



Hydrate Technology for the Concentration of Aqueous Salt Solutions using Fluorinated Refrigerants

By

Peterson Thokozani Ngema

MTech (Chemical Engineering) – DUT
MScEng (Chemical Engineering) – UKZN

Thesis submitted in fulfilment of the academic requirements for the

Doctor of Philosophy in the field of Chemical Engineering

at the University of KwaZulu-Natal, South Africa

EXAMINERS' COPY

March 2019

Supervisors: Prof. Deresh Ramjugernath, Prof. Amir H. Mohammadi, Prof. Paramespri Naidoo,

As the candidate's supervisor, I agree to the submission of this dissertation/thesis

Prof. D. Ramjugernath

Prof. A. H. Mohammadi

Prof. P. Naidoo

DECLARATION 1 - PLAGIARISM

I, ..Peterson Thokozani Ngema....., declare that

1. Except where I mean otherwise, the research work in this dissertation is my original work.
2. This dissertation has not been submitted to any other university for any degree or examination.
3. This dissertation shall not contain any data, images, text, graphics or other information or tables of other persons copied and pasted from the Internet unless specifically recognized as originating from other persons. The source information is listed in the reference sections of the dissertation.

Signature

.....

DECLARATION 2 - PUBLICATIONS

Publication 1: The Journal of Chemical Thermodynamics (*Accepted Manuscript*)

Journal Title: Phase Stability Conditions for Refrigerant (R410a or R507) + Water + (NaCl, CaCl₂, MgCl₂ and Na₂SO₄) + Cyclopentane: Experimental Measurements and Thermodynamic Modelling Using Developed Hydrate Electrolyte–Cubic Plus Association (HE–CPA) Equation of State

Authors: Peterson Thokozani Ngema, Paramespri Naidoo, Amir H. Mohammadi*, Deresh Ramjugernath*

Publication 2: Journal of Chemical and Engineering Data (*Accepted*)

Journal Title: Experimental Measurements and Modelling of the Dissociation Conditions of Clathrate Hydrates for CO₂ + (NaCl or CaCl₂ or MgCl₂) + Water + Cyclopentane Systems

Authors: Peterson Thokozani Ngema, Paramespri Naidoo, Amir H. Mohammadi*, Deresh Ramjugernath*

***This paper was presented on the *Flouro-Chemical Expansion Initiative Conference*, Cape Town, South Africa, 14–17 November 2015

Publication 3: Desalination (*Manuscript in preparation*)

Journal Title: Water Desalination using Clathrate Hydrates: State of the Art

Authors: Peterson Thokozani Ngema, Paramespri Naidoo, Amir H. Mohammadi*, Deresh Ramjugernath*

ACKNOWLEDGEMENTS

I would like to acknowledge the following people for their support and enormous contribution to this project:

- My God who gave me power and strength to stand and overcome all challenges encountered during this investigation and I thank God for making this project successful.
- My family, my sister (Mbali) and three brothers who gave me support in my studies and in my tough times. In addition, their passion for me to complete this project.
- My supervisors, Professor Deresh Ramjugernath, Professor Amir H. Mohammadi and Professor Paramespri Naidoo for their assistance, knowledge, guidance and support during my PhD degree.
- University of KwaZulu-Natal for their financial support
- Supporter, Zamandaba Ndaba
- Laboratory Assistance, Ayanda Khanyile
- My friend, Siyabonga Buthelezi
- My colleagues, Mxolisi Cele and Mohammed Bux (DUT Masters students); Dr. Kaniki Tumba, Dr. Marc Tshibangu, Dr. Matthew Lasich, Dr. Khalid Osman, Dr. Samuel Iwarere
- The workshop staff for their assistance during the gas hydrates equipment breakdowns.

ABSTRACT

The world is facing a challenge with the scarcity of fresh water, due to an increase in the world population and the large expansion of industrial projects. This results in greater demand for fresh water. In such a scenario, seawater shows the potential as an alternative source of fresh water, if a suitable purification system can be economically incorporated. Desalination is a process used to remove salts from seawater, in so doing, converting into fresh water. In general, there are two desalination processes, which are thermal processes and membrane processes. These processes are used in water industries to treat seawater and wastewater. Seawater and industrial wastewater contain higher concentration of minerals such as NaCl, Na₂SO₄, MgCl₂ and CaCl₂, which need to be eliminated from drinking water. However, the thermal and membrane processes consume a large amount of energy. They are costly to operate because of the scaling and membrane damage that is caused by saturated sulphates and the presence of chlorides, respectively. It is important to recover fresh water from concentrated brine solutions at ambient conditions, consequently, desalination using gas hydrate technology has been proposed by several researchers to be an alternative technology. This is simply because gas hydrate technology offers one of the most promising economical alternatives for desalination of seawater and industrial wastewater, especially in the use of fluorinated refrigerants as hydrate former in the presence of a promoter.

The use of fluorinated refrigerants to form gas hydrate is attractive because it may facilitate hydrate formation in ambient environments. Then, the dissociation of gas hydrate results in the production of fresh water after all the minerals and contaminants are eliminated. However, there is a lack of research regarding the formation of hydrate using fluorinated refrigerants with single and mixed electrolytes, as well as in the presence of promoter. Consequently, one of the objectives of this study was to conduct the extensive research that is required for the hydrate phase equilibrium data for refrigerants, with electrolyte solution (single and mixed electrolytes), as well as in the presence of the promoter. The generated hydrate dissociation data and the apparent rate constant obtained from the kinetic data were used to design the gas hydrate reactor for the proposed process for the treatment of seawater and industrial wastewater using gas hydrate technology. Another objective of this study was to develop a hydrate electrolyte equation of state to model the generated data as well as to undertake future predictions.

Hydrate dissociation data were measured using the non-visual isochoric equilibrium cell designed by author in the MSc programme in 2014 to conduct a gas hydrate measurement. In this study, gas hydrate measurements were conducted using the pressure-search method.

The synthetic saline solutions were prepared within a typical range for industrial wastewater concentrations, such as those found at Tutuka Eskom, and seawater concentrations. It was found that the hydrate was formed, but phase boundary condition was shifted slightly, to lower dissociation temperatures. In the presence of promoter, it was revealed that dissociation temperatures were closed to ambient conditions. Moreover, higher concentrations of electrolytes above seawater concentration were investigated. It was revealed that as the concentration of electrolytes increases, hydrates dissociation temperatures shifted more towards lower values. In the presence of a promoter the dissociation temperatures increases, but they were below ambient temperatures. The solubility of electrolytes was measured to ensure that no salts are above the solubility limits.

Among the studied refrigerants (hydrate former), it was found that hydrate former (R410a) was suitable to be utilised for the desalination gas hydrate technology due to its properties such as being environmentally-friendly, not harmful to human, availability, lower cost and form hydrate at lower pressures near ambient temperatures. The use of R410a as hydrate former shows that hydrates are formed near ambient temperatures, where the main purpose is to design the process to operate at ambient conditions. Cyclopentane was used as a promoter. It shows impressive results on hydrate systems, because it was able to shift dissociation temperatures near to ambient conditions, and can therefore can be used as a promoter in hydrate processes.

All gas hydrate measurements were modelled using the developed combinations contributions terms, namely the Hydrate Electrolytes Cubic Plus Association (HE-CPA) equation of state. The results obtained show that the hydrate dissociation data strongly agree with the model results. Consequently, it is recommended that this model can be used for predictions for hydrate systems and can be used in water industry to optimise processes. It was concluded that for the proposed desalination process using gas hydrate technology, the R410a could be used as hydrate former in the hydrate reactor to form hydrates slurry. The proposed process was designed at a high level, where only hydrate reactor, separator and compressor were designed. It is recommended that one has to design and scale up a process in full.

TABLE OF CONTENT

DECLARATION 1 - PLAGIARISM	ii
DECLARATION 2 - PUBLICATIONS.....	iii
ACKNOWLEDGEMENTS	iv
ABSTRACT.....	v
TABLE OF CONTENT.....	vii
LIST OF FIGURES	xii
LIST OF TABLES	xviii
NOMENCLATURE.....	xxiii
ABBREVIATIONS.....	xxvii
CHAPTER 1: INTRODUCTION.....	1
CHAPTER 2: LITERATURE REVIEW	6
2.1 Desalination	6
2.1.1 Traditional processes.....	6
2.1.2 Gas hydrate technology.....	10
2.1.3 Summary of the desalination.....	14
2.2 Electrolytes	14
2.2.1 Solubility of electrolytes in water	18
2.2.2 Summary of electrolytes	23
2.3 Industrial wastewater and seawater	23
2.3.1 Electrolytes in the oil and gas industry	27
2.3.2 Behaviour of mixtures containing electrolytes in industry	28
2.3.2 Summary of the industrial wastewater and seawater	30
2.4 Gas hydrates.....	30
2.4.1 Introduction to gas hydrates.....	30
Physical properties of gas hydrates.....	31

2.4.2 Structures of gas hydrates	33
2.4.3 Hydrate formation	35
2.4.4 Hydrate dissociation.....	36
2.4.5 Hydrate promoters.....	37
Cyclopentane.....	39
2.6 Refrigerants.....	41
Solubility of fluorinated refrigerants in water	43
2.7 Kinetic and thermodynamic behaviour of clathrate hydrates	44
2.8 Economics.....	44
2.9 Summary for the gas hydrates.....	48
CHAPTER 3: DEVELOPMENT OF HYDRATE ELECTROLYTE–CUBIC PLUS ASSOCIATION (HE-CPA) MODEL EQUATION OF STATE	49
3.1 Activity coefficient models for electrolytes.....	50
3.1.1 Long range interactions (LR).....	53
3.1.2 The middle range (MR) interaction term	60
3.1.3 The short range (SR) interaction term.....	62
3.1.4 The Born term	63
3.2. The Cubic-Plus-Association (CPA) equation of state (EoS)	65
3.2.1 Calculation of fugacity coefficients with CPA EoS.....	71
3.2.2 Calculation of fugacity coefficients for the association term of the CPA EoS	74
3.2.3 Calculation of the volume	77
3.3 Modeling of hydrate phase.....	79
3.3.1 Model parameters.....	83
3.3.2 The Langmuir constants.....	84
3.4 Development of thermodynamic hydrate modelling (HE-CPA)	85
3.5 Kinetic model.....	86
CHAPTER 4: GAS HYDRATE EQUIPMENT AND EXPERIMENTAL PROCEDURE . 91	
4.1 The isochoric equilibrium cell	91
4.1.1 Method of agitation within the equilibrium cell	95
4.1.2 Pressure measurements	97
4.1.3 Temperature measurements	98

4.1.4 Data logging.....	98
4.2 Preparation of the equilibrium cell	98
4.2.1 Cleaning of the equilibrium cell.....	98
4.2.2 Leak detection	99
4.3 Calibrations	99
4.3.1 Temperature and pressure calibration	99
4.3.2 Temperature probe calibration	100
4.3.3 Pressure transmitter calibration.....	101
4.3.4 Vapour pressure measurements	102
4.4 Materials	102
4.5 Sample preparation	102
4.6 Operating procedure for equilibrium cell	103
4.6.1 Loading of equilibrium cell.....	103
4.6.2 Hydrate measurements	103
4.6.3 Kinetics measurements	105
4.6.4 Shutdown procedure	105
4.7 Operating procedure for measuring salt solubility.....	106
4.7.1 Samples preparation.....	106
4.7.2 Solubility measurements	106
4.7.3 Shutdown of DTG.....	107
4.8 Safety in the laboratory	107
CHAPTER 5: RESULTS AND DISCUSSIONS	109
5.1 Purities, vapour pressure and calibrations	109
5.1.1 Chemical purities	109
5.1.2 Vapour pressures for refrigerants.....	110
5.1.3 Temperature calibration	111
5.1.4 Pressure calibration	112
5.2 Refrigerant with water systems.....	113
5.2.1 Binary test systems for refrigerant + water	113
5.2.2 Refrigerants + water + CP systems	116
5.2.3 R507 + water + CP systems	118

5.3 Refrigerant + single electrolytes in the presence of CP	118
5.4 Refrigerant + mixed electrolytes in the presence of CP	123
5.4.1 Industrial concentration.....	123
5.4.2 R507 + water + CaCl ₂ + NaCl + CP system	126
5.4.3 R410a systems at higher concentration.....	128
5.4.4 The effect of CP on the formation and dissociation of gas hydrates.....	130
5.5 Enthalpy of hydrate dissociation.....	131
5.6 Kinetic measurements	135
5.7 Carbon dioxide + water + single salt + CP systems	139
5.8 Desalination using gas hydrate technology.....	143
5.8.1 Solubility of refrigerants	145
5.8.2 Separation of residual by hydrate formation.....	145
5.9 Solubility measurement of electrolytes.....	146
5.10 Hydrate Electrolyte – Cubic Plus Association (HE-CPA) model discussion.....	150
5.10.1 Fugacity calculation	152
5.11 Modelling Results	153
5.11.1 Refrigerant + water + CP systems.....	156
5.11.2 Refrigerant + water + single salts in the presence of CP	158
5.11.3 Refrigerant + water + mixed salts in the presence of CP.....	160
5.11.4 R410a high concentration of salt	163
5.11.5 Model parameters.....	165
5.12 Carbon dioxide system.....	166
5.12.1 CO ₂ + water + single salt in the presence of CP	166
CHAPTER 6: CONCEPTUAL DESIGN FOR DESALINATION PROCESS	169
6.1 Proposed hydrate desalination process	169
6.2 Hydrate reactor design	172
6.3 Horizontal belt filter separation design.....	174
6.4 Compressor design.....	176
6.4.1 Sizing and selection	176
6.5 Economic feasibility study.....	178
6.5.1 The capital cost	179

6.5.2 Operation and maintenance costs.....	180
CHAPTER 7: CONCLUSIONS	182
<u>CHAPTER 8: FUTURE WORK</u>.....	185
REFERENCES.....	186
APPENDIX A: CALIBRATION AND UNCERTAINTIES.....	218
A.1 Calibrations	218
A.2 NIST uncertainty determinations	220
Estimation of uncertainty for temperature and pressure	220
APPENDIX B: PARAMETERS.....	222
APPENDIX C: MEASURED AND CALCULATED HYDRATE DISSOCIATION DATA WITH THEIR AAD.....	225
APPENDIX D: DESIGN EQUATIONS	234
D.1 Reactor design.....	234
D.2 Compressor design.....	235
D.3 Horizontal belt filter design	236
APPENDIX E: KINECTICS MEASUREMENTS	243
APPENDIX F: JOURNAL PAPERS ABSTRACT	250

LIST OF FIGURES

CHAPTER 2

Figure 2. 1: An early desalination process design.....	12
Figure 2. 2: Solubility of different salts above 100°C	19
Figure 2. 3: Effect of NaCl concentration at 298.15 K on mean ionic activity coefficient, water activity and osmotic activity (left). Effect of different salts on the freezing point of water as a consequence of reduced water activity (right)	29
Figure 2. 4: Apparent molar volume as a function of ionic strength (left); and heat capacity of selected aqueous electrolyte solutions (right)	29
Figure 2. 5: Formation of a gas hydrate in a sapphire cell.....	33
Figure 2. 6: Polyhedral structures of the sI, sII and sH.....	34
Figure 2. 7: Elements of gas hydrate formation.....	35
Figure 2. 8: Demonstration of the hydrate formation and dissociation curve	36
Figure 2. 9: Energy consumption for distillation, membrane and hydrate	47

CHAPTER 3

Figure 3. 1: Cubic Plus Association equation of state to hydrate and electrolyte (HE-CPA)	86
---	----

CHAPTER 4

Figure 4. 1: Schematic diagram of the isochoric equilibrium cell	92
Figure 4. 2: Schematic flow diagram of the equipment.....	94
Figure 4. 3: A schematic diagram of the stirring mechanism	96
Figure 4. 4: Demonstration of hydrate formation and dissociation curve	104

CHAPTER 5

Figure 5. 1: Vapour pressure plots for the R134a, R410a and R507	111
Figure 5. 2: Deviation for temperature calibration	112
Figure 5. 3: Deviation in pressure calibration.....	113
Figure 5. 4: Comparison between the measured hydrate data and literature for the R134a (1) + water (2) system.....	114
Figure 5. 5: Comparison between the measured hydrate data and literature for R410a (1) + water (2) system.....	115
Figure 5. 6: Measured data for hydrate–liquid water–vapour for the R507 (1) + water (2) system	116
Figure 5. 7: Measured data for hydrate–liquid water–liquid promoter–vapour for the R410a (1) + water (2) in the absence and presence of CP systems.....	117
Figure 5. 8: Measured data for hydrate–liquid water–liquid promoter–vapour for the R507 (1) + water (2) + CP (3) system	118
Figure 5. 9: Measured data for hydrate–liquid water–liquid promoter–vapour for the R410a (1) + water (2) + NaCl (3) + CP (4) system.....	120
Figure 5. 10: Measured data for hydrate–liquid water–liquid promoter–vapour for the R410a (1) + water (2) + CaCl ₂ (3) + CP (4) system	122
Figure 5. 11: Measured data for hydrate–liquid water–liquid promoter–vapour for the R410a (1) + water (2) + Na ₂ SO ₄ (3) system	123
Figure 5. 12: Measured data for hydrate–liquid water–liquid promoter–vapour for the R410a (1) + water (2) + 0.0020 mass fraction of CaCl ₂ (3) + 0.017 mass fraction of NaCl (4) + CP (5) systems.....	124
Figure 5. 13: Measured data for hydrate–liquid water–liquid promoter–vapour for the R410a (1) + water (2) + 0.013 mass fraction of MgCl ₂ (3) + 0.019 mass fraction of NaCl (4) + CP (5) system	126
Figure 5. 14: Measured data for hydrate–liquid water–liquid promoter–vapour for the R507 (1) + water (2) + 0.0020 mass fraction of CaCl ₂ (3) + 0.017 mass fraction of NaCl (4) + CP (5) system	127
Figure 5. 15 Measured data for hydrate–liquid water–liquid promoter–vapour for the R410a (1) + water (2) + 0.05 mass fraction of NaCl (3) + 0.08 mass fraction of CaCl ₂ (4) + CP (5) system	129

Figure 5. 16: Measured data for hydrate–liquid water–liquid promoter–vapour for the R410a (1) + water (2) + 0.05 mass fraction of NaCl (3) + 0.15 mass fraction of CaCl ₂ (4) + CP (5) system	130
Figure 5. 17: Enthalpy of measured hydrate dissociation data in the absence and presence of single and mixed salt as well as CP	134
Figure 5. 18: Initial conditions and degree of subcooling for R410a (1) + water (2) + 0.013 mass fraction of MgCl ₂ (3) + 0.019 mass fraction of NaCl system.....	135
Figure 5. 19: Kinectic measurements for R410a (1) + water (2) + 0.002 mass fraction of CaCl ₂ (3) + 0.017 mass fraction of NaCl (4) system at 281.8 K at the following initial pressures	136
Figure 5. 20: The algorithm to calculate the water to hydrate conversion	138
Figure 5. 21: Measured data for hydrate–liquid water–liquid promoter–vapour for the CO ₂ (1) + water (2) + NaCl (3) + CP (4) system.....	140
Figure 5. 22: Measured data for hydrate–liquid water–liquid promoter–vapour for the CO ₂ (1) + water (2) + CaCl ₂ (3) + CP (4) system.....	142
Figure 5. 23: Measured data for hydrate–liquid water–liquid promoter–vapour for the CO ₂ (1) + water (2) + MgCl ₂ (3) + CP (4) system	143
Figure 5. 24: Solubility data for measured salts	148
Figure 5. 25: Solubility data for calcuim sulphate	149
Figure 5. 26: Computational algorithm flow diagram	152
Figure 5. 27: Measured and estimated data for hydrate–liquid water–vapour for the R134a (1) + water (2) test system	154
Figure 5. 28: Measured and estimated data for hydrate–liquid water–vapour for the R410a (1) + water (2) test system	155
Figure 5. 29: Measured and estimated data for hydrate–liquid water–vapour for the R152a (1) + water (2) test system	155
Figure 5. 30: Measured and estimated data for hydrate–liquid water–vapour for the R507 (1) + water (2) system.....	156
Figure 5. 31: Measured and estimated data for hydrate–liquid water–liquid promoter–vapour for the R410a (1) + water (2) in the absence and presence of CP (3) systems.....	157
Figure 5. 32: Measured and estimated data for hydrate–liquid water–liquid promoter–vapour for the R507 (1) + water (2) in the absence and presence of CP (3) system	157

Figure 5. 33: Measured and estimated data for hydrate–liquid water–liquid promoter–vapour for the R410a (1) + water (2) + NaCl (3) + CP (4) system	159
Figure 5. 34: Measured and estimated data for hydrate–liquid water–liquid promoter–vapour for the R410a (1) + water (2) + CaCl ₂ (3) + CP (4) system	159
Figure 5. 35: Measured and estimated data for hydrate–liquid water–vapour for the R410a (1) + water (2) + Na ₂ SO ₄ (3) system	160
Figure 5. 36: Measured and estimated data for hydrate–liquid water–liquid promoter–vapour for the R410a (1) + water (2) + 0.0020 mass fraction of CaCl ₂ (3) + 0.017 mass fraction of NaCl (4) + CP (5) systems	161
Figure 5. 37: Measured and estimated data for hydrate–liquid water–liquid promoter–vapour for the R410a (1) + water (2) + 0.013 mass fraction of MgCl ₂ (3) + 0.019 mass fraction of NaCl (4) + CP (5) system.....	162
Figure 5. 38: Measured and estimated data for hydrate–liquid water–liquid promoter–vapour for the R507 (1) + water (2) + 0.0020 mass fraction of CaCl ₂ (3) + 0.017 mass fraction of NaCl (4) + CP (5) system.....	162
Figure 5. 39. Measured and estimated data for hydrate–liquid water–liquid promoter–vapour for the R410a (1) + water (2) + 0.08 mass fraction of CaCl ₂ (3) + 0.05 mass fraction of NaCl (4) + CP (5) system.....	164
Figure 5. 40: Measured and estimated data for hydrate–liquid water–liquid promoter–vapour for the R410a (1) + water (2) + 0.15 mass fraction of CaCl ₂ (3) + 0.05 mass fraction of NaCl (4) + CP (5) system.....	164
Figure 5. 41: Measured and estimated data for hydrate–liquid water–liquid promoter–vapour for the CO ₂ (1) + water (2) + NaCl (3) + CP (4) system	167
Figure 5. 42: Measured and estimated data for hydrate–liquid water–liquid promoter–vapour for the CO ₂ (1) + water (2) + CaCl ₂ (3) + CP (4) system.....	167
Figure 5. 43: Measured and estimated data for hydrate–liquid water–liquid promoter–vapour for the CO ₂ (1) + water (2) + MgCl ₂ (3) + CP (4) system.....	168

APPENDIX A

Figure A1. 1: Calibration temperature curve for T_{std} against T_{exp} for the isochoric pressure cell: T_{exp} is the experimental temperature and T_{std} is the standard probe from WIKA.....	218
Figure A1. 2: Deviation for temperature sensor (Pt-100) for isochoric pressure cell: T_{act} is the calculated temperature using equation obtained in Figure A1.1.....	218
Figure A1. 3: Calibration for pressure transmitter curve range (0–60 bar) for P_{std} against P_{exp} for the isochoric pressure cell: P_{exp} is the experimental temperature and P_{std} is the standard transmitter from WIKA.....	219
Figure A1. 4: Deviation for pressure transmitter sensor for isochoric pressure cell: P_{act} is the calculated pressure using equation obtained in Figure A1.3	219

APPENDIX E

Figure E1. 1: Kinetic measurements for R410a (1) + water (2) + 0.013 mass fraction of $MgCl_2$ (3) + 0.019 mass fraction of NaCl (4) system at 276.8 K at the following initial pressures	243
Figure E1. 2: Kinetic measurements for R410a (1) + water (2) + 0.013 mass fraction of $MgCl_2$ (3) + 0.019 mass fraction of NaCl (4) + CP system at 280.8 K at the following initial pressures	244
Figure E1. 3: Kinetic measurements for R410a (1) + water (2) + 0.013 mass fraction of $MgCl_2$ (3) + 0.019 mass fraction of NaCl (4) + CP system at 282.8 K at the following initial pressures	244
Figure E1. 4: Kinetic measurements for R410a (1) + water (2) + 0.002 mass fraction of $CaCl_2$ (3) + 0.017 mass fraction of NaCl (4) system at initial pressure of 0.90 MPa; at different temperature	245
Figure E1. 5: Kinetics measurements for R410a (1) + water (2) + 0.002 mass fraction of $CaCl_2$ (3) + 0.017 mass fraction NaCl (4) system at 281.8 K at the following initial pressures.....	246
Figure E1. 6: Initial conditions and degree of subcooling for R410a (1) + water (2) + 0.013 mass fraction of $MgCl_2$ (3) + 0.019 mass fraction of NaCl (4) + CP (5) system	246
Figure E1. 7: Kinetics measurements for R410a (1) + water (2) + 0.013 mass fraction of $MgCl_2$ (3) + 0.019 mass fraction of NaCl (4) system + CP (5) at 277.2 K at the following initial pressures.....	247

Figure E1. 8: Kinetics measurements for R410a (1) + water (2) + 0.002 mass fraction of CaCl₂ (3) + 0.017 mass fraction of NaCl (4) system at 282.9 K at the following initial pressures 247

Figure E1. 9: Kinetics measurements for R410a (1) + water (2) + 0.013 mass fraction of MgCl₂ (3) + 0.019 mass fraction of NaCl (4) system + CP at 277.2 K at the following initial pressures 248

Figure E1. 10: Kinetics measurements for R410a (1) + water (2) + 0.013 mass fraction of MgCl₂ (3) + 0.019 mass fraction of NaCl (4) system at 276.8 K at the following initial pressures 248

Figure E1. 11: Kinetics measurements for R410a (1) + water (2) at the following initial pressures 249

Figure E1. 12: Kinetics measurements for R410a (1) + water (2) + 0.002 mass fraction of CaCl₂ (3) + 0.017 mass fraction NaCl (4) + CP system at 277.2 K at the following initial pressures; 249

LIST OF TABLES

CHAPTER 2

Table 2. 1: Traditional desalination processes	7
Table 2. 2: Comparison of desalination technologies	9
Table 2. 3: Single electrolytes with fluorinated refrigerants at different concentrations.....	16
Table 2. 4: Mixed electrolytes with fluorinated refrigerants at different concentrations	17
Table 2. 5: Salts solubility with various solvents	21
Table 2. 6: Brine stream concentrations of constituents at various industries.....	25
Table 2. 7: The major constituents of water at seawater level.....	26
Table 2. 8: The quality of treated water from Tutuka power station Eskom	27
Table 2. 9: Characteristics and physical properties of gas hydrates	31
Table 2. 10: Comparison of structure sI and sII.....	32
Table 2. 11: Criteria for selecting hydrate formers.....	42
Table 2. 12: Reviewed hydrate former and water systems	43
Table 2. 13: Comparison of MSF, RO and gas hydrate technology	46

CHAPTER 3

Table 3. 1: Activity coefficient models for electrolyte solutions and their applications	52
Table 3. 2: Coefficients for the calculation of the dielectric constant in Equation 3.2.....	54
Table 3. 3: Example of a charge component.....	55
Table 3. 4: Schematic of association schemes	67
Table 3. 5: CPA parameters for associating compound (pure water)	70
Table 3. 6: Kinetic for the selected refrigerant	87

CHAPTER 5

Table 5. 1: Purities, critical properties and suppliers of refrigerant studied	110
Table 5. 2: Temperature calibration correlation and deviations	112
Table 5. 3: Pressure calibration correlation and deviations	113
Table 5. 4: Hydrate dissociation data for refrigerants (1) + water (2) test systems.....	114
Table 5. 5: Measured data for hydrate–liquid water–vapour for R507 (1) + water (2) system ..	116
Table 5. 6: Measured data for hydrate–liquid water–liquid promoter–vapour for the refrigerant (1) + water (2) + CP (3) systems.....	117
Table 5. 7: Measured data for hydrate–liquid water–liquid promoter–vapour for the R410a (1) + water (2) + NaCl (3) + CP (4) system at various salt concentrations	120
Table 5. 8: Measured data for hydrate–liquid water–liquid promoter–vapour for the R410a (1) + water (2) + CaCl ₂ (3) + CP (4) system at various salt concentrations	121
Table 5. 9: Measured data for hydrate–liquid water–vapour for R410a (1) + water (2) + Na ₂ SO ₄ (3) system at 0.10 wt% concentrations of salt	122
Table 5. 10: Measured data for hydrate–liquid water–liquid promoter–vapour for the R410a (1) + water (2) + CaCl ₂ (3) + NaCl (4) + CP (5) system at various salt concentrations.....	124
Table 5. 11: Measured data for hydrate–liquid water–liquid promoter–vapour for the R410a (1) + water (2) + MgCl ₂ (3) + NaCl (4) + CP (5) system at various salt concentrations.....	125
Table 5. 12: Measured data for hydrate–liquid water–liquid promoter–vapour for the R507 (1) + water (2) + CaCl ₂ (3) + NaCl (4) + CP (5) system at various salt concentrations.....	127
Table 5. 13: Measured data for hydrate–liquid water–liquid promoter–vapour for the R410a (1) + water (2) + NaCl (3) + CaCl ₂ (4) + CP (5) system at various salt concentrations.....	128
Table 5. 14: Enthalpy of hydrate dissociation	132
Table 5. 15: Water to hydrate conversion, apparent rate constant and induction time for studied systems.....	137
Table 5. 16: Measured data for hydrate–liquid water–liquid promoter–vapour for the CO ₂ (1) + water (2) + NaCl (3) + CP (4) system at various salt concentrations	140
Table 5. 17: Measured data for hydrate–liquid water–liquid promoter–vapour for the CO ₂ (1) + water (2) + CaCl ₂ (3) + CP (4) system at various salt concentrations	141
Table 5. 18: Measured data for hydrate–liquid water–liquid promoter–vapour for the CO ₂ (1) + water (2) + MgCl ₂ (3) + CP (4) system at various salt concentrations.....	143

Table 5. 19: Comparison of solubility of measured salt and at 298.2 K.....	147
Table 5. 20: Solubility data for sodium sulphate and sodium chloride	147
Table 5. 21: Solubility data for magnesium chloride and calcium chloride	148
Table 5. 22: Solubility data for calcium sulphate	149
Table 5. 23: Temperature and pressure ranges for hydrate dissociation data for (R134a, R410a, R152a and R507) + water systems	154
Table 5. 24: Temperature and pressure ranges for hydrate dissociation data in the presence of CP	156
Table 5. 25: Temperature and pressure ranges investigated for hydrate dissociation data in the absence and presence of CP at various salt concentration (w_i = mass fraction)	158
Table 5. 26: Temperature and pressure ranges investigated for gas hydrate measurements in the absence and presence of CP at various salt concentration (w_i = mass fraction)	161
Table 5. 27: Temperature and pressure ranges investigated for gas hydrate measurements in the absence and presence of CP at various salt concentration (w_i = mass fraction)	163
Table 5. 28: Regressed Langmuir constants parameters used in this study.....	165
Table 5. 29: Temperature and pressure ranges investigated for gas hydrate measurements	166
Table 5. 30: Regressed Langmuir constants parameters for the CO ₂ (1) + water (2) system.....	168

APPENDIX B

Table B1. 1: Constant parameters.....	222
Table B1. 2: Relative dielectric constant of selected solvents at T = 298.15 K	222
Table B1. 3: The charge of electrolytes	223
Table B1. 4: Selected interaction parameters for the MR term	223
Table B1. 5: Impeller diameter	223
Table B1. 6: M–Line and MB–Line frame data	224
Table B1. 7: Nominal Ψ	224

APPENDIX C

Table C1. 1. Measured and calculated data for hydrate–liquid water–liquid promoter–vapour for the R410a (1) + water (2) + NaCl (3) + CP (4) system at various salt concentrations	225
Table C1. 2. Measured and calculated data for hydrate–liquid water–liquid promoter–vapour for the R410a (1) + water (2) + CaCl ₂ (3) + CP (4) system at various salt concentrations.....	226
Table C1. 3. Measured and calculated data for hydrate–liquid water–vapour for the R410a (1) + water (2) + Na ₂ SO ₄ (3) system at various salt concentrations and literature systems for (R134a and R152b) (1) + water (2)	227
Table C1. 4. Measured and calculated data for hydrate–liquid water–liquid promoter–vapour for the R507 (1) + water (2) + mixed salts (3) + CP (4) system at industrial salt concentrations....	228
Table C1. 5. Measured and calculated data for hydrate–liquid water–liquid promoter–vapour for the R410a (1) + water (2) + mixed salts (3) + CP (4) system at industrial salt concentrations..	229
Table C1. 6. Measured and calculated data for hydrate–liquid water–liquid promoter–vapour for the R410a (1) + water (2) + mixed salts (3) + CP (4) system at higher salt concentrations	230
Table C1. 7. Measured and calculated data for hydrate–liquid water–liquid promoter–vapour for the CO ₂ (1) + water (2) + NaCl (3) + CP (4) system at various salt concentrations	231
Table C1. 8. Measured and calculated data for hydrate–liquid water–liquid promoter–vapour for the CO ₂ (1) + water (2) + CaCl ₂ (3) + CP (4) system at various salt concentrations.	232
Table C1. 9. Measured and calculated data for hydrate–liquid water–liquid promoter–vapour for the CO ₂ (1) + water (2) + MgCl ₂ (3) + CP (4) system at various salt concentrations.	233

APPENDIX D

Table D1. 1. Separation and filtration phase.....	241
Table D1. 2. Washing phase	241
Table D1. 3. Deliquoring phase	242

LIST OF PHOTOGRAPHS

CHAPTER 4

Photograph 4. 1: Top view of the equilibrium cell and cap.....	92
Photograph 4. 2: The isochoric equilibrium cell.....	93
Photograph 4. 3: Side view of the cap	93
Photograph 4. 4: A layout of the equipment.....	95
Photograph 4. 5: Stirring device made with neodymium magnets	97
Photograph 4. 6: Differential thermal analysis	107

NOMENCLATURE

Symbol	Description	Units
AAD	Absolute average deviation	%
a,b c,d	Adjustable parameter for the Langmuir constant	K.MPa ⁻¹
a _{ij} and b _{ij}	Cross parameters for the terms a _m and b _m	
a _m and b _m	EOS parameters for the mixture	
a _o	Parameter in the energy term	bar.L ² mol ⁻²
α	Energy term in the SRK term	bar.L ² mol ⁻²
A _i	Site A in molecule <i>i</i>	
<i>b</i>	Co-volume parameter	L.mol ⁻¹
B _j	Site B in molecule <i>j</i>	
C and D	Langmuir constant	
<i>c</i> ₁	Parameter in the energy term	
<i>d</i> _m	Density of the salt-free mixture	kg.m ⁻³
<i>e</i>	Electronic charge	
<i>f</i>	Fugacity	MPa
<i>g</i>	Radial distribution function	
h _{is}	Interaction parameter between the dissolved salt and non-electrolyte component	
<i>I</i>	Ionic strength	
<i>k</i>	Boltzmanns constant	
k _{ij} and l _{ij}	Concentration in a binary-independent binary interaction parameters and they are different for each binary system	
<i>m</i> _{<i>i</i>}	Molality	mol/kg
M _m	Salt-free mixture molecular weight	kg
N _A	Avogadro's number	
<i>N</i>	Number of experimental data	
<i>n</i>	Number of moles	
OF	Objective function	

P	Pressure	MPa
P_c	Critical pressure	MPa
Q_{sp}	Stationary point	
q_i	Surfaces area of the solvent	m
r	Radial coordinate	\AA^0
r_i	Van der Waals volume	
r	Distance between ion	m
R	Universal gas constant	$\text{J}\cdot\text{mol}^{-1}\cdot\text{K}^{-1}$
s	Structure of gas hydrate	
T	Temperature	K
T_c	Critical temperature	K
V	Vapour	
v'_i	Number of cavities of type I per water molecule in a unit hydrate cell	
v	Partial molar volume	m^3
V_m	Molar volume	L/mol
x	Mole fraction of liquid	
y	Mole fraction of vapour	
Z	Compressibility factor	
Z_i	Charge component i	

Greek symbol

Symbol	Description
μ	Chemical potential
γ	Activity coefficient
ϕ	Fugacity coefficient
α	EOS temperature dependent parameter
κ	Constant characteristic of each component
ω	Acentric factor
φ	Correction for the deviation of the saturated vapour of pure lattice from ideal behaviour
Δ	Change in a property or association strength
ε_m	Salt-free mixture dielectric constant
ε_N	Dielectric constant of water
β	Association volume parameter
η	Reduced density or packing factor
ϵ	Association energy parameter
ρ	Molar density
π	Pie
ν	Stoichiometric coefficient
Ψ	Electric potential

Superscripts

Symbol	Description
β	Empty hydrate phase
α	Ice phase
L	Liquid water phase
H	Hydrate phase
EOS	Equation of state
MT	Empty hydrate
EL	Effect of the electrolytes
Cal	Calculated
Exp	Experimental
sat	Saturation

Subscripts

Symbol	Description
m	Cavity type m
w	Water
I	Ice
i,j	Component

ABBREVIATIONS

Abbreviation	Description of abbreviation
CPA	Cubic Plus Association equation of state
CP	Cyclopentane
EDR	Electrodialysis reversal
EoS	Equation of state
GC	Gas chromatograph
GH	Gas hydrate
H-L _w -V	Hydrate – liquid water –vapour
ICP-AES	Inductively Coupled Plasma Atomic Emission Spectroscopy
MD	Membrane distillation
MSF	Multi-stage flash distillation
NF	Nano-filtration
RO	Reverse osmosis
SRK	Soave – Redlich – Kwong
TCD	Thermal conductivity detector
TDS	Total dissolved solid
VC	Vapour compression
VLE	Vapour-liquid equilibrium

CHAPTER 1

INTRODUCTION

This study seeks to determine whether environmentally-friendly fluorinated refrigerants, with the addition of a suitable promoter, can be used to provide a cost effective gas hydrate separation technology for water desalination. Desalination is a process used to purify water at industrial wastewater treatment plants or to purify seawater. It was defined as a process that removes minerals from saline water (seawater or industrial wastewater) that contains salts such as sodium chloride (NaCl), sodium sulphate (Na₂SO₄), magnesium chloride (MgCl₂), calcium chloride (CaCl₂), calcium sulphate (CaSO₄) and other salts. These salts need to be removed because they make water unsuitable for use for any purposes, and are causing corrosion or damage on pipeline and process equipment.

Desalination technology is important because freshwater has become a scarce commodity. The growth of population and industrial expansion has increased the demand for freshwater (Park et al., 2011). Seawater is in abundant supply, and it has potential as an alternative source of freshwater if suitable, economical purification technologies can be developed.

Finding a means of desalination at ambient temperatures and pressures is central to the question of cost. Traditional desalination technologies are utilising multi-stage flash (MSF) distillation, and reverse osmosis (RO) membrane. However, these technologies are uneconomical because they consume a large amount of energy. They operate at high temperatures and/or pressures. In addition, they are costly to operate because of the scaling, corrosion and membrane damage that is caused by saturated sulphates and chlorides. To be economical, it is necessary to be able to recover freshwater from concentrated brine at ambient conditions, where gas hydrate technology is widely believed to have this potential.

The aim is to determine the suitable hydrate former (refrigerant) that could be used to design a viable gas hydrate system for the treatment of industrial wastewater and seawater.

While the use of gas hydrates is well established as an effective means of desalination, no publication of research has been found on the formation of hydrates from water containing mixed electrolytes, using a fluorinated refrigerant as hydrate former and a promoter, except for propane (R290). As a result, this study sets out to undertake extensive laboratory measurements of hydrate formation and dissociation data, resulting from the use of four selected fluorinated refrigerants and four types of electrolyte solution in the presence of a promoter.

The use of fluorinated refrigerants in gas hydration has been well established, but they have not been investigated for use in desalination. Moreover, while a number of commercial refrigerants have been phased out owing to their impact on the environment, only refrigerants that are not harmful are used in this study. In addition, while refrigerants on their own do not meet the requisite of operating at ambient conditions, a promoter (cyclopentane), can be used to shift the phase equilibrium boundary towards ambient conditions, making the process more cost-effective.

Globally, gas hydrates have attracted significant interest for their potential use in natural gas production, natural gas storage and transportation, gas separation, hydrogen storage, industrial wastewater treatment, particularly in the desalination process. Hydrates were discovered in 1810. They are a solid crystalline compound physically resembling ice, in which guest molecules are surrounded inside cages by hydrogen-bonded water molecules (Mohammadi and Richon, 2010). Hydrates can be formed between ambient temperature and the freezing point of water. They typically comprise of three crystalline structures: structure I (sI), structure II (sII) and structure H (sH), which contain cages of different size and shape. More on the detailed the characteristics of these structures can be found elsewhere (Sloan and Koh, 2008).

Research has been undertaken into gas hydrate desalination technology using hydrocarbons and refrigerants as the hydrate former, the research has been focus on single electrolyte and other refrigerant such R152, R141b, R22 and others (Barduhn et al., 1962; Barduhn, 1967; Sugi and Saito, 1996; Kubota et al., 1984; McCormack and Anderson, 1995; Ngan and Englezos, 1996; McCormack and Niblock, 1998; Park et al., 2011). Fluorinated refrigerants (hydrate formers) are of interest because the chemical structure of gas hydrates form a hydrate with water only, thereby excluding all salts and other impurities from the crystalline structure (Cha et al., 2013; Eslamimanesh et al., 2011 and 2012). According to the review by Eslamimanesh

et al. (2012), the dissociation of hydrate results in the production of clean/pure water. The released refrigerant can be recycled to form hydrates.

Hydrocarbons have been mentioned as one amongst the potential hydrate formers, and these have traditionally attracted most of the research in the gas hydrate field. A hydrocarbon is a gas that contains a carbon atom. While hydrocarbon hydrate technology has shown promise, compared to distillation and membrane technologies, hydrocarbons operate at higher pressures and lower temperatures when compared to refrigerants, making them unsuitable for use at ambient temperatures and pressures. In addition, practical issues still need to be resolved, such as the complexity of hydrate solids handling (Miller, 2003). Although, this is also a practical problem that will arise at the design stage of a desalination process using refrigerants.

Refrigerants have more potential than do hydrocarbons for desalination applications at ambient conditions. A refrigerant is a compound that contains fluorine atoms. However, certain refrigerants, by destroying ozone, have been discredited because of their harmful effect on the environment. Consequently, four environmentally-friendly fluorinated refrigerants were selected for this research. They are {1,1,1,2-tetrafluoroethane (R134a), (difluoromethane + 1,1,1,2,2-pentafluoroethane) (R410a), (1,1,1-trifluoroethane + 1,1,1,2,2-pentafluoroethane) (R507) and carbon dioxide (R744)}.

Due to the focus on desalination of seawater and industrial wastewater, it is important to understand the relationship between the solution of electrolytes in water and the action of the refrigerants in the process of gas hydration. Precise electrolyte (salt) solubility data is essential for the design desalination processes using a gas hydrate technology (Bader, 1998; Pinho and Macedo, 2005). Apart from process design factors, an understanding of solubility properties is essential for the safe operation of various industrial processing equipment (Wagner et al., 1998). As a result, the four most commonly found electrolytes in water are selected and each is separately studied in pure water. These are NaCl, CaCl₂, MgCl₂, and Na₂SO₄, which are available at a lower cost.

Detailed knowledge of hydrate formation and dissociation kinetics is important in the design of hydrate processes due to the complexity of their dynamics (Eslamimanesh et al., 2011; Ilani-Kashkouli et al., 2012). To this end, hydrate formation and dissociation data are measured using an isochoric pressure equilibrium cell that was designed, built and tested by this researcher in

fulfilment of an MScEng degree in 2014. The technique used to measure gas hydrate formation and dissociation is the pressure-search method.

Finally, in addition to this experimental data, a model is developed that will combine aspects of the Cubic-Plus-Association (CPA), the Soave-Redlich-Kwong (SRK) Equation of State (EoS), the van der Waals-Platteeuw, and the Deybe–Hückel model. This has been called the Hydration Electrolyte–Cubic-Plus-Association (HE–CPA) model. It will be used to describe the behaviour of refrigerants and electrolytes and their effects on the formation and dissociation of gas hydrates. The model has been designed to calculate the commercial feasibility of using refrigerants and a promoter for hydrate formation, as a means to desalinate industrial wastewater and seawater.

The Cubic-Plus-Association (CPA) equation of state, developed by Kontogeorgis et al. (1996), has been selected for use in this study to provide the inputs for the co-existing fluid phases. The combination of CPA and SRK models will be used as a basis to describe the liquid or/and vapour phase. The van der Waals-Platteeuw hydrate solid theory, proposed by J. H. van der Waals and J. C. Platteeuw in 1959, constitute the basis for the hydrate modelling. This model will describe the hydrate phase only. The Deybe–Hückel model will describe the behaviour of electrolytes in the aqueous solution.

Dissertation outline

Chapter 2: A Literature review

This chapter provides a review of the presence of different desalination processes, and their application. The potential for the use of gas hydrate technology for the eliminating salts and impurities from water. It provides a review for gas hydrates, fluorinated refrigerants, promoter, electrolytes, solubilities, kinetics of gas hydrate, and economic viability.

Chapter 3: Development of HE-CPA equation of state

This chapter shows the development of HE-CPA equation of state that can be used to describe the properties and the behaviour of electrolyte solutions to employ gas hydrate technology in the purification of saline water.

Chapter 4: Gas hydrate equipment and experimental procedure

This chapter presents a review of gas hydrate equipment and experimental techniques. It provides the design and the description of the isochoric equilibrium cell and the layout procedures of the formation and dissociation of gas hydrates, temperature sensor calibration, pressure transducer calibration and salt solubility measurements.

Chapter 5: Results and Discussion

This chapter represents the results and discussions for all hydrate measurements introduced in Chapter 1. It provides the results of using the HE-CPA equation of state, which was developed in Chapter 3.

Chapter 6: Conceptual design for desalination process

This chapter provides a proposed desalination process and the high level of design of the hydrate reactor, the separator and the compressor. It also provides an economic feasibility study of gas hydrate technology for desalination.

Chapter 7: Conclusions

This chapter provides the concrete conclusions able to be drawn from Chapter 5 and 6.

Chapter 8: Future work

This chapter provides recommendation for hydrate systems that need to be measured and a fully designed economical evaluation for the proposed desalination process.

CHAPTER 2

LITERATURE REVIEW

The current state of research into the treatment and desalination of industrial wastewater and seawater will be reviewed. The various methods used for desalination, the special influence of electrolytes, and the potential for the use of gas hydrate technology for the separation of salts and impurities from water, will be covered. Salt solubility for the systems of interest is also addressed.

Gas hydrates and refrigerants are reviewed in this chapter. The important role of cyclopentane, as a promoter in the formation and dissociation of gas hydrates, using fluorinated refrigerants as hydrate formers, is clarified. Studies on the kinetics of gas hydrates; as well as the economic viability of commercial use of gas hydrate technology for desalination are included.

2.1 Desalination

Desalination is the production of fresh water from saline waters such as seawater, industrial wastewater and brackish water. The fresh water can then be used for agricultural, industrial and domestic purposes. Seawater and industrial wastewater are highly saline, which causes scaling, foaming, corrosion, biological growth, and fouling on equipment (Kalogirou, 2005). Consequently, chemical pre-treatment and post-treatment are required. Desalination of seawater and industrial wastewater can be undertaken using traditional process and hydrate technologies.

2.1.1 Traditional processes

The traditional thermal (phase change) and semi-permeable membrane (single-phase) processes are the currently employed industrial desalination technologies used to separate solvents and solutes, as shown in Table 2.1.

Table 2. 1: Traditional desalination processes

Thermal processes	Membrane processes
Multi-stage flash distillation (MSF)	Reverse osmosis (RO)
Multiple effect boiling (MEB)	Electrodialysis (ED)
Vapour compression (VC)	
Freezing	
Humidification–dehumidification	
Solar stills	

The energy source for each desalination technique in the thermal process can be attained from conventional fossil-fuels, nuclear energy or non-conventional solar energy. In membrane processes, electricity is utilized to drive the high pressure pumps or the current electrodes used in ED process for ionization of salts contained in the wastewater or seawater.

Multi-stage flash (MSF) distillation consists of multiple stages where the pressure and temperature decreases. The MSF process involves the generation of vapour from raw water (seawater or wastewater) due to a sudden pressure decrease when raw water enters an evacuation chamber. A decrease in pressure is repeated stage-by-stage (Kalogirou, 2005). External steam supply is required at a maximum temperature of 373.2 K. This maximum temperature of the MSF process is restricted by the concentration of salt, to prevent scaling on the equipment.

Multiple effect boiling (MEB) is similar to the MSF process, but it involves generating vapours from the absorption of thermal energy by raw water. The steam produced in one stage is used to heat the aqueous solution in the next stage, because the next stage is at a lower temperature and pressure. External steam supply is required for the MEB process at a maximum temperature of 343.2 K.

Vapour compression (VC) is the distillation process whereby the saline water feed is preheated and boiled. The released vapours are compressed by a mechanical compressor, and passed through tubes where it condenses (Ribeiro, 1996). The latent heat released is used to boil the saline water in the feed and the vent is used to remove the non-condensable gases. At the start-

up, the VC required steam is supplied. VC is capable of recovering 0.01 g/L TDS in the water product. Total dissolved solids (TDS) refers to the measure of salts contained in water

Freezing is a separation process associated with a solid-liquid phase change. In this process the temperature of raw water is decreased to its freezing point, producing hydrate crystal solid ice (pure water). Pure water is obtained by washing the ice crystals and re-melting (Kalogirou, 2005). The freezing method has been recommended as an alternative for seawater desalination, purification of mixtures, wastewater treatment, and food liquid concentration (Fattahi et al., 2015).

The humidification/dehumidification process is similar to the refrigeration system but the operating procedure is different and it is not similar to any mentioned processes. In this process, wastewater is added to an air stream to raise its humidity. This humidified air is directed to a cooled coil on the surface of which water vapour, contained in the air, is condensed and collected as fresh water.

The reverse osmosis (RO) process is simple and effective compared to other membrane processes. It consists of thin, semi-permeable spiral or hollow fibre membranes, which are supported by a number of non-selective membranes. The membranes are permeable to water and the dissolved salt cannot pass through as the membrane pore size is 0.1 nm. Osmotic pressure, which is higher than the feed water, is exerted on the saline water to allow the pure water to pass through the membrane, while leaving the concentrated brine at retentate stream. The required pressure depends on the concentration of salt in the saline water. This process requires electricity or shaft power to drive a pump that increases the pressure of the saline solution (van der Bruggen and Vandecasteele, 2002).

The electrodialysis (ED) process consists of compartments on both ends, containing electrodes that pass direct current through all the chambers. Cation and anions travel in opposite directions in response to the voltage applied. The ED process needs electricity for the ionisation of water, which is cleaned by using appropriate membranes situated at oppositely charged electrodes. Due to the membrane selectivity, the concentration of the ions increases and decreases in alternating chambers (Miller, 2003). The concentration decreases in a chamber and increases in an adjacent chamber. This process is suitable for concentrations above 12 g/l TDS. Membranes require cleaning often due to fouling of salt (Ribeiro, 1996).

MSF, RO and ED are the most commonly employed desalination processes. But RO is the most effective of the membrane processes (Kalogirou, 2005). It is estimated that MSF accounts for 40% and RO accounts for 50% of the total world desalination capacity (volume of water produced). The MSF process tends to be used at an industrial scale, with a capacity of over 5000 m³/day (Sangwai et al., 2013). The RO process is more for small-scale unit production. However, the RO process has gained interest because it has a lower cost and simplicity compared to MSF.

Table 2.2 has been assembled for comparison of MSF and RO process capacities in industry. It is difficult to compare production rate and volume of water produced for MSF and RO with hydrate technology because, currently, the gas hydrate is only carried out on a laboratory scale and pilot plant. The MSF consume more energy than RO as indicated in Table 2.2. It has higher removal efficiency for Na⁺, Ca²⁺, K⁺ and Mg²⁺ than RO. This show that MSF is more costly compared to RO process. Due to higher cost for these processes, this study is the improvement of gas hydrate technology because it is a promising technique that can be utilized to treat industrial wastewater and seawater at a lower cost. Park et al. (2011); Kang et al. (2013) recommend that a gas hydrate technology can be employed in industry due to impressive removal efficiency of 72% for Na⁺, Ca²⁺, K⁺ and Mg²⁺, because once the hydrate is being formed, the water is free salinity.

Table 2. 2: Comparison of desalination technologies

	Minerals	World Capacity ^a (%)	Removal efficiency (%)	Production rate ^b (%)	°SEC (kWh)	References
Thermal process (MSF)	K, Na, Ca, Mg	44	83	93	20	Mendez and Gasco, (2005)
Membrane process (RO)	K, Na, Ca, Mg	42	70	88	3.3	Kalogirou, 2005; and Mohamed et al. (2006)

^aWorld capacity, ^bproduction rate and ^c(SEC) specific energy consumption are expressed in percentages because they are calculated from worldwide capacity and production drawn from different countries

Seawater, for example, that represents the largest water reservoir of the earth, contains on average 3.5 wt% of dissolved salts compared to industrial wastewater, such as Tutuka power station at Eskom, containing on average 2.4 wt%. Some industrial water contains more than 3.5 wt% salt concentrations. The high concentration of salts in industrial wastewater and seawater makes it unsuitable for most purposes prior to desalination. Desalination by means of the commonly-used, distillation and membrane technologies can reduce the total dissolved solids (TDS) of seawater or industrial wastewater to less than 0.5 g TDS/L.

Several countries, particularly in the Middle East, depend on desalination for fresh water. It is estimated that about 75 million people use desalinated seawater or brackish water (Sangwai et al., 2013). The five leading countries, according to desalination production capacity (%), are as follows: Saudi Arabia (17.4%), USA (16.2%), United Arab Emirates (14.7%), Spain (6.4%) and Kuwait (5.8%) (Khawajia et al., 2008).

2.1.2 Gas hydrate technology

While desalination using gas hydrates has not yet been commercialised, it looks promising as a future technology. Gas hydrates show the potential to produce pure/clean water that can be used as drinking water, as well as for industrial or agricultural purposes, requiring lower energy consumption in comparison to the traditional technologies.

The use of fluorinated refrigerants to form gas hydrates for desalination has gained attention because they can further reduce energy and operational costs (Chun et al., 2000; Seo and Lee, 2001; Javanmardi and Moshefeghian, 2003; and Eslamimanesh et al., 2011). According to Park et al. (2011), gas hydrate formation technology is more effective than traditional methods, and it shows the potential to be an improved technology that will reduce the cost of desalination.

As mentioned in Chapter 1, gas hydrate technology is already used in several other applications, including gas separation, CO₂ sequestration, gas storage and transportation, energy, refrigeration. Hydrate technology for desalination was first developed in the 1940s and gained more interest in the 1970s.

It has been reported (Parker, 1942; Knox et al., 1961; Barduhn, et al., 1962; Barduhn, 1967 and 1968) that the Sweet Water Development Co. and Koppers Co., firstly developed desalination

by means of gas hydrates, in 1961. Researchers (Barduhn, et al., 1962; Barduhn, 1967 and 1968) investigated the kinetics and separation of minerals, using gas hydrate technology.

The main challenge in implementing gas hydrate technology on an industrial scale is the separation of the hydrate phase from concentrated brine, resulting in an uneconomical operation, that time they have not got an idea how to separate the two and to recover a hydrate former (Rautenbach and Seide, 1978; Park et al., 2011). In addition, seawater has a high concentration of NaCl, which inhibits gas hydrate formation. Salts such as NaCl, CaCl₂ and MgCl₂ are good inhibiting agents that can lower the formation and dissociation temperatures. More description later. Once hydrate is being formed, the water has zero salinity, that can be achieved by separating the salts from the water.

The Bureau of Reclamation in the US had sponsored an investigation conducted by McCormack and Andersen (1995), the study was followed by a pilot plant scale conducted at the Natural Energy Laboratory of Hawaii (McCormack and Nga, 1998). The test was effective, while a wash column was not built and tested as the part of the effective operation. Although the test was successful but they were experiencing difficulties in separating hydrate crystal and materials which led to determine the filterability of hydrate crystal, the design and operation of wash column, and surveying alternate higher temperature hydrate former (McCormack and Nga, 2000)

Taking the technology forward, a simple desalination process was designed by Sangwai et al., (2013) to produce fresh water, as shown in Figure 2.1. As was mentioned in Chapter 1, hydrate can be formed by using either hydrocarbon gases or fluorinated refrigerants as hydrate formers. The gas hydrate technology has an advantage of operating at ambient temperatures and pressures, and it is required less energy compared to freezing process.

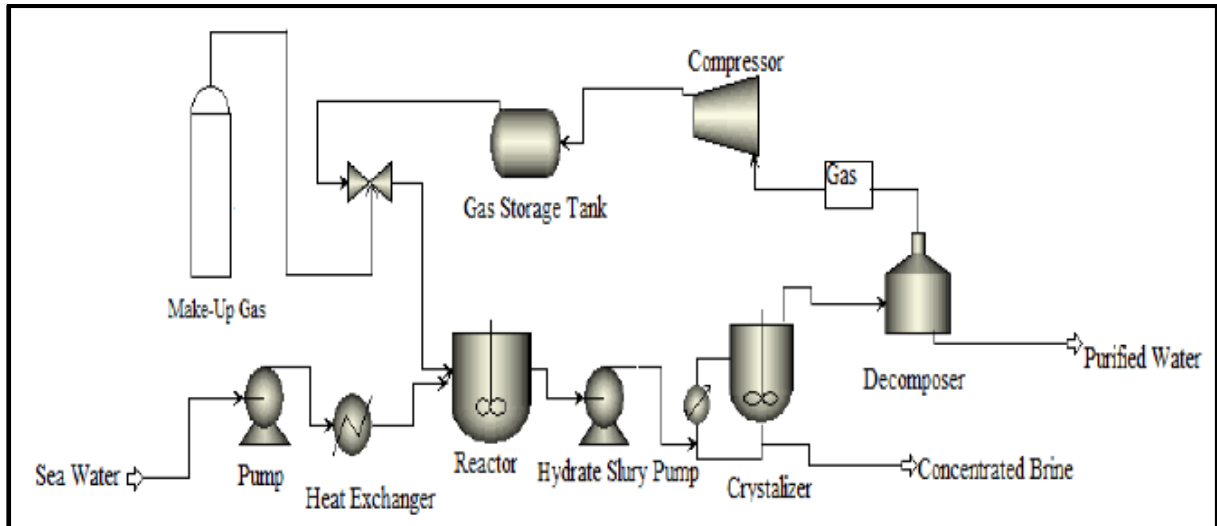


Figure 2. 1: An early desalination process design (Sangwai et al., 2013)

Barduhn and Lee (1978) studied the refrigerant F-22 (CHClF) hydrate system in aqueous sodium chloride solution. They reported on thermodynamic information including hydrate decomposition conditions, the eutectic point, and the invariant points. It was found that the eutectic point can be used to check the performance of F-22 as an agent for use in the hydration process for desalination of seawater.

A study by McCormack and Andersen (1995) showed that hydrate technology had the potential to provide an economical desalination process at a rate of \$0.46 – 0.52/m³ of saline water. Ngan and Englezos (1996) investigated the retrieval of water from wastes or effluents and 2.5 wt% NaCl solutions, using hydrate propane in a moderately operated vessel in which hydrate nucleation, growth, separation and melting occurred. The average reduction in the salt content of the recovered water from the NaCl solutions was found to be 31%. In 2011, Park et al., compared a unit for seawater desalination, based on hydrate formation, with other methods. It was drawn out that hydrate formation process can be useful for more effective seawater desalination process instead of RO or MSF process.

Younos and Tolou (2005) reviewed the performance of traditional desalination technology. They briefly gave an introduction for a gas hydrate as a potential future desalination technology, which is under research and development. Sabil et al. (2010) presented a kinetic study in water and sodium chloride aqueous solution on the formation of single carbon dioxide, mixed carbon dioxide and tetrahydrofuran hydrates. The presence of tetrahydrofuran in the hydrate system has been shown to reduce the consumption of CO₂ in hydrate formation, which has demonstrated its potential in desalination processes using CO₂ as a hydrate.

Sarshar and Sharafi (2011) carried out an experimental study on simultaneous seawater desalination and CO₂ capture, using gas hydrate technology. They evaluated process conditions for CO₂ hydrate formation in Persian Gulf water, and it was found that up to 52% of minerals or salts were removed. Corak et al., (2011) provided thermodynamic and kinetic data for a cyclopentane hydrate in brine. They also observed the effect of sub-cooling, with amount of cyclopentane present, on hydrate formation. A high degree of sub-cooling favoured the hydrate method of desalination.

Park et al., (2011) designed a hydrate based desalination process to extract dehydrated gas from a reactor containing hydrate slurries. They recommended different hydrate formers, such as fluorinated refrigerants, for further desalination research. Karamoddin and Varaminian (2013) investigated the hydrate growth process using HCFC-141b refrigerant in different brine solutions for desalination of water; and they designed a new apparatus for hydrate formation under high pressure to undertake water desalination measurements. Aliev et al., (2011) developed mathematical modelling for a Freon R-142b water hydrate system. They used a column type reactor with a sieve plate for a gas-liquid process of hydrate formation in a Freon-water system. They carried out an optimization study to determine design condition for desalination processes by means of hydrate technology. They found the values of the mode parameters and the number of sieve plates at a specified fresh charge that would ensure the highest throughput of the reactor with respect to gas hydrate formation. It was also found that the mathematical model of the reactor might be applicable for optimum designing of the seawater desalination process.

Fattahi et al., (2015) compared the performance, in a reactor, of salt removal using a freezing method and hydrate formation, in the presence of tetrahydrofuran as hydrate former. They found that the salt removal efficiency of the hydrate formation technique was higher than that of the freezing method. The efficiency of removal decreased with an increased concentration of salt in the freezing method while a different trend in the hydrate formation technique was observed. They also investigated the effect of ionic size on salt removal efficiency. Their results showed that the performance of desalination improved with increasing ionic radius. The measurements were performed with NaCl, NaBr, NaF, and NaI, which have the same cation (positive ion).

2.1.3 Summary of the desalination

Conventional traditional desalination processes such as MSF and RO are commonly used to treat industrial wastewater and seawater. These technologies are well reviewed, and distillation (MSF) shows that it is costlier, it consumes more energy, and it has higher removal efficiency for Na^+ , Ca^{2+} , K^+ and Mg^{2+} than RO.

A gas hydrate technology is promising as a future technology to be used to separate solvent and solutes due to its advantages. It consumes less energy compared to traditional processes. The use of fluorinated refrigerants to form gas hydrates for desalination has gained attention because they can further reduce energy and operational costs. The refrigerants form a gas hydrate with water only. Park et al. (2011) found that the gas hydrate technology has the removal efficiency of (72 to 80%) for Na^+ , Ca^{2+} , K^+ and Mg^{2+} . The challenge part to implement gas hydrate technology on the industrial scale is the separation of hydrate phase and saline brine water. Some pilot plants are conducted and they were successful in separation.

Electrolytes are present on the industrial wastewater and seawater, which make water to be unsuitable to be used for any purpose. In order to produce pure water, these electrolytes need to be removed. It is important to know, which electrolytes are found on industrial wastewater and seawater. Based on the information, the separation of electrolyte and hydrate is easy because the hydrate former (refrigerant) forms hydrate with water only, then the clean/pure water is produced by dissociating the hydrate phase.

2.2 Electrolytes

Industrial wastewater and seawater contains electrolytes such as NaCl , CaCl_2 , MgCl_2 , Na_2SO_4 and other salts, which are needed to be removed, in order to produce pure water. These electrolytes have high concentration in water compared to the others; refer to Table 2.6. Electrolytes are well known to prevent the formation of hydrate by reducing water activity during the coexisting liquid stage. They form gas hydrates at lower temperatures and at higher pressures in comparison with pure water hydrate formation (Dhloabhai et al., 1996). According to a study published by this researcher in 2014, the single electrolytes (NaCl , CaCl_2 and MgCl_2) have an inhibitory effect on hydrate formation, as exhibited through the measurement of the hydrate equilibrium conditions of R410a, R507 and R134a.

When electrolytes dissolved in water, most electrolytes dissociate into ions. Strong electrolytes dissociate completely, while weak electrolytes dissociate partly (Thomsen, 2009; Kontogeorgis and Folas, 2010). The presence of charged ions causes the aqueous solution to deviate more than in a non-electrolyte solution even at very low electrolyte concentrations from the ideal solution behavior (Thomsen, 2009). Moreover, after the ionization of electrolytes in aqueous solution, they form a Coulombic bond with the dipoles of water. This bond is much stronger than the hydrogen bond or the forces of van der Waals (Sloan and Koh, 2008).

The Coulombic bond formation causes clustering by water molecules around the ions. This inhibits the formation of hydrate because water is more attracted to ions than to the structure of the hydrate. (Sloan and Koh, 2008). A secondary effect, reported by Sloan and Koh (2008), is that the clustering of water molecules causes a decrease in the solubility of gas molecules in water. Then, the hydrate formation temperature can decrease slightly.

Both ion clustering and salting-out result in significantly more subcooling for the formation of hydrate. Sloan and Koh (2008) reported that the more ions present, and the higher the concentration of salt in the solution, the larger the hydrate inhibiting effect.

From Table 2.3 and 2.4 have been assembled below, this is a review for the formation of a gas hydrate in the presence of a single electrolyte at different concentrations, using a fluorinated refrigerant as hydrate former. However, the use of single and mixed electrolytes in the presence of a promoter was recommended for further investigation.

Table 2. 3: Single electrolytes with fluorinated refrigerants at different concentrations

Hydrate former	Salt	Conc/mass fraction	T/K	P/MPa	Reference
R13	NaCl	0.020 – 0.050	271.70 – 279.70	0.305 – 2.030	Kubota et al. (1984)
R23	NaCl	0.020 – 0.050	272.60 – 290.60	0.344 – 3.440	Kubota et al. (1984)
R152a	NaCl	0.020 – 0.050	271.00 – 286.60	0.059 – 0.413	Kubota et al. (1984)
R290	NaCl	0.020 – 0.050	271.00 – 276.60	0.138 – 0.471	Kubota et al. (1984)
R290	CaCl ₂	0.150	268.70 – 271.70	0.205 – 0.412	Englezos and Ngan (1993)
R22	NaCl	0.050 – 0.150	274.0 to 287.3	0.273 to 0.775	Chun et al. (2000)
R22	KCl	0.050 – 0.150	275.1 to 287.8	0.199 to 0.790	Chun et al. (2000)
R22	MgCl ₂	0.050 – 0.150	273.9 to 287.4	0.319 to 0.783	Chun et al. (2000)
R290	NaCl	0.050 – 0.150	271.5 to 275.1	0.200 to 0.400	Mohammadi et al. (2008)
R290	KCl	0.050 – 0.150	273.8 to 278.0	2.010 to 3.350	Mohammadi et al. (2008)
R410a	NaCl	0.050 – 0.100	276.10 – 290.90	0.240 – 1.345	Ngema (2014)
R410a	CaCl ₂	0.038 – 0.060	280.80 – 291.40	0.315 – 1.341	Ngema (2014)
R410a	MgCl ₂	0.023 – 0.047	274.90 – 291.80	0.154 – 1.343	Ngema (2014)
R507	NaCl	0.050 – 0.100	273.90 – 281.00	0.226 – 0.802	Ngema (2014)
R507	CaCl ₂	0.038 – 0.060	274.70 – 282.50	0.191 – 0.834	Ngema (2014)
R507	MgCl ₂	0.023 – 0.047	274.30 – 282.60	0.174 – 0.823	Ngema (2014)
R134a	NaCl	0.050 – 0.150	268.10 – 280.60	0.086 – 0.383	Ngema (2014)
R134a	CaCl ₂	0.038 – 0.060	276.20 – 281.20	0.125 – 0.392	Ngema (2014)
R134a	MgCl ₂	0.047 – 0.070	274.70 – 282.20	0.116 – 0.410	Ngema (2014)

Table 2. 3: Single electrolytes with fluorinated refrigerants at different concentrations continue.....

Hydrate former	Salt	Conc/mass fraction	T/K	P/MPa	Reference
R22	NaCl	0.030 – 0.180	273.2 to 290.2	0.089 to 0.893	Maeda et al. (2008)
R141b	NaCl or CaCl ₂ or KCl or MgCl ₂	0.010 – 0.060	273.2 to 277.2	No pressure readings.	Karamoddin and Varaminian, (2013)

Table 2. 4: Mixed electrolytes with fluorinated refrigerants at different concentrations

Hydrate former	Salt	Conc/mass fraction	T/K	P/MPa	Reference
R290	NaCl + KCl	0.075 + 0.075	265.20 – 269.05	0.157 – 0.372	Englezos and Ngan (1993)
	NaCl + CaCl ₂	0.075 + 0.075	265.90 – 269.40	0.172 – 0.418	Englezos and Ngan (1993)
	CaCl ₂ + KCl	0.075 + 0.075	266.30 – 270.10	0.181 – 0.432	Englezos and Ngan (1993)
	CaCl ₂ + NaCl + KCl	0.050 + 0.075 + 0.075			Englezos and Ngan (1993)
R290	NaCl + KCl	0.050 + 0.050	270.40 – 272.40	0.234 – 0.441	Tohidi et al. (1997)
	NaCl + CaCl ₂	0.049 + 0.038	270.90 – 273.50	0.234 – 0.441	Tohidi et al. (1997)
R290	NaCl + KCl + CaCl ₂		248.00 – 278.00	0.100 – 0.540	Javanmardi et al. (1998)

2.2.1 Solubility of electrolytes in water

Solubility is measured by the amount of electrolyte solute required to concentrate a solution to its saturation at a given temperature. Where salt dissolves in water, it forms a homogenous solution. There is a maximum amount of solute at a given temperature, which can be dissolved in a given amount of solvent. Consequently, the solubility of a substance depends on temperature.

Solubility data are essential for the design of wastewater treatment and desalination processes. Solubility is a property required for the design of separation processes, including extractive crystallization (Bader, 1998; Pinho and Macedo, 2005). This property is essential for the safe operation of industrial processing equipment, including distillation, absorption columns, and extraction columns or plants (Wagner et al., 1998).

Some researchers (Linke and Seidell, 1958, 1965; and Stephen and Stephen, 1963, 1964), have compiled information on aqueous electrolyte system solubility for many salts. Pinho and Macedo (2005) have reported that solubility changes as temperature increases, up to a certain temperature, depending on the salt and solvent (water) used. However, beyond the particular temperature, solubility is almost constant due to breaking behaviour, corresponding to a solid phase transition. For example, the transition of NaBr takes place at 323.98 K. The solid phase is NaBr.2H₂O below 323.98 K and above 323.98 K, the solid phase is NaBr (Rard and Archer, 1995). The salt solubility is inversely proportional to the temperature when alcohol is used as a solvent (Pinho and Macedo, 2005).

In most cases, the solubility of a substance increases with increasing temperature, as shown in Figure 2.2. However, the rate of solubility varies from compound to compound. Figure 2.2 shows that NaCl has a relatively weak temperature dependence, compared to KNO₃, at a water temperature of 373 K. NaCl solubility changes from 35.7 to 39.8 g/100g of water over 373 K, while KNO₃ changes from 13.4 to 247 g/100g water at the same temperatures.

Solubility information is very important in gas hydrate processes since it is used to determine the amount of cooling required to form a hydrate. The solubility of Ce₂(SO₄)₃ decreases as temperature increases, as indicated in Figure 2.2.

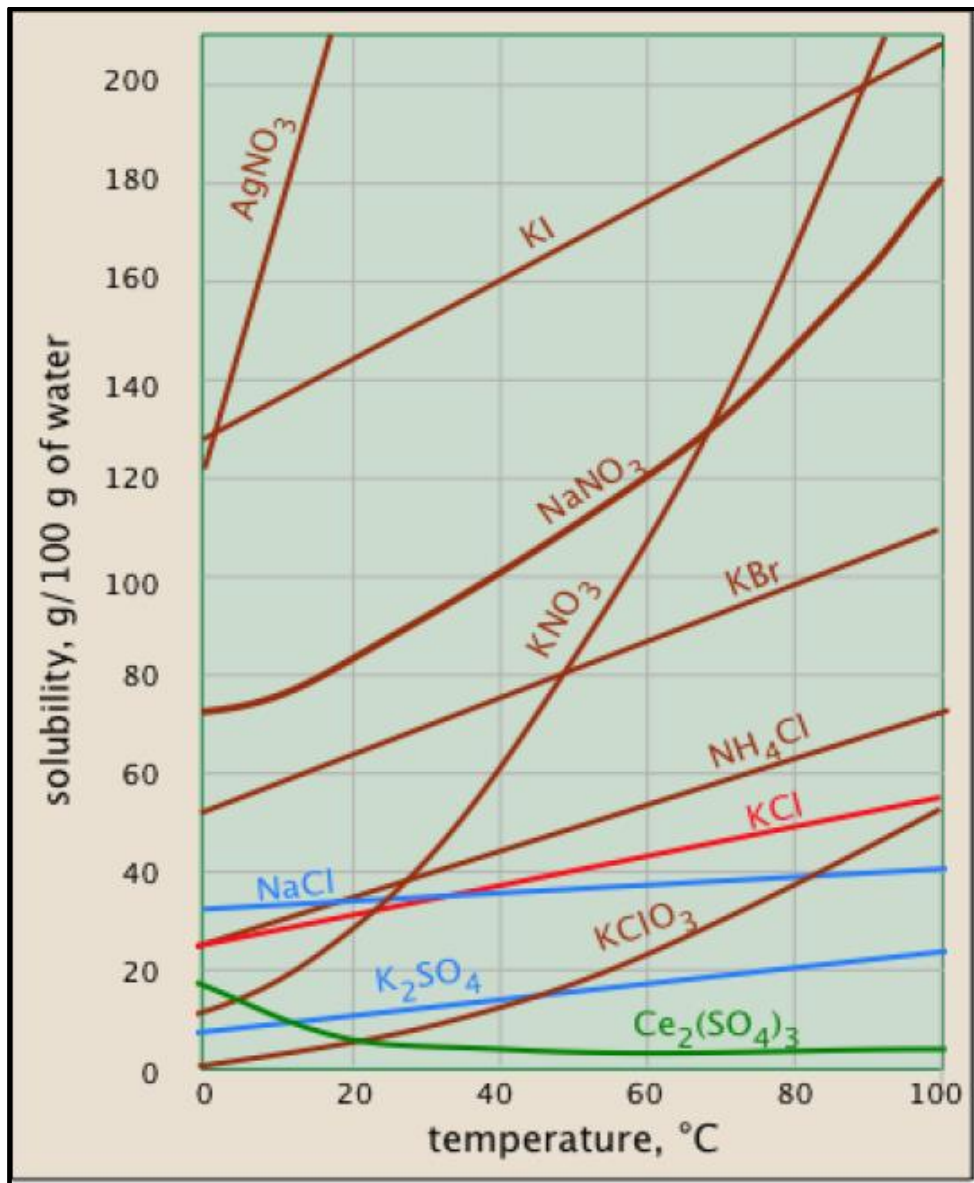


Figure 2. 2: Solubility of different salts above 100°C (Davis, 2014)

Wastewater from petroleum reservoirs contains various salts, including NaCl, KCl, CaCl₂, MgCl₂, BaSO₂, CaCO₃, Na₂SO₄, and CaSO₄. Generally, NaCl, KCl, CaCl₂, and MgCl₂ are highly soluble in water, and BaSO₂, CaCO₃, Na₂SO₄, and CaSO₄ precipitate at a certain temperature and pressure, due to low solubility in water. Those salts with low solubility in water tend to cause scale precipitation in pipelines and equipment in water treatment plants using a reverse osmosis membrane (Zhu and Elimeleh, 1997; Lee et al., 2004).

These salts in aqueous solutions are highly corrosive in nature. However, they play an important role as inhibiting agents (Kang et al., 1998). Salts, methanol and ethylene glycol are commonly used inhibitors for shifting the point for hydrate formation in industrial pipelines.

Table 2.5 is compiled for salt solubility using various solvents. When salt begins to dissolve in the solvent, solubility decreases gradually because the interactions between water molecules and ions are stronger than the interactions between water and dissolved gases (refrigerants).

Precipitation of salts will occur at a high temperature of 423.15 K, a pressure of 1000 bar, and at a high concentration of mixed electrolytes, above 250 000 mg/L (Chawathe et al., 2009). Nevertheless, solubility data at high temperatures, pressure and concentrations are rarely reported in the literature, and there are few prediction models.

Furthermore, the application of scale precipitation models in a certain temperature and pressure range is usually limited to certain salts, due to the complex ion interactions in mixed electrolytes and their undetermined temperature and pressure dependences (He and Morse, 1993). As a result, a thermodynamic model to predict the solubility and scaling risks of different salts with mixed salts over a wide range of temperatures, pressures and concentrations were recommended.

Subsequently, some researchers (Stumm and Morgan, 1996; Shi et al., 2013) have developed a thermodynamic model to predict solubility and scaling risks for the CaSO_4 , BaSO_4 , BaCl_2 , Na_2SO_4 and CaBr_2 . It was revealed that the model results agreed with experimental measurements at the temperature of 298.15 K and pressure of 101.325 kPa. Dai et al., (2015) reported on salt solubility predictions for CaSO_4 , BaSO_4 , BaCl_2 , Na_2SO_4 and CaBr_2 , and it was found that it is difficult to estimate the scaling risk at high temperature, pressure, and ionic strength with mixed salts.

Table 2. 5: Salts solubility with various solvents

Salts	Solvent	Temperature range (K)	Reference
CaSO ₄	Water	373.15 to 348.15	Hullet and Allen, (1902)
		373.15 to 473.15	Partridge and White, (1929)
		453.15 to 480.15	Straub, (1932)
		298.15 to 373.15	Hill and Yanick, (1935)
		298.15 to 348.15	Hill and Wills, (1938)
		298.15 to 373.15	Posjnak, (1938)
		278.15 to 383.15	Sborgi and Bianchi, (1940)
		413.15 to 573.15	Booth, (1950)
		298.15 to 323.15	Bock, (1961)
		298.15 to 473.15	Marshall et al. (1964)
		298.15 to 368.15	Power et al. (1966)
		273.15 to 473.15	Marshall and Slusher, (1966)
		523.15 to 598.15	Templeton and Rodgers, (1967)
CaCl ₂ , MgCl ₂	Water	298.15 to 368.15	Dutrizac, (2002)
		298.15 to 368.15	Ghazal, (2010)
CaCl ₂ , MgCl ₂	Water	243.15 to 273.15	Prutton and Tower, (1932)
NaCl	Water	273.15 to 373.15	Linke, (1965)
CaSO ₄	HCl	293.15 to 373.15	Gupta, (1968)
NaCl	Water	273.15 to 473.15	Potter et al. (1975)

Table 2. 5: Salts solubility with various solvents continue....

Salts	Solvent	Temperature range (K)	Reference
CaCO ₃	Water	273.15 to 363.15	Plummer and Busenburg, (1982)
NaCl	Water	273.15 to 553.15	Pitzer et al. (1984)
CaCO ₃	Water	348.15 to 473.15	Segnit et al. (1996)
KBr	Water, methanol, ethanol and mixed binary solvents	298.15 to 353.15	Pinch and Macedo, (2002)
NaCl, NaBr, KCl	Water, methanol, ethanol and mixed binary solvents	298.15 to 353.15	Pinch and Macedo, (2005)
NaCl, NaBr, KBr	Tetradecyltrimethylammonium bromide and sodium dodecyl sulfate	298.15 to 353.15	Zhou and Hao, (2011)

2.2.2 Summary of electrolytes

Electrolytes are completely dissolved in water up to a certain concentration. They can inhibit hydrate by reducing water activity in the liquid phase. Some electrolytes such as NaCl, CaCl₂ and MgCl₂ have been shown by this researcher in 2014 that they have ability to shift dissociation temperatures and pressures to lower values in the presence of fluorinated refrigerants. Previously, work has been conducted in the presence of single and mixed electrolytes with refrigerant; it is presented in Table 2.3 and 2.4.

As the electrolyte is soluble in water, the solubility of each electrolyte is important to be known or measured because the experimental work in this study have to be conducted below its saturation point at that particular temperature. Solubility is a thermodynamic property that is required for the design of wastewater treatment, desalination and separation process. Figure 2.2 shows the solubility of different electrolytes between the temperature ranges of (0⁰C and 100⁰C).

In this study, it is important to know the concentrations of all electrolytes present in the industrial wastewater and seawater because the gas hydrate measurements will be conducted at those concentrations and at higher concentrations closer its saturation to evaluate its effect on hydrate formation and dissociation.

2.3 Industrial wastewater and seawater

Biological treatment methods are currently used on industrial wastewater that contains a high concentration of salt (Smythe et al., 2006). However, the high salt content tends to add to the cost and sensitivity of the treatment system. The following types of biological treatment systems are used on salty wastewater:

- Conventional activated sludge systems can handle a salt concentration of up to 5 wt%.
- Anaerobic systems can treat wastewater to a concentration of 1.5 wt%.
- Specialized systems, such as fluid bed/SBR/Zeno-Gem, can treat wastewater with a salt concentration of up to 10 wt%.
- Special bacteria can treat wastewater containing a salt concentration of up to 15 wt%.

According to the study carrier out by Diaz et al., (2002) wastewater from industries contained higher concentrations of salt (> 3.5% w/v) as well as waste organics. Their focus was on waste

organics. They reported that the large capacities of oily wastewater are produced during the production, transport, and refining of crude oil. Produced wastewater contains a wide range of salinities from almost fresh water to three times that of seawater. (Diaz et al., 2002). High salinities or wide salinity ranges make wastewater difficult to be treated using a simple conventional tradition process, because it is required a number stages to reduce concentration, which increase operation cost.

Table 2.6 and 2.7 have been assembly to provide information on the concentration of electrolytes found in brine streams at different industries and at seawater. This information is very important in this study because it gives the indication for the typical concentration range of salts can be used to undertake experimental measurements. As the focus of this study is to design the desalination process using gas hydrate technology to treat industrial wastewater and seawater, it is essential to know concentration and all salts present in both type of water. The measurements are performed by selecting those salts that have higher concentration such as NaCl, CaCl₂, MgCl₂, and Na₂SO₄

Table 2. 6: Brine stream concentrations of constituents at various industries

Constituent	Units	^a Tutuka Eskom	^b FAM Secunda	^b TRO Secunda	^c Oil-field brine	^d Tannery brine	^e Secunda mine water	Min wt%	Max wt%
<i>Calcium</i>	<i>mg/l</i>	<i>329</i>	<i>770</i>	<i>790</i>	<i>1900</i>		<i>291</i>	<i>0.0291</i>	<i>0.19</i>
<i>Chloride</i>	<i>mg/l</i>	<i>3443</i>	<i>1000</i>	<i>2260</i>	<i>17600</i>		<i>280</i>	<i>0.028</i>	<i>1.76</i>
<i>Magnesium</i>	<i>mg/l</i>	<i>201</i>	<i><0.04</i>	<i>2</i>	<i>166.5</i>		<i>174</i>	<i>4x10⁻⁶</i>	<i>0.02</i>
<i>Sodium</i>	<i>mg/l</i>	<i>7262</i>	<i>1400</i>	<i>2300</i>	<i>9400</i>	<i>16559.2</i>	<i>1115</i>	<i>0.14</i>	<i>1.66</i>
<i>Sulphate</i>	<i>mg/l</i>	<i>12130</i>	<i>2780</i>	<i>7440</i>	<i>11.9</i>		<i>3211</i>	<i>1.2x10⁻³</i>	<i>1.21</i>
Potassium	mg/l	316	100	220	66.2		6.5		
Nitrate	mg/l	15.8	22.3	24.5					
Zinc	mg/l	0.05							
Aluminium	mg/l	0.03							
Barium	mg/l	0.07	<0.01		30.0		0.02		
Cadmium	mg/l	<0.005							
Copper	mg/l	0.35							
Cyanide	mg/l	<0.025							
Iron	mg/l	0.2			3.8				
Lead	mg/l	0.06							
Manganese	mg/l	0.12							
Silica as SiO ₂	mg/l	84.2							
Fluoride	mg/l	1.31	1653	8.31					
NH ₃ as N	mg/l	86							
Lithium	mg/l			4.8	0.48				
Ammonium	mg/l		80	19	57.3				
Strontium	mg/l				72.0		6.3		

References: ^aLalla et al. (2014); ^bLewis et al. (2010); ^cDalmacija et al. (1996); ^dSivaprakasam et al. (2008); ^eNyamhingura, (2009)

Table 2. 7: The major constituents of water at seawater level

(Portoes, 1983)

Constituent	Symbol	Standard limits	Unit
<i>Calcium</i>	<i>Ca</i>	<i>411.9</i>	<i>mg/L</i>
<i>Magnesium</i>	<i>Mg</i>	<i>1284</i>	<i>mg/L</i>
<i>Sodium</i>	<i>Na</i>	<i>10781</i>	<i>mg/L</i>
<i>Potassium</i>	<i>K</i>	<i>399</i>	<i>mg/L</i>
<i>Chloride</i>	<i>Cl</i>	<i>19353</i>	<i>mg/L</i>
Strontium	Sr	7.94	mg/L
Fluoride	F	1.30	mg/L
Sulphate	SO ₄	2712	mg/L
Bicarbonate	HCO ₃	126	mg/L
Bromide	Br	67	mg/L
Borate	H ₃ BO ₄	25.7	mg/L
Total	11	35169	mg/L

Tutuka power station, as an example, designed a new brine concentration desalination plant to include **acidic coagulation, lime-soda softening, pressurised granular activated carbon filtration, and ultra-filtration processes**, these stages are discussed in this Chapter. The quality of the feed water stream presented in Table 2.6 is treated using these mentioned processes and the result achieved is presented in Table 2.8. The results show an impressive reduction of concentrations for the various salt present in the brine stream. The treat quality water is achieved at different temperatures ranges between 1⁰C and 35⁰C, these was done to find the optimum temperature and to check what concentration can have achieved at ambient temperature. It is indicated that at a lower temperature of 1⁰C more salt is being removed, because Table 2.8 shows that as the temperature increase and the concentration of treat water increases. The produced quality is re-used in plant for any purpose where water is required. Consequently, Tutuka power station is saving to use fresh water and the cost is reducing.

An acidic coagulation process was first used to reduce the total organic carbon (TOC) content in the feed water (that had a concentration of 110 mg/l, which was 36.6 times higher than the desired concentration of 3 mg/l of TOC), as specified by the membrane manufacturers (Lalla et al., 2014). This process reduces the TOC concentration but not to the desired level. This has

the advantages that the organic load on the activated carbon is reduced, as well as the risk of biological fouling on the RO membranes.

A lime-soda softening process was used to reduce calcium and adsorb silica concentrations. This process was followed by the use of pressurised granular activated carbon filters (GAC) that were designed for a minimum contact time of 10 minutes. The GAC reduced the TOC concentrations, although the removal was not higher than 70%. Biological fouling was controlled by means of non-oxidising biocides. Subsequently, ultra-filtration was employed to remove any colloidal particles present in the water. The RO plant was designed for temperatures of between 1°C and 35°C, and for pressures up to 78 bar.

Table 2. 8: The quality of treated water from Tutuka power station Eskom (Lalla et al., 2014)

Constituent	@ 1°C	@ 15°C	@ 25°C	@ 35°C	Unit
<i>Calcium</i>	<i>0.1</i>	<i>0.2</i>	<i>0.3</i>	<i>0.7</i>	<i>mg/L</i>
<i>Magnesium</i>	<i>0.2</i>	<i>0.3</i>	<i>0.5</i>	<i>0.7</i>	<i>mg/L</i>
<i>Sodium</i>	<i>17.5</i>	<i>35.0</i>	<i>62.5</i>	<i>105.0</i>	<i>mg/L</i>
<i>Potassium</i>	<i>2.0</i>	<i>4.5</i>	<i>7.5</i>	<i>12.5</i>	<i>mg/L</i>
<i>Chloride</i>	<i>20.0</i>	<i>40.0</i>	<i>75.0</i>	<i>117.5</i>	<i>mg/L</i>
Silica	0.5	1.0	1.5	2.5	mg/L
Sulphate	12.5	22.0	41.0	65.0	mg/L
TDS	50.0	100.0	185.0	300.0	mg/L

2.3.1 Electrolytes in the oil and gas industry

In the oil and gas industry, the presence of salts causes a salting out of hydrocarbons from the brine stream. They reduce solubility compared to pure water, and the presence of electrolytes may improve the inhibitory effect of methanol or/and glycol on the formation of gas hydrates in natural gas pipelines (Maribo-Mogensen, 2014).

In petroleum and wastewater industries, it is well known that too much rain and water flood recovery can reduce the concentration of salinity brine water from the outlet stream of the process (Robertson, 2007). This means less operating cost, less scaling and corrosion on equipment. Salt can be an economic and operational hazard when it precipitates inside

pipelines, processing equipment or near the wellbore (Crabtree et al., 1999). Mackay et al. (2005) have stated on the conditions for salt precipitation:

- A water flood brine, containing sulfate, mixes with formation water, leading to the precipitation of sulfate scales such as BaSO_4 , CaSO_4 , SrSO_4 or $\text{CaSO}_4 \cdot 2\text{H}_2\text{O}$
- A sudden decrease in pressure or temperature increase causes carbonate salts such as CaCO_3 to be deposited
- A dry gas stream is mixed with a brine stream, causing evaporation of water, inducing a super-saturation of salts and leading to the formation of NaCl .

Industrial wastewater is well known to contain high concentrations of salts, which can damage equipment by causing corrosion and scaling. Thus, it is very important that the industry can plan and to select suitable strategies and materials that can assist in managing scale formation and corrosion from the reservoir onwards. For example, by injecting low-sulfate brine and by squeezing scale inhibitors into the reservoir to prevent scaling in the reservoir and near the wellbore areas (Maribo-Mogensen, 2014).

2.3.2 Behaviour of mixtures containing electrolytes in industry

The complex behaviour of mixtures containing electrolytes has gained the attention of scientists and engineers for hundreds of years. Despite their interest, there are still many unanswered questions in relation to thermodynamic models for electrolytes. Figure 2.3 and 2.4 show known examples of the typical behaviour of mixtures containing various salts.

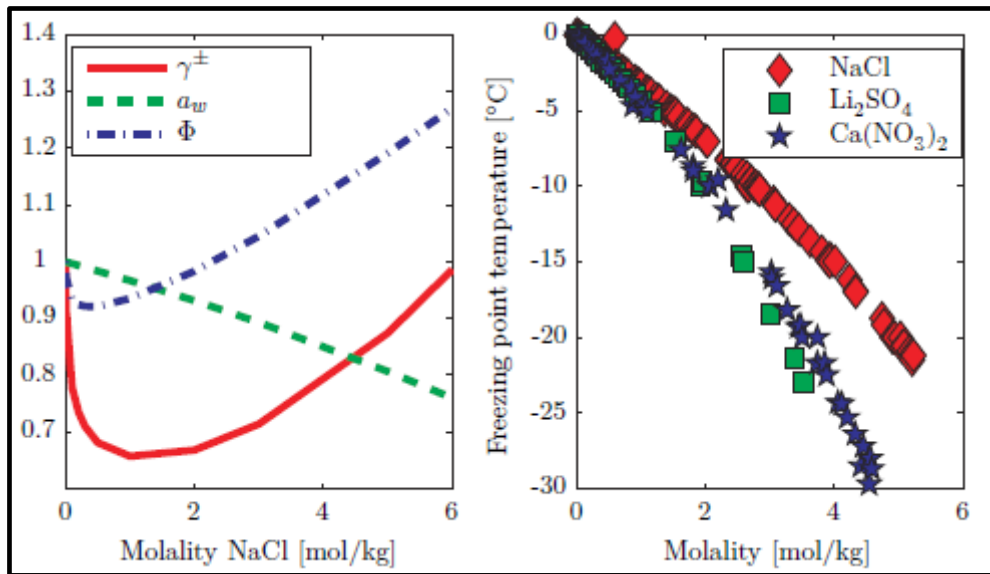


Figure 2. 3: Effect of NaCl concentration at 298.15 K on mean ionic activity coefficient, water activity and osmotic activity (left). Effect of different salts on the freezing point of water as a consequence of reduced water activity (right) (Maribo-Mogensen, 2014)

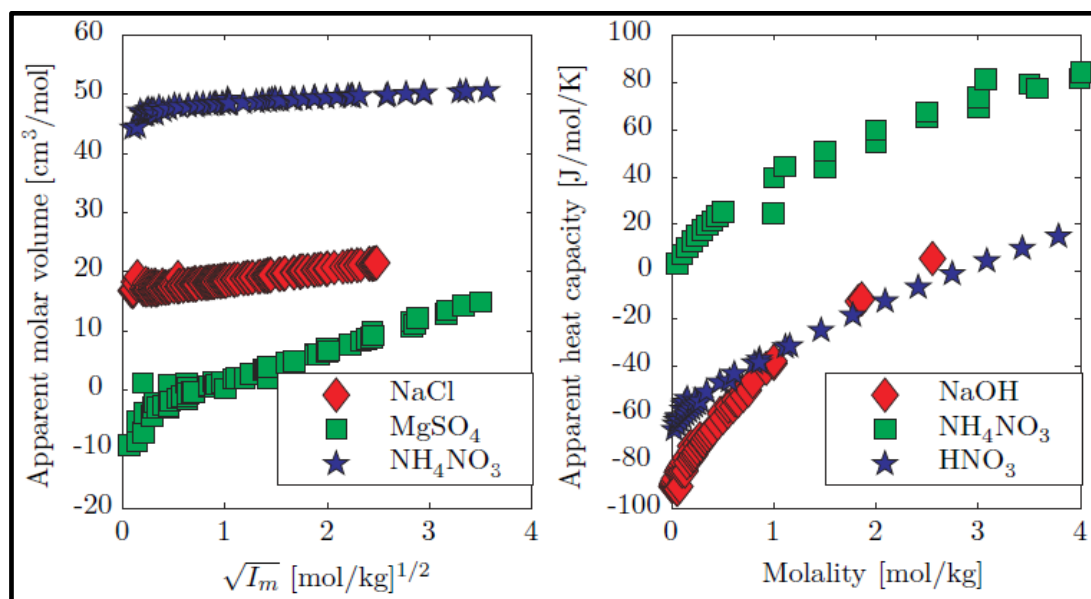


Figure 2. 4: Apparent molar volume as a function of ionic strength (left); and heat capacity of selected aqueous electrolyte solutions (right) (Maribo-Mogensen, 2014)

In general, salts reduce the activity of water and they cause a reduction in freezing point and vapour pressure. The apparent molar volume or heat capacity of the solution can be observed

to either increase or decrease, depending on the ions in the solution, due to the effect ions have on the structure of the solvent, for example, in the formations of solvation shells surrounding the ions (Maribo-Mogensen, 2014).

2.3.2 Summary of the industrial wastewater and seawater

Conventional traditional (MSF and RO) and biological (Anaerobic) methods are currently used on wastewater treatment plant. These methods are preferable to be used to treat wastewater with a high concentration of salt. The above Table 2.6 and 2.7 provide information on the concentration of electrolyte found in saline streams for South African industries such as Tutuka Eskom and others as well as at seawater. The concentration of saline streams will be used as a guide on undertaken gas hydrate measurements in the laboratory. The measurements are performed by selecting those salts that have higher concentration such as NaCl, CaCl₂, MgCl₂, and Na₂SO₄. The concentration of saline brine water can be reduced by rain, which reduce operating cost, reduce scaling and corrosion on equipment. Salt can be an economic and operational hazard when it saturated or precipitates inside pipelines, processing equipment.

The hydrate dissociation data collect in the laboratory will be used to design a desalination process using gas hydrate technology. Consequently, it is important to understand the formation and dissociation of a gas hydrate and its behaviour in the process. A gas hydrate will be produce by mixing electrolyte solution and fluorinated refrigerant (hydrate former), which led to the production of clean/pure water.

2.4 Gas hydrates

2.4.1 Introduction to gas hydrates

A gas hydrate is a solid structure that consists of hydrogen water molecules, as described in Chapter 1. Kontogeorgis and Gani (2004) reported that each oxygen atom is connected to two hydrogen atoms by covalent bonds and to two hydrogen atoms by hydrogen bonds. According to them, the composition of ordinary hydrates cannot be fixed or expressed in small integers, such as vapour-liquid equilibrium (VLE) data measurements. The nature of the comparison of the type and strength of the interactions are involved.

In a typical gas hydrate, the energy stored in a covalent bond is 430 kJ.mol^{-1} , in a hydrogen bond it is 20 kJ.mol^{-1} , and in the lattice-hydrate (water molecules) van der Waals interactions it is 1.3 kJ.mol^{-1} (Kontogeorgis and Gani, 2004). The hydrate cannot be formed without “help” gas molecules (hydrate former) because it is thermodynamically unstable or metastable. Nevertheless, the binding of the gas molecules to the lattice hydrate is comparatively weak.

Physical properties of gas hydrates

Kontogeorgis and Gani (2004) reported that the advantageous physical properties of gas hydrates are density, low thermal conductivity, and varying heats of dissociation. These properties depend on the composition of the hydrate formed at a specific pressure and temperature. The amount of heat required to dissociate the gas hydrate is 1.5 times the heat required to dissociate ice into liquid water. The thermal conductivity of the gas hydrate is approximately 1/4 of the thermal conductivity of ice, which is approximately $0.5 \text{ W.m}^{-1}\text{K}^{-1}$ at a temperature of 273.15 K . In Table 2.9 the characteristics and physical properties of gas hydrates are provided.

Table 2. 9: Characteristics and physical properties of gas hydrates (Kontogeorgis and Gani, 2004)

Characteristics/ Physical properties	Values	Units
Density	900 – 950	kg.m^{-3}
Thermal conductivity	2.22	$\text{W.m}^{-1}\text{K}^{-1}$
Dissociation heat of 1 kg of hydrate	400 – 500	kJ

Generally, two types of crystalline gas hydrate structure were initially detected. These are called structure I (sI) and structure II (sII). Table 2.10 has been compiled to provide comparisons between structure I and structure II hydrates. Later, Ripmeester et al. (1987) detected a third structure, H (sH),, but it is less common. The details concerning the characteristics of these structures are elsewhere (Sloan and Koh, 2008).

Table 2. 10: Comparison of structure sI and sII (Carroll, 2003)

	Structure I	Structure II
Water molecules per unit cell	46	136
Cages per cell		
Small	2	16
Large	6	8
Theoretical formula		
All cages occupied	$X * \frac{5.3}{4} H_2O$	$X * \frac{5.2}{3} H_2O$
Mole fraction hydrate former	0.1481	0.1500
Only large cages occupied	$X * \frac{7.2}{3} H_2O$	$X * 17 H_2O$
Mole fraction hydrate former	0.1154	0.0556
Cavity diameter (Å)		
Small	7.9	7.8
Large	8.6	9.5
Volume of unit cell (m³)	1.728×10^{-27}	5.178×10^{-27}
Hydrate formers	CH ₄ , C ₂ H ₆ , H ₂ S, CO ₂	C ₃ H ₈ , i-C ₄ H ₁₀ , N ₂

where X is the hydrate former

Figure 2.5 shows the formation of a gas hydrate that surrounds gas molecules with water molecules to form a cage. The entire gas hydrate structure is stabilized by hydrogen bonds and van der Waals forces. (Avlonitis, 1992). These crystalline structures are generally dependent on the different size and shape of cages formed or on the guest molecule (Sloan and Koh, 2008; Eslamimanesh et al., 2011). A gas hydrate is a solid, crystalline structure consisting of a host water lattice composed of cavities, as shown in Figure 2.5. This lattice contains cavities, which are stabilized by small apolar molecules such as hydrate formers. Gases (CH₄, C₂H₆, CO₂, refrigerants and other gases) are used to form the gas hydrate and are called hydrate formers. The gas hydrate cannot be formed without the presence of a hydrate former.



Figure 2. 5: Formation of a gas hydrate in a sapphire cell (Chapoy, 2004)

2.4.2 Structures of gas hydrates

A structure I hydrate contains 46 water molecules with small and larger cavities. A small cavity is a pentagonal dodecahedral cavity consisting of 12 pentagonal rings of water, known as 5^{12} . A larger cavity is a tetrakaidecahedral cavity made up of 12 pentagonal rings, and two hexagonal rings of water, as shown Figure 2.6. Typical hydrate formers include CH_4 , C_2H_6 , ethylene, acetylene, H_2S , CO_2 , SO_2 , and Cl_2 .

A structure II hydrate contains 136 water molecules with small and larger cavities. The small cavities are similar to that of structure I. The larger cavities are hexakaidecahedral cavities made up of 12 pentagonal rings of water and four hexagonal rings of water, known as $5^{12}6^4$, as shown in Figure 2.6. Hydrate formers for sII include propane, iso-butane, propylene, and iso-butylene.

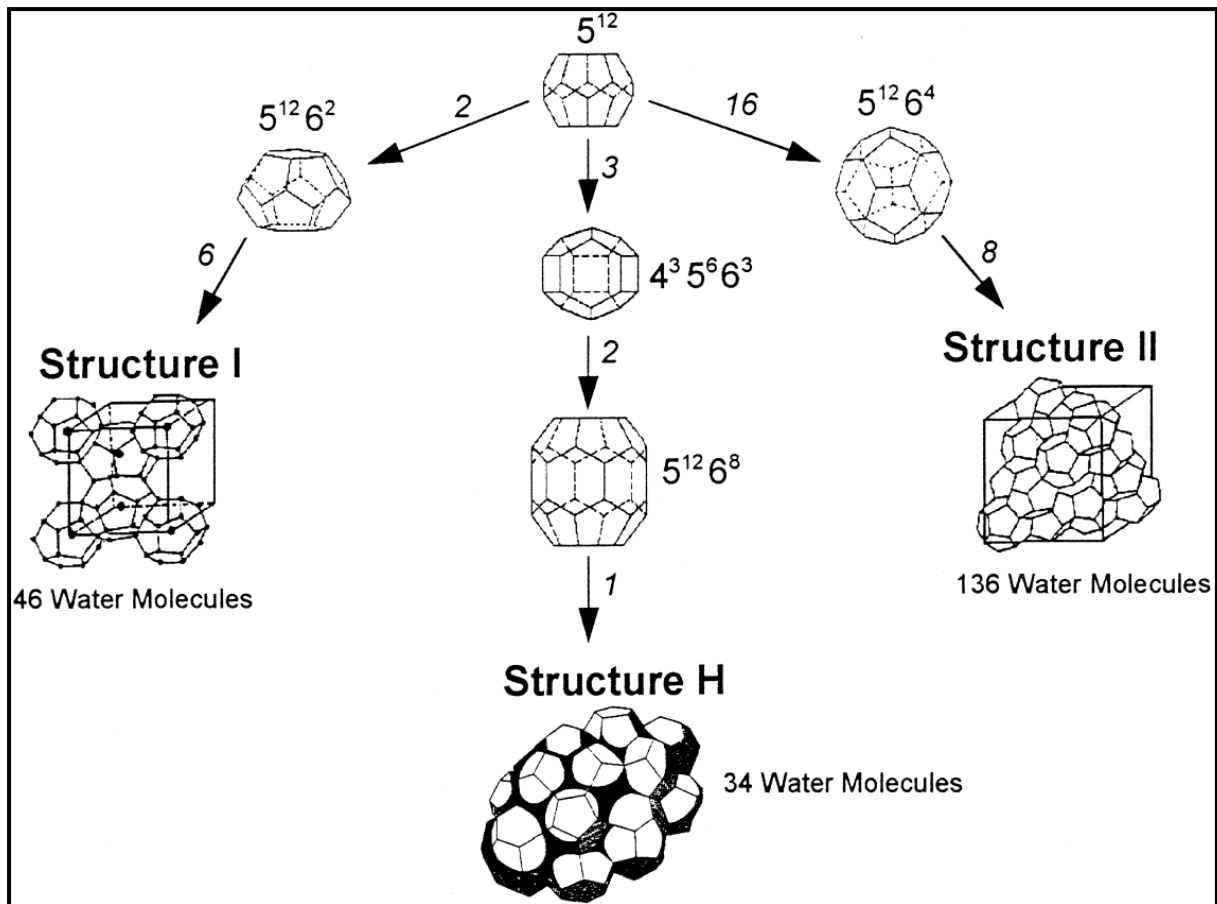


Figure 2. 6: Polyhedral structures of the sI, sII and sH (Khokhar et al., 1998)

Figure 2.6 shows the third hydrate structure discovered by Ripmeester et al., (1987), called structure H. It is formed by means of 40 water molecules with three different types of cavities. These are:

- A small pentagonal dodecahedral cavity consisting of 12 pentagonal rings of water, known as 5^{12}
- An intermediate cavity, consisting of three squares, and six pentagonal and three hexagonal rings of water, known as $4^3 5^6 6^3$.
- A larger hexakaidecahedral cavity of 12 pentagonal rings and eight hexagonal rings of water, known as $5^{12} 6^8$

Small gas molecules can occupy intermediate and small cavities. Larger molecules, such as, cycloalkanes and cycloalkanes (Babae et al. 2012), can occupy the large cavity. Some researchers (Carroll, 2003; Sloan and Koh, 2008; Eslamimanesh et al., 2012) have reported that typical hydrate formers for large cavities are 2-methylbutane, 2,2-dimethylbutane, 2,3-

dimethylbutane, 2,2,3-trimethyl-butane, 2,2-dimethylpentane, 3,3-dimethylpentane, methylcyclopentane, ethylcyclopentane, methylcyclohexane, cycloheptane and cyclooctane

The crystalline structures, sI and sII, can form a hydrate in the presence of a single guest molecule, but structure H requires two guest molecules to be present. For sH hydrate formation, a small molecule, such as, methane, and one larger molecule, are required (Carroll, 2003).

2.4.3 Hydrate formation

Figure 2.7 is drawn to show the guest molecules inside the cages that are not bonded with water but are held inside by van der Waals forces. However, free to rotate inside the cages, known as host molecules.

The formation of a gas hydrate requires the following conditions (Carroll, 2003):

- The right combination of temperature and pressure
- A hydrate former
- A sufficient amount of water.

The formation of a gas hydrate consists of four elements, as indicated in Figure 3.3.

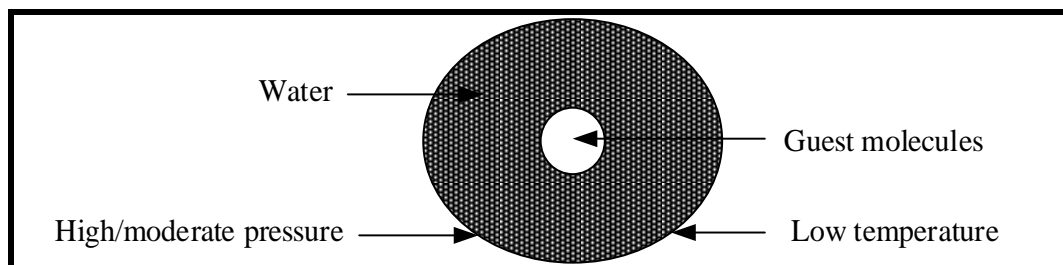


Figure 2. 7: Elements of gas hydrate formation

Gas hydrate formation is usually divided into two processes: a nucleation process and a stable growth process. These are described in more details by a number of researchers: (Vysniaskas and Bishnoi, 1983; Englezos et al., 1987; Natarajan et al., 1994; Kashchiev and Firoozabadi, 2003; Sloan and Koh, 2008).

Figure 2.8 shows how gas hydrate is formed and dissociated. Hydrate formation conditions depend on the rate of cooling, degree of subcooling, fluid used for cooling and the presence of foreign material (Sloan and Koh, 2008; Mohammadi and Richon, 2010).

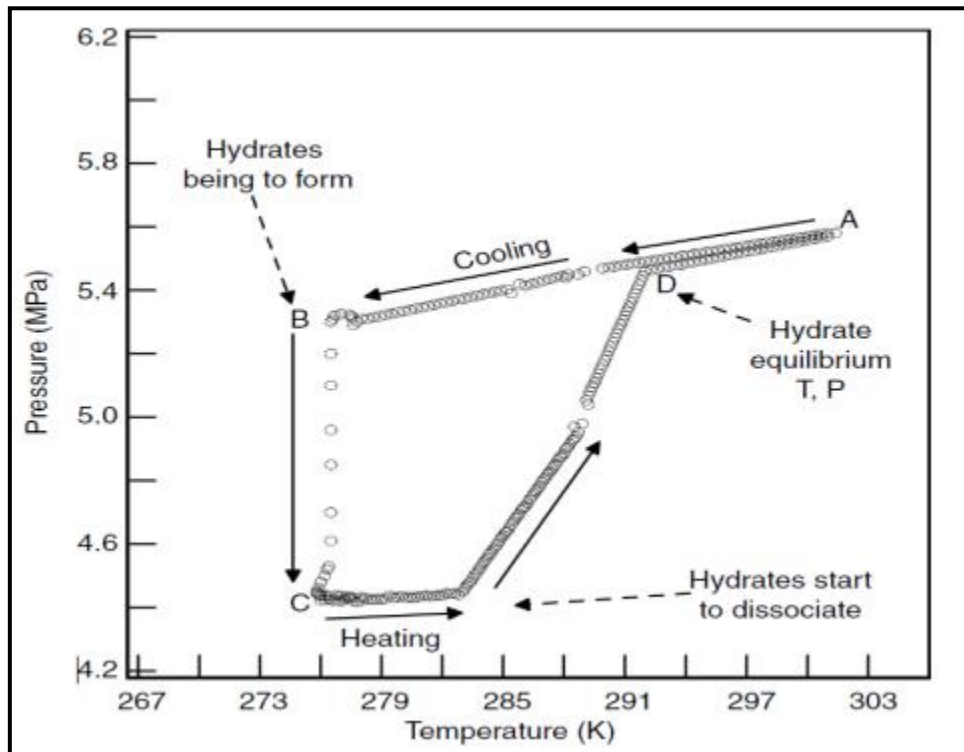


Figure 2. 8: Demonstration of the hydrate formation and dissociation curve (Sloan and Koh, 2008)

Typically, three different procedures can be used for the formation and dissociation of gas hydrates: the isothermal, isochoric, and isobaric methods (Sloan and Koh, 2008). All three procedures are described in detail in Makogon and Sloan, (1994). The isothermal technique requires changing the system pressure in the equilibrium cell; while the isochoric and isobaric procedures require the system temperature to be decreased for hydrate formation, and increased for dissociation of gas hydrates.

In this study, the isochoric method was selected to investigate the systems of interest and the description of the isochoric method is found in Chapter 5. The content inside the equilibrium cell could not be viewed. Thus, the gas hydrate dissociation point was determined by measuring the pressure versus temperature as illustrated in Figure 3.4.

2.4.4 Hydrate dissociation

Hydrate dissociation requires the reduction of pressure, an increase of temperature, chemical (thermodynamic) inhibition, and kinetic inhibition. It is an endothermic process. In order for

the gas hydrate to dissociate, heat must be supplied gradually to break the van der Waals interaction forces and the hydrogen bonds between water molecules. Subsequently, the guest and water molecules of the hydrate lattice decompose the hydrate into water and gas (hydrate former). The hydrate dissociation point is a thermodynamic temperature and pressure equilibrium points, shown as point D in Figure 2.8. This is the final point where the last crystals of the hydrate dissipate.

Generally, heat transfer in hydrate dissociation is more important than intrinsic kinetics. (Hong et al., 2003). Intrinsic kinetics only control the very early phase of hydrate decay. Later, the existing temperature gradient at the hydrate zone forces heat to be conducted from the hydrate zone to the interface due to the removal of heat during decay. Thus, the heat transfers during the later stages (Sabil, 2009) controls the process of dissociation. Based on Fourier's Law, Sloan and Koh (2008) created a heat transfer model that can predict precisely the time of dissociation without any modifiable parameters.

2.4.5 Hydrate promoters

Industrial application of hydrate technology has been hindered by the slow rate of formation of hydrates, coupled with the energy costs of hydrate formation at low temperatures and high pressures. This is why promoters are useful to enable the rapid formation of hydrates.

A promoter facilitates the formation of hydrate by lowering the required pressure and increasing the temperature. It also adjusts the selectivity of the hydrate cages so that several guest molecules can be absorbed. Promoters also reduce mass transfer and kinetic challenges during hydrate formation (Mandal and Laik, 2004). Promoters are normally hydrophobic and they are classified according to their shape, size and chemical nature. The size of the molecules and type of structure occupied affect the position of the gas within the structure of the hydrate. This, in turn, alters the hydrate formation pressure and temperature.

A promoter is a large molecule that fills the gas hydrate with large cavities, and smaller cavities are filled with small gas molecules like methane and hydrogen. Tetrahydrofuran (THF), for example, as a promoter, can stabilize H₂ in hydrates of H₂ + THF structure II at lower pressure than for pure hydrogen hydrates (Ilani-Kashkouli et al., 2013). Kang et al. (2001) and Linga et al. (2007) have found that the dissociation pressure of hydrates in the presence of THF is less than the dissociation pressure without this type of promoter (THF). Promoters can be used in different applications in industry, such as CO₂ capture, gas separation and hydrogen storage.

There are two distinct categories of gas hydrate promoters: “water-soluble” and “water-insoluble” (Eslamimanesh et al., 2011). Water-soluble promoters can be either **thermodynamic** or **kinetic** promoters. Thermodynamic promoters are organic compounds consisting of two types of molecules that shift the equilibrium conditions of hydrate formation to higher temperatures and lower pressures. The first type of molecule does not take part in the structure of hydrate cavities. These molecules include THF, acetone and 1,4-dioxane, and 1,3-dioxalane. These molecules form structure II clathrate hydrates in the presence or absence of guest molecules (Ilani-Kashkouli et al., 2013). The second type of former molecules take part in the structuring of cavities in hydrates including tetra-n-butylammonium bromide (TBAB) and tetrabutyl phosphonium bromide (TBPB). Some researchers have investigated the effect of THF and TBAB water soluble promoters (Kamata et al., 2004; Fan et al., 2009; Acosta et al., 2010; Deschamps and Dalmazzone, 2010; Li et al., 2010; Oshima et al., 2010; Rodionova et al., 2010; Sugahara et al., 2010; Sun and Sun, 2010; Ilani-Kashkouli et al., 2013). It was found that TBAB change the structure of cavities while THF had not, but both promoters increase the formation and dissociation temperatures.

Kinetic water-soluble promoters are surfactant molecules, such as sodium dodecyl sulfate (SDS), that affect the rate of hydrate formation (Sum et al., 2009; Castellania et al., 2012). An ionic surfactant (SDS) increases methane hydrate formation, and decreases the hydrate formation pressure (Link et al., 2003; Lin et al., 2004; Yoslim et al., 2010). The use of a surfactant in hydrate formation is an effective method for reducing power consumption. Roosta et al. (2013) reported on the promotion effect of a surfactant on gas hydrate formation kinetics. In addition, surfactants are used to improve the gas uptake rate during hydrate crystallization without affecting the equilibrium formation conditions (Sun et al., 2003; Hao et al., 2008).

The second category of gas hydrate promoters, water-insoluble promoters, consist of heavy hydrocarbons that include methylcyclohexane, cyclopentane, cyclohexane, cycloheptane, cyclooctane, acetone, neopentane, tetrahydropyran, neohexane, methyl-cyclopentane, 1,3-dimethylcyclohexane, 1,1-dimethylcyclohexane, 2,2-dimethylpentane, methylcyclohexane, cyclobutanone, cis-1,2-dimethylcyclohexane (Ilani-Kashkouli et al., 2013). These heavy hydrocarbons normally form structure H hydrates, except for cyclopentane and cyclohexane that form structure II hydrates. Structure H hydrate formers occupy the large cages of the hydrate structure. They can be used to increase the gas storage capacity of clathrate hydrates (Eslamimanesh et al., 2011).

Researchers (Khokhar et al., 1998; Mohammadi and Richon, 2009, 2010 and 2011; Mooijer-van den Heuvel et al., 2000 and 2001) have focus at the effect of water-insoluble hydrate formers on the hydrate dissociation conditions of various gases, including methane. On the one hand, results show that methylcyclohexane increases the temperature and decreases the pressure of the hydrate dissociation of the methane + water system. On the other hand, Mohammadi and Richon (2009 and 2010) measured a hydrogen sulphide + water system in the presence of methylcyclohexane, cyclopentane and cyclohexane. The results show that the methylcyclohexane does not have a strong promotion effect compared to cyclopentane and cyclohexane. Mohammadi and Richon (2009) studied the effect of cyclopentane, cyclohexane, methyl-cyclopentane, methyl-cyclohexane + CO₂ systems; it was found that cyclopentane has the highest promotion effect. Consequently, the promotion effects of cyclopentane is established as optimal for use in gas hydrate systems.

In this study, cyclopentane is chosen as the promoter for the selected systems, because it has the following advantages (Mohammadi and Richon, 2009 and 2010):

- It is water immiscible due to its low solubility in water
- It does not affect the hydrate structure
- It allows the desalinated water and concentrated brine to be separated easily
- It is environmental friendly and it is not a harmful organic chemical
- It is easily recovered due to its immiscibility.

Cyclopentane

Generally, cyclopentane forms structure sII hydrate. It has an added advantage in that it stabilises the temperature and pressure conditions to lower pressures and higher temperatures, compared to hydrate formers of sI and sH hydrates. Herslund, (2013) compared the use of promoters, cyclopentane (sII) and methyl-cyclohexane (sH), in the presence of methane gas as hydrate former. The equilibrium conditions for both systems were shifted to higher temperatures and lower pressures. It was also found that the cyclopentane (sII) promoted at milder conditions than the methyl-cyclohexane (sH).

Cyclopentane made an impressive pressure reduction and increase of temperature in systems where the gas phase species enters the small cavities of the sII hydrate structure. This means that the cyclopentane is more stable, if the small and large cavities are fully occupied.

However, cyclopentane has very low solubility in water under certain conditions of hydrate formation, for example, the solubility is 86 mg/L at 283 K. It forms an organic liquid phase when used in excess amounts. In the case of an excess amount of cyclopentane present in the system, the aqueous phase is always saturated (Herslund, 2013). Herslund revealed that cyclopentane solubility in water is limited in relation to its concentration with changing temperature and pressure. Consequently, the gas hydrate formation conditions are dependent on only a small amount of cyclopentane. Due to its limited solubility, little is available in the aqueous phase. The appearance of hydrate-like aggregates in the aqueous phase, combining to form the hydrate nucleus, becomes less probable from a statistical point of view (Herslund, 2013).

Chen et al. (2010) investigated the effects of the electrolyte, NaCl, on hydrate formation in the presence of cyclopentane and methane. It was found that NaCl had an inhibiting effect on the measured hydrate dissociation pressure. It was also shown that the increase of electrolyte concentration from 3.5 wt% to 10 wt% provided an increase in inhibition.

Corak et al. (2011) and Cha et al. (2013) reported that the formation of a hydrate in the presence of cyclopentane could be employed for seawater desalination. However, the hydrate formation without a promoter was slow, as was the case with any other hydrate formation. Cha et al. (2013) have suggested that either cyclopentane or cyclohexane be added in the presence of CO₂ as hydrate former, in order to raise the temperature required for desalination of seawater with a high concentration of salt, for the production of fresh water.

Both cyclopentane and cyclohexane are known to form structure II hydrates with small gaseous molecules of CH₄ or CO₂ (Cha et al., 2013). The large 5¹²6⁴ cages for structure II hydrates are filled by cyclopentane and cyclohexane and the smaller 5¹² cages are occupied with CH₄ or CO₂ molecules (Ripmeester et al., 1991). When hydrate formation is compared in the presence of cyclopentane or cyclohexane with single guest molecules, CO₂ or CH₄, the phase boundary of sII hydrates shifts into a hydrate promotion region by lowering pressure and increasing temperature (Sun et al., 2002). Komastu et al., (2010) reported that the promotion effect was larger than that of THF, which was normally used as the hydrate promoter. Also, Zhang et al., (2009); and Trueba et al., (2011), emphasize that the use of cyclopentane has been also recommended for H₂ storage and CO₂ separation from pre- and post-combustion gases.

Kang and Lee (2000) and Arjmandi et al., (2007) reported on the use of THF and tetraalkylammonium salts as promoters having the ability to shift the hydrate phase boundary

of the promotion region, even at near ambient pressure. Cha et al. (2013) studied the effect of using cyclopentane in water to raise the temperature of the hydrate from subzero Celsius to near ambient temperature. It was found that the addition of cyclopentane increases the hydrate formation temperature from 271 to 289 K.

There is limited information on the use of cyclopentane as a promoter in the presence of fluorinated refrigerants. This study explores its use in the presence of single and mixed electrolytes in a desalination process using gas hydrates technology. The use of single electrolytes in the presence of fluorinated refrigerants as hydrate formers without a promoter were investigated by this author for a Master of Science in engineering degree in 2014.

2.6 Refrigerants

In the current study, fluorinated refrigerants were selected to be used as hydrate formers in the presence of a promoter. Several criteria were considered when determining suitable commercial fluorinated hydrating agents for the desalination of industrial wastewater. Firstly, a list of commercially available fluorinated refrigerants was obtained and compared to the chemicals listed in the Montreal Protocol. The Montreal Protocol considers ozone depletion due to the presence of chlorine as well as greenhouse effects. Table 2.11 presents the criteria used for selection of the fluorinated refrigerants.

Table 2. 11: Criteria for selecting hydrate formers (Petticrew, 2011)

Characteristic	Appropriate criteria
Environmental acceptability	The hydrate former must have a low ozone depletion and greenhouse effect and was accepted by the Montreal Protocol.
Non-toxicity	The hydrate former must have a low acute toxicity as it was non-carcinogenic and non-mutagenic.
Non-flammability	The hydrate former must have a high flash point temperature to minimize the risk of starting a fire.
Chemical stability	The hydrate former reacted slowly with chemicals.
Compatibility with standard materials	The hydrate former must have a low chemical activity.
Forms a structure II hydrate	An easier separation of hydrate and salt was recognized in the wash column.
Reduce cost	Operating costs have been reduced
Availability	The hydrate former was made from a reliable supplier in commercial capacity.
Water solubility	

Table 2.12 has been compiled from a list of fluorinated refrigerants that can be used as hydrate formers in the presence of water for the formation of gas hydrates. Only those that are not banned, nor are in danger of being phased out, are selected. They are environmentally friendly. They have the potential to form hydrates at lower pressures compared to natural hydrate formers, with the exception of carbon dioxide. These fluorinated refrigerants were not extensively investigated in the literature, in particular in the presence of electrolytes. The corresponding phase equilibrium data for some of these refrigerants in the presence of pure water are available in the literatures as presented in Table 2.12.

Table 2. 12: Reviewed hydrate former and water systems

Hydrate former	Solvent	T/K	P/MPa	Reference
R134a	Water	273.5 to 283.1	0.566 to 4.144	Liang et al. (2001)
R141b	Water	273.4 to 281.5	0.078 to 0.402	Liang et al. (2001)
R152a	Water	273.4 to 288.2	0.772 to 4.437	Liang et al. (2001)
R141b	Water	274.2 to 280.2	Atmospheric pressure	Li et al. (2008)
R32	Water	275.5 to 290.7	0.200 to 1.090	Hashimoto et al. (2010)
R134a	Water	265.3 to 283.5	0.047 to 0.417	Eslamimanesh et al. (2011)
R141b	Water	268.4 to 281.5	0.008 to 0.040	Eslamimanesh et al. (2011)
R32	Water	264.7 to 288.2	0.077 to 0.444	Eslamimanesh et al. (2011)
R152a	Water	274.0 to 294.1	0.174 to 1.489	Eslamimanesh et al. (2011)
R410a	Water	277.50 – 293.00	0.179 – 1.421	Ngema et al. (2014)
R507	Water	277.70 – 283.70	0.221 – 0.873	Ngema et al. (2014)
R134a	Water	277.10 – 283.00	0.114 – 0.428	Ngema et al. (2014)

Solubility of fluorinated refrigerants in water

Fluorinated refrigerants as hydrate formers, including R134a, R410a and R507, have low solubility in water and in salt aqueous solution. Several assumptions were made by Eslamimanesh et al., (2011), first is the vapour pressures of refrigerants might be equal to the partial pressure of that particular refrigerant in the aqueous solutions. The second is the vapour phase is an ideal gas of that particular refrigerant, due to the low solubility. The third is the fugacity of refrigerants in the vapour phase is equal to the dissociation pressure of gas hydrates. These assumptions are used in this study to calculate the fugacity of refrigerants.

2.7 Kinetic and thermodynamic behaviour of clathrate hydrates

Ilani-Kashkouli et al. (2012) and Babaei et al. (2015) mentioned that the kinetic rate of gas hydrate formation is required for the reliable and efficient design of industrial separation processes. The parameters affecting the kinetic rate of hydrate formation are the initial temperature, initial pressure, interfacial area, water history and degree of subcooling (Vysniauskas and Bishnoi, 1983). A semi-empirical kinetic model was developed, and it was found that water history increases the induction time. Englezos et al. (1987) developed a kinetic model to be used to estimate the kinetic constant and the rate of hydrate formation. They also studied crystallization and mass transport theories that indicate that the rate of gas consumption is dependent on crystal growth rate.

According to Englezos et al. (1987), the crystallization theory is based on the difference between the fugacity of gas molecules in the vapour and hydrate phases. Skovborg and Rasmussen (1994) studied the model proposed by Englezos et al. (1987). They indicated that the rate of hydrate formation is dependent on the mass transport between the water and gas molecule and is independent of the total particle surface area. They concluded that there is no need to know the particle size distribution in the hydrate processes.

Mork and Gudmundson, (2002) reported that hydrate formation involves (i) the dispersion of a hydrate former from the interface of a vapour-liquid phases to a liquid phase, (ii) the latter from the liquid to the interface of hydrate phases, and (iii) the physical reaction of water molecules and hydrate former at the interface of a hydrate phase. Good results were obtained when modelling hydrate formation using a combination of either (i), (ii) and (iii) or (i) and (ii).

2.8 Economics

An economic study of desalination using hydrates is an important factor in determining the feasibility of the application. The operation cost of desalination, either industrial wastewater or seawater, using gas hydrate technology depends on wastewater/seawater temperature, salt concentration, mobility of salt and yield (Javanmardi and Moshfeghian, 2003). The efficiency of the removal of salt in a desalination process depends on the ionic radius and the ionic charge of the cations present in the form of minerals (Park et al., 2011).

The traditional desalination processes, which include reverse osmosis (RO), Multi-stage flash distillation (MSF) are mostly used in the Middle-East countries where there is shortage of fresh water and local abundance of oil and gas (He et al., 2018). The water recovery from MSF

process is up 20%, and the specific energy consumption is 13.5 – 25.5kWh/m³ depending on the operating conditions (He et al., 2018; Igunnu and Chen, 2012; Al-Sahali and Ettouney, 2007). MSF overall cost is 0.56–1.75 \$/ton (Al-Karaghoulis and Kazmerski, 2013; Younos, 2005). The reverse osmosis operates at a higher pressure of 50 to 80 bar, and consume a large amount of energy and it is sensitive to impurities (He et al., 2018). It can recovery water up to 55% which is high than the MSF process. The specific energy consumption for RO process is 1.85–36.3 kWh/m³, and overall cost is ranging between 0.45 – 0.66 \$/ton (He et al., 2018; Al-Karaghoulis and Kazmerski, 2013; Gude, 2011). The gas hydrate process built in hawaii and San Diego by Thermal energy systems where R141b was used as hydrate former with a formation temperature of 5.6 °C. The overall cost of water produced was 0.46 – 0.52 \$/ton and the specific energy consumption was 1.5 kWh/m³, which are less than MSF and RO processes, respectively (He et al., 2018; Lee et al., 2016; McCormark and Niblock, (2000, 1998, 1996,1995)). It was found that 90% of salt removal by using gas hydrate technology (Lee et al., 2016).

Table 2.13 has been assembled for comparison of typical operating conditions of reverse osmosis (RO), Multi-stage flash distillation (MSF) and gas hydrate processes, when used in desalination. MSF distillation operates at a high temperature range compared to hydrate technology and RO, while the pressure is below 0.1 MPa. The capital investment for hydrate technology is higher while the operating cost and the total production cost are lower compared to MSF and RO processes. The operating cost of hydrate technology can be further reduced by using suitable nontoxic promoters. In Table 2.13, it is indicated that the product cost of MSF and RO is higher than the gas hydrate technology in the production of fresh water. The product cost depends on the concentration of salt and the temperature of the wastewater or seawater.

Table 2. 13: MSF, RO and gas hydrogen technology comparisons (Sangwai et al., 2013)

Parameter	MSF	RO	Hydrate	Units
Physio-chemical principal	Flash evaporation	Solute diffusion	Phase change process	–
Temperature	90 – 120	20 – 35	Vicinity of 0	°C
Pressure	Below 0.1	5.5 – 7.0	0.45 – 0.65 (propane hydrate)	MPa
Capacity	1000	1000	1000	ton/day
Capital investment	2.93	2.3	5.46	M\$
Operating cost	2	3.23	1.2	\$/ton
Total product cost	3.26	4.27	2.76	\$/ton
Maintenance	Corrosion problem	Membrane replacement	No maintenance	–

Figure 2.9 shows the energy consumption (kJ/kg) with respect to salt content in water. It is observed that gas hydrate technology (clathrate hydrate) for desalination is more economical compared to distillation and membrane methods. The use of hydrate technology has been gaining interest, but further research is required to decrease the capital investment.

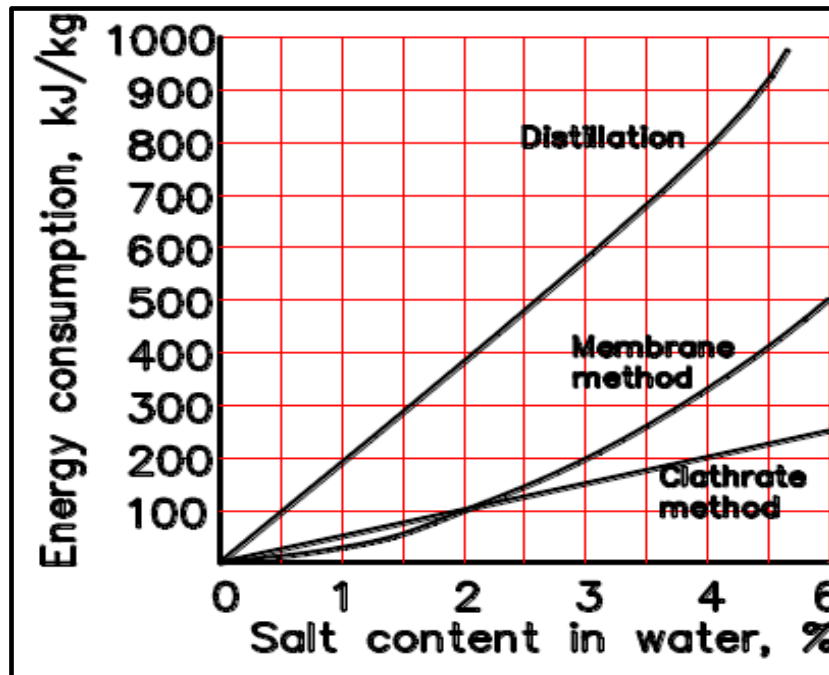


Figure 2. 9: Energy consumption for distillation, membrane and hydrate (Lee, 2011; Sangwai et al., 2013)

Eslamimanesh et al. (2012) reported that, since the 1940s, a number of studies have been carried out to design desalination processes using gas hydrate technology efficiently and economically. An economic study including total capital investment, operating and maintenance costs and depreciation costs showed that the total cost of drinking water production is reduced by the use of fluorinated refrigerants as a hydrate former.

The investigations conducted by Chun et al. (2000); Javanmardi and Moshfeghian (2003); Seo and Lee (2003) showed that the formation of gas hydrates without a hydrate former or promoter is not an economical method for a desalination process compared to distillation and membrane methods. The use of a promoter has an impact in reducing the energy cost of the process and it can lead to a lower fresh water production cost (Eslamimanesh et al., 2012).

Some researchers (Cakmakci, et al., 2008; El-Dessouky and Ettouney, 2008; Cha et al., 2013) have reported that the treatment of wastewater using RO has an estimated cost of \$5.19–\$5.98/m³, while seawater treatment costs \$0.46–\$0.79/m³. This difference is caused by a decrease in membrane lifespan due to increases in operating pressures and pretreatment processes for removing electrolytes and other impurities. On the other hand, with distillation

technology, energy consumption creases from 2.3 to 13.6 kWh/m³ as salt concentration increases from 37 g/L in seawater to 55 g/L in produced water (Koren and Nadadrate, 1994; Wade, 2001). However, the treatment of highly saline water, to produce fresh water, using gas hydrate technology can also be subject to increased operation costs. This is due to the hydrate being formed at higher pressure and lower temperature, especially when using natural hydrate formers such as CH₄, CO₂ etc. The addition of a promoter causes the phase boundary to shift to lower pressures and to increase the temperatures for hydrate formation so that hydrate formation can be achieved at atmospheric conditions. The cost reduction for hydrate technology depends on the type of hydrate former used, such as refrigerant.

2.9 Summary for the gas hydrates

Gas hydrate technology is an alternated technology to be considered over tradinational desalination processes, due to economically especial in the presence of the promoter. The gas hydrates structured were identinty as sI, sII and sH. The gas hydrates were formed using fluorinate refrigerant as the hydrate former. The selected fluorinated refrigerants were those not phase out. The selected refrigerants were environmental friendly, low pressures, available at the market at the lower cost and not harmful to human. The gas hydrates were formered when the hydrate former was trapped inside water molecule as the temperature of the system decreases and it dissociate when the system temperature increases gradually until the dissociation is being achived.

Once hydrate dissociation data is achieved than the kinetic rate of gas hydrate formation is required for the design of industrial separation processes. The parameters affecting the kinetic rate of hydrate formation are the initial temperature, initial pressure, interfacial area, water history and degree of subcooling. In addition, an economic study of desalination using gas hydrate technology is an important factor in determining the feasibility of the application. The operation cost of this technology compare to the traditional desalination processes were discussed.

Once hydrate dissociation data is generated, it is important to model the experimental data. Consequently, in this study, the Hydrate Electrolyte–Cubic Plus Association equation of state was developed to model hydrate systems in the presence of single and mixed electrolyte as well as in the presence of the promoter. The developed model is presented in the next chapter.

CHAPTER 3

DEVELOPMENT OF HYDRATE ELECTROLYTE– CUBIC PLUS ASSOCIATION (HE-CPA) MODEL EQUATION OF STATE

Desalination eliminates the mixed electrolytes contained in industrial wastewater and seawater. To this end, a thermodynamic model is developed to describe the properties and the behaviour of electrolyte solutions in order to employ gas hydrate technology in the purification of saline water.

In this study, three models are combined into one model to be used for the optimization of water desalination employing gas hydrate technology, namely, the Van der Waals and Platteeuw, CPA EoS and Deybe–Hückel models. The Van der Waals and Platteeuw is used to model the hydrate phase, the CPA equation of state is used to model the liquid or vapour phase, and the Deybe–Hückel model is used to model electrolytes. This combination is used to measure hydrate dissociation data for single and mixed electrolytes in the presence of a fluorinated refrigerant as hydrate former. It is essential to have good models for the description of electrolyte and hydrate properties.

The Deybe–Hückel that is only represents the long range interactions and UNIQUAC covers the middle and short-range interactions that are discussed later in this Chapter. The Deybe–Hückel is the starting point for the development of activity coefficient models for electrolyte solutions, which was developed in 1923 by P. Deybe and E. Hückel. It is considered as an exact equation to describe the behaviour of an electrolyte system at infinite dilution (Gmehling et al., 2012). Gmehling et al. (2012) for the derivation of the Deybe–Hückel limiting law made the following assumptions:

- Only electrostatic forces were considered between the ions and all other forces were insignificant;
- The electrostatic interactions in comparison with thermal energies were small;
- The ions were regarded as punctual charges with a spherical field;
- The dielectric constant of the solution was equal to that of the solvent;
- The electrolyte was completely dissociated;

- Each ion was surrounded by ions of an opposite charge;
- Solutions of electrolyte(s) were diluted to lower concentrations;
- Boltzmann 's law controls the distribution of ions around a center ion due to the existing electrical potential.

This information is essential for the modelling of electrostatic interactions. Models for electrolytes have used one of three approaches:

- Primitive models assume that the static permittivity is equal to that of the solvent (Maribo-Mogensen, 2014). Several researchers reported that the static permittivity correlation at the saturation line of solvent (water) with temperature is generally applied in activity coefficient models (Deybe–Hückel, 1923; Pitzer, 1973; Chen and Evans, 1986; Thomsen and Rasmussen, 1999; Anderko et al., 2002). Some researchers used this method with equation of state modelling and in molecular simulation (Raatschen et al., 1987; Copeman and Stein, 1987; Jin and Donohue, 1988a and 1988b; Liu et al., 1989; Aasberg-Petersen et al., 1991; Vu et al., 2002; Myers et al., 2002; Haghghi et al., 2009). These models include empirical terms to consider the effect of salt in the mixture.
- Non-primitive models use the pair of all the electrostatic interactions (ion-ion, ion-dipole, dipole-dipole). These models have not included static permittivity (Liu et al., 2005; Herzog et al., 2010).
- Civilized models are non-primitive models that consider the steric effects, ion-hydration and ion-ion association (Robison and Stokes, 1970; Clano-Restrepo and Chapman, 1994). These models have not been used within an equation of state (Maribo-Mogensen, 2014).

3.1 Activity coefficient models for electrolytes

Some authors, including (Kontogeorgis and Folas, 2010; Gmehling et al., 2012; Maribo-Mogensen, 2014), addressed the fundamentals of electrolytes in thermodynamics. This section is focussed on thermodynamics models for electrolytes systems that can be applicable in desalination process. These thermodynamic models describe different contributions to excess Gibbs energy. Normally, they consist of explicit terms to take into account short-range (SR), intermediate-range (MR) and long-range (LR) interactions in the specified solution, as presented in the following expression:

$$G^E = G^{SR} + G^{MR} + G^{LR} \quad (3.1)$$

Table 4.1 presents some common activity coefficient models used in chemical and wastewater industries (Lin et al., 2010). These models are based on extension of a local composition term (modified NRTL or UNIQUAC) with an additional model to consider the electrolytes. Lin et al. (2010) reported that these models required a large number of interaction parameters to be estimated against the existing experimental data. These parameters, in general, are not transferable outside the regime where they were estimated.

Thomsen, (2009) state that the standard state properties of electrolytes are not well established for many electrolytes, and that intermediate species make it necessary to infer standard state properties from measured data, for example, heat of dilution, chemical speciation and apparent molal heat capacity.

Table 3. 1: Activity coefficient models for electrolyte solutions and their applications
(Maribo-Mogensen, 2014)

Model	Electrolyte NRTL ^{a,b}	OLI mixed solvent electrolyte ^(e,f,g,h,i)	Extended UNIQUAC ^(l,m,n)
Non-electrostatic term	Modified NRTL ^a	UNIQUAC ^j + 2 nd virial term ^k	UNIQUAC ^j
Electrostatic term	Modified Pitzer- Debye–Hückel ^(b,c) and Born ^d	Modified Pitzer- Debye–Hückel ^(c,e)	Extended-Debye– Hückel ^o
Parameters	2-4 per binary (on ion pair basis)	3 per binary	4 per molecule, 2 per per binary
Availability	Aspen Plus/Properties	Aspen Plus / HYSYS, Honeywell UniSim, gPROMS, Pro/II	Aspen Plus and Excel

^aChen and Evans (1986); ^bSong and Chen (2009); ^cPitzer and Simonson (1986); ^dBorn (1920); ^eWang et al. (2002); ^fWang et al. (2004); ^gWang et al. (2006); ^hWang et al. (2013); ⁱAnderko et al. (2002); ^jAbrams and Prausnitz (1975); ^kPitzer (1973); ^lThomsen (2009); ^mThomsen et al. (1996); ⁿThomsen and Rasmussen (1999) and ^oDebye–Hückel (1923)

Lin et al. (2010) compared the activity coefficient models listed in Table 3.1 by conducting ten test systems. These systems included an aqueous mixture with salts (NaCl, Na₂SO₄, MgCl₂, KNO₃, K₂SO₄, MgSO₄, MgNO₃) and a mixed solvent system with water and ethanol. They compared the model predictions of VLE and SLE against measured data at temperatures ranging from 251.15 to 383.15 K, using standard parameters. It was found that these activity coefficient models give reasonable results for VLE vapour pressures, but they sometimes give incorrect SLE data, because of incorrect speciation.

On other hand, the Extended UNIQUAC gave good results in the case of mixed solvent solutions, even at higher concentrations, despite the Debye–Hückel assumption that the solvent is pure water and it does not include the Born term for the Gibbs energy transfer (see section 3.1.4 for more information on the Born term). It was also found that the interaction parameters of the UNIQUAC model could be employed to compensate for the alternative representation of electrostatic interactions. Nevertheless, there was a query about whether the correlation

models could produce accurate predictions in regions with limited data, which include high temperature or pressure (Lin et al., 2010). In such cases the fundamentals of thermodynamic modelling of electrolyte aqueous solutions was required.

3.1.1 Long-range interactions (LR)

The Deybe-Hückel model for electrostatic interactions between charged ions in aqueous electrolyte systems takes into account long - range interactions. It describes the thermodynamics of ideal solutions of ions. The Deybe-Hückel model does not describe the interactions between ions and water. (Thomsen, 2009).

In the use of the Deybe-Hückel model, the solvent only plays an essential role due to its relative permittivity (dielectric constant) and its density. This model cannot stand alone as a model for electrolyte solutions. There is a need to describe the properties of concentrated electrolyte solutions by including short and intermediate-range interactions (Thomsen, 2009). The Deybe-Hückel theory was derived with the following assumptions (Kontogeorgis and Folas, 2010):

- The ions are not distributed randomly;
- The solution is electrically neutral;
- The ions are taken as a sphere of radius with a point charge in the centre of the sphere;
- Around a central ion there will be an overweight of ions with the opposite charge.

Electrolytes dissociate into ions when dissolved in polar solvents such as water or water-alcohol mixtures (Kontogeorgis and Folas, 2010). Strong electrolytes, such as NaCl, MgCl₂ and CaCl₂, dissociate completely in a polar solvent because of a longer range of Coulombic forces, compared to the van der Waals and other related forces. Such solutions, containing charged ions, are more non-ideal than solutions containing only neutral molecules (Kontogeorgis and Folas, 2010). In the Deybe-Hückel theory, Coulombs law expresses the electrostatic force that a positive ion exerts on a negative, through the solvent medium:

$$F = -\frac{1}{4\pi\epsilon_0\epsilon_r} \frac{e^2}{r^2} \quad (3.2)$$

where e is the electronic charge; ϵ_0 is the permittivity in vacuum; ϵ_r is the dielectric constant or relative permittivity of the solvent; and r is the distance between the ions. The values of the

electronic charge, the permittivity in vacuum and dielectric constant or relative permittivity of water at 298.15 K are presented in Appendix B.

The dielectric constant is strongly temperature-dependent (Gmehling et al., 2012). It has a polynomial correlation that can be used over wide temperature ranges. Table 3.2 presented the coefficients used for the polynomial correlation in Equation 3.2

$$\varepsilon_r = A + BT + CT^2 + DT^3 + ET^4 \quad (3.3)$$

where A , B , C , and D are coefficients; and T is temperature in Kelvin.

Table 3. 2: Coefficients for the calculation of the dielectric constant in Equation 3.2

(Gmehling et al., 2012)

Component	A	B	C	D	E	T _{min} /K	T _{max} /K
Water	289.8229	-1.1480	1.7843*10 ⁻³	-1.053*10 ⁻⁶	0.000	273	643
Methanol	301.6681	-2.3343	7.9275*10 ⁻³	-1.2858*10 ⁻⁵	7.964*10 ⁻⁹	163	511
Ethanol	191.9472	-1.3540	3.8877*10 ⁻³	-4.1286*10 ⁻⁶	0.000	163	353

Thomsen (2009) and Kontogeorgis and Folas (2010) reported that the expression for Helmholtz energy in the Deybe–Hückel theory was derived by solving the Piosson’s equation, giving a relation between the charge density, ρ_i (Cm⁻³) around ion, i , and the electrical potential, ψ_i (J / C), for a sphere with radius, r , around ion, i :

$$\frac{1}{r^2} \frac{d}{dr} \left(r^2 \frac{d\psi_i}{dr} \right) = - \frac{\rho_i}{\varepsilon_0 \varepsilon_r} \quad (3.4)$$

The ions are not distributed uniformly or randomly in the solution because of the charges. Near a cation, anions tend to be in excess and near an anion, cations tend to be in excess (Kontogeorgis and Folas, 2010). An ion, j , has the electrical potential energy of $z_j e \psi_i$, if it is in the distance of r , from the ion, i . Deybe–Hückel assumed that the distribution of ions in solution was a Boltzmann distribution. This assumption gives the relation between the charge density and the electrical potential.

$$\rho_i = e N_A \sum_{allions} \frac{n_j z_j}{nV} e^{-\frac{z_j e \psi_i}{kT}} \quad (3.5)$$

where n_j is the mol number of component, j ; z_j is the charge of component, j ; N_A is Avogadro's number; k is the Boltzmann constant; T is the temperature in Kelvin; and V is the molar volume of the solution. The Boltzmann distribution describes how the distribution of the ions differs from the average distribution because of the electrostatic interactions. The values of Avogadro's number and Boltzmann constant are presented in Appendix B.

In this study, the electrolyte solutions consist of the particular ions which are formed by dissociation reactions, for example:



The Z_j gives the total charge of an ion, Table 3.3 presents the charge component Z_j , for the above chemical equations. (The charge components for all electrolytes used in this study are present in Appendix B.)

Table 3. 3: Example of a charge component

Charge	Value of Z
Na ⁺	+1
Cl ⁻	-1
Ca ²⁺	+2
SO ₄ ²⁻	-2

The Poisson and Boltzmann equations were combined by Deybe–Hückel to remove the charge density. For electrical potential, the resulting Poisson-Boltzmann equation has been solved. Deybe–Hückel had finally come to an excess Helmholtz function for an ideal solution of charged ions. Ideal solutions do not have excess terms. The excess Helmholtz function takes only the non-ideality of electrostatic interactions into account. It does not deal with traditional short-range non-ideality. Equation can express the molar excess Helmholtz function for electrostatic interactions.

$$\frac{A^E}{RT} = -\frac{1}{3} \sum x_i z_i^2 s \kappa \chi(\kappa a_i) \quad (3.8)$$

where the terms s and κ are defined by:

$$s = \frac{e^2}{4\pi\epsilon_0\epsilon_r kT} \quad (3.9)$$

and:

$$\kappa = \left(\frac{e^2 N_A}{\epsilon_0 \epsilon_r kT} \frac{\sum n_i z_i^2}{nV} \right)^{1/2} \quad (3.10)$$

where the function χ is given by:

$$\chi(x) = \frac{3}{x^3} \left(\frac{3}{2} + \ln(1+x) + 2(1+x) + \frac{1}{2}(1+x)^2 \right) \quad (3.11)$$

There are a wide of explanations of the Deybe–Hückel equation that have been used for model development, mentioned in text books (Thomsen, 2009).

A simplification of the original Deybe–Hückel equation was derived from the relation between Gibbs energy and Helmholtz energy which is given by $G = A + PV$. The term PV was not added to the Helmholtz function. This chemical term was derived from the energy function by molar differentiation at constant temperature and pressure. It was not derived at molar differentiation at constant temperature and volume. The chemical potential is derived from the different energy functions as:

$$\mu_i \equiv \left[\frac{\partial G}{\partial n_i} \right]_{T,P,n_j} = \left[\frac{\partial H}{\partial n_i} \right]_{S,P,n_j} = \left[\frac{\partial A}{\partial n_i} \right]_{T,V,n_j} = \left[\frac{\partial U}{\partial n_i} \right]_{S,V,n_j} \quad (3.12)$$

The Helmholtz function in Equation 4.8 generated a Gibbs energy function by replacing the molarity concentration unit with molality and by simplifying the equation for κ in Equation 3.10. The density of an electrolyte solution with the molar volume V and the total volume nV can be written as:

$$\rho_{sol} = \frac{n_w M_w + \sum_{ions} n_i M_i}{nV} \quad (3.13)$$

This equation is converted to an expression for nV , which is inserted into Equation 3.10:

$$\kappa = \left(\frac{e^2 N_A \rho_{sol}}{\varepsilon_0 \varepsilon_r kT} \frac{\sum n_i z_i^2}{n_w M_w + \sum_{ions} n_i M_i} \right)^{1/2} \quad (3.14)$$

According to Thomsen (2009) the assumption was made that the capacity and the mass of the ions is zero. This assumption represents a minor inaccuracy for dilute solutions and a greater error for concentrated solutions. This assumption means that the density of the solution is equal to the density of pure water.

Lewis and Randall (1921) introduced the concept of ion strength

$$I = 0.5 \sum_i m_i Z_i^2 \quad (3.15)$$

where m_i is the molality (mol/kg); and Z is the charge component:

$$m_i = \frac{n_i}{n_{solvent} M_{solvent}}$$

The expression for κ can be written:

$$\kappa = \left(\frac{2e^2 N_A \rho_o}{\varepsilon_0 \varepsilon_r kT} \right)^{1/2} I^{1/2} \quad (3.16)$$

Then, the products $s\kappa$ from Equation 3.7 can be written as:

$$s\kappa = 2(2\pi N_A \rho_o)^{1/2} \left(\frac{e^2}{\varepsilon_0 \varepsilon_r kT} \right)^{3/2} I^{1/2} \quad (3.17)$$

The approximated value of product $s\kappa$ is expressed as $2AI^{1/2}$ where A is the Deybe–Hückel parameter:

$$A = (2\pi N_A \rho_o)^{1/2} \left(\frac{e^2}{\varepsilon_0 \varepsilon_r kT} \right)^{3/2} \quad (3.18)$$

The value of the Deybe–Hückel parameter A is $1.1717 (kg/mol)^{1/2}$ at 298.15 K (Thomsen, 2009) and it can be approximated in the temperature range (273.15 to 383.15) K by:

$$A = 1.131 + 1.335 * 10^{-3}(T - 237.15) + 1.164 * 10^{-5}(T - 273.15)^2 \quad (3.19)$$

The product term, κa_i , from Equation 4.8 was substituted by $BaI^{1/2}$ where a is a common ion size parameter substituting the individual distance of closest approach, a_i . The ion size parameter, a , is within the range 3.5 to 6.2×10^{-10} m (Thomsen, 2009). B is derived from the estimated value of κ in Equation 3.10:

$$B = \left(\frac{2e^2 N_A \rho_o}{\epsilon_0 \epsilon_r kT} \right)^{1/2} \quad (3.20)$$

Consequently, **the activity coefficient of ion** is calculated by an extended Deybe–Hückel, which is derived from the total Gibbs excess function by molar differentiation:

$$\left[\frac{\partial(nG_{DH}^E / RT)}{\partial n_i} \right]_{T,P,n_j,j \neq i} = -Z_i^2 \frac{A\sqrt{I}}{1 + Ba\sqrt{I}} \quad (3.21)$$

$$\ln \gamma_i^{DH} = -Z_i^2 \frac{A\sqrt{I}}{1 + Ba\sqrt{I}} \quad (3.22)$$

Equation 3.22 calculates the rational activity coefficient and it is not calculating the molal activity coefficient as some claimed (Thomsen, 2009). The definition of the molal activity coefficient is expressed as:

$$\ln \gamma_i^m = x_w \gamma_i^{DH} \quad (3.23)$$

Thus, the molal activity coefficient according to the extended Deybe–Hückel can be calculated from:

$$\ln \gamma_i^{DH} = \ln(x_w \gamma_i^{DH}) = \ln x_w - Z_i^2 \frac{A\sqrt{I}}{1 + Ba\sqrt{I}} \quad (3.24)$$

According to Thomsen (2009) and Gmehling et al. (2012), the mean molal activity coefficient of an electrolyte with cation (C) and anion (A) is defined as:

$$\ln \gamma_i^m = \left((\gamma_C^m)^{\nu_C} (\gamma_A^m)^{\nu_A} \right)^{1/\nu} \quad (3.25)$$

where ν is the sum of the stoichiometric coefficients, shown as:

$$V = V_C + V_A \quad (3.26)$$

The extended Deybe–Hückel mean molal activity coefficient for electrolytes from Equation 3.24 is:

$$\ln \gamma_i^{DHm} = \ln x_w - \frac{1}{\nu} \sum_i \nu_i Z_i^2 \frac{A\sqrt{I}}{1 + Ba\sqrt{I}} \quad (3.27)$$

$$\ln \gamma_i^{DHm} = \ln x_w - |Z_C Z_A| \frac{A\sqrt{I}}{1 + Ba\sqrt{I}} \quad (3.28)$$

where x_w is the mole fraction of water.

In addition, the activity coefficient of water, calculated using the extended Deybe–Hückel equation is given by:

$$\left[\frac{\partial (nG_{ExtendedDbye-Huckel}^E) / RT}{\partial n_w} \right]_{T,P,n_i} = \ln \gamma_w = \frac{2}{3} M_w A I^{3/2} \sigma \left(BaI^{1/2} \right) \quad (3.29)$$

where M_w is the molar mass of water:

$$\sigma(x) = \frac{3}{x^3} \left\{ 1 + x - \frac{1}{1+x} - 2 \ln(1+x) \right\} \quad (3.30)$$

Calculation of the activity coefficient of the solvent

According to Macedo et al. (1990); Lei et al. (2005); Gmehling et al. (2012), the Deybe–Hückel **solvent** activity coefficient can be calculated utilizing the following expression:

$$\ln \gamma_{solvent}^{DH} = \left[\frac{2AM_{solvent}\rho_{m-s}}{b^3 \rho_{solvent}} \right] \left[1 + b\sqrt{I} - \frac{1}{1+b\sqrt{I}} - 2 \ln(1+b\sqrt{I}) \right] \quad (3.31)$$

where Deybe–Hückel solvent parameters A and b can be calculated as follows:

$$A = \frac{1.327757 * 10^5 \rho_{m-s}^{0.5}}{(\epsilon T)^{1.5}} \quad (3.32)$$

and:

$$b = \frac{6.359696 \rho_{m-s}^{0.5}}{(\varepsilon T)^{0.5}} \quad (3.33)$$

where ρ_{m-s} is the mixed-solvent density or density of solution, which is calculated using Equation 3.13.

The dielectric constant, ε , for the binary mixture can be calculated using the Oster rule:

$$\varepsilon = \varepsilon_1 + \left[\frac{(\varepsilon_2 - 1)(2\varepsilon_2 - 1)}{2\varepsilon_2} - (\varepsilon_1 - 1) \right] \varphi_2 \quad (3.34)$$

where the index 1 is water and 2 is the other component.

For a multicomponent mixture, ε can be estimated as:

$$\varepsilon = \sum_{\text{solvent}} \varphi_{\text{solvent}} \varepsilon_{\text{solvent}} \quad (3.35)$$

Where φ_i is the volume fraction of the solvent I that can be defined as:

$$\varphi_i = \frac{V_i}{\sum_{\text{solvent}} V_j} \quad (3.36)$$

3.1.2 The middle range (MR) interaction term

The middle range (MR) contribution term takes into account the indirect effects of the charge interactions, which include charge-dipole, and charge-induced interactions to the excess Gibbs energy. The middle-range contribution term can be calculated using the LIQUAC model. The MR term is given by:

$$\frac{G_{MR}^E}{RT} = m_{\text{sol,kg}} \sum_i \sum_j B_{ij} m_i m_j \quad (3.37)$$

where B_{ij} is the interaction coefficient between species i and j (ion or molecule).

It is similar to the virial coefficient representing the indirect effects. In this model, B_{ij} represents all indirect effects caused by the charges, where the ionic strength dependence is described by following a simple expression:

$$B_{ij}(I) = b_{ij} + c_{ij} \exp(a_1 I^{0.5} + a_2 I) \quad (3.38)$$

where b_{ij} and c_{ij} are the adjustable MR interaction parameters between species i and j ($b_{ij} = b_{ji}$, $c_{ij} = c_{ji}$), a_1 and a_2 are empirical constant parameters, determined using the few reliable experimental data for electrolyte systems. (The adjustable MR interaction parameters are presented in Appendix B.)

The best values were obtained using equations 3.39 and 3.40:

$$B_{ion,ion} = b_{ion,ion} + c_{ion,ion} \exp(-I^{0.5} + 0.13I) \quad (3.39)$$

$$B_{ion,sol} = b_{ion,sol} + c_{ion,sol} \exp(-1.2I^{0.5} + 0.13I) \quad (3.40)$$

Equation 3.39 and 3.40 reveal that the ion-ion interactions are not the same as ion-solvent interactions. This is due to charge–charge and charge–induced dipole interactions between ions and charge–dipole interactions being between ion and molecule.

In the LIQUAC model the interactions between like-charges are negligible in the MR term, consequently, Equation 3.37 can be simplified to:

$$\frac{G_{MR}^E}{RT} = m_{sol,kg} \left[\sum_{sol} \sum_{ion} B_{sol,ion}(I) m_{sol} m_{ion} + \sum_c \sum_a B_{ca}(I) m_c m_a \right] \quad (3.41)$$

where c and a indices cover all cations and all anion, respectively.

Equations 3.42 and 3.43 are obtained by differentiating Equation 3.41 with respect to the number of moles of solvent and ions. Therefore, the activity coefficient of the MR term for the solvent and ions are calculated using the following equations:

$$\begin{aligned} \ln \gamma_{sol}^{MR} = & \sum_{ion} B_{sol,ion}(I) m_{ion} - \frac{M_{sol}}{M_m} \sum_{sol} \sum_{ion} [B_{sol,ion}(I) + IB'_{sol,ion}(I)] x'_{sol} m_{ion} \\ & - M_{sol} \sum_c \sum_a [B_{ca}(I) + IB'_{ca}(I)] m_c m_a \end{aligned} \quad (3.42)$$

$$\begin{aligned} \ln \gamma_j^{MR} = & \frac{\sum_{sol} B_{j,sol}(I) x_{sol}}{M_m} + \left[\frac{z_j^2}{2M_m} \right] \sum_{sol} \sum_{ion} B'_{sol,ion}(I) x'_{sol,ion} \\ & + \sum_a B_{j,a}(I) m_a + \left[\frac{z_j^2}{2} \right] \sum_c \sum_a B'_{ca}(I) m_c m_a - \frac{B_{j,sol}(I)}{M_{sol}} \end{aligned} \quad (3.43)$$

where x'_{sol} is the salt-free mole fraction; and M_m is molecular weight of mixed solvent calculated by Equation 3.45:

$$M_m = \sum x'_{sol} M_{sol} \quad (3.44)$$

$$B'_{ij}(I) = \frac{dB_{ij}(I)}{dI} \quad (3.45)$$

3.1.3 The short-range (SR) interaction term

The SR term contribution in the LIQUAC model involves the Combinatorial (C) and Residual (R) activity coefficient terms for the UNIQUAC model as given in:

$$\ln \gamma_i^{SR} = \ln \gamma_i^C + \ln \gamma_i^R \quad (3.46)$$

The Van der Waals surface areas and volumes are required for the calculation of the activity coefficient for the temperature-dependent combinatorial part only:

$$\ln \gamma_i^C = 1 - V_i + \ln V_i - 5q_i \left[1 - \frac{V_i}{F_i} + \ln \left(\frac{V_i}{F_i} \right) \right] \quad (3.47)$$

whereas, for the residual part the interaction parameters are essential, besides the surface area:

$$\ln \gamma_i^R = q_i \left[1 - \ln \frac{\sum_j q_j x_j \tau_{ij}}{\sum_j q_j x_j} - \sum_j \frac{q_j x_j \tau_{ij}}{\sum_k q_k x_k \tau_{kj}} \right] \quad (3.48)$$

where

$$V_i = \frac{r_i}{\sum_k r_k x_k} \quad (3.49)$$

$$F_i = \frac{q_i}{\sum_k q_k x_k} \quad (3.50)$$

where j and k cover all solvent and ions; r_i is the Van der Waals volumes; and q_i is the surface area of the solvent:

$$\tau_{ij} = \exp\left(-\frac{a_{ij}}{T}\right) \quad (3.51)$$

where a_{ij} is the UNIQUAC interaction parameters between species i and j , whereby a_{ij} is not the same as a_{ji} .

The final equation for the activity coefficient of the **solvent** is given by:

$$\ln \gamma_{sol} = \ln \gamma_{sol}^{LR} + \ln \gamma_{sol}^{MR} + \ln \gamma_{sol}^{SR} \quad (3.52)$$

where the activity coefficient is defined according to the mole fraction scale.

The activity coefficient of **ion** for the SR term has to be normalized to the infinite dilution reference state using the following relation:

$$\ln \gamma_{ion}^{SR} = \left(\ln \gamma_{ion}^C + \ln \gamma_{ion}^R\right) - \left(\ln \gamma_{ion}^{C,\infty} + \ln \gamma_{ion}^{R,\infty}\right) \quad (3.53)$$

For the combinatorial and the residual part of the UNIQUAC equation, one obtains the following expression for the values at infinite dilution:

$$\ln \gamma_{ion}^{C,\infty} = 1 - \frac{r_{ion}}{r_{sol}} + \ln\left(\frac{r_{ion}}{r_{sol}}\right) - 5q_{ion} \left[1 - \frac{r_{ion}q_{sol}}{r_{sol}q_{ion}} + \ln\left(\frac{r_{ion}q_{sol}}{r_{sol}q_{ion}}\right) \right] \quad (3.54)$$

$$\ln \gamma_{ion}^{R,\infty} = q_{ion} \left(1 - \ln \tau_{sol,ion} - \tau_{ion,sol} \right) \quad (3.55)$$

The final equation for the calculation of the activity coefficient of an **ion j** at the chosen standard state is given by:

$$\ln \gamma_j = \ln \gamma_j^{LR} + \ln \gamma_j^{MR} + \ln \gamma_j^{SR} - \ln \left[\frac{M_{sol}}{M_m} + M_{sol} \sum_{ion} m_{ion} \right] \quad (3.56)$$

3.1.4 The Born term

The Deybe–Hückel term must be corrected by means of the Born term. This term takes into account the difference between the dielectric constants of water and the solvent mixture (Austgen et al., 1989; Gmehling et al., 2012). A solvent made up of polar molecules is polarized and it is called a dielectric medium. Highly polarized solvents are highly permitted in relative terms.

In Equation (3.2), Coulomb's law showed that solvents with high relative permittivity reduce electrostatic interactions. Salts do not instinctively dissociate in a vacuum because the

electrostatic interactions between the ions are too strong. In water, the electrostatic interactions between ions are reduced by a factor $\epsilon_r = 78.4$ at 298.15 K. The water molecules protect the ions from each other and separate them. The relative permittivity of a solvent is expressed as the ratio between the permittivity of a solvent and a vacuum:

$$\epsilon_r = \frac{\epsilon}{\epsilon_0} \quad (3.57)$$

Due to the limitations of the Debye–Hückel theories in accounting for all the ion-related interactions. Many engineering models have been developed which contain additional terms associated with ionic interactions: (1) Born term (Born, 1920) and (2) a short-range ionic term.

The term Born describes the effect of ion solvation or hydration because solvent molecules are polarized by electrical charges when ions are dissolved in a dielectric medium (Thomsen, 2009). The Born term represents the extent of ion-solvent interactions or of the single ions, even when they do not interact at all (Kontogeorgis and Folas, 2010). Hydration is not the formation of ion hydrates of a particular stoichiometric composition, but the redirection of the polar water molecules around the charged ions.

The energy change associated with solvation is the solvation energy, or in the case of water it is called hydration energy. The Born term in Equation 3.39 has been used to calculate the energy to transfer an ion from a vacuum to a solvent with a dielectric constant. Equation 4.39 is an expression used for the change in total Helmholtz energy:

$$\Delta_{solv}A = \frac{Z_i^2 N_A e^2}{8\pi\epsilon_0 r_i} \left(\frac{1}{\epsilon_r} - 1 \right) \quad (3.58)$$

Gmehling et al. (2012) has recommended the value for the ionic radius to be $r_i = 3 \times 10^{-10}$ m. The Born term in Equation 4.40 has been used to calculate the activity coefficient for electrolyte solution:

$$\ln \gamma_i^{Born} = \frac{Z_i^2 N_A e^2}{8\pi\epsilon_0 R T r_i} \left(\frac{1}{\epsilon_{r,solv}} - \frac{1}{\epsilon_{r,H_2O}} \right) \quad (3.59)$$

The mixing rule of the dielectric constant is expressed as:

$$\epsilon_{r,solv} = \sum_i x_i \epsilon_i \quad (3.60)$$

The dielectric constant of the pure solvents is expressed as a function of temperature:

$$\varepsilon_i(T) = A + B \left(\frac{1}{T} - \frac{1}{298.15} \right) \quad (3.61)$$

where A and B are pure solvent constants, as presented in Table 3.2.

The Born term contributes to the activity coefficients because of the variation of the relative permittivity with pressure. In addition, it is also used for calculating the Gibbs energy transfer. On the other hand, Planche and Renon (1981) presented a short-range ionic term and it was derived from a non-primitive model for electrolyte systems.. It was used in the Fürst and Renon (1993) electrolyte EoS and in other electrolytes models (Kontogeorgis and Folas, 2010).

3.2. The Cubic-Plus-Association (CPA) equation of state (EoS)

The CPA EoS combines the classical Soave-Redlich-Kwong (SRK) EoS of 1972 with an additional term that takes into account the association. The CPA EoS was developed by Kontogeorgis et al. (1996), it was widely used in petroleum industries to describe the complex mixtures containing hydrocarbons and polar/association chemicals, including water, alcohols, glycols, esters and organic acids. The CPA EoS provides the following advantages (Kontogeorgis and Folas, 2010):

- Multi-component calculation results accurately using only the parameters estimated from binary data;
- It uses a modest mathematical formulation, but with a theoretical contextual in order to describe complex compounds;
- It reduces the classical SRK EoS as it provides a representation of hydrocarbon phase equilibria. SRK is considered satisfactory and successful to calculate the cubic EoS of petroleum fluids.

Kontogeorgis et al. (1996 and 1999) proposed CPA EoS for mixtures that can be expressed in terms of P as:

$$P = \frac{RT}{V_m - b} - \frac{a(T)}{V_m(V_m + b)} - \frac{1}{2} \frac{RT}{V_m} \left(1 + \rho \frac{\partial \ln g}{\partial \rho} \right) \sum_i x_i \sum_{A_i} (1 - X_{A_i}) \quad (3.72)$$

where ρ is the molar density and V_m is molar volume:

$$\rho = \frac{1}{V_m} \quad (3.73)$$

$$V_m = \frac{ZRT}{P} \quad \text{or} \quad V_m = \frac{M_{\text{solvent}}}{\rho_{\text{solvent}}} \quad (3.74)$$

where Z is the compressibility factor obtained from a Peng-Robinson (PR) EoS and M is the molecular mass of pure solvent.

The important element of the association term is X_{A_i} , which represents the fractions of site A on molecule i that do not form bonds with other active sites; and x_i is the mole fraction of component i . The X_{A_i} is related to the association strength, $\Delta^{A_i B_j}$, between two sites belonging to two different molecules, which include site A on molecule i and site B on molecule j . X_{A_i} was determined from:

$$X_{A_i} = \frac{1}{1 + \frac{1}{V_m} \sum_j x_j \sum_{B_j} X_{B_j} \Delta^{A_i B_j}} \quad (3.75)$$

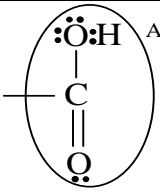
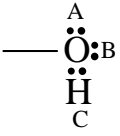
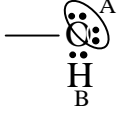
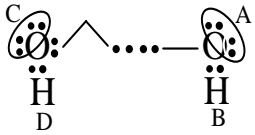
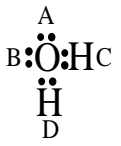
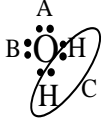
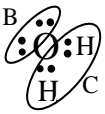
$$\rho \frac{\partial \ln g}{\partial \rho} = \frac{1.9\eta}{1 - 1.9\eta} \quad (3.76)$$

where the association strength $\Delta^{A_i B_j}$ can be expressed as:

$$\Delta^{A_i B_j} = g(\rho) \left[\exp\left(\frac{\varepsilon^{A_i B_j}}{RT}\right) - 1 \right] b_{ij} \beta^{A_i B_j} \quad (3.77)$$

The association strength of CPA is dependent on the choice of association scheme. Table 3.4 presents the number and type of association sites for the compound. According to Haghighi et al. (2009) the association scheme and maximum number of association sites can be determined by checking, at the location, its constituting hydrogen atoms and lone pairs on proton acceptor atoms (oxygen for water molecules). Huang and Radosz, (1990) have classified eight different association schemes. These association schemes can be applied to different molecules depending on the number and type of associating sites.

Table 3. 4: Schematic of association schemes (Huang and Radosz, 1990)

Species	Formula	Type	Site fraction (X)
Acids		1A	$X_1 = X_A$
Alcohols		3B	$X_A = X_B; X_C = 2X_A - 1$ $X_1 = X_A X_B X_C$
		2B	$X_A = X_B$ $X_1 = X_A X_B$
Glycols		4C	$X_A = X_B = X_C = X_D$ $X_1 = X_A X_B X_C X_D$
Water		4C	$X_A = X_B = X_C = X_D$ $X_1 = X_A X_B X_C X_D$
		3B	$X_A = X_B; X_C = 2X_A - 1$ $X_1 = X_A X_B X_C$
		3B ^a	$X_A = X_B; X_C = 2X_A - 1$ $X_1 = X_A X_B X_C$
		2B	$X_A = X_B$ $X_1 = X_A X_B$

^aAssuming one proton donor and two proton acceptors for water results in the same mathematical expression as if two proton donors and one proton acceptor

The one site (1A) scheme in Table 3.4 is used for acids based on the assumption that the site behaves as a glue spot. The site can be able to bond with a lone pair of electrons of an H atom or a site of the same type. For alcohols and amines, two-site (2B) or three-site (3B) systems are used. In the formalism of 3B for alcohol, sites A and B correspond to oxygen lone pairs, while site C corresponds to an H atom.

Due to the asymmetry of the association, the fraction of non-bonded H atoms (X_C) is not equal to the fraction of non-bonded lone pairs (X_A or X_B). In the 2B formalism, the two lone pairs for oxygen are taken as a single site (Kontogeorgis et al., 2006). The association scheme for four sites (4C) is used for highly hydrogen-bonded substances including water and glycols. These substances have two proton donors and two proton acceptors (Kontogeorgis et al., 2006).

The selection of association scheme is based on the key component. Water is a key component of all investigated systems in this study. Thus, the four-site (4C) association scheme was selected to be used in this study (Kontogeorgis et al., 2006). This type of association scheme is traditionally used for water within the CPA framework (Kontogeorgis et al., 1999; Voutas et al., 1999, 2000; Dewari et al., 2003; Folas, 2006). In the 4C formalism, the bonding arrangement means that all non-bonded site fractions are equal (Folas, 2006).

In all cases, the fraction of monomers (completely non-bonded molecules, X_1) is equal to the product of the fractions of all non-bonded site types (Folas, 2006; Kontogeorgis et al., (2006). In the case where bonding is symmetrical (2B and 4C), the fraction of non-bonded sites is assumed to be equal for all types of site (Folas, 2006).

In this study water is the only associating compound (self-association), consequently, this significantly simplifies Equation 3.75 as the sum is removed, and the expression becomes:

$$X_A = \frac{1}{1 + \frac{1}{V_m} x_w \sum X_B \Delta^{AB}} \quad (3.78)$$

As indicated in Table 3.4, $X_A = X_B = X_C = X_D$. This information is used when solving Equation 3.78. In the case where site A and B are positive sites, and site C and D are negative sites (Kontogeorgis and Folas, 2010), the expression becomes:

$$\Delta^{AA} = \Delta^{BB} = \Delta^{CC} = \Delta^{DD} = \Delta^{AB} = \Delta^{AD} = 0 \quad (3.79)$$

whereas,

$$\Delta^{AC} = \Delta^{AD} = \Delta^{BC} = \Delta^{BD} \neq 0 \quad (3.80)$$

Then, the expression in Equation 4.78 becomes:

$$X_A = \frac{1}{1 + \frac{1}{V_m} x_w (X_C \Delta^{AC} + X_D \Delta^{AD})} \quad (3.81)$$

The same equation for solving X_B , where there is simply replacement of A with B, becomes:

$$\Delta^{AC} = \Delta^w = g(\rho) \left[\exp\left(\frac{\varepsilon^w}{RT}\right) - 1 \right] b_w \beta^w \quad (3.82)$$

By introducing $X_A = X_B = X_C = X_D$ and Equation 3.81, site A (X_A) molecule i expression becomes:

$$X_A = \frac{1}{1 + \frac{1}{V_m} x_w (X_A \Delta^w)} \quad (3.83)$$

According to Kontogeorgis and Folas (2010), the solution of Equation 3.83 becomes:

$$X_A = \frac{-1 + \sqrt{1 + \left(\frac{8}{V_m}\right) x_w \Delta^w}}{\left(\frac{4}{V_m}\right) \Delta^w} \quad (3.84)$$

Equation 3.83 can be rewriting as follow in terms of molar density:

$$X_A = \frac{-1 + \sqrt{1 + 8\rho x_w \Delta^w}}{4\rho \Delta^w} \quad (3.85)$$

From Equation 3.82, the radial distribution function is:

$$g(\rho) = \frac{1}{1 - 1.9\eta} \quad (3.86)$$

The packing factor can be expressed as:

$$\eta = 0.25b\rho \quad (3.87)$$

where ρ is the fluid density.

The cross-association energy is:

$$\varepsilon^{A_i B_j} = \frac{\varepsilon_{A_i} + \varepsilon_{B_j}}{2} \quad (3.88)$$

The cross-association volume parameters are:

$$\beta^{A_i B_j} = \sqrt{\beta^{A_i B_i} \beta^{A_j B_j}} \quad (3.89)$$

Table 3. 5: CPA parameters for associating compound (pure water)

(Kontogeorgis et al., 1999, 2006; Kontogeorgis and Folas, 2010)

Compound	b (L.mol ⁻¹)	a_0 (bar.L ² mol ⁻²)	c_1	ε (bar.L.mol ⁻¹)	β	ε/k_B (K)
Water	1.4515	0.12277	0.6736	16655	69200	2003.25

Table 3.5 presents the CPA cross-association energy and volume parameters for water only. It also presents the energy parameter of the EoS, given by a Soave type temperature dependency, while b is temperature independent.

In terms of critical temperature and critical pressure for component i :

$$a(T) = a_o \left[1 + c_1 \left(1 - \sqrt{\frac{T}{T_c}} \right) \right]^2 \quad (3.90)$$

$$a_o = 0.42747 \frac{R^2 T_c^2}{P_c} \quad (3.91)$$

$$b = 0.08664 \frac{R T_c}{P_c} \quad (3.92)$$

Parameter c_1 can be connected directly with the acentric factor of the related compounds:

$$c_1 = 0.480 + 1.574\omega_i - 0.176\omega_i^2 \quad (3.93)$$

The Van der Waals one-fluid-mixing rules are given by the following expression:

$$a_m = \sum_{i=1}^n \sum_{j=1}^n x_i x_j a_{ij} = x_i^2 a_{ii} + x_j^2 a_{jj} + 2x_i x_j a_{ij} \quad (3.94)$$

where:

$$a_{ij} = \sqrt{a_i a_j} (1 - k_{ij}) \quad (3.95)$$

$$b_m = \sum_{i=1}^n \sum_{j=1}^n x_i x_j b_{ij} = x_i^2 b_{ii} + x_j^2 b_{jj} + 2x_i x_j b_{ij} \quad (3.96)$$

The co-volume parameter, b , is assumed to be temperature independent:

$$b_{ij} = \frac{b_i + b_j}{2} (1 - l_{ij}) \quad (3.97)$$

In the case where $l_{ij} = 0$, the mixing rule for the co-volume parameter is simplified to:

$$b = \sum_{i=1}^n x_i b_i \quad (3.98)$$

3.2.1 Calculation of fugacity coefficients with CPA EoS

This section presents all the equations necessary to calculate the CPA EoS fugacity coefficient.

The fugacity coefficient, ϕ_i , of a component, i , in a mixture is given by:

$$RT \ln \phi_i = \left(\frac{\partial A^r}{\partial n_i} \right)_{T,V,n_j} - RT \ln Z \quad (3.99)$$

where A^r is the residual Helmholtz energy for the mixture and Z is the compressibility factor, defined as:

$$Z = \frac{PV}{nRT} \quad (3.100)$$

The CPA EoS combines the SRK EoS with the association term, derived from Wertheim's first order perturbation theory (Kontogeorgis and Folas, 2010), hence:

$$A^r(T, P, n) = A_{SRK}^r(T, P, n) + A_{ass}^r(T, P, n) \quad (3.101)$$

The fugacity coefficient for the SRK term can be determine using Equation 3.102 (Michelsen and Mollerup, 2007):

$$\frac{A_{SRK}^r(T, P, n)}{RT} = -n \ln \left(1 - \frac{B}{V} \right) - \frac{D(T)}{RTB} \ln \left(1 + \frac{B}{V} \right) \quad (3.102)$$

where V is the total volume of the system, while:

$$nB = n^2 b = \sum_i n_i \sum_i n_j b_{ij} \quad (3.103)$$

$$D(T) = n^2 \alpha = \sum_i n_i \sum_i n_j \alpha_{ij}(T) \quad (3.104)$$

$$n = \sum_i n_i \quad (3.105)$$

According to Michelsen and Mollerup (2007), $D(T)$ is used instead of $\alpha(T)$ for consistency. The energy, $\alpha(T)$, and co-volume parameter b are determined using the classical Van der Waals one-fluid-mixing rule as follows:

$$\alpha_{ij}(T) = \sqrt{\alpha_i(T)\alpha_j(T)}(1 - k_{ij}) \quad (3.106)$$

$$b_{ij} = b_{ji} = 0.5(b_{ii} + b_{jj}) \quad (3.107)$$

Equation 3.105 and Equation 3.107 reduces to:

$$B = \sum_i n_i b_{ii} \quad (3.108)$$

Assuming that:

$$\frac{A_{SRK}^r(T, V, n)}{RT} = -n \ln \left(1 - \frac{B}{V} \right) - \frac{D(T)}{RTB} \ln \left(1 + \frac{B}{V} \right) = F^{SRK} \quad (3.109)$$

$$g(V, B) = \ln \left(1 - \frac{B}{V} \right) \quad (3.110)$$

$$f(V, B) = \frac{1}{RB} \ln \left(1 + \frac{B}{V} \right) \quad (3.111)$$

By substitution of Equation 3.110 and 3.111 into Equation 3.109, the expression for F^{SRK} becomes:

$$F^{SRK} = ng(V, B) - \frac{D(T)}{T} f(V, B) \quad (3.112)$$

Consequently, the calculation of the fugacity coefficient, ϕ_i , of a component, i , for the SRK term in Equation 3.99, the derivative of the function F^{SRK} is required:

$$\left(\frac{\partial F^{SRK}}{\partial n_i} \right)_{T, V, n_j} = F_n + F_B B_i + F_D D_i \quad (3.113)$$

where:

$$F_n = -g = -\ln \left(1 - \frac{B}{V} \right) \quad (3.114)$$

$$F_B = -ng_B - \frac{D(T)}{T} f_B \quad (3.115)$$

$$g_B = -\frac{1}{V - B} \quad (3.116)$$

$$f_B = -\frac{f + Vf_V}{B} \quad (3.117)$$

$$f_V = -\frac{1}{R(V + B)} \quad (3.118)$$

$$F_D = -\frac{f}{T} \quad (3.119)$$

where B_i and D_i are the composition derivatives of the energy term in Equation 3.104 and the co-volume term in Equation 3.108, given by the following equations:

$$B_i = \frac{2 \sum_j n_j b_{ij} - B}{n} \quad (3.120)$$

$$D_i = 2 \sum_j n_j \alpha_{ij} \quad (3.121)$$

Therefore, the fugacity from CPA is:

$$f_i^\alpha = x_i \phi_i^{SRK} P \quad (3.122)$$

where α can be a vapour or liquid.

3.2.2 Calculation of fugacity coefficients for the association term of the CPA EoS

Michelsen and Mollerup (2007) proposed a method for estimating the contribution of residual Helmholtz energy for the association term, $A_{ass}^r(T, P, n)$. The Q function was introduced in order to calculate the derived properties of the association term. Because the benefit of the association's contribution to Helmholtz energy itself is the result of a reduction. By considering the Q function, the following expression is derived:

$$Q(n, T, V, X) = \sum_i n_i \sum_{A_i} (\ln X_{A_i} - X_{A_i} + 1) - \frac{1}{2V} \sum_i \sum_j n_i n_j \sum_{A_i} \sum_{B_j} X_{A_i} X_{B_j} \Delta^{A_i B_j} \quad (3.123)$$

where X_{A_i} presents the fraction of A-sites on molecule, i , that do not form bonds with other active sites; n presents the total composition of the mixture; and V presents is the total volume. The association contribution of the CPA EoS equals the value of Q at a stationary point (sp), with respect to the site fractions, X . At a stationary point, the following conditions are applied:

$$\frac{\partial Q}{\partial X_{A_i}} = 0, \text{ for all sites}$$

By differentiating Equation 3.123:

$$n_i \left(\frac{1}{X_{A_i}} - 1 \right) - \frac{1}{V} n_i \sum_j n_j \sum_{B_j} X_{B_j} \Delta^{A_i B_j} = 0 \quad (3.124)$$

Equation 3.124 yields to:

$$\frac{1}{X_{A_i}} = 1 + \frac{1}{V} \sum_j n_j \sum_{B_j} X_{B_j} \Delta^{A_i B_j} \quad (3.125)$$

The value of Q at a stationary point is:

$$Q_{sp} = \sum_i n_i \sum_{A_i} (\ln X_{A_i} - X_{A_i} + 1) - \frac{1}{2} \sum_i n_i \sum_{A_i} X_{A_i} \left(\frac{1}{V} \sum_j n_j \sum_{B_j} X_{B_j} \Delta^{A_i B_j} \right) \quad (3.126)$$

$$Q_{sp} = \sum_i n_i \sum_{A_i} (\ln X_{A_i} - X_{A_i} + 1) - \frac{1}{2} \sum_i n_i \sum_{A_i} X_{A_i} \left(\frac{1}{X_{A_i}} - 1 \right) \quad (3.127)$$

$$Q_{sp} = \sum_i n_i \sum_{A_i} \left(\ln X_{A_i} - \frac{1}{2} X_{A_i} + \frac{1}{2} \right) = \frac{A_{ass}^r(T, P, n)}{RT} \quad (3.128)$$

The calculation of the fugacity coefficient from the association term is performed by using the chain rule (Kontogeorgis and Folas, 2010). According to the chain rule the derivative of Q_{sp} with respect to n_i is given by Equation 3.129:

$$\frac{\partial Q_{sp}}{\partial n_i} = \frac{\partial Q}{\partial n_i} \Big|_X + \sum_i \sum_{A_i} \frac{\partial Q}{\partial X_{A_i}} \frac{\partial X_{A_i}}{\partial n_i} \quad (3.129)$$

At the stationary point, the derivatives $\frac{\partial Q}{\partial X_{A_i}}$ are by definition zero, meaning that the fugacity coefficient for the association term can now be calculated using the explicit derivative of Q with respect to n_i as follows:

$$\begin{aligned} \frac{\partial}{\partial n_i} \left(\frac{A_{ass}^r}{RT} \right)_{T,P,n_j} &= \frac{\partial}{\partial n_i} \left(\sum_i n_i \sum_{A_i} (\ln X_{A_i} - X_{A_i} + 1) - \frac{1}{2} \sum_i n_i \sum_{A_i} X_{A_i} \left(\frac{1}{V} \sum_j n_j \sum_{B_j} X_{B_j} \Delta^{A_i B_j} \right) \right)_{T,P,n_j} = \\ &= \sum_{A_i} (\ln X_{A_i} - X_{A_i} + 1) - \frac{1}{2V} \frac{\partial}{\partial n_i} \left(\sum_i \sum_j n_i n_j \sum_{A_i} \sum_{B_j} X_{A_i} X_{B_j} \Delta^{A_i B_j} \right) - \frac{1}{2V} \left(\sum_i \sum_j n_i n_j \sum_{A_i} \sum_{B_j} X_{A_i} X_{B_j} \frac{\partial \Delta^{A_i B_j}}{\partial n_i} \right) = \\ &= \sum_{A_i} (\ln X_{A_i} - X_{A_i} + 1) - \frac{2}{2V} \sum_j n_j \sum_{A_i} \sum_{B_j} X_{A_i} X_{B_j} \Delta^{A_i B_j} - \frac{1}{2V} \left(\sum_i \sum_j n_i n_j \sum_{A_i} \sum_{B_j} X_{A_i} X_{B_j} \frac{\partial \Delta^{A_i B_j}}{\partial n_i} \right) \end{aligned} \quad (3.130)$$

The above equation combined with Equation 3.125, which yields:

$$\begin{aligned} \frac{\partial}{\partial n_i} \left(\frac{A_{ass}^r}{RT} \right)_{T,P,n_j} &= \sum_{A_i} (\ln X_{A_i} - X_{A_i} + 1) - \sum_{A_i} X_{A_i} \left(\frac{1}{X_{A_i}} - 1 \right) - \frac{1}{2V} \left(\sum_i \sum_j n_i n_j \sum_{A_i} \sum_{B_j} X_{A_i} X_{B_j} \frac{\partial \Delta^{A_i B_j}}{\partial n_i} \right) = \\ & \sum_{A_i} \ln X_{A_i} - \frac{1}{2V} \left(\sum_i \sum_j n_i n_j \sum_{A_i} \sum_{B_j} X_{A_i} X_{B_j} \frac{\partial \Delta^{A_i B_j}}{\partial n_i} \right) \end{aligned} \quad (3.131)$$

For the calculation of the derivative, $\frac{\partial \Delta^{A_i B_j}}{\partial n_i}$, one has to consider that for CPA the function of the cross-association strength is given by:

$$\Delta^{A_i B_j} = g \left(\frac{1}{V_m} \right)^{ref} \left[\exp \left(\frac{\varepsilon^{A_i B_j}}{RT} \right) - 1 \right] b_{ij} \beta^{A_i B_j} = g(n, V) \lambda(T) \quad (3.132)$$

Hence the derivative can be calculated as follows:

$$\frac{\partial \Delta^{A_i B_j}}{\partial n_i} = \frac{\partial g}{\partial n_i} \lambda = \frac{\partial \ln g}{\partial n_i} g \lambda = \Delta^{A_i B_j} \frac{\partial \ln g}{\partial n_i} \quad (3.133)$$

Therefore:

$$\frac{\partial}{\partial n_i} \left(\frac{A_{ass}^r}{RT} \right)_{T,P,n_j} = \sum_{A_i} \ln X_{A_i} - \frac{1}{2V} \left(\sum_i \sum_j n_i n_j \sum_{A_i} \sum_{B_j} X_{A_i} X_{B_j} \frac{\partial \Delta^{A_i B_j}}{\partial n_i} \right) \quad (3.134)$$

By combining Equation 3.134 with Equation 3.125, the resulting equation is given as:

$$\frac{\partial}{\partial n_i} \left(\frac{A_{ass}^r}{RT} \right)_{T,P,n_j} = \sum_{A_i} \ln X_{A_i} - \frac{1}{2} \sum_i n_i \sum_{A_i} (1 - X_{A_i}) \frac{\partial \ln g}{\partial n_i} \quad (3.135)$$

Finally, the calculation of the association term contribution, the derivative of g with regard to the mole number, n_i is required, given that for the CPA EoS:

$$g(V, n) = \frac{1}{1 - 1.9\eta}, \text{ where } \eta = \frac{B}{4V} \quad (3.136)$$

Equation 3.108 gives B:

$$\frac{\partial g}{\partial n_i} = \frac{\partial g}{\partial B} B_i, \quad (3.137)$$

where B_i can be calculated from Equation 3.120, while:

$$\frac{\partial g}{\partial B} = 0.475V \left(\frac{1}{V - 0.475B} \right)^2 \quad (3.138)$$

3.2.3 Calculation of the volume

Michelsen and Mollerup (2007) calculated the total volume using a Newton-Raphson iteration approach. The volume was utilized for the calculation of the fugacity coefficient, ϕ_i , of a component, i , in the mixture. The capacity corresponding to a specific pressure, temperature and mixture composition can be calculated from the pressure equation:

$$P = \frac{nRT}{V} - \left(\frac{\partial A^r}{\partial V} \right)_{T,n} = \frac{nRT}{V} - \left(\frac{\partial A_{SRK}^r}{\partial V} \right)_{T,n} - \left(\frac{\partial A_{ass}^r}{\partial V} \right)_{T,n} \quad (3.139)$$

From Equation 3.109 the expression of the SRK term is:

$$\left(\frac{\partial A_{SRK}^r}{\partial V} \right)_{T,n} = RT \left(\frac{\partial F^{SRK}}{\partial V} \right) \quad (3.140)$$

From Equations 3.126, 3.127 and 3.128 the expression of the association term is:

$$\left(\frac{\partial A_{ass}^r}{\partial V} \right)_{T,n} = RT \left(\frac{\partial Q_{sp}}{\partial V} \right)_{T,n} \quad (.141)$$

By substituting Equation 3.140 and 3.141 into Equation 3.139, the pressure equation becomes:

$$P = \frac{nRT}{V} - RT \left(\frac{\partial F^{SRK}}{\partial V} \right)_{T,n} - RT \left(\frac{\partial Q_{sp}}{\partial V} \right)_{T,n} \quad (3.142)$$

According Michelsen and Mollerup (2007) the following equations are for the estimation of the contribution of the physical term:

$$\left(\frac{\partial F^{SRK}}{\partial V} \right)_{T,n} = F_V \quad (3.143)$$

$$F_V = -ng_V - \frac{D(T)}{T} f_V \quad (3.144)$$

$$g_V = -\frac{B}{V(V-B)} \quad (3.145)$$

$$f_V = -\frac{1}{RV(V+B)} \quad (3.146)$$

Michelsen and Mollerup, (2007) showed that the Q function, presented before and the chain rule, give rise to:

$$\left(\frac{\partial Q_{sp}}{\partial V}\right) = \left(\frac{\partial Q}{\partial V}\right)_X + \sum_i \sum_{A_i} \frac{\partial Q}{\partial X_{A_i}} \frac{\partial X_{A_i}}{\partial V}, \quad (3.147)$$

the derivative, $\left(\frac{\partial Q_{sp}}{\partial V}\right)$, is given by:

$$\left(\frac{\partial Q_{sp}}{\partial V}\right) = \frac{1}{2V} \left(1 - V \left(\frac{\partial \ln g}{\partial V}\right)\right) \sum_i n_i \sum_{A_i} (1 - X_{A_i}) \quad (3.148)$$

By taking into account Equation 3.136, the required derivative $\left(\frac{\partial \ln g}{\partial V}\right)$ for the calculation of the contribution of the association term is given by:

$$\frac{\partial g}{\partial V} = -0.475B \left(\frac{1}{V - 0.475B}\right)^2 \quad (3.149)$$

For a Newton-Raphson variant to calculate the total volume V , Equation 3.142 gives the function to be minimized as follows:

$$H(V) = P - \left[\frac{nRT}{V} - \left(\frac{\partial A^r}{\partial V}\right)_{T,n} = \frac{nRT}{V} - \left(\frac{\partial A_{SRK}^r}{\partial V}\right)_{T,n} - \left(\frac{\partial A_{ass}^r}{\partial V}\right)_{T,n} \right] \quad (3.150)$$

The derivative of the volume function $H(V)$ is also required, which means that second volume derivatives of A^r are necessary. The second derivative, however, can be numerically calculated from equation 3.150. An analytical method to estimate the second derivatives is therefore not necessary or required (Michelsen and Mollerup, 2007; Konteorgis and Folas, 2010).

3.3 Modeling of hydrate phase

Some researchers have modified the Van der Waals and Plateeuw (1959) model to minimize the error between the experimental and predicted H-L_w-V equilibrium data. The modified models are simple and applicable for industrial purposes. The following is a list of researchers who modified the fundamental model of Van der Waals and Plateeuw, (1959), so that it can be utilized to predict hydrate dissociation data:

- Parrish and Prausnitz (1972)
- Ng and Robinson (1980)
- Dharmawardhana et al. (1980)
- Holder and Grigoriou (1980)
- Sloan et al. (1987)
- Chen and Guo (1998)
- Mohammadi and Richon (2008)
- Eslamimanesh et al. (2011).

A combination of the Eslamimanesh et al. (2011) and CPA EoS were selected to be studied to model a hydrate phase. This model is very simple and is able to predict reliable results with a relatively small absolute average deviation (AAD).

The liquid water-hydrate-vapour (L_w-H-V) system in equilibrium balance conditions can be calculated by equating the water fugacity in the liquid water phase, f_w^L , and hydrate phase, f_w^H , ignoring water content of the gas/vapour phase (Sloan and Koh, 2008; Mohammadi et al., 2008; Mohammadi and Richon, 2009; Tumba et al., 2011):

$$f_w^L = f_w^H \quad (3.151)$$

The fugacity of water in the hydrate phase, f_w^H , by means of the following equation 3.152, is associated to the chemical potential difference of water in the filled and empty hydrate cage.

$$f_w^H = f_w^{MT} \exp \frac{\mu_w^H - \mu_w^{MT}}{RT} \quad (3.152)$$

where f_w^{MT} present the water fugacity in the hypothetical empty hydrate phase; $\mu_w^H - \mu_w^{MT}$ presents the chemical potential of water in the filled (μ_w^H) and empty (μ_w^{MT}) hydrate; and R and T present the universal gas constant and temperature, respectively.

The solid solution theory of Van der Waals and Platteeuw, (1959) can be utilized for calculating

$$\frac{\mu_w^H - \mu_w^{MT}}{RT} \quad (\text{Mohammadi et al., 2008; Mohammadi and Richon, 2009; Tumba et al., 2011;}$$

Eslamimanesh et al., 2011):

$$\frac{\mu_w^H - \mu_w^{MT}}{RT} = -\sum_i v'_i \ln\left(1 + \sum_j C_{ij} f_j\right) = \sum_i \ln\left(1 + \sum_j C_{ij} f_j\right)^{-v'_i} \quad (3.153)$$

where v'_i is the number of cavities of type i per water molecule in a unit hydrate cell (Eslamimanesh et al., 2011); and f_j is the fugacity of refrigerants which was obtained from the CPA EoS.

From Equation 3.153, C_{ij} presents the Langmuir constant, which describes the interaction between the former structures. This interaction varies between the cavities (Mohammadi et al., 2008; Mohammadi and Richon, 2009; Tumba et al., 2011; Eslamimanesh et al., 2011). Consequently, Eslamimanesh et al. (2011), proposed the expression for the fugacity of water in the hypothetical empty hydrate phase to be as follow:

$$f_w^{MT} = P_w^{MT} \phi_w^{MT} \exp \int_{P_w^{MT}}^P \frac{v_w^{MT}}{RT} dP \quad (3.154)$$

where P_w^{MT} present the vapour pressure of the empty hydrate lattice, ϕ_w^{MT} present the correction for the deviation of the saturated vapour of pure lattice from ideal behaviour, and v_w^{MT} present the partial molar volume of water in the empty hydrate (Eslamimanesh et al., 2011). The exponential term is the Poynting correction term.

Eslamimanesh et al. (2011) made two assumptions in Equation (3.154):

- (1) The partial molar volume of hydrate is equal to the molar volume and independent of the pressure.

(2) P_w^{MT} is quite small (in the order of 10^{-3} MPa), hence, the fugacity coefficient, ϕ_w^{MT} , of water vapour over empty hydrate phase is set to unity.

Therefore, Equation (3.154) can be simplified:

$$f_w^{MT} = P_w^{MT} \exp \frac{v_w^{MT}(P - P_w^{MT})}{RT} \quad (3.155)$$

By the substitution of Equation (3.155) into Equation (3.152), the fugacity of water in the hydrate phase can be expressed as:

$$f_w^H = P_w^{MT} \exp \left[\frac{v_w^{MT}(P - P_w^{MT})}{RT} \right] \ln \left[\left(1 + C_{small} f_{refrigerant}^V \right)^{-v'_{small}} * \left(1 + C_{large} f_{refrigerant}^V \right)^{-v'_{large}} \right] \quad (3.156)$$

where the subscripts *small* and *large* refer to the small and large cavities, respectively. The $f_{refrigerant}^V$ was the fugacity of the hydrate former in the vapour phase obtained from the CPA EoS.

It was assumed that Equation 3.156 is valid for all temperatures and pressures. In addition, it is not limited in an ice region and it does not influence the overall performance of the hydrate model (Kontogeorgis and Folas, 2010). The Poynting correction term can be taken into account in the calculation if the dissociation pressure is greater than 2 MPa (Eslamimanesh et al., 2011). It is set to a unity when the Poynting correction term is less than 2 MPa, then the fugacity of water in the hydrate phase in Equation 3.156 can be simplified to:

$$f_w^H = P_w^{MT} \ln \left[\left(1 + C_{small} P \right)^{-v'_{small}} * \left(1 + C_{large} P \right)^{-v'_{large}} \right] \quad (3.158)$$

The fugacity of water in the liquid water phase can be expressed by (Poling et al., 2001; Mohammadi and Richon, 2008 and 2009; Eslamimanesh et al., 2011):

$$f_w^L = x_w^L \gamma_w^L P_w^{sat} \quad (3.159)$$

where x_w^L and γ_w^L are the water mole fraction and the activity coefficient of water in the liquid phase, respectively. At intermediate pressure ranges, liquid water is not compressible, the solubility of the hydrate former is low, and the activity coefficient is equal to unity. At higher pressures, the activity coefficient is not equal to a unity because of the solubility of the

refrigerant and the non-ideality of the liquid water phase (Poling et al., 2001; Mohammadi and Richon, 2008, and 2009; Eslamimanesh et al., 2011).

Therefore, Equation 3.159 becomes:

$$f_w^L = P_w^{sat} \quad (3.160)$$

Eslamimanesh et al. (2011) assumed that the vapour phase (refrigerant) is an ideal gas to use as a hydrate former. Consequently, it was concluded that $f_{refrigerant}^v = P$ as presented in Equation 3.156. By the substitution of Equation 3.160, at low to intermediate pressures, into Equation 3.151, and then into Equation 3.158, the following expression is yielded:

$$P_w^{sat} = P_w^{MT} \ln \left[(1 + C_{small} P)^{-v'_{small}} * (1 + C_{large} P)^{-v'_{large}} \right] \quad (3.161)$$

The following expressions are obtained for calculating the dissociation conditions for gas hydrates of hydrate formers for liquid water-hydrate-vapour equilibrium:

$$1 - \left(\frac{P_w^{MT}}{P_w^{sat}} \right) \left[(1 + C_{small} P)^{-v'_{small}} * (1 + C_{large} P)^{-v'_{large}} \right] = 0 \quad (3.162)$$

For ice-hydrate-vapour equilibrium:

$$1 - \left(\frac{P_w^{MT}}{P_I^{sat}} \right) \left[(1 + C_{small} P)^{-v'_{small}} * (1 + C_{large} P)^{-v'_{large}} \right] = 0 \quad (3.163)$$

where subscript I is ice.

Equations 3.162 and 3.163 allow for the easy calculation of the equilibrium pressures of gas hydrates of the refrigerant at liquid or ice. The advantages of the Eslamimanesh et al. (2011) model are:

- (1) The availability of input data;
- (2) The calculation is simple as it can be done on an Excel spreadsheet.

3.3.1 Model parameters

The vapour pressure of the empty hydrate lattice, P_w^{MT} is calculated by equating the water fugacity in the hydrate phase with pure ice in the three-phase line. Dharmawardhan et al. 1980) achieved the following vapour pressure equation of the empty hydrate structure (Mohammadi et al., 2008; Mohammadi and Richon, 2009; Tumba et al., 2011; Eslamimanesh et al., 2011).

For structure I:

$$P_w^{MT} = 0.1 \exp\left(17.440 - \frac{6003.9}{T}\right) \quad (3.164)$$

and for structure II:

$$P_w^{MT} = 0.1 \exp\left(17.332 - \frac{6017.6}{T}\right) \quad (3.166)$$

where P_w^{MT} present in MPa and T is in K.

The saturation pressure of water/ice is calculated using Equations 3.167 and 3.168 (Daubert and Danner, 1985). Equation 3.167 is used for systems at temperatures below 273.15 K (Tohidi-Kalorazi, 1995; Mohammadi et al., 2004; Eslamimanesh et al., 2011):

$$P_w^{sat} = 10^{-6} \exp\left(73.649 - \frac{7258.2}{T - 7.3037 \ln(T) + 4.1653 * 10^{-6} T^2}\right) \quad (3.167)$$

where P_w^{sat} is the saturation pressure of water in MPa. Equation 3.168 is used for systems at temperatures above 273.15 K:

$$P_I^{sat} = \frac{\left[10^{\left(\frac{-1032558}{T+51.0561 \log(T)} - 0.0977T + 7.0357 \cdot 10^{-5} T^2 - 98.512\right)}\right]}{7600} \quad (3.168)$$

where P_I^{sat} is the saturation pressure of ice in MPa.

Sloan and Koh (2008), Eslamimanesh et al. (2011), Mohammadi et al. (2008) and Mohammadi and Richon, (2009) used the following values in Equations 3.169 and 3.170 for the number of cavities of type i per water molecule in the unit hydrate cell (v_i').

For structure I of the gas hydrate:

$$v'_{small} = \frac{1}{23} \quad \text{and} \quad v'_{large} = \frac{3}{23} \quad (3.169)$$

For structure II of the gas hydrate:

$$v'_{small} = \frac{2}{17} \quad \text{and} \quad v'_{large} = \frac{1}{17} \quad (3.170)$$

3.3.2 The Langmuir constants

The Langmuir constants are assumed to be temperatures (Kontogeorgis and Folas, 2010), as presented in Equations 3.169 and 3.170. They are accountable for the interaction between the refrigerants and water molecules in the cavities, as reported by Parrish and Prausnitz, (1972), for a certain hydrate former evaluated over a certain range of temperatures (Eslamimanesh et al., 2011). However, the integration procedures for determining the former Langmuir constants, evaluated for the range of temperatures, using the Kihara potential function with a spherical core, are not applicable in the model of Eslamimanesh et al., (2011). As a result, the model parameters for the Langmuir constants for the various refrigerants were determined in this study using the equations of Parrish and Prausnitz (1972).

For small cavity (pentagonal dodecahedral):

$$C_{small} = \frac{a}{T} \exp\left(\frac{b}{T}\right) \quad (3.171)$$

For large cavities (tetrakaidecahedra (sI) and hexakaidecahedra (sII)):

$$C_{large} = \frac{c}{T} \exp\left(\frac{d}{T}\right) \quad (3.172)$$

where T is in K and C has units of reciprocal MPa.

The optimum values of the parameters of a Langmuir constant correlation ($a-d$) are evaluated by tuning the thermodynamic model against the measured experimental gas hydrate dissociation data obtained in the literature.

3.4 Development of thermodynamic hydrate modelling (HE-CPA)

In section 3.1 the fundamentals of modelling electrolyte solutions were presented. These models included extended Debye–Hückel (DH) and the Born term. Similarly, the fundamentals of CPA EoS were investigated, which described the fugacity of the liquid or vapour phase. This chapter describes the combination of gas hydrate, CPA EoS and electrolyte solution. The combination will present the model for measured hydrate dissociation data and will finally show how the Langmuir constant parameters are obtained.

For any system at equilibrium, the chemical potential of each component in all coexisting phases is equal. The fugacity of each component in the hydrate phases were calculated using the combination of CPA EoS and Soave-Redlich-Kwong (SRK) EoS. This was done to describe the physical interactions, which can be useful to different types of hydrogen bonding compounds such as water (Kontogeorgis et al., 2006). Since water is the only associating component in this study (Kontogeorgis et al., 1999), the water parameters were determined from pure liquid water properties. Table 3.6 presents the CPA EoS pure compound (water) parameters that were used for the fugacity calculations in this study.

In the presence of salt, the activity coefficient in the aqueous solution is calculated using the Debye–Hückel model. The hydrate phase is modelled using the solid solution theory of Van der Waals and Platteeuw (1959). Eslamimanesh et al., (2011), modified the hydrate phase model used in this study. The Langmuir constants were obtained by tuning the model, using the measured hydrate dissociation data. Consequently, Figure 3.1 and Equation 3.173 present the combination CPA equation of state, gas hydrate and electrolytes, which are named as Hydrate Electrolytes-Cubic Plus Association (HE-CPA) equation of state.

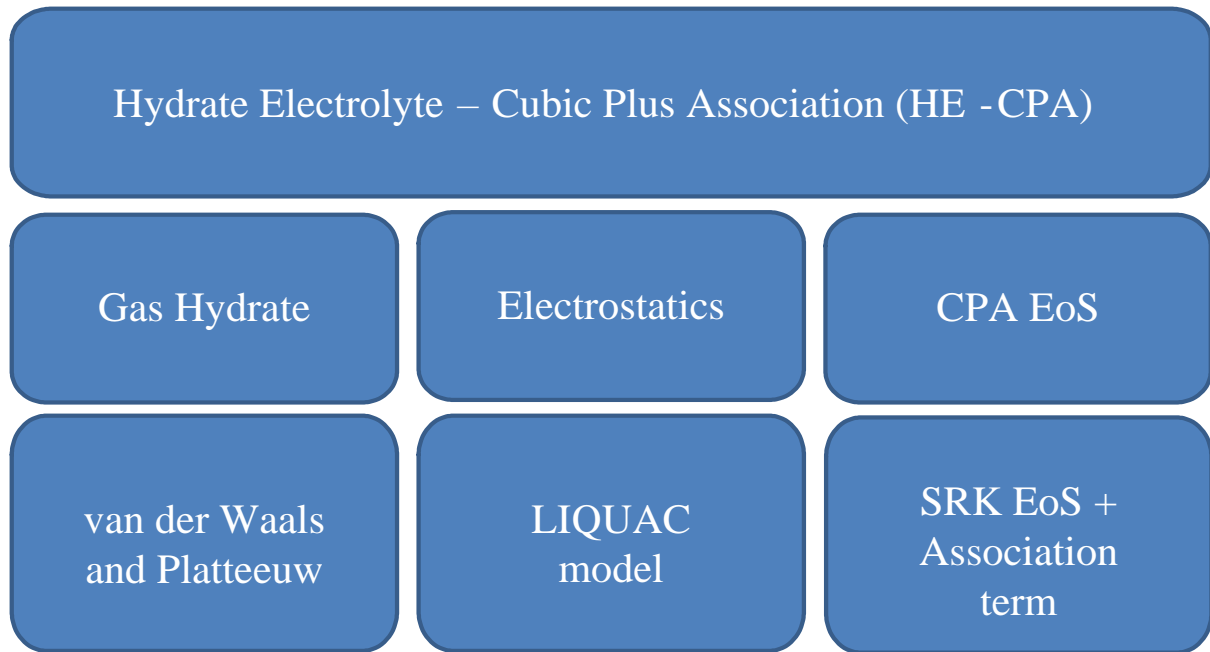


Figure 3. 1: Cubic Plus Association equation of state to hydrate and electrolyte (HE-CPA)

Thus, the hydrate–electrolyte CPA equation of state has the following contributions:

$$A^{HE-CPA} = A^{CPA} + A^{SRK} + A^{DH} + A^{Hydrate} \quad (3.173)$$

3.5 Kinetic model

The details of the hydrate kinetic models have been presented in the literature of Sloan and Koh (Sloan and Koh, 2008). Mohammadi et al., (2014) have studied the kinetic for carbon dioxide (CO₂) in the presence of silver nanoparticles and sodium dodecyl sulfate (SDS). It was revealed that SDS and silver nanoparticles do not have significant effect on decreasing the induction time, but they can increase the storage capacity of CO₂ hydrates. Babaei et al., (2015) have studied the kinetic and thermodynamic behaviour of tetrafluoromethane (CF₄) clathrate hydrate. It was found that by increasing the initial pressure at constant temperature decreased the induction time, while the formation rate of CF₄ hydrate, the apparent rate of reaction constant and the conversion of water to hydrate increased. Table 3.6 shows the induction time and the apparent rate constant of reaction studied by Hashemi, (2015), for several refrigerants with water.

The most critical parameter in studying kinetic is apparent rate constant of reaction, consequently, Englezos et al., (1987) showed the equation for the rate of hydrate formation. The equation was based on the kinetic model for hydrocarbon (methane and ethane) and Englezos developed their mixtures with co-workers (Englezos et al., 1987). It was assumed

that clathrate hydrate nucleation and growth occurred in the liquid layer at the gas-liquid boundary. The rate of hydrate formation can be formulated as

$$r(t) = \frac{dn}{dt} = k_{app}(f - f_{eq}) \quad (3.174)$$

where k_{app} represent the rate constant of hydrate reaction, f presents the fugacity of the hydrate former at instantaneous pressure and temperature, and f_{eq} shows the fugacity of the hydrate former at the equilibrium pressure and initial temperature.

Table 3. 6: Kinetic for the selected refrigerant (Hashemi, 2015)

Refrigerant	^a T ₀ /K	^b P ₀ /MPa	^c IT/min	^d K _{app} x 10 ⁹ / [mole G/(mole W). min. Pa]
R410a	282.8	0.81	335	2.1
		0.93	0	4.8
		1.00	0	5.2
	283.8	0.92	39	3.2
		1.0	4	4.4
		1.1	2	8.5
	284.8	1.0	1673	2.1
		1.1	7	4.2
		R407C	281.8	0.73
0.83	4			18.5
0.90	0			29.3
282.8	0.71		65	12.9
	0.82		5	16.2
283.8	0.82		4.8	12.8
R507C	279.9	0.91	5.6	28.1
		0.64	5	3.1
		0.71	4	3.5
	280.9	0.75	3	5.0
		0.81	5	5.3
		R404A	281.0	1.17
282.0	1.15		12	4.8
283.0	1.22		^e n.f	-
R406A	282.0	0.65	0	25
	283.0	0.65	^e n.f	
R408A	281.0	0.86	165	0.6
R427A	183.1	1.05	40	0.4

^aInitial temperature, ^bInitial pressure, ^cInduction time, ^dApparent rate constant, ^eno hydrate form

Apparent rate constant during hydrate growth

The hydrate growth rate can be presented using the following equation (Englezos et al., 1987, Zhang et al., 2007, Mohammadi et al., 2014)

$$r(t) = \left. \frac{dn_R}{dt} \right|_{t_i} = \frac{\Delta n_R}{\Delta t} \Big|_{t_i} = \frac{n_{R,i-1} - n_{R,i+1}}{(t_{i+1} - t_{i-1})n_{w_o}} \quad (3.175)$$

where $n_{R,i-1}$ and $n_{R,i+1}$ represent the number of moles of hydrate former in the gas phase at t_{i-1} and t_{i+1} respectively and n_{w_o} represent the initial moles of water or solution in the liquid phase. Thus, the apparent rate constant at a specific time t_i is determined by the following equation:

$$k_{app} = \frac{\left(\frac{n_{R,i-1} - n_{R,i+1}}{(t_{i+1} - t_{i-1})n_{w_o}} \right)}{(f - f_{eq})_{t_i}} \quad (3.176)$$

Water to hydrate conversion

The hydrate formation can be expressed as a reaction between the refrigerant and water molecules as follows (Sloan and Koh, 2008)



where M signifies the hydrate number (number of water molecules per guest molecules) which can be calculated by the succeeding equation for structure II (Sloan and Koh, 2008)

$$M = \frac{136}{8\theta_L + 16\theta_S} \quad (3.178)$$

where

$$\theta_{ki} = \frac{C_{ki}f_k}{1 + \sum_j C_{ji}f_j} \quad (3.179)$$

where f_k represent the fugacity of hydrate former in the gas phase and C_k represents the Langmuir constant. More details on the above sections for the calculation of Langmuir constants and the fugacities of the studied hydrate former using CPA equation of state. The gas law was used to determine the number of moles of the hydrate former consumed during the formation of the hydrate (Englezos et al., 1987, Mohammadi et al., 2014).

$$\Delta n_R = \frac{P_0 V_0}{Z_0 R T_0} - \frac{P_t V_t}{Z_t T_t} \quad (3.180)$$

where P and T represents the pressure and temperature of the cell respectively, and R stands for the Universal gas constant, and Z represent the compressibility factor for the former which can be calculated by the SRK equation of state. Subscripts “0” and “ t ” denote the initial conditions and condition at time, t , of the system respectively.

The volume of the hydrate former inside the cell at time, t (V_t) was calculated using the following equation (Mohammadi et al., 2014)

$$V_t = V_{cell} - V_{w_0} + V_{RW_t} - V_{H_t} \quad (3.181)$$

where V_{cell} represent the total volume of the cell which is 38 cm³, V_{w_0} represent the volume of the aqueous solution which is 20 cm³. Then, the volume of solution or water reacted, V_{RW_t} at time, t is estimated by the following equation

$$V_{RW_t} = M * \Delta n_R * v_w^L \quad (3.182)$$

where v_w^L represent the molar volume of water which can be calculated by the following expression (Mohammadi et al., 2014)

$$v_w^L = 18.015 * \left[\frac{1 - 1.0001 * 10^{-2} + 1.33391 * 10^{-4} (1.8(T - 273.15) + 32)}{5.50654 * 10^{-7} (1.8(T - 273.15) + 32)^2} \right] * 10^{-3} \quad (3.183)$$

The molar volume, V_{H_t} , of the hydrate at time, t , can be determine by the following equation (Mohammadi et al., 2014)

$$V_{H_t} = M * \Delta n_R * v_w^{MT} \quad (3.184)$$

where v_w^{MT} represent the volume of the empty hydrate lattice which can be estimated using the following equation

$$v_w^{MT} = \left(17.13 + 2.249 * 10^{-5} T + 2.013 * 10^{-6} T^2 \right)^3 \left(\frac{10^{-30} N_A}{136} \right) - 8.006 * 10^{-9} P + 5.448 * 10^{-12} P \quad (3.185)$$

where T is in K and P is in MPa. The water to hydrate conversion which is known as the number of moles of water converted to hydrate per mole of feed solution can be determine using the following expression:

$$\text{water to hydrate conversion} = \frac{M * \Delta n_R}{n_{w_0}} \quad (3.186)$$

CHAPTER 4

GAS HYDRATE EQUIPMENT AND EXPERIMENTAL PROCEDURE

The review of gas hydrate equipment and experimental techniques are presented in Ngema, (2014). Details concerning the design and the description of the isochoric equilibrium cell and agitation device used herein are given in Ngema et al. (2014). This cell has been used to measure hydrate dissociation data. The main purpose of this study is to perform accurate measurements of gas hydrates dissociation data for refrigerants + water + electrolyte systems in the presence of a promotor (cyclopentane) as well as mix electrolytes. The gas hydrate dissociation data were measured based on the pressure-search method. This chapter presents the summary of isochoric equilibrium cell and the layout procedures of the formation and dissociation of gas hydrates, temperature sensor calibration, pressure transducer calibration and salt solubility measurements.

4.1 The isochoric equilibrium cell

The isochoric equilibrium cell was built and constructed in the study conducted by this researcher in 2014, a 316 stainless steel was used because of its impressive properties that include a mechanical strength and the corrosion resistance. In addition, the 316 stainless steel had the advantages of being suitable at extremely high or low temperatures and high pressures (Sinnott, 2006). The cell was designed to withstand pressures up to 20 MPa. The volume of the equilibrium cell is approximately 38 cm³. All dimensions of the isochoric equilibrium cell are presented in the previous study of this author in 2014.

In this study, O-rings are made of Viton, as this material is compatible with the studied electrolytes and refrigerants. A Viton O-ring is placed into a groove to provide good sealing between the cell body and its cap. The equilibrium cell has a loading line, which is used as an evacuation line for gas and venting, a drain line, a pressure transducer line and a slot for inserting a Pt-100 sensor. Figure 4.1 shows the inner part of equilibrium cell with a stirring device (body and cap). The cap is tightened to the equilibrium cell body using six stainless steel bolts as shown in Photograph 4.1, 4.2 and 4.3. The equilibrium cell has a stirring device with impellers in order to improve the stirring efficiency.

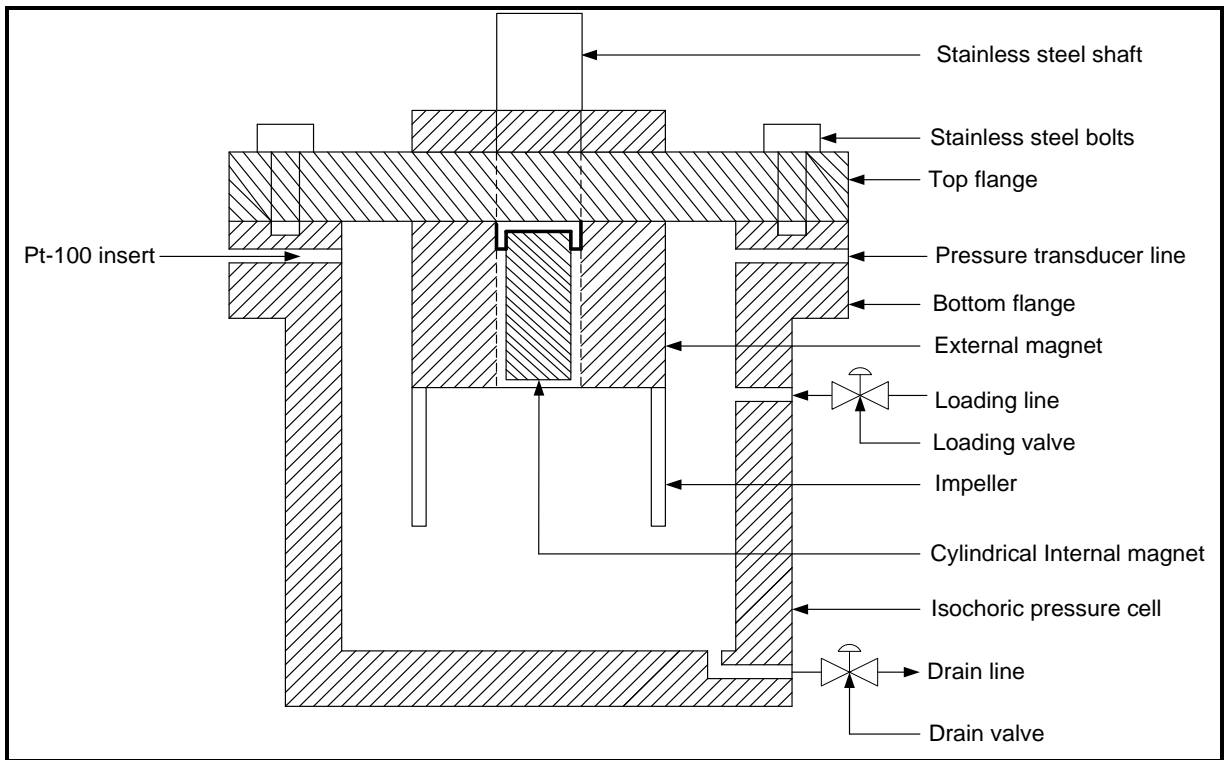
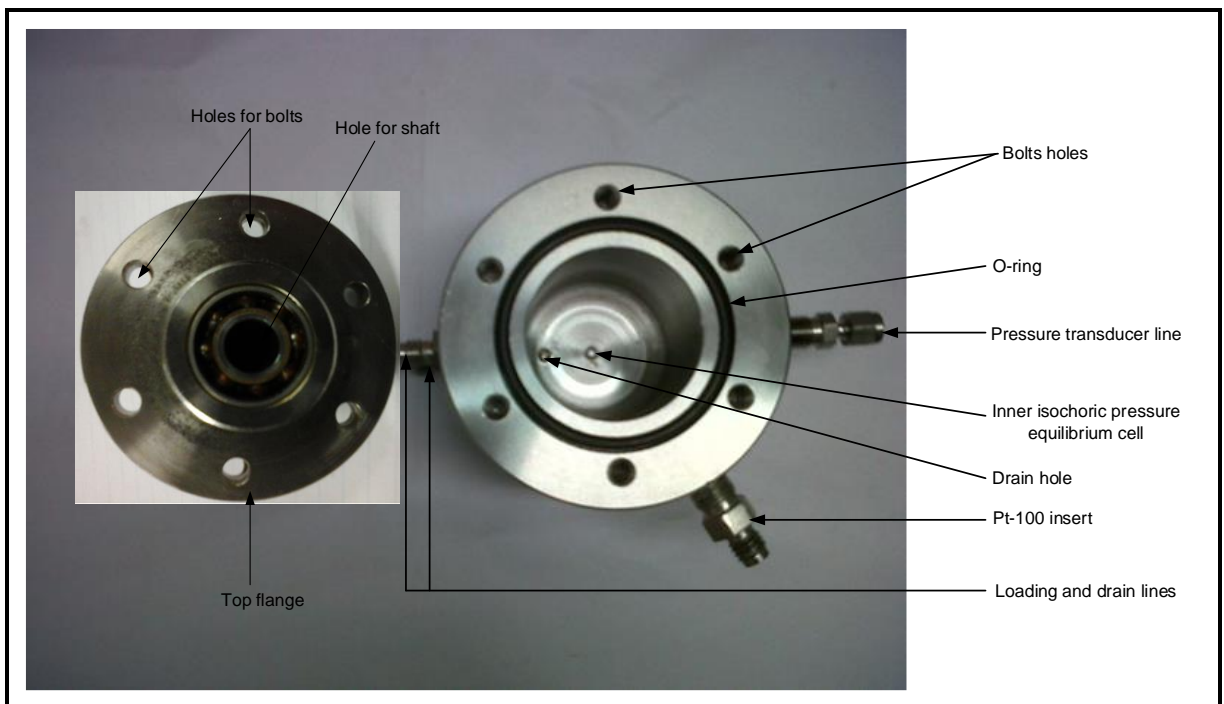
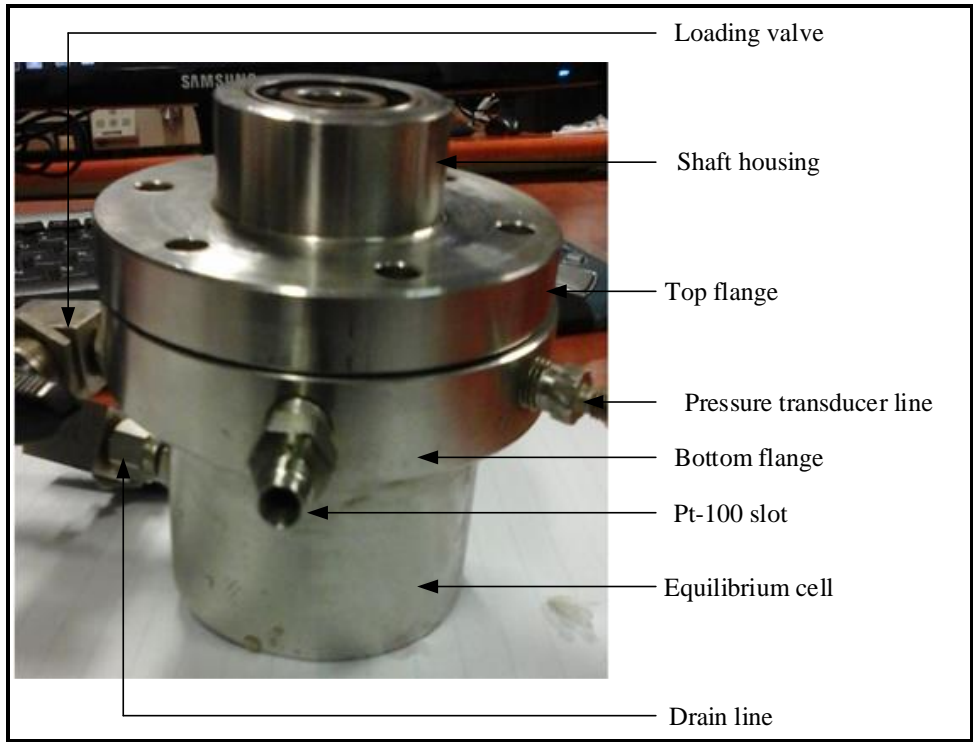


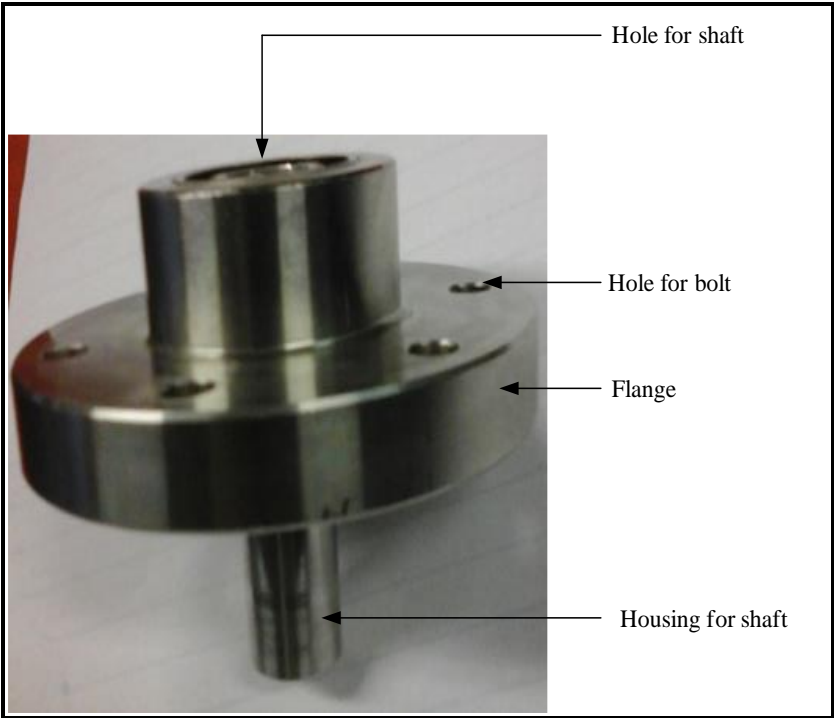
Figure 4. 1: Schematic diagram of the isochoric equilibrium cell



Photograph 4. 1: Top view of the equilibrium cell and cap



Photograph 4. 2: The isochoric equilibrium cell



Photograph 4. 3: Side view of the cap

The isochoric equilibrium cell consists of the following:

- A 34972A Agilent data acquisition unit
- A pressure transducer WIKA model P-10 range from 0 – 10 MPa
- A class A temperature probe (Pt-100)
- A TDGC2 model variac voltage regulator
- A Grant TX 150 programmable temperature circulator
- A Polyscience model KB 80 chiller unit
- A mechanical jack
- An Edward's model RV3 vacuum pump
- A Shinko ACS-13A temperature controller
- A water bath with an internal dimension of 300 mm x 260 mm x 250 mm. For external dimension, 20 mm thickness was added, for insulation, on each side.

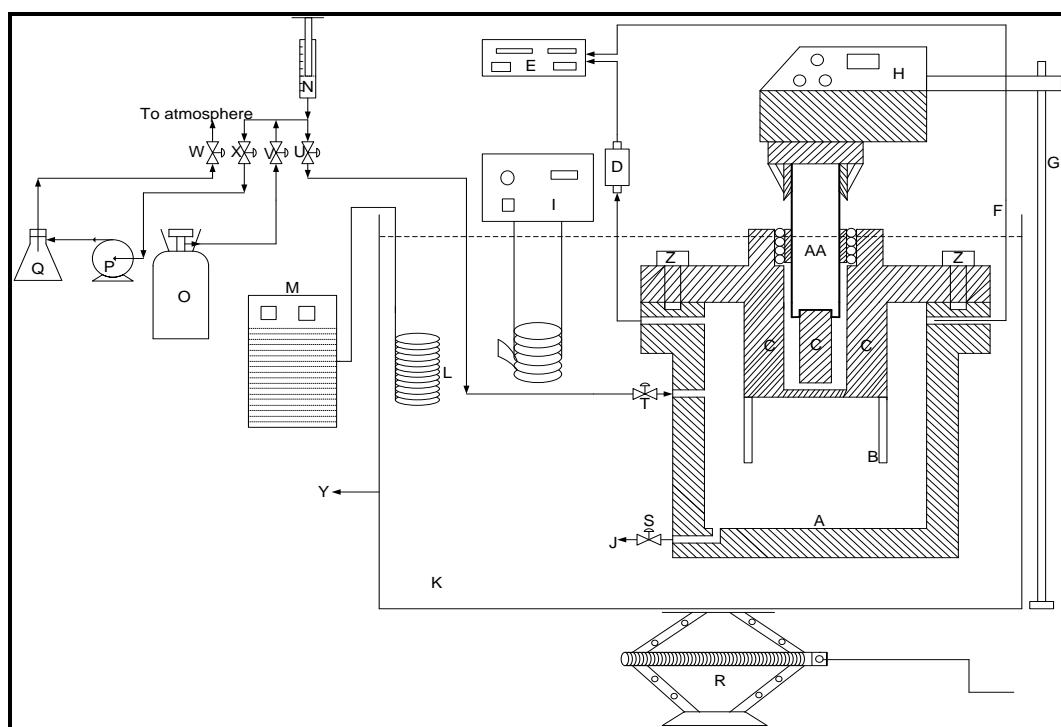
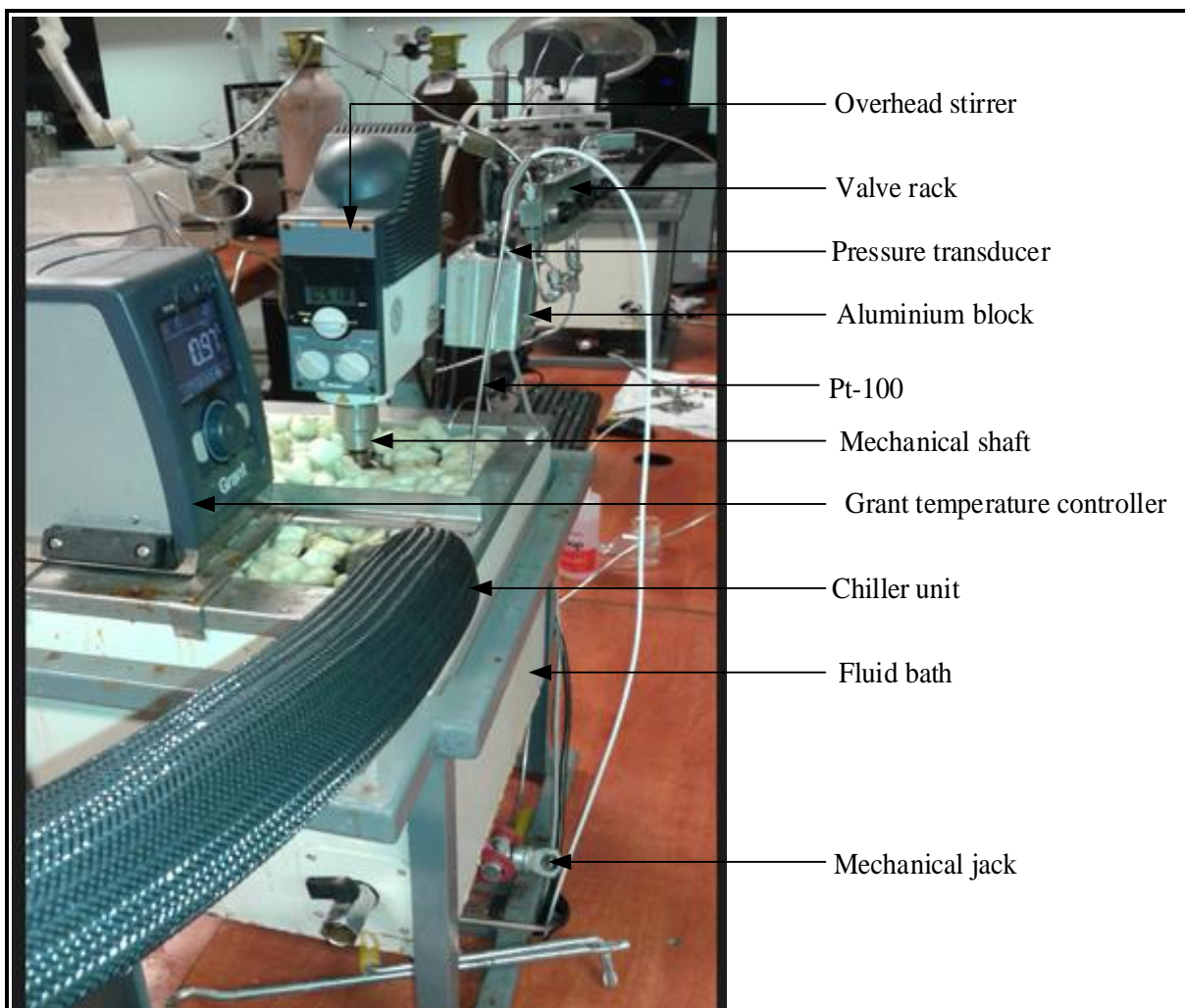


Figure 4. 2: Schematic flow diagram of the equipment: A, Equilibrium cell; B, Impeller; C, Magnet; D, Pressure transmitter; E, Data acquisition unit; F, Pt-100; G, Holder; H, Overhead mechanical agitator; I, Temperature controller; J, Discharge line; K, Chilling fluid; L, Cooling coil; M, Cold finger; N, Liquid syringe with aqueous solution; O, Gas supply cylinder; P, Vacuum pump; Q, Vacuum flask; R, Mechanical jack; S, Discharge valve; T, Inlet valve; U, Loading valve; V, Gas supply valve, W, Vent valve; X, Vacuum valve; Y, Water bath and Z, Bolts.



Photograph 4. 4: A layout of the equipment

4.1.1 Method of agitation within the equilibrium cell

Efficient agitation within the equilibrium cell was required to improve stirring power and to reduce time taken for the hydrate formations and dissociations. The stirring device consists of a Neodymium type of larger external magnet and smaller internal magnet, which is situated inside the stainless steel shaft. The neodymium has an extremely strong magnetic field. The detailed information and properties of the neodymium magnet are found in previously study of this author in 2014.

The stirring device is placed at the bottom of the top flange of the equilibrium cell as shown in Figure 4.3. A Heidolph RZR 2041 overhead mechanical agitation was used to drive the mechanical shaft, which successively drives the magnetic stirrer as shown in Figure 4.2 and 4.3. The overhead stirrer consists of two gear speeds, which range from 40 to 400 rpm and 200

to 2000 rpm with an accuracy of 0.1 of the final value. The stirring mobile consists of four impeller blades. These impeller blades are attached to an external magnet as shown in Photograph 4.5. A thin layer of vesconite material was used inside the shell of the external magnet and the stainless steel shaft in order to limit friction issues. The external magnet with impeller blades is removable from the shaft. The blades were designed to throw out liquid in the equilibrium cell as it agitates. With this agitation mechanism, the content inside the cell was able to attain equilibrium more rapidly.

The stirring device provides the following advantages, which were ascertained by the author by means of fulfilment of MSc Degree in Chemical Engineering:

- Stirring power and efficiency improved compared with the previously used magnetic bar stirring device
- Reducing the time of dissociation of gas hydrate by more rapid homogenisation
- Increase in accuracy of reading as the overhead displayed the same rotating speed than inside the equilibrium cell, while the rotation speed of the previously used magnetic bar was sometimes slower or even null.
- Promotion of a homogeneous aqueous solution by means of direct agitation in the cell

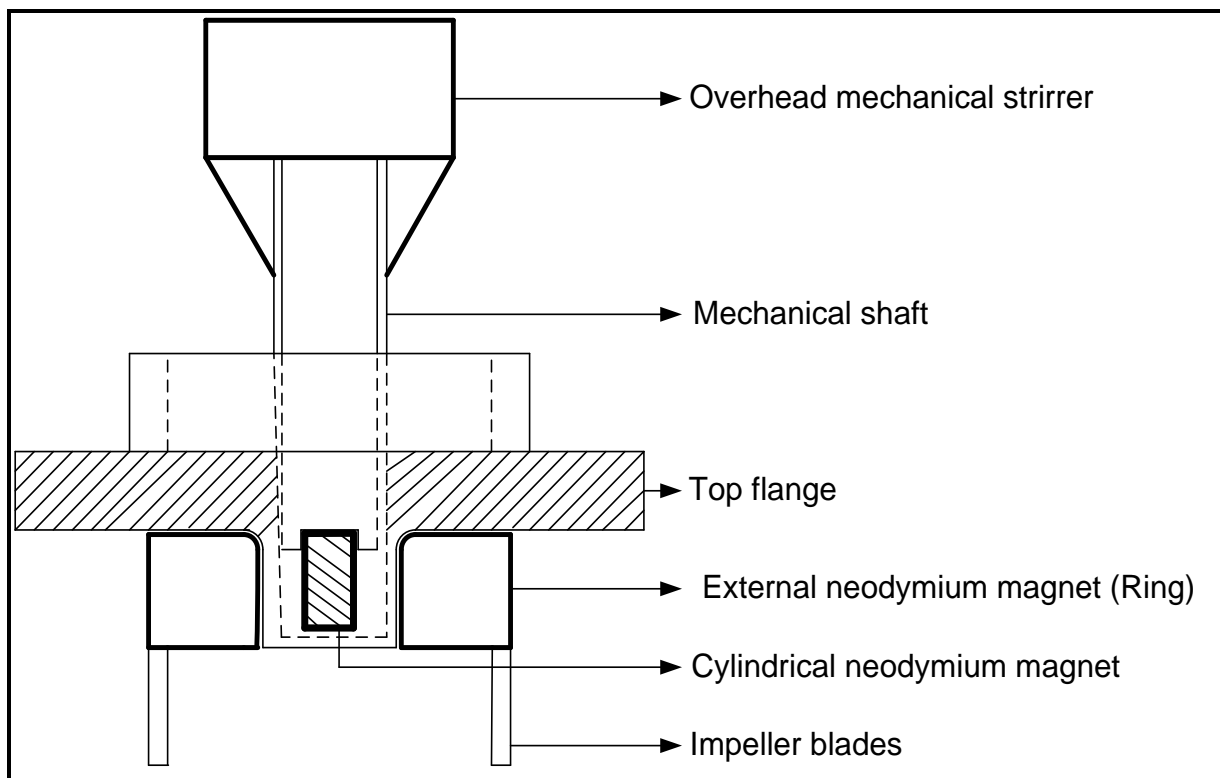
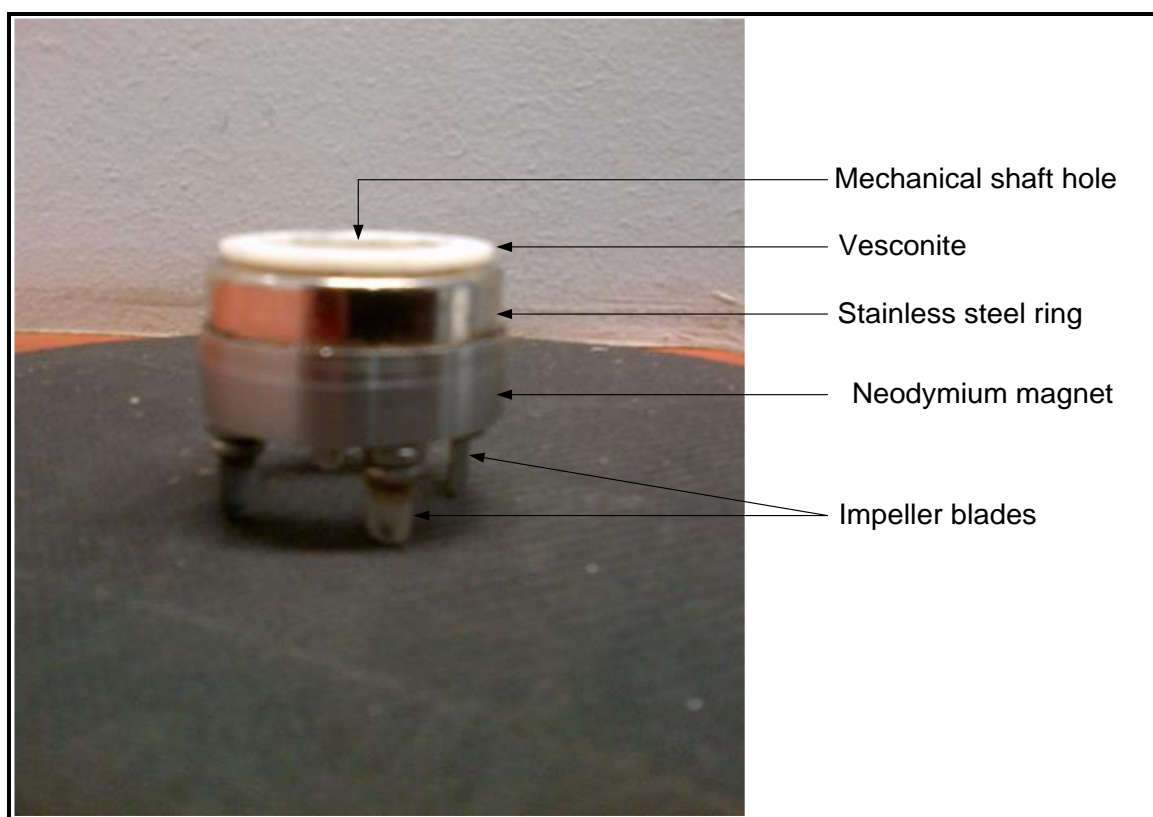


Figure 4. 3: A schematic diagram of the stirring mechanism



Photograph 4. 5: Stirring device made with neodymium magnets

4.1.2 Pressure measurements

In this study, the pressure readings were obtained using a WIKA model P-10 pressure transmitter and display, using a 34972A Agilent data acquisition unit. The pressure transmitter had a pressure range from 0 to 10 MPa, and its supplier guaranteed an accuracy of 0.05%. The pressure transmitter was mounted as close as possible to the equilibrium cell to limit dead volumes. It was connected to the equilibrium cell using a 1.5875 mm (1/16 inch) OD stainless steel pipe and was placed into an aluminium block housing regulated at constant temperature of 313.2 K. This is the temperature higher than the maximum studied temperature in order to avoid condensation. The aluminium block was heated using a heater cartridge taking power from a variac voltage regulator (TDGC2 model). A Shinko ACS-13A digital controller was used to display the temperature of the block and to control the energy supplied by the variac. The controller was able to maintain constant temperature of ± 0.01 K.

4.1.3 Temperature measurements

In this study, ethylene glycol was used as cooling fluid. The water bath was filled with ethylene glycol. The bath temperature was controlled by using a TX 150 Grant circulator programmable temperature controller. It was able to maintain temperature stability within 0.01 K. The equilibrium temperature in the equilibrium cell was measured by using a WIKA model REB Pt-100 with a class A ceramic bulb type sensor temperature probe. A hole of 6 mm diameter and 30 mm depth was drilled into the top of the bottom 316 stainless steel flange, to insert the Pt-100. It had a 3.175 mm (1/8 inch) diameter and was 300 mm long with a 90° bend 50 mm from the sensor tip. The Pt-100 was connected to a 34972A Agilent acquisition unit, through which the temperatures were read and logged using a computer. The temperature probes (aluminium block and equilibrium cell) were calibrated using the WIKA CTB 9100 oil bath. A WIKA standard temperature probe was connected to a WIKA CTH 6500 multi-meter with a manufacture temperature uncertainty of ± 0.03 K. The equilibrium cell and aluminium block temperature probes were calibrated within the temperature range 253.2 K and 323.2 K. The temperature calibration curves are presented in Appendix A.

4.1.4 Data logging

The temperatures and pressures readings were all logged using the 34972A Agilent data acquisition unit. The readings were logged continuously every 2 seconds for a specified time interval using BenchLink Data software. All log data were saved and stored in the computer. After data acquisition unit completed logging the data for the specified settings, then the data was exported to a Microsoft® Excel spreadsheet for further analysis. The pressure data was plotted against temperature data to obtain the hydrate dissociation point.

4.2 Preparation of the equilibrium cell

4.2.1 Cleaning of the equilibrium cell

It is very important to clean the equilibrium cell before undertaking any new experimental measurements. The equilibrium cell was filled with 50 ml of ethanol (cleaning solvent). Ethanol was allowed to agitate inside the cell at 600 rpm for 70 minutes to recover any contaminants on the walls as well as in the agitating device. Subsequently, the cleaning solvent was drained out by applying nitrogen at a pressure of 1 MPa. The cell was rinsed two times

with acetone. Once again nitrogen was supplied to a pressure of 5 MPa to flush the remaining acetone residue.

This was carried out to ensure that the equilibrium cell was clean and dry. Then, the cell was evacuated for 30 minutes using an Edward vacuum pump model RV3, to a low pressure of 0.0002 MPa. This was conducted to remove any volatile components still present in the cell. Once this cleaning process was completed, the cell was ready for leak testing. The entire cleaning procedure was conducted after completing the study of each system of interest.

4.2.2 Leak detection

Leak detection was conducted after cleaning the cell to obtain accurate results. The equilibrium cell was filled with nitrogen gas to a pressure of 10 MPa. All inlet valves were opened, except the drain valve that was closed. Once the cell reached the desired detection pressure, the nitrogen cylinder was closed.

SNOOPY was the leak detector selected to be used in this study. It was made with high viscous liquid soap and water. Then, it was applied to all fittings and around the cell. A leak was identified by observing the bubbles in that particular fitting. All fittings were retightened when leaks were observed.

Subsequently, the equilibrium cell was pressurized with nitrogen gas at a pressure of 10 MPa. It was fully immersed in the fluid bath at a constant temperature of 298.2 K for 24 hours. The pressure readings were recorded by computer. The trend was observed for the entire period. If there was a significant decrease in the pressure reading, this meant there was a leak in the fittings or, bubbles were observed if the leak was on the cell. The above procedure was repeated until no leaks were detected, and the pressure reading stayed constant for the entire period of 24 hours.

4.3 Calibrations

4.3.1 Temperature and pressure calibration

The temperature and pressure sensors had to be calibrated before starting the actual measurements to quantify uncertainties. The instrument (sensors) calibrations were important because the quality of measured data depends on the precision and quality of calibrations. The instruments had to be frequently calibrated, at least two or three times over 12 months, as they

were likely to drift with time. In this study, the validation of the calibration was performed by measuring the vapour pressure of the components used.

4.3.2 Temperature probe calibration

The temperature probe (probe for equilibrium cell) was calibrated using the WIKA CTB 9100 temperature calibration unit. This calibration unit had a standard temperature probe and WIKA CTH 6500 multi-meter. The standard temperature probe was calibrated using a WIKA instruments with an uncertainty of 0.03 K. Two temperature probes (standard and equilibrium cell) were aligned together with a tiny copper wire to minimize the temperature gradient.

All probes were deeply submerged into a WIKA CTB 9100 silicon oil bath. The temperature of the bath was initially set at 253.2 K. The probes were calibrated over the required working temperature ranges from (253.2 to 323.2) K. The temperature of the bath fluid was incrementally increased by 5 K per point. At each 5 K point, there was a waiting period until the equilibrium was reached, and only then was the final values recorded. The data was collected in increments of 5 K per data point, and subsequently decreased and increased again over the working temperature range. The hysteresis is discussed in Chapter 5 and plotted in Figure 5.1.

At each equilibrium point, the temperatures of the probe were recorded for 5 minutes. The values of temperatures in the equilibrium cell were logged via a 34972A Agilent data acquisition unit; while the values of the standard temperature probe were read on the display of a WIKA CTH 6500 multi-meter. The data obtained over 5 minutes were averaged, as the response times between the probes of the equilibrium and standard probe differed.

The data from the standard temperature probe was plotted against the measured probe to ascertain the equilibrium cell data. A linear curve was observed. The temperature calibration curve is presented in Appendix A. The curve was fitted with both first and second order polynomials by least square regression to obtain equation(s). The measured values obtained from the equilibrium cell temperature probe were fitted into these equations. It was important to obtain the closest or most similar values compared to those from the standard temperature probe.

The uncertainty was obtained by the difference between calculated values and standard values. The combined temperature measurement uncertainty was ± 0.03 K (*the confidence level, k = 2*). If a larger discrepancy exists between the calculated values and standard values, then the

Pt-100 is damaged. The temperature probe may require re-calibrating. Calibration should be checked regularly, at least two or three times a year as the probe may experience an internal resistance drift.

4.3.3 Pressure transmitter calibration

In this study, a WIKA P-10 pressure gauge transmitter was used to measure equilibrium pressures. The P-10 pressure gauge has a pressure range of 0 – 10 MPa and was calibrated using a 0 – 25 MPa (gauge) WIKA (MENSOR) CPC 8000 High –End Pressure Controller. The P-10 was calibrated in the pressure range of 0 – 10 MPa. The MENSOR unit was calibrated directly using WIKA Instruments. The supplier claimed a combined uncertainty of $\pm 0.01\%$. The pressure transmitter was fitted in the housing of the aluminium block. The block was kept at a constant temperature of 313.2 K. The empty equilibrium cell was submerged in the isothermal liquid bath at a temperature of 298.2 K. The equilibrium cell was pressurized with nitrogen gas via the MENSOR unit. The equilibrium cell pressure was then increased by an increment of 1 MPa, and subsequently decreased and increased again over the pressure range of 0 – 10 MPa. All increments were controlled using the MENSOR unit. At each equilibrium point, the P-10 pressures were recorded and logged via the 34972A Agilent data acquisition unit for 5 minutes. The values of the standard pressures were read and manually recorded from the display of a MENSOR CPC 8000 calibration unit. The pressure data obtained over 5 minutes were averaged, as the response times between the P-10 pressure transmitter and the MENSOR standard pressure transmitter differ.

The standard pressures values were plotted against the measured P-10 pressure values and linear curves were observed. Curves for pressure calibration are shown in Appendix A. The curve was fitted by least square regression to obtain equation(s). The P-10 measured values fitted into those equations. It was important to obtain the closest or similar values compared to standard pressure values. The uncertainty was obtained by the difference between calculated values and standard values. The combined pressure measurement uncertainty was ± 0.0007 MPa (*the confidence level, k = 2*). If a larger discrepancy is observed between the calculated values and standard values, then the pressure transmitter is damaged. With a change in bath temperature, the P-10 pressure transmitter may require to re-calibrating. Calibration should be undertaken at each temperature of use and be checked at least two or three times per annum.

4.3.4 Vapour pressure measurements

Once the pressure and temperature calibrations were completed, the vapour pressures of R410a, R134a and R507 refrigerants were measured. This researcher at MSc program in 2014 measured the vapour pressures. These were measured to verify the calibrations, the reliability of the equilibrium cell, and to confirm the purity of the refrigerants studied. The measured vapour pressures were compared with literature data for that particular refrigerant. The results of measured vapour pressure are discussed in Chapter 5. The vapour pressures measurements were undertaken between temperature ranges of 258.2 to 303.2 K. This temperature range was within the hydrate formation and dissociation data range.

4.4 Materials

All refrigerants (high purity R410a, R507, and R134a) used for this study were purchased from Afrox (Linde Group). The purity of the chemicals is discussed in Chapter 5 and presented in Table 5.1.

The electrolytes (high purity NaCl, CaCl₂, MgCl₂, and Na₂SO₄) were purchased from Capital Laboratory and Supplies. These electrolytes were used to prepare aqueous solutions.

Ultrapure Millipore Q water was supplied by the analytical laboratory at the University of KwaZulu-Natal. It had an electrical resistivity of 18 MΩ.cm at 298.2 K.

4.5 Sample preparation

The gravimetric method was used to prepare all aqueous solutions. Water and salt were measured by means of double weighing using an accurate analytical balance (Ohaus Adventurer balance, model No. AV 114) with an uncertainty of ±0.0001 g in mass. Ultrapure Millipore Q water was used in all aqueous solution preparations. A volume of 20 cm³ aqueous solutions was prepared at ambient temperatures and pressures. They were stirred for 5 to 10 minutes to ensure the salt particles were completely dissolved in water. The promoter (cyclopentane) was added, 10% of the total volume of the prepared aqueous solution. Then, the mixture was stirred for 5 to 10 minutes.

4.6 Operating procedure for equilibrium cell

4.6.1 Loading of equilibrium cell

Once the cleaning and calibration of sensors were completed, and a sample of aqueous solution was prepared. The equilibrium cell was evacuated for 30 minutes at a pressure of 0.0002 MPa, using an Edward vacuum pump. The inlet valve was closed to maintain the cell under vacuum. The pressure transmitter device allowed readings and the data logger recorded the data.

The volume of 20 cm³ of prepared aqueous solution was drawn from a beaker using a plastic syringe. The air bubbles were removed from the syringe by tapping it lightly. The filled syringe was connected to the loading line and the valve was opened slightly to allow the content to be fed into the equilibrium cell. Subsequently, the loading valve was closed and the gas line was opened. The equilibrium cell was pressurised, using the fluorinated refrigerant of the system being studied. The desired pressure was controlled using a pressure regulator connected to the gas cylinder. Finally, hydrate measurements are taken.

4.6.2 Hydrate measurements

The equilibrium cell was filled with the aqueous solution and refrigerant being studied. The overhead was switch on to agitate the mixture inside the cell at 600 rpm. Initially, the fluid bath temperature was set at 293.2 K, which was outside the hydrate formation region. The equilibrium cell was immersed in the temperature-controlled bath by lifting up the bath using a mechanical jack under the bath.

The contents inside the cell were left for equilibrium to take place until the pressure stabilized. Then, the Grant TX 150 programmable temperature controller was programmed to promote the formation and dissociation of gas hydrate. The temperature was programmed to cool from 293.2 K, until 10 K below the anticipated hydrate dissociation temperature.

The system temperature was decreased slowly at the rate of 1 K/h to allow for the formation of gas hydrate. During the formation of gas hydrate, the separation of hydrate and salt was taking place, because fluorinated refrigerants only form hydrates with water. This procedure is known as a cooling curve. This curve consists of a nucleation process and hydrate growth. The nucleation process involves a small cluster of water and gas growing and dispersing as pressure and temperature decreases very slowly, as shown in Figure 4.4 from point A to B. The rapid drop in pressure indicated hydrate growth, meaning that at this stage the hydrate had formed

as shown in Figure 4.4. The temperatures and pressures readings were logged every 2 seconds continuously for the entire programmable time.

After the formation of hydrate, the system temperature was increased very slowly in a stepwise method. This is known as the heating curve. At the beginning, large temperature steps were used (3 K/h), but when the system temperature approached the dissociation point, the temperature was increased with at a step of 0.1 K/h. A typical hydrate formation and dissociation cycle is illustrated in Figure 4.4. At each temperature increment of 0.1 K, the system was given 60 minutes to achieve equilibrium.

As temperature increase, the pressure also increased and the hydrate dissociated until the last hydrate crystal dissolved. The method used for the formation and dissociation is non-visual, and is known as the isochoric pressure-search method. The pressure and temperature readings were monitored until the last hydrate crystal disappeared, as shown in Figure 4.4. The point at which the slope of the heating curve intersected with a cooling curve was considered to be the point at which all hydrate crystals had dissociated. Thus, this point was recorded as the gas hydrate dissociation point. The above procedure was repeated by changing the system pressure.

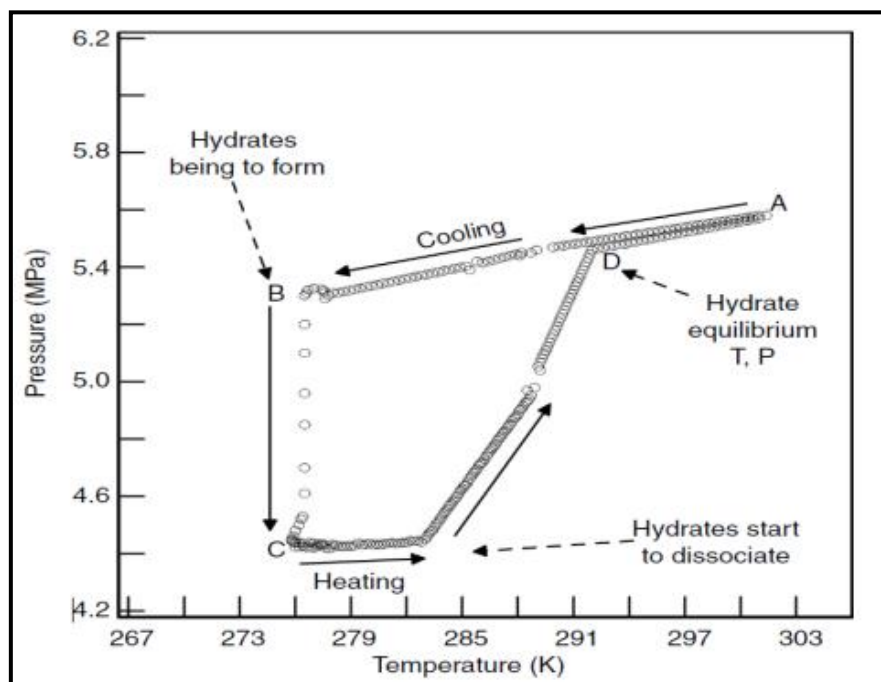


Figure 4. 4: Demonstration of hydrate formation and dissociation curve

(Sloan and Koh, 2008)

4.6.3 Kinetics measurements

The kinetics of gas hydrate formation was investigated. The objective was to examine the effect of the initial temperature and the initial pressure on the rate of hydrate formation, the apparent rate constant of hydrate reaction, water to hydrate conversion, induction time and gas consumption. Some of the factors that affect the kinetics of hydrate formation include volume and shape of the equilibrium cell, the amount of aqueous solution, water history, stirrer speed, initial pressure and initial temperature.

To investigate the effect of the initial pressure and temperature on the kinetics of hydrate formation, all parameters were kept constant except the initial temperature and pressure.

Prior of the measurements, the equilibrium cell was washed using deionized water. Then the cell was evacuated to a pressure of 0.00039 MPa using an Edward vacuum pump for 30 minutes to eliminate any impurities. Consequently, a volume of 30 cm³ of pure water or aqueous solution was introduced to the equilibrium cell using the injection line installed at the top-side the cell. To minimise effect of water history in the kinetics measurements, pure water should be used. The equilibrium cell was then evacuated again for 1 minute to remove any air and contaminants. Subsequently, the cell was immersed inside the water bath and the temperature was set to the desired initial temperature that is within the hydrate stability zone at the expected pressure.

Once the system temperature become stable, the hydrate former was introduced slowly into the cell to pressurize the cell to the desired initial pressure that is the hydrate stability zone. Once the cell was pressurized, the valve for loading the hydrate former was closed and the content inside was stirred at the stirrer speed of 600 rpm. As the hydrate was being formed inside the cell, and the hydrate former molecules were trapped inside the hydrate cavities, the pressure was dropping gradually until it reached a steady state condition. The induction time was evaluated if a particular, system shows it in the trend that was monitored by computer.

4.6.4 Shutdown procedure

Once the system study had been completed, it was important to shut down the equipment in an appropriate manner. The data acquisition unit was switched to manual and stopped. The overhead stirrer, the chiller unit, and the programmable temperature controller were switched off. The bath was lowered using a mechanical jack and the drain valve was opened to allow the content inside the cell to be discharged. Nitrogen gas was used to flush residue left inside the

equilibrium cell. Subsequently, the cleaning procedure mentioned in section 4.2 was followed before undertaking the next gas hydrate system study.

4.7 Operating procedure for measuring salt solubility

4.7.1 Samples preparation

Samples were prepared using 5 ml vials. Initially, the vials were washed with soap and distilled water was used to rinse them. The vials were filled with acetone and then placed them in a MRC ULTRASONIC DC200H at 303.2 K for 20 minutes. The acetone was emptied into a waste bottle. The vials were dried by using a Scientific oven at the temperature of 333.2 K for a period of 15 minutes. This was done to ensure that no residual acetone was found in the vials and ready for sample preparation.

A gravimetric method was used to prepare the electrolyte solutions. The samples were prepared using on OHAUS PIONEER analytical balance, which has a manufacturing stated uncertainty of ± 0.0001 g in mass. The desired amount of distilled water was added into the vial and a small amount of salt was added to achieve a saturated solution. The salts, NaCl, CaCl₂, MgCl₂, Na₂SO₄ and CaSO₄ were studied. For solubility measurements, the samples were kept in the ULTRASONIC bath for four hours at the desired temperature. At one point in the water bath, the samples were finally kept for 20 to 24 hours at the desired temperature for measuring salt solubility.

4.7.2 Solubility measurements

Before measuring solubility, it was important to verify that the syringe and the sampling pan were at the desired (room temperature) temperature for measuring solubility. This was done to minimize error. A small amount of sample (as described in 4.7.1) was extracted using a syringe from its vial. The empty sampling pan was placed on the calibrated mass balance, and the pan was filled with aqueous solution. A mass of aqueous solution was then recorded. The weighed amount of aqueous solution was placed into the chamber of a Differential Thermal Analysis (DTG 60AH) SHIMADZU which was connected to a SHIMADZU Thermal Analyser (TA 60WS) and SHIMADZU Flow Controller (FC 60A). This analytical instrument is shown in Photograph 5.6. The carrier gas (nitrogen) was connected via FC 60A, TA 60 WS to DTG 60AH. The estimated time of 120 minutes was programmed to allow for the evaporation of the solvent. The chamber temperature was set at 10 K below the solvent boiling point. Then, the

TA program began and the solvent evaporated slowly until the constant mass was reached. The dry salt pan was weighed by means of a mass balance and the value was finally recorded.

4.7.3 Shutdown of DTG

It was important to shutdown the DTG analyser using the proper procedure to prevent any damage. Firstly, the computer program was stopped, and the carrier gas to DTG 60AH was stopped, using FC-60A. Subsequently, the DTG 60AH, TA 60WS was switched off, and followed by the FC 60A. Lastly, the valve for the carrier gas (nitrogen) was closed.



Photograph 4. 6: Differential thermal analysis

4.8 Safety in the laboratory

The practice of safety in a laboratory is important to ensure that all personnel are working in a protected environment. Consequently, all safety procedures are adhered to during the experiments and the following precautions are taken:

- Latex gloves and goggles are required to be worn during the preparation and loading of the samples
- A laboratory coat is worn all times in the laboratory

- An industrial extractor hood is installed above the equipment to extract fumes from the cell. The extractor hood is switch on all times
- The equipment is built and framed to ensure that no piece of equipment could fall and cause an accident
- Gas cylinders are chained properly either on the wall or on a trolley and unused cylinders are secured at a cylinder area.
- Appropriate safety signs are placed at the door and against the wall in the laboratory
- All signs are proper, clear and understandable
- A pressure regulator is used to control the amount of gas supplied to the equilibrium cell. It is connected to the gas cylinder to measure the amount of gas inside the cylinder and to control the desired amount needed in the equilibrium cell
- The material safety data sheet (MSDS) for all chemicals used in this study were kept in a file near the apparatus
- All chemicals and hazardous waste are clearly labelled and stored under the fume hood
- The work place and laboratory are kept clean all time
- There is no obstruction in the walking area
- The walking area is demarcated
- The sirens are checked on a regular basis.

CHAPTER 5

RESULTS AND DISCUSSIONS

This chapter focuses on the results and discussions for all measured systems, which includes the hydrate former (refrigerant) + water + (single and mixed electrolytes) systems in the absence and the presence of promoter (CP), kinetics measurements and the solubility of electrolytes. The HE-CPA equation of state developed in Chapter 3, was used to model the experimental hydrate dissociation data using the isochoric equilibrium cell and pressure-search method. The HE-CPA equation of state and the results of the model are discussed in this chapter, respectively.

5.1 Purities, vapour pressure and calibrations

5.1.1 Chemical purities

The purities of the chemicals used in this study together with the details of the chemical supplier have been captured in Table 5.1. A Shimadzu 2010 gas chromatograph (GC) with a thermal conductivity detector (TCD) was used to check the refrigerant purity. A Poropak Q column was utilized in the GC. The column has a mesh range of 100/120, length of 2 m, internal diameter of 2.2 mm, a maximum operating temperature of 523 K and it was constructed of stainless steel. It was found that there were no significant impurities in the studied fluorinated refrigerants. It showed 100% peak area and the single peak in the chromatogram at 30 minutes. Ultrapure Millipore Q water was used in all the experiments. It had an electrical resistivity of 18 M Ω .cm at 298.2 K. Millipore water was generated using PURE ALGAE UNIT in the laboratory. The aqueous salt solutions {NaCl or CaCl₂ or Na₂SO₄ or MgCl₂} were prepared using the gravimetric method. An accurate analytical balance (Ohaus Adventurer balance, Model No. AV 114) with an uncertainty of ± 0.0001 g (0.1mg) in mass was used to prepare the aqueous solutions.

Table 5.1 presents the pure refrigerant properties, such as critical temperature, critical pressure, critical volume and acentric factor, which plays an essential role in the thermodynamic

modelling. Thus, the use of accurate properties is important for the accurate theoretical treatment of measured hydrate dissociation data.

Table 5. 1: Studied purities, critical properties and suppliers of refrigerant

Chemicals	Formula	Molecular weight (g.mol ⁻¹)	Supplier	Purity (mass fraction)	T _c /K	P _c /kPa	ω
Water	H ₂ O	18.015	UKZN	1.000 ^e	647.14 ^a	22064.00 ^a	0.344 ^a
R507	0.5CHF ₂ CF ₃ + 0.5 CH ₃ CF ₃ ^g	98.8	Afrox	0.998 ^e	343.96 ^b	3797.00 ^b	0.304 ^f
Cyclopentane	C ₅ H ₁₀		Merck	0.999 ^e	374.18 ^c	4057.24 ^c	0.326 ^c
R410a	0.5CH ₂ F ₂ + 0.5 CHF ₂ CF ₃ ^g	72.6	Afrox	0.998 ^e	345.65 ^d	4964.20 ^d	0.279 ^f
Sodium chloride	NaCl	58.44 ^h	Merck	0.990 ^h			
Calcium chloride dihydrate	CaCl ₂	110.98 ^h	Merck	0.990 ^h			
Magnesium chloride hexahydrate	MgCl ₂	95.21 ^h	Merck	0.990 ^h			
Sodium Sulfate	Na ₂ SO ₄		Merck				

Critical properties from: ^aPoling and Prausnitz (2001), ^bDöring et al. (1997), ^cAspen Plus (2011), ^dCalm (2008), ^eCheck by GC analysis for the gases and liquid, ^fShouzhi et al. (2005), ^gmass fraction, ^hAs stated by the supplier

5.1.2 Vapour pressures for refrigerants

This author in the MSc program in 2014 measured experimental vapour pressure data for all fluorinated refrigerants (R410a, R507, and R134a) used in this study. The literature vapour pressure values for R134a and R507 were calculated using Wagner equations 2.5 and 3.5 respectively, with the parameters for the Wagner equations taken from the Aspen software, (2011) and Döring et al. (1997), respectively. The literature values of vapour pressure for R410a were taken from Calm (2008). The measured data were agreed very well compared with

literature values as shown in Figure 5.1. The accuracy of the measured data is within the uncertainty of pressure measurement, which is ± 0.0007 MPa. The vapour pressure measurement is a part of the validated sensor calibrations and operating procedure for the isochoric equilibrium cell, and checks the purity of the refrigerants or chemicals used.

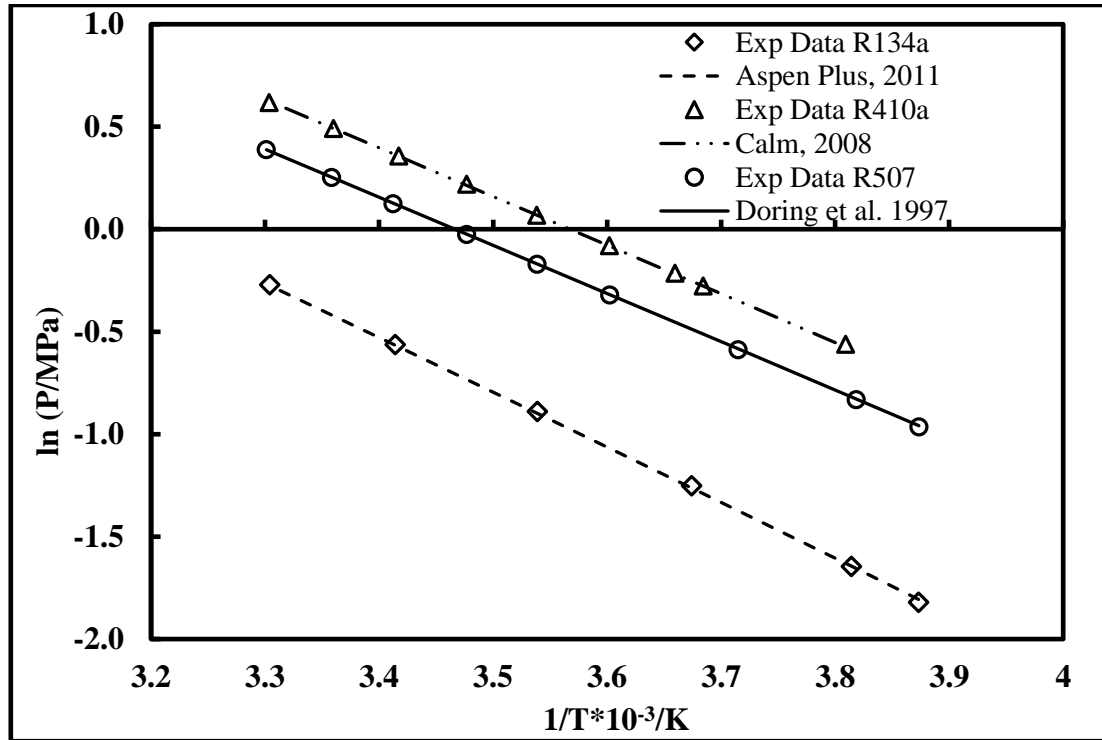


Figure 5. 1: Vapour pressure plots for the R134a, R410a and R507

5.1.3 Temperature calibration

The temperature probe (Pt-100) was calibrated in the temperature ranges from (253.2 to 323.2) K before measuring the gas hydrate. The measured temperatures were plotted against the standard temperatures, and the linear curve was obtained. Then, the second-order polynomial was fitted in the linear curve to obtain the correlation used to calculate the hydrate dissociation temperatures, the linear curve is presented in Appendix A in Figure A.1. Table 5.2 presents the resultant temperature calibration polynomials for the specified temperature ranges. It shows the maximum and minimum errors for the temperature probe. The combined uncertainty in the temperature was ± 0.031 with a confidence level of $k = 2$. Figure 5.2 presents the deviation results obtained from the calibration polynomial. The measured temperature was corrected using the correlation obtained in Table 5.2 in degrees Celsius, and it was then converted to Kelvin.

Table 5. 2: Temperature calibration correlation and deviations

Sensor	^a ΔT_{\min} /°C	^a ΔT_{\max} /°C	Correlation /°C
Pt-100	-0.0079	0.0099	$T_{\text{calc}} = 6.9868\text{E-}06x^2 + 0.999x - 1.3566$

^a $\Delta T = |T_{\text{std}} - T_{\text{calc}}|$ is the maximum and minimum error induced by the calibration correlation, T_{std} is the temperature of the standard probe and T_{calc} is the calculated temperature from the correlation.

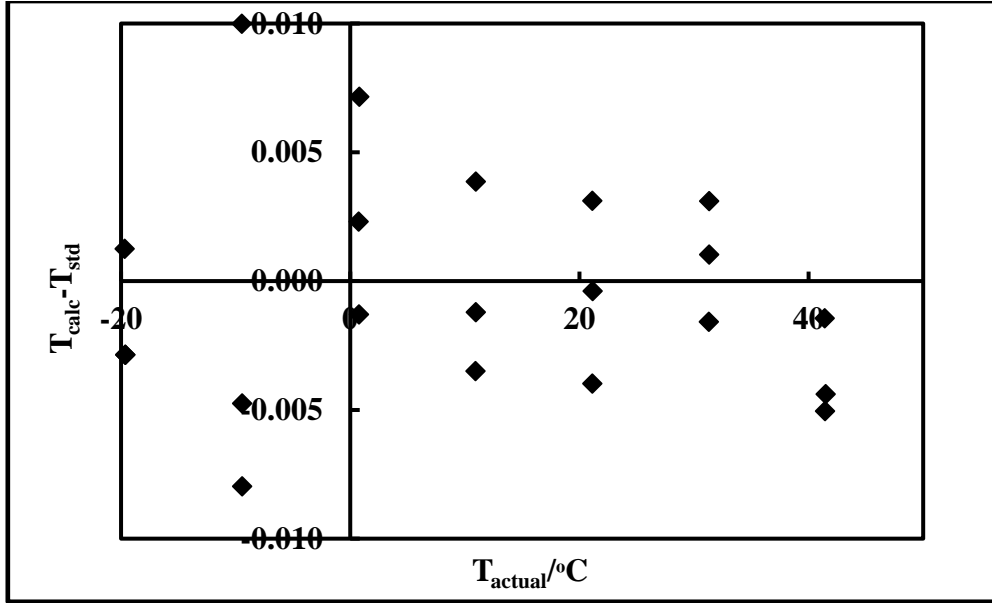


Figure 5. 2: Deviation for temperature calibration

5.1.4 Pressure calibration

The second order polynomial was used to fit the measured pressure against the standard pressure. The P-10 pressure transmitter was calibrated at pressure range between 1 and 10 MPa. Table 5.3 presents the pressure resultant calibration polynomial for the specified pressure ranges. It shows the maximum and minimum errors for the pressure transmitter. Figure 5.3 presents the deviation results obtained from the calibration polynomial. The combined uncertainty in the pressure was calculated to be ± 0.051 with a confidence level of $k = 2$. The linear curve for pressure calibration is presented in Appendix A in Figure A3. The measured pressure was corrected using correlation obtained in Table 5.3 in bars, and it was then converted to MPa

Table 5. 3: Pressure calibration correlation and deviations

Sensor	${}^a\Delta P_{\min}$ /bar	${}^a\Delta P_{\max}$ /bar	Correlation /bar
P-10	-0.0069	0.0089	$P_{\text{calc}} = -1.4445\text{E-}06x^2 + 0.9998x + 0.3601$

${}^a\Delta P = |P_{\text{std}} - P_{\text{calc}}|$ is the maximum and minimum error induced by the calibration correlation, P_{std} is the pressure of the standard pressure transmitter and P_{calc} is the calculated temperature from the correlation.

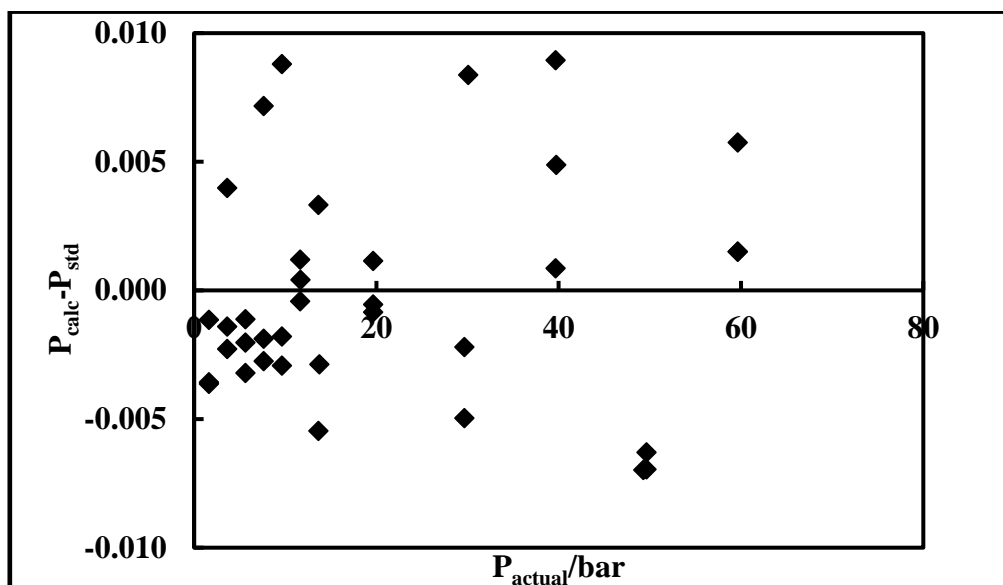


Figure 5. 3: Deviation in pressure calibration

5.2 Refrigerant with water systems

5.2.1 Binary test systems for refrigerant + water

This author in the MSc level in 2014 measured the binary test systems for (R410a and R134a) + water. The hydrate dissociation data is presented in Table 5.4 and shown in Figures 5.4 and 5.5. The test systems were measured to verify, the reliability of the isochoric equilibrium cell. The binary test systems for the {R410a or R134a} + water agrees very well with the existing literature values of (Akiya et al., 1999; Liang et al., 2001; Petticrew, 2011), which confirms and provides confidence that the isochoric equilibrium cell can be used to perform unpublished hydrate dissociation data. In this study, the method used to obtain the hydrate dissociation data was the isochoric pressure-search method. This method is well described in detail in Chapter 4.

Table 5. 4: Measured data for refrigerants (1) + water (2) test systems^a

R134a (1) + water (2)		R410a (1) + water (2)	
T/K	P/MPa	T/K	P/MPa
283.0	0.4047	293.0	1.4213
282.6	0.3671	291.3	1.1847
281.9	0.3218	290.3	1.0339
281.4	0.2806	289.0	0.8676
281.4	0.2763	287.8	0.7414
280.7	0.2471	286.0	0.5824
280.4	0.2336	284.6	0.4837
280.0	0.2147	283.1	0.3955
280.0	0.2113	280.3	0.2568
279.3	0.1824	277.5	0.1788
278.4	0.1445		
277.6	0.1231		
275.8	0.0916		

^aU(T) (0.95 level of confidence) = 0.1 K, U(P) (0.95 level of confidence) = 0.0007 MPa

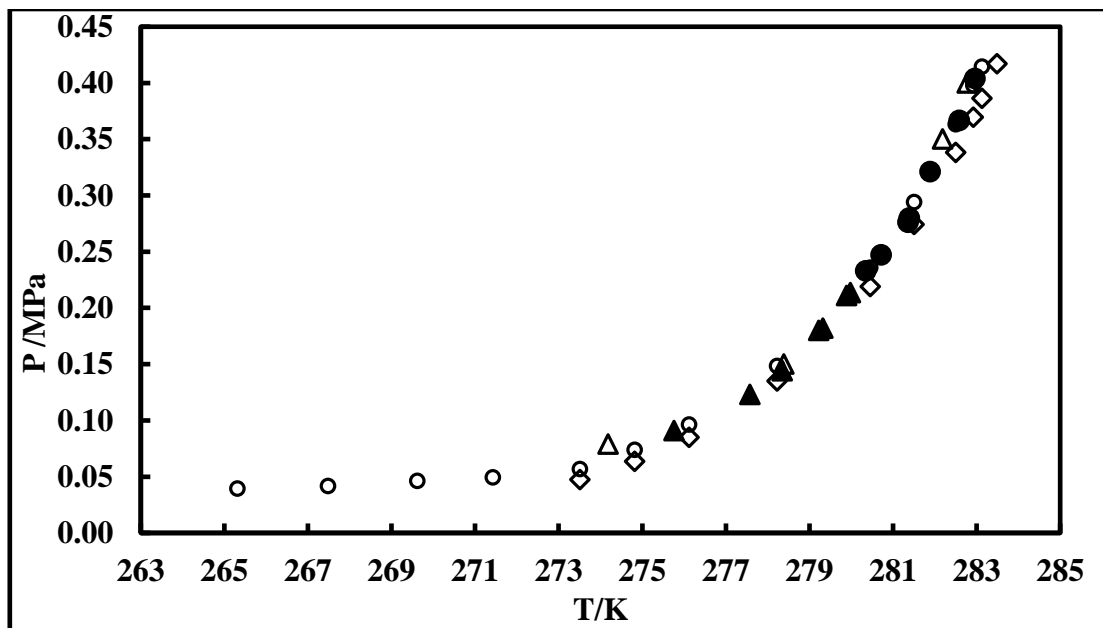


Figure 5. 4: Comparison between the measured hydrate data and literature for the R134a (1) + water (2) system; [●, experimental data at 400 rpm; ▲, experimental data at 600 rpm] This work; ◇, Akiya et al., (1999); ○, Liang et al., (2001); △, Petticrew, (2011)

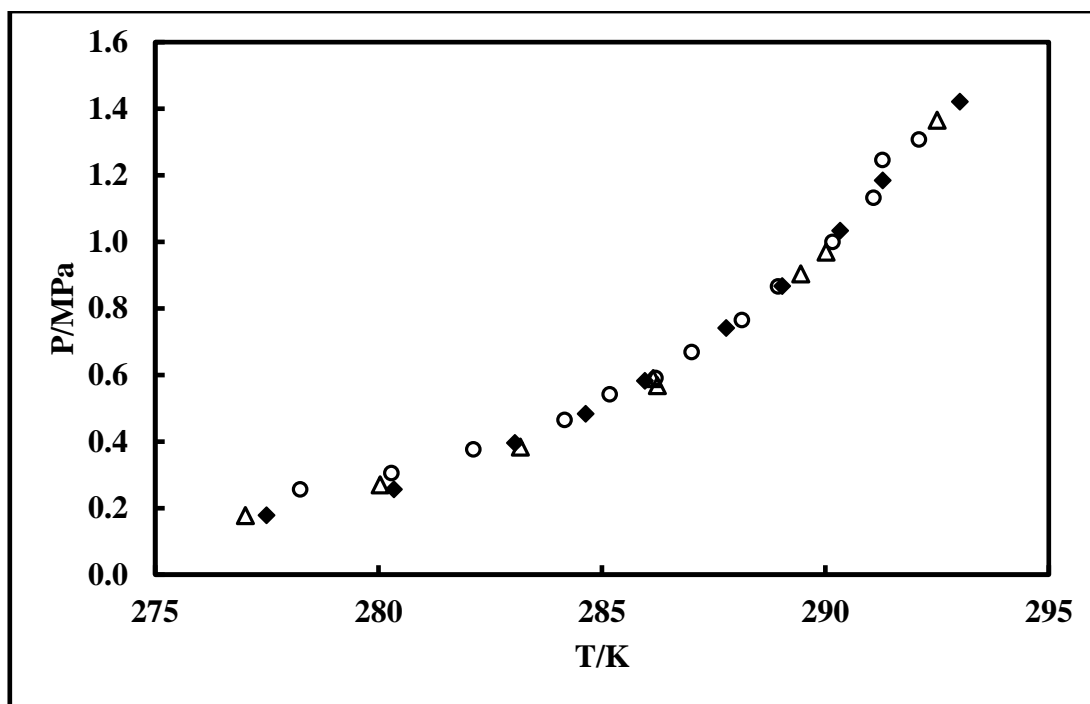


Figure 5.5: Comparison between the measured hydrate data and literature for R410a (1) + water (2) system; ◆, This work; ○, Akiya et al. (1999); △, Hashemi (2015).

Table 5.5 presents the hydrate dissociation data for R507 + water system and it is shown in Figure 5.6. This author at MSc level in 2014 measured the binary systems for (R134a, R410a and R507) + water as shown in Figures 5.4 to 5.6. It was found that R410a is suitable for gas hydrate technology for desalination because dissociation temperatures are closed to ambient temperatures. It was also found that R134a and R507 were not suitable for the desalination process because their dissociation temperatures were far below in comparison to ambient temperatures. Consequently, from the study of this author in 2014, it was recommended that further research is required for R410a, R507 and R134a systems in the presence of cyclopentane (CP) to study the effect of CP in increasing the hydrate dissociation temperatures.

Table 5. 5: Measured data for hydrate–liquid water–vapour for R507 (1) + water (2) system^a

T/K	P/MPa
283.3	0.8733
283.0	0.7401
282.2	0.6110
281.3	0.5043
280.7	0.4442
280.0	0.3704
279.0	0.2979
278.1	0.2417
277.7	0.2212

^aU(T) (0.95 level of confidence) = 0.1 K, U(P) (0.95 level of confidence) = 0.0007 MPa

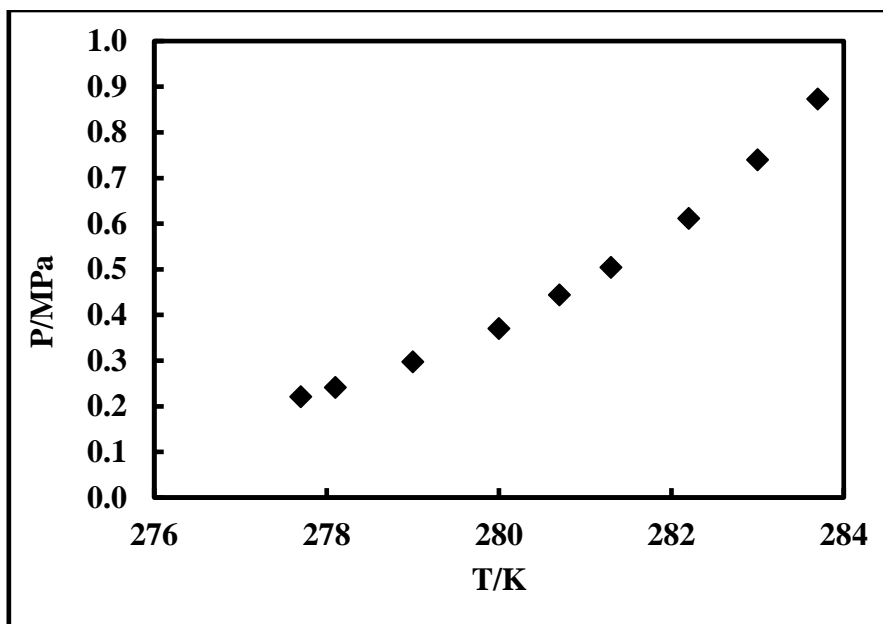


Figure 5. 6: Measured data for hydrate–liquid water–vapour for the R507 (1) + water (2) system

5.2.2 Refrigerants + water + CP systems

Hydrate dissociation data for ternary systems consisting of fluorinated refrigerant (R410a or R507) + water in the presence of CP were measured in this study. The measured hydrate dissociation data are presented in the Table 5.6 as shown in Figures 5.7 and 5.8.

Table 5. 6: Measured data for hydrate–liquid water–liquid promoter–vapour for the refrigerant (1) + water (2) + CP (3) systems^a

R410a (1) + water (2)		R410a (1) + water (2) + CP (3)		R507 (1) + water (2)		R507 (1) + water (2) + CP (3)	
T/K	P/MPa	T/K	P/MPa	T/K	P/MPa	T/K	P/MPa
293.0	1.4213	294.4	1.3852	283.3	0.8733	284.6	0.8580
291.3	1.1847	293.7	1.1877	283.0	0.7401	284.2	0.7445
290.3	1.0339	292.6	0.9970	282.2	0.6110	283.6	0.6041
289.0	0.8676	290.3	0.7424	281.3	0.5043	282.6	0.4744
287.8	0.7414	287.0	0.4699	280.7	0.4442	282.6	0.4823
286.0	0.5824	283.8	0.2719	280.0	0.3704	281.1	0.3459
284.6	0.4837	280.9	0.1588	279.0	0.2979	279.8	0.2489
283.1	0.3955			278.1	0.2417		
280.3	0.2568			277.7	0.2212		
277.5	0.1788						

^aU(T) (0.95 level of confidence) = 0.1 K, U(P) (0.95 level of confidence) = 0.0007 MPa

Figure 5.7 shows the measured system for R410a + water + CP. The effect of adding CP shows impressive results by shifting hydrate dissociation temperatures to higher temperatures. It was revealed that the presence of CP increases the hydrate dissociation temperatures by 1.4 K at higher temperatures and 2.4 K at lower temperature and pressures as shown in Figure 5.7. This shows that R410a in the presence of CP can be employed for gas hydrate technology for the desalination process because the hydrate dissociation temperatures are at ambient temperatures, consequently, the desalination process can operate at ambient temperatures.

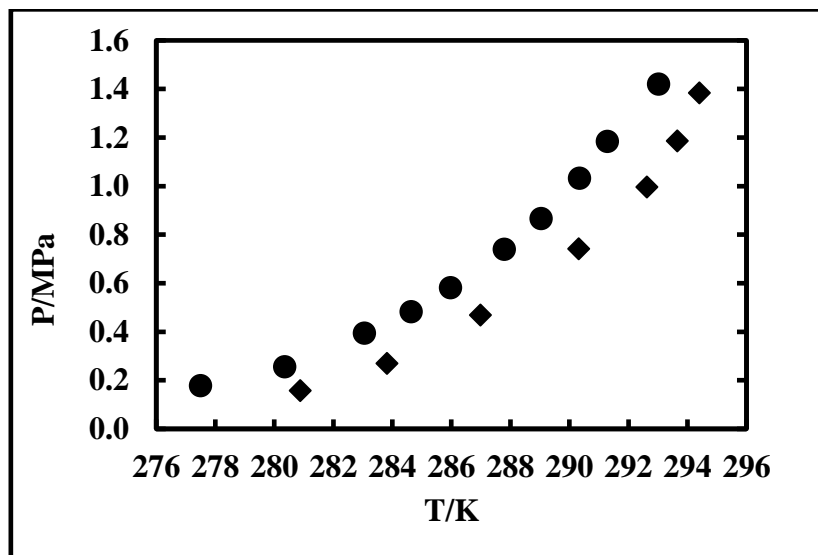


Figure 5. 7: Measured data for hydrate–liquid water–liquid promoter–vapour for the R410a (1) + water (2) in the absence and presence of CP systems: This work: ●, in the absence of CP; ◆, in the presence of CP.

5.2.3 R507 + water + CP systems

This author measured the binary system for R507 + water in the absence of CP in the MSc program in 2014. The ternary system for R507 + water + CP was measured in this study. The hydrate dissociation data is presented in Figure 5.8. The experimental data is presented in Table 5.8. The result for R507 + water + CP system shows an increase in hydrate dissociation temperatures by 1.3 K when compared to the system without CP. Although, the presence of CP increases dissociation temperatures but the hydrate dissociation temperatures were still far below ambient temperatures. Consequently, R507 is not suitable for gas hydrate technology for the desalination process. Although, the measured hydrate dissociation pressures were found below atmospheric pressures, which is good for gas hydrate technology for the desalination process.

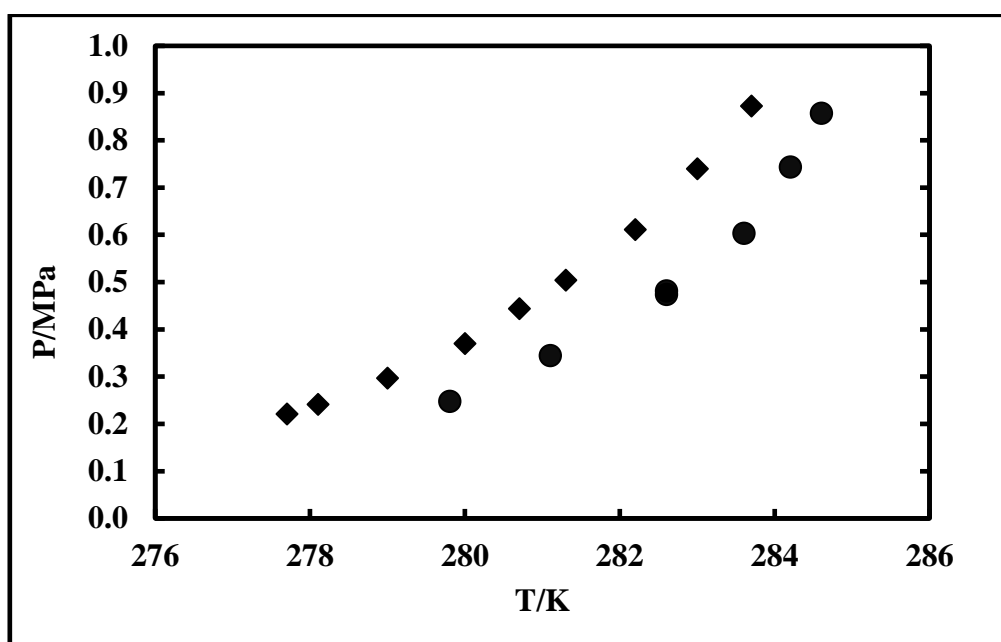


Figure 5. 8: Measured data for hydrate–liquid water–liquid promoter–vapour for the R507 (1) + water (2) + CP (3) system: This work: ◆, absence of CP; ●, in the presence of CP.

5.3 Refrigerant + single electrolytes in the presence of CP

This author measured the hydrate dissociation data for R134a, R507 and R410a + water + {NaCl or CaCl₂ or MgCl₂} systems at various salt concentrations previously in the MSc program in 2014. It was found that R410a is suitable fluorinated refrigerant to be used in gas

hydrate technology for a desalination process because the dissociation temperatures are closed to ambient temperatures. Previous results revealed that R410a + water system shows higher dissociation pressures compared to the {R507 or R134a} + water systems in the absence and presence of electrolytes such as {NaCl or CaCl₂ or MgCl₂}. The maximum dissociation pressure for the {R410a or R507 or R134a} + water systems were 1.421, 0.873 and 0.421 MPa, respectively. Consequently, from the research conducted by this author in 2014, it was recommended that further research is required for R410a + single and mixed electrolytes in the presence of water-insoluble promoter (CP).

In this study, gas hydrate dissociation data for R410a + water + (NaCl, MgCl₂, CaCl₂, and Na₂SO₄) systems were measured at various salt concentrations in the absence and presence of CP. All measured concentrations were below their solubility at 298.15 K. The solubility measurements are discussed later in this Chapter. The solubility was measured to ensure that no salt formed the precipitate or became saturated. All studied salts were completely dissolved in water, before hydrate formation.

The experimental hydrate dissociation data for R410a + water + NaCl + CP systems are presented in Table 5.7 and shown in Figure 5.9. This system shows that the addition of promoter (CP) causes the phase equilibrium boundary to increase hydrate dissociation temperatures compared to the system in the absence of CP at similar salt concentrations of (0.10 and 0.20) mass fraction. It is clearly shown in Table 5.7 that at the maximum dissociation temperature of 0.10 mass fraction, the temperature increases from 288.6 to 290.5 K in the presence of CP. It was also noted that the equilibrium phase boundary shifts to lower temperatures as salt concentration increases to 0.20 mass fraction. The results show that R410a can be employed as a hydrate former because it enables the elimination of electrolytes even at a high concentration of 0.20 mass fraction. The R410a + water + 0.10 mass fraction NaCl + CP system shows that the dissociation temperatures increase by 2.7 K compared to R410a + water + 0.10 mass fraction NaCl system measured by this author in 2014 as shown in Figure 5.9. There is no hydrate dissociation data published for R410a + water + NaCl + CP system that can be used to compare to the measured hydrate dissociation with CP.

Table 5. 7: Measured data for hydrate–liquid water–liquid promoter–vapour for the R410a (1) + water (2) + NaCl (3) + CP (4) system at various salt concentrations^a

R410a (1) + water (2)		R410a (1) + water (2) + CP (3)		^b R410a (1) + water (2) + 0.10 ^c NaCl (3)		R410a (1) + water (2) + 0.10 ^c NaCl (3) + CP (4)		R410a (1) + water (2) + 0.20 ^c NaCl (3) + CP (4)	
T/K	P/MPa	T/K	P/MPa	T/K	P/MPa	T/K	P/MPa	T/K	P/MPa
293.0	1.4213	294.4	1.3852	288.6	1.2706	290.5	1.1791	285.8	0.8790
291.3	1.1847	293.7	1.1877	286.9	1.0315	289.6	1.0413	285.2	0.7922
290.3	1.0339	292.6	0.9970	285.5	0.8529	288.6	0.9015	284.1	0.6761
289.0	0.8676	290.3	0.7424	283.9	0.7029	287.4	0.7673	283.1	0.5873
287.8	0.7414	287.0	0.4699	282.1	0.5697	286.0	0.6339	281.5	0.4760
286.0	0.5824	283.8	0.2719	280.7	0.4724	283.2	0.4448	280.1	0.3865
284.6	0.4837	280.9	0.1588	278.4	0.3487	280.2	0.2869		
283.1	0.3955			276.1	0.2399				
280.3	0.2568								
277.5	0.1788								

^aU(T) (0.95 level of confidence) = 0.1 K, U(P) (0.95 level of confidence) = 0.0007 MPa

^bNgema et al. (2014); ^cValues are in mass fraction.

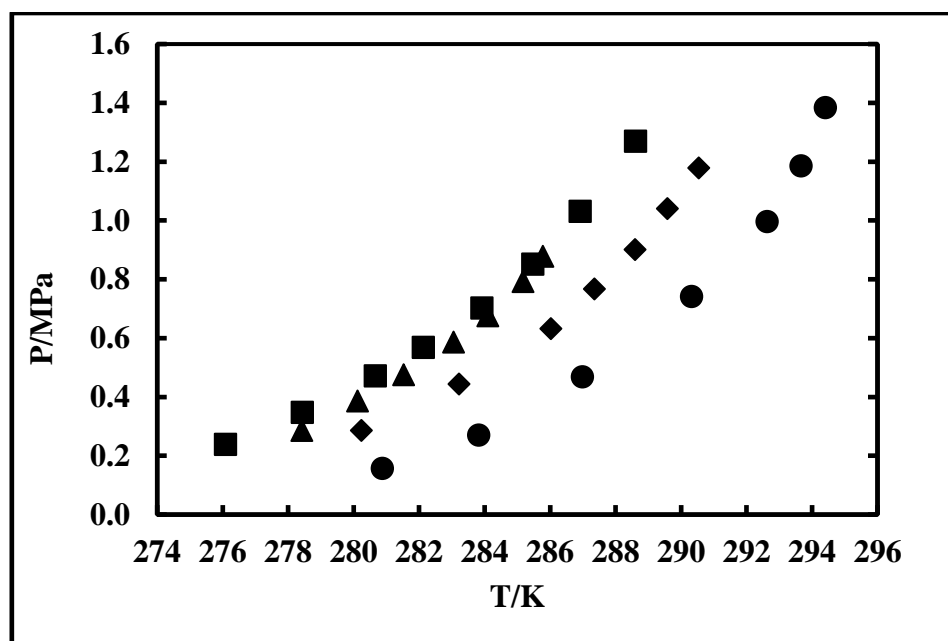


Figure 5. 9: Measured data for hydrate–liquid water–liquid promoter–vapour for the R410a (1) + water (2) + NaCl (3) + CP (4) system: ■, Ngema et al. (2014); This work: ●, absence of salt + CP; ◆, 0.10 mass fraction + CP; ▲, 0.20 mass fraction + CP.

The experimental hydrate dissociation data for R410a + water + CaCl₂ + CP systems are presented in Table 5.8 and shown in Figure 5.10. The R410a + water + CaCl₂ + CP system in Figure 5.10 shows that the presence of CP causes the phase equilibrium boundary to increase dissociation temperatures closed to ambient temperatures even at a higher electrolyte concentration of 0.15 mass fraction. This system was measured at salt concentration of 0.10 and 0.15 mass fraction. It was also noted that there is a slight shift for the equilibrium phase boundary to lower temperatures as electrolyte concentration increases to 0.15 mass fraction.

Table 5. 8: Measured data for hydrate–liquid water–liquid promoter–vapour for the R410a (1) + water (2) + CaCl₂ (3) + CP (4) system at various salt concentrations^a

R410a (1) + water (2)		R410a (1) + water (2) + CP (3)		R410a (1) + water (2) + 0.10 ^b CaCl ₂ (3) + CP (4)		R410a (1) + water (2) + 0.15 ^b CaCl ₂ (3) + CP (4)	
T/K	P/MPa	T/K	P/MPa	T/K	P/MPa	T/K	P/MPa
293.0	1.4213	294.4	1.3852	293.7	1.0561	291.9	1.0561
291.3	1.1847	293.7	1.1877	292.7	0.8359	290.1	0.8359
290.3	1.0339	292.6	0.9970	292.0	0.7772	287.7	0.7772
289.0	0.8676	290.3	0.7424	290.2	0.5873	287.8	0.5873
287.8	0.7414	287.0	0.4699	290.2	0.5981	285.4	0.5981
286.0	0.5824	283.8	0.2719	287.9	0.3859	282.6	0.3859
284.6	0.4837	280.9	0.1588	285.3	0.2148		
283.1	0.3955						
280.3	0.2568						
277.5	0.1788						

^aU(T) (0.95 level of confidence) = 0.1 K, U(P) (0.95 level of confidence) = 0.0007 MPa

^bValues are in mass fraction.

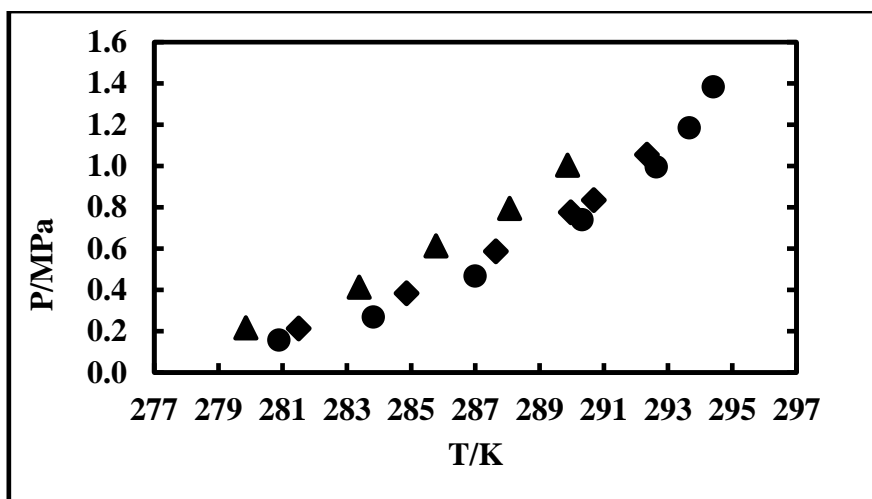


Figure 5. 10: Measured data for hydrate–liquid water–liquid promoter–vapour for the R410a (1) + water (2) + CaCl₂ (3) + CP (4) system: This work: ◆, absence of salt + CP; ●, 0.10 mass fraction + CP; ▲, 0.15 mass fraction + CP.

The experimental hydrate dissociation data for R410a + water + Na₂SO₄ system is presented in Table 5.9 and shown in Figure 5.11. The R410a + water + Na₂SO₄ system in Figure 5.11 was measured at salt concentration of 0.10 mass fraction. It was found shows that the addition of Na₂SO₄ causes the phase equilibrium boundary to shift slightly lower dissociation temperatures, but these temperatures are closed to ambient temperatures even at salt concentration of 0.10 mass fraction.

Table 5. 9: Measured data for hydrate–liquid water–vapour for R410a (1) + water (2) + Na₂SO₄ (3) system at 0.10 wt% concentrations of salt^a

R410a (1) + water (2)		R410a (1) + water (2) + 0.100 ^b Na ₂ SO ₄ (3)	
T/K	P/MPa	T/K	P/MPa
293.0	1.4213	291.6	1.3733
291.3	1.1847	289.6	1.0671
290.3	1.0339	288.2	0.9016
289.0	0.8676	285.4	0.6274
287.8	0.7414	283.3	0.4639
286.0	0.5824	281.0	0.3167
284.6	0.4837	278.3	0.1997
283.1	0.3955		
280.3	0.2568		
277.5	0.1788		

^aU(T) (0.95 level of confidence) = 0.1 K, U(P) (0.95 level of confidence) = 0.0007 MPa

^bValues are in mass fraction.

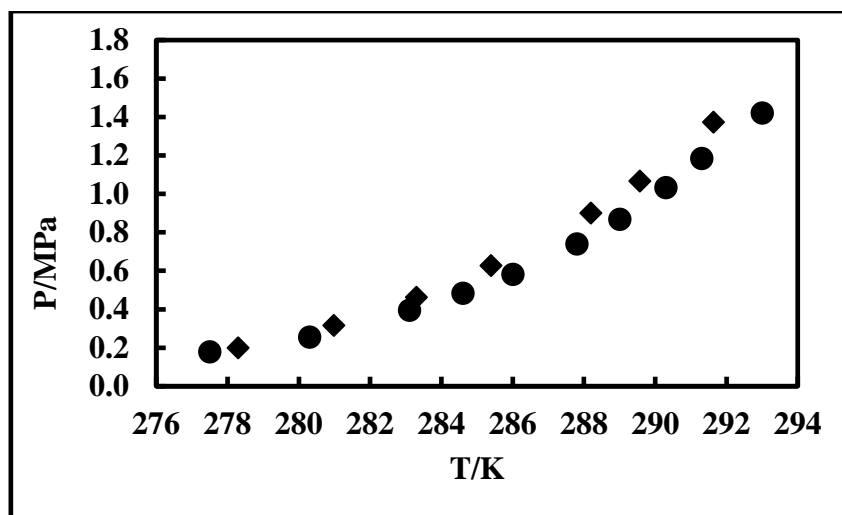


Figure 5. 11: Measured data for hydrate–liquid water–liquid promoter–vapour for the R410a (1) + water (2) + Na₂SO₄ (3) system: symbols represent experimental data: ●, Akiya et al., (1999) in the absence of salt; This work in the presence of salt: ◆, 0.10 mass fraction.

5.4 Refrigerant + mixed electrolytes in the presence of CP

5.4.1 Industrial concentration

Experimental gas hydrate dissociation data for {R410a or R507} + water + mixed electrolytes (NaCl, CaCl₂ and MgCl₂) systems were measured at maximum concentrations of electrolytes at an industrial wastewater treatment plant as indicated in Table 2.6 in Chapter 2. The selected maximum concentration covers the electrolytes concentrations in seawater as tabulated in Table 2.7 in Chapter 2.

The R410a + water + 0.002 mass fraction CaCl₂ + 0.017 mass fraction NaCl system was measured at industrial maximum concentrations of 0.002 mass fraction and 0.017 mass fraction respectively for electrolyte in the absence and presence of CP. The measured hydrate dissociation data are presented in Table 5.10. These measurements are undertaken in the absence and presence of CP and the results are presented in Figure 5.12. It was revealed that in the addition of CP the dissociation temperatures increase by 2.4 K as shown in Figure 5.12. It was also found that the mixed of electrolytes have an inhibition effect by shifting phase equilibrium boundary to lower dissociation temperatures by 0.9 K in the absence and the presence of CP for this system.

Table 5. 10: Measured data for hydrate–liquid water–liquid promoter–vapour for the R410a (1) + water (2) + CaCl₂ (3) + NaCl (4) + CP (5) system at various salt concentrations^a

R410a (1) + water (2)		R410a (1) + water (2) + CP (3)		R410a (1) + water (2) + 0.002 ^b CaCl ₂ (3) + 0.017 ^b NaCl (4)		R410a (1) + water (2) + 0.002 ^b CaCl ₂ (3) + 0.017 ^b NaCl (4) + CP (5)	
T/K	P/MPa	T/K	P/MPa	T/K	P/MPa	T/K	P/MPa
293.0	1.4213	294.4	1.3852	289.4	1.0197	292.5	1.1193
291.3	1.1847	293.7	1.1877	289.3	1.0083	290.8	0.9075
290.3	1.0339	292.6	0.9970	288.4	0.8935	289.5	0.7427
289.0	0.8676	290.3	0.7424	286.9	0.7308	289.5	0.7319
287.8	0.7414	287.0	0.4699	284.7	0.5629	286.2	0.4683
286.0	0.5824	283.8	0.2719	281.3	0.3549	283.3	0.2993
284.6	0.4837	280.9	0.1588	279.6	0.2500		
283.1	0.3955						
280.3	0.2568						
277.5	0.1788						

^aU(T) (0.95 level of confidence) = 0.1 K, U(P) (0.95 level of confidence) = 0.0007 MPa

^bValues are in mass fraction.

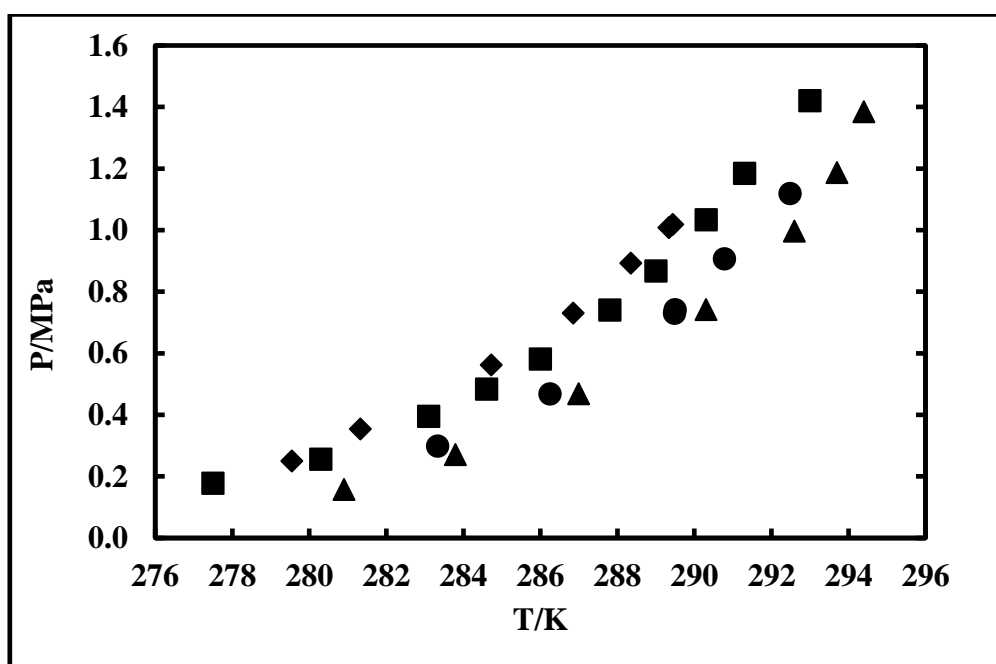


Figure 5. 12: Measured data for hydrate–liquid water–liquid promoter–vapour for the R410a (1) + water (2) + 0.0020 mass fraction of CaCl₂ (3) + 0.017 mass fraction of NaCl (4) + CP (5) systems: ■, Akiya et al., (1999) in the absence of CP; This work: ◆, mixed salt in the absence of CP; ●, mixed salt in the presence of CP; ▲, R410a in the presence of CP.

The measured hydrate dissociation data for R410a + water + 0.013 mass fraction MgCl₂ + 0.019 mass fraction NaCl systems are presented in Table 5.11. These measurements are undertaken in the absence and presence of CP and the results are shown in Figure 5.13. It shows an increase in dissociation temperatures by 2.9 K at a higher pressure of 1.017 MPa and increase by 3.2 K at a lower pressure of 0.238 MPa as shown in Figure 5.13. The phase equilibrium boundary shifts to lower dissociation temperatures by 1.4 K in the absence of CP and 0.8 in the presence of CP for this system presented in Figure 5.13.

Table 5. 11: Measured data for hydrate–liquid water–liquid promoter–vapour for the R410a (1) + water (2) + MgCl₂ (3) + NaCl (4) + CP (5) system at various salt concentrations^a

R410a (1) + water (2)		R410a (1) + water (2) + CP (3)		R410a (1) + water (2) + 0.0013 ^b MgCl ₂ (3) + 0.019 ^b NaCl (4)		R410a (1) + water (2) + 0.0013 ^b MgCl ₂ (3) + 0.019 ^b NaCl (4) + CP (5)	
T/K	P/MPa	T/K	P/MPa	T/K	P/MPa	T/K	P/MPa
293.0	1.4213	294.4	1.3852	288.9	1.0183	292.9	1.1693
291.3	1.1847	293.7	1.1877	287.6	0.8606	291.8	0.9903
290.3	1.0339	292.6	0.9970	287.5	0.7674	291.8	0.9766
289.0	0.8676	290.3	0.7424	286.7	0.6146	290.0	0.8044
287.8	0.7414	287.0	0.4699	285.0	0.4777	288.2	0.6573
286.0	0.5824	283.8	0.2719	283.2	0.3923	285.9	0.4556
284.6	0.4837	280.9	0.1588	281.6	0.2442	282.3	0.2381
283.1	0.3955			279.1	0.2446		
280.3	0.2568						
277.5	0.1788						

^aU(T) (0.95 level of confidence) = 0.1 K, U(P) (0.95 level of confidence) = 0.0007 MPa

^bValues are in mass fraction.

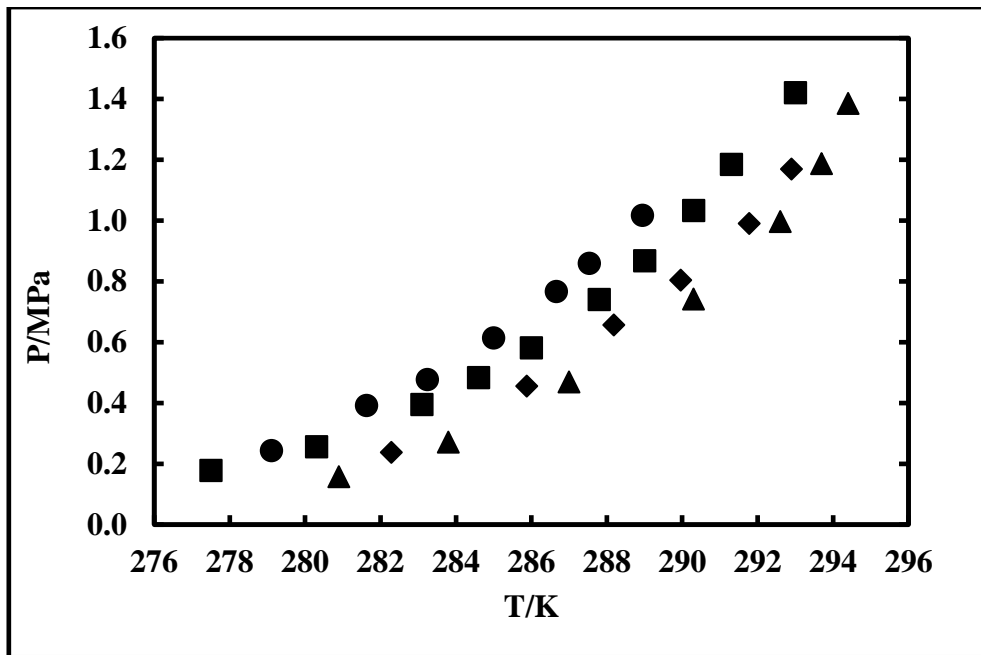


Figure 5. 13: Measured data for hydrate–liquid water–liquid promoter–vapour for the R410a (1) + water (2) + 0.013 mass fraction of MgCl₂ (3) + 0.019 mass fraction of NaCl (4) + CP (5) system: ■, Ngema et al., (2014) in the absence of CP; This work:●, mixed salt in the absence of CP; ◆, mixed salt in the presence of CP; ▲, R410a in the presence of CP.

5.4.2 R507 + water + CaCl₂ + NaCl + CP system

In this study, the R507 + water + 0.002 mass fraction CaCl₂ + 0.017 mass fraction NaCl system was measured in the absence and presence of CP. The measured hydrate dissociation data are presented in Table 5.12 and shown in Figure 5.14. It was found that the dissociation temperatures for this system increases by 1.2 K at a higher pressure of 0.759 MPa and increase by 1.7 K at a lower pressure of 0.250 MPa as shown in Figure 5.14. It was revealed that the mixed of electrolytes have an inhibition effect by shifting the phase equilibrium boundary to lower dissociation temperatures by 0.3 K in the absence of CP and 0.9 K in the presence of CP at a higher pressure of 0.604 MPa and 0.3 K at lower pressure of 0.345 MPa. It was found that R507 + water system has lower dissociation temperatures in the presence of CP, as shown in Figures 5.8, as result R507 is not suitable for gas hydrate technology for the desalination process.

Table 5. 12: Measured data for hydrate–liquid water–liquid promoter–vapour for the R507 (1) + water (2) + CaCl₂ (3) + NaCl (4) + CP (5) system at various salt concentrations^a

R507 (1) + water (2)		R507 (1) + water (2) + CP (3)		R507 + water (2) + 0.002 ^b CaCl ₂ (3) + 0.017 ^b NaCl (4)		R507 (1) + water (2) + 0.002 ^b CaCl ₂ (3) + 0.017 ^b NaCl (4) + CP (5)	
T/K	P/MPa	T/K	P/MPa	T/K	P/MPa	T/K	P/MPa
283.3	0.8733	284.6	0.8580	283.0	0.8311	284.0	0.7783
283.0	0.7401	284.2	0.7445	282.9	0.7591	284.1	0.7784
282.2	0.6110	283.2	0.6041	281.5	0.6783	281.8	0.6675
281.3	0.5043	282.6	0.4744	282.4	0.6704	280.9	0.5370
280.7	0.4442	282.6	0.4823	282.3	0.5552	279.5	0.4479
280.0	0.3704	281.1	0.3459	281.0	0.5026	283.4	0.3649
279.0	0.2979	279.8	0.2489	280.1	0.4087	282.5	0.2483
278.1	0.2417			279.3	0.3506		
277.7	0.2212			277.8	0.2503		

^aU(T) (0.95 level of confidence) = 0.1 K, U(P) (0.95 level of confidence) = 0.0007 MPa

^bValues are in mass fraction.

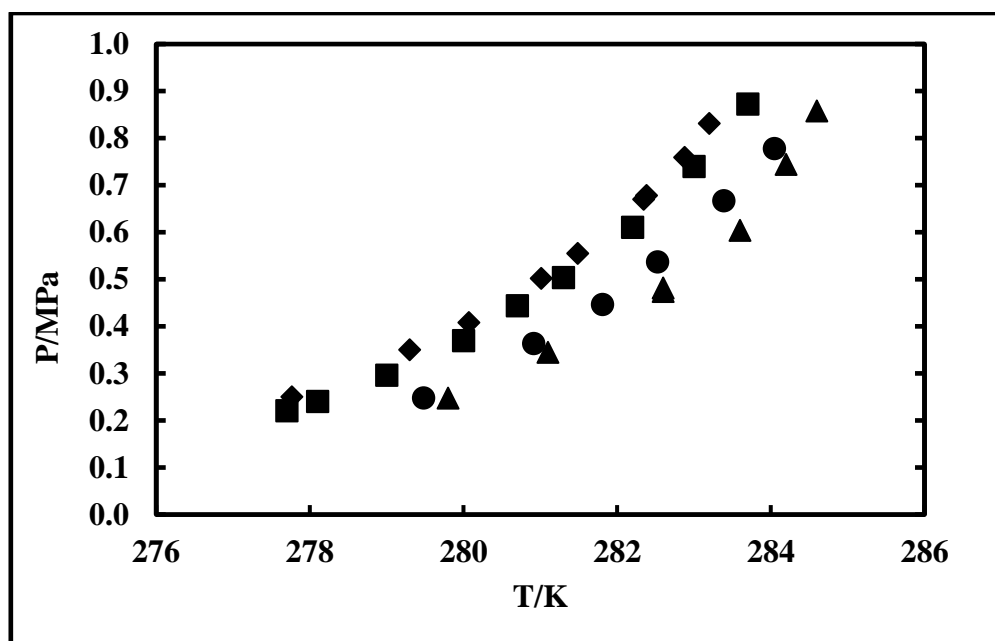


Figure 5. 14: Measured data for hydrate–liquid water–liquid promoter–vapour for the R507 (1) + water (2) + 0.0020 mass fraction of CaCl₂ (3) + 0.017 mass fraction of NaCl (4) + CP (5) system: ■, Ngema et al., (2014); This work: ◆, mixed salt in the absence of CP; ●, mixed salt in the presence of CP; ▲, R507 + water + CP.

5.4.3 R410a systems at higher concentration

It is important to measure hydrate dissociation data at a higher concentration than industrial wastewater concentration, because the salt concentration can increase way above the targeted concentration. Secondly, to ensure that the gas hydrate can be formed at higher concentration and no is precipitate formed. In this study, gas hydrate dissociation data for R410a + water + mixed electrolytes (NaCl and CaCl₂) systems were measured at a higher concentration range of (0.05 to 0.15) mass fraction of electrolytes. The gas hydrate systems were measured in the absence and presence of CP.

The experimental hydrate dissociation data for R410a + water 0.08 mass fraction CaCl₂ and 0.05 mass fraction NaCl and R410a + water + 0.05 mass fraction NaCl + 0.15 mass fraction CaCl₂ systems in the absence and presence of CP are presented in Table 5.13 and shown in Figures 5.15 and 5.16. It was found that the dissociation temperature for R410a + water 0.08 mass fraction CaCl₂ and 0.05 mass fraction NaCl system increases by 3.2 K in presence of CP as shown in Figure 5.15. Further, by increasing the concentration of CaCl₂ to 0.15 mass fraction and keeping NaCl constant at 0.05 mass fraction, it was found that dissociation temperature increases by 7.6 K at a higher pressure of 1.074 MPa and increases by 5.7 K at lower pressure of 0.279 MPa as shown in Figure 5.16. As the concentration of CaCl₂ increases up 0.15 mass fraction while NaCl remains constant at 0.05 mass fraction, the phase equilibrium boundary shifts to lower dissociation temperatures. These systems show that the hydrate can be formed at even higher concentrations of salt, but the measured concentrations were below the salt saturation. This was verified by measuring the solubility of salts, which is discussed later in this chapter.

Consequently, all results for R410a systems show that it can be utilised as a hydrate former for gas hydrate technology for the desalination processes in the presence of CP, because their dissociation temperatures are very close to ambient temperatures even at higher concentrations.

Table 5. 13: Measured data for hydrate–liquid water–liquid promoter–vapour for the R410a (1) + water (2) + NaCl (3) + CaCl₂ (4) + CP (5) system at various salt concentrations^a

R410a (1) + water (2) + 0.05 ^b NaCl (3) + 0.05 ^b CaCl ₂ (4)		R410a (1) + water (2) + 0.05 ^b NaCl (3) + 0.08 ^b CaCl ₂ (4)		R410a (1) + water (2) + 0.05 ^b NaCl (3) + 0.08 ^b CaCl ₂ (4) + CP (5)		R410a (1) + water (2) + 0.05 ^b NaCl (3) + 0.15 ^b CaCl ₂ (4)		R410a (1) + water (2) + 0.05 ^b NaCl (3) + 0.15 ^b CaCl ₂ (4) + CP (5)	
T/K	P/MPa	T/K	P/MPa	T/K	P/MPa	T/K	P/MPa	T/K	P/MPa
291.5	1.4025	288.8	1.0672	294.6	1.0992	282.2	1.0744	289.4	1.0413
289.8	1.1455	288.8	1.0834	292.7	0.8093	281.8	0.9963	286.6	0.7424
286.8	0.7757	286.6	0.8091	291.2	0.6640	280.6	0.8110	286.6	0.7615
282.3	0.4748	284.6	0.6510	289.2	0.4995	280.7	0.8324	285.1	0.6211
280.8	0.3841	282.9	0.5320	289.2	0.5130	279.7	0.6991	283.4	0.4660
275.1	0.1993	281.2	0.4379	286.2	0.3144	279.3	0.6486	281.1	0.3069
		279.3	0.3588	283.8	0.1919	277.9	0.5197	279.3	0.2041
		276.4	0.2498			276.1	0.3749		
						274.5	0.2796		

^aU(T) (0.95 level of confidence) = 0.1 K, U(P) (0.95 level of confidence) = 0.0007 MPa

^bValues are in mass fraction.

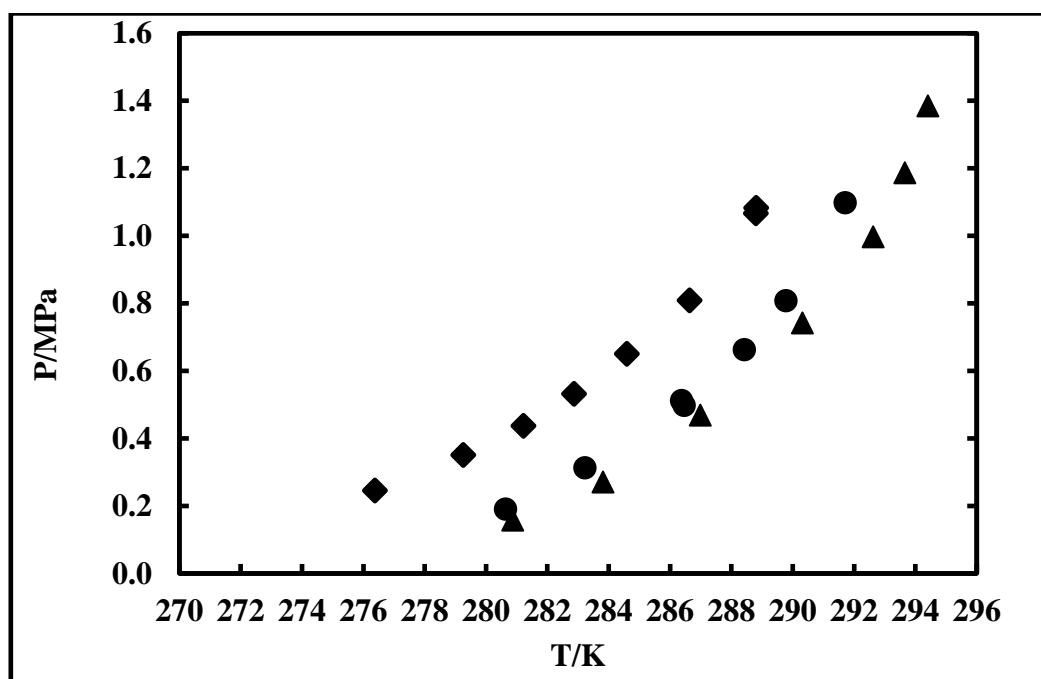


Figure 5. 15 Measured data for hydrate–liquid water–liquid promoter–vapour for the R410a (1) + water (2) + 0.05 mass fraction of NaCl (3) + 0.08 mass fraction of CaCl₂ (4) + CP (5) system: This work: ▲, R410a in the presence of CP; ◆, mixed salt in the absence of CP; ●, mixed salt in the presence of CP.

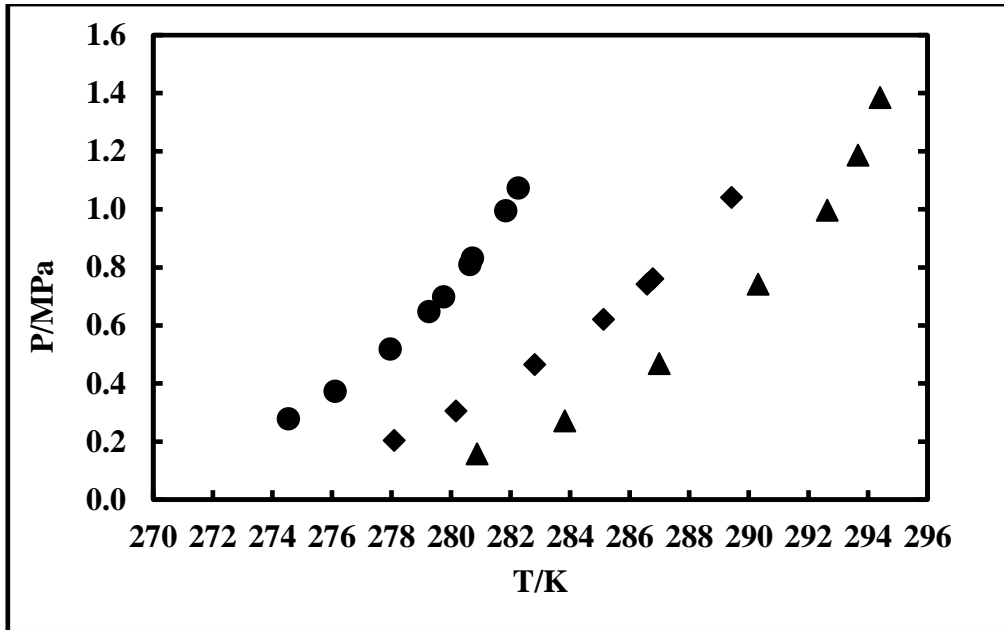


Figure 5. 16: Measured data for hydrate–liquid water–liquid promoter–vapour for the R410a (1) + water (2) + 0.05 mass fraction of NaCl (3) + 0.15 mass fraction of CaCl₂ (4) + CP (5) system: This work: ▲, R410a in the presence of CP; ●, mixed salt in the absence of CP; ◆, mixed salt in the presence of CP.

5.4.4 The effect of CP on the formation and dissociation of gas hydrates

Experimental results show that the addition of single and mixed electrolytes {NaCl or MgCl₂ or CaCl₂ or Na₂SO₄} on hydrate formation have an inhibiting effect to the shift phase equilibrium boundary to slightly lower dissociation temperature, but in the presence of CP the hydrate dissociation temperatures for R410a systems were increased near ambient temperatures. Consequently, the CP promoter made an impressive increase of dissociation temperatures for R410a systems in the presence of single and mixed electrolytes. However, R507 systems show the hydrate dissociation temperatures were still lower than ambient temperatures even in the presence of CP, as the results were presented in Figures 5.8 and 5.14.

Normally, cyclopentane forms structure sII hydrate, in this study, CP made an impressive increase of dissociation temperatures in systems where the gas phase species enters the small cavities of the sII hydrate structure. This means that CP is more stable, if the small and large cavities are fully occupied.

Some researchers investigated promoters, which include cyclopentane, cyclohexane, neopentane, isopentane, methylcyclopentane and methylcyclohexane. It was found that CP demonstrates the largest promotion effect compared to the others on the measured hydrate

phase boundaries (Herslund, 2013). Sun et al. (2002) reported hydrate dissociation data for methane using cyclohexane or cyclopentane as a promoter. It was revealed that CP was more powerful compared to cyclohexane. Therefore, the cyclopentane was selected as a promoter in this study because research indicated that it was powerful in comparison to other mentioned promoters. Cyclopentane can lower the dissociation pressure and raise dissociation temperature compared to the pure gas hydrate systems of the pure refrigerants.

5.5 Enthalpy of hydrate dissociation

The energy required for the hydrate systems containing electrolytes is determined by the enthalpy of hydrate dissociation. This is an essential property for the design of gas hydrate desalination process. The Clausius-Clapeyron equation was used to estimate enthalpy of hydrate dissociation.

$$\Delta H = -RZ \left(\frac{d(\ln P)}{d\left(\frac{1}{T}\right)} \right) \quad (5.2)$$

where Z represents the compressibility factor, which is calculated by using SRK equation of state (Soave, 1972), R represents the universal gas constant and $d(\ln P)/d(1/T)$ is the gradient obtained by plotting $\ln P$ vs $1/T$ using experimental hydrate dissociation data. Table 5.14 represent the calculated values for enthalpy of dissociation and they are plotted in Figure 5.17. Three hydrate formers are reported in Table 5.28 (R410a, R507 and R134a). , It was observed in Figure 5.17 that R507 systems have high enthalpy compared to R134 and R410a. It was noted that the measured dissociation temperatures for R507 hydrate systems are lower than R410a, which means more energy is required for R507. Consequently, it is not a suitable hydrate former for the hydrate process as well as R134a for the same reasons.

It was found that the enthalpy of dissociation ranging from (139.76 to 209.77) kJ/mol for R507, (124.14 to 147.04) kJ/mol for R134a and (66.00 to 134.25) kJ/mol for R410a systems in the absence and presence of salt and cyclopentane. Consequently, shows that R410a can be utilized as a hydrate former for gas hydrate desalination process, because it requires less energy compare to the R507 and R134a.

Table 5. 14: Enthalpy of hydrate dissociation

R410a (1) + water (2)		R134a (1) + water (2)		R410a (1) + water (2) + 0.1NaCl (3)		R410a (1) + water (2) + 0.1NaCl (3) + CP (4)	
T/K	ΔH /kJ/mol	T/K	ΔH /kJ/mol	T/K	ΔH /kJ/mol	T/K	ΔH /kJ/mol
293.0	69.58	283.0	124.15	288.6	69.94	290.5	76.21
291.3	75.91	282.6	125.38	286.9	73.31	289.6	78.19
290.3	78.04	281.9	126.85	285.5	75.73	288.6	80.16
289.0	80.31	281.4	128.24	283.9	77.67	287.4	81.97
287.8	81.99	281.4	128.37	282.1	79.36	286.0	83.75
286.0	84.07	280.7	129.29	280.7	80.61	283.2	86.21
284.6	85.33	280.4	129.73	278.4	82.17	280.2	88.28
283.1	86.46	280.0	130.34	276.1	83.56		
280.3	88.26	280.0	130.45				
277.5	89.26	279.3	131.37				
		278.4	132.59				
		277.6	133.25				
		275.8	134.25				
R410a (1) + water (2) + 0.2NaCl (3) + CP (4)		R410a (1) + water (2) + 0.1CaCl ₂ (3) + CP (4)		R410a (1) + water (2) + 0.15CaCl ₂ (3) + CP (4)		R410a (1) + water (2) + 0.1Na ₂ SO ₄ (3)	
T/K	ΔH /kJ/mol	T/K	ΔH /kJ/mol	T/K	ΔH /kJ/mol	T/K	ΔH /kJ/mol
285.8	85.11	293.7	109.33	291.9	95.94	291.6	77.33
285.2	86.44	292.7	113.48	290.1	99.28	289.6	82.07
283.1	89.43	292.0	114.48	287.7	102.35	288.2	84.50
281.5	91.01	290.2	117.83	287.8	102.08	285.4	88.39
280.1	92.29	290.2	117.62	285.4	105.22	283.3	90.68
278.4	93.73	287.9	121.35	282.6	108.35	283.3	90.97
		285.3	124.33			281.0	92.72
						278.3	94.35
R410a (1) + water (2) + 0.05NaCl (3) + 0.08CaCl ₂ (4)		R410a (1) + water (2) + 0.05NaCl (3) + 0.08CaCl ₂ (4) + CP (5)		R410a (1) + water (2) + 0.05NaCl (3) + 0.15CaCl ₂ (4)		R410a (1) + water (2) + 0.05NaCl (3) + 0.15CaCl ₂ (4) + CP (5)	
T/K	ΔH /kJ/mol	T/K	ΔH /kJ/mol	T/K	ΔH /kJ/mol	T/K	ΔH /kJ/mol
288.8	66.21	294.6	93.04	282.2	90.75	289.4	92.47
288.8	66.00	292.7	97.60	281.8	92.24	286.6	97.29
286.6	69.28	291.2	99.76	280.6	95.65	286.6	96.96
284.6	71.08	289.2	101.99	280.7	95.26	285.1	99.19
282.9	72.42	289.2	102.20	279.7	97.63	283.4	101.64
281.2	73.48	286.2	104.93	279.3	98.53	281.1	104.15
279.3	74.44	283.8	106.77	277.3	100.69	279.3	105.75
276.4	75.63			276.1	103.21		
				274.5	104.81		

Table 5.14: Enthalpy of hydrate dissociation continue.....

R410a (1) + water (2) + 0.002CaCl ₂ (3) + 0.017NaCl (4)		R410a (1) + water (2) + 0.002CaCl ₂ (3) + 0.017NaCl (4) + CP (5)		R410a (1) + water (2) + 0.0013MgCl ₂ (3) + 0.019NaCl (4)		R410a (1) + water (2) + 0.0013MgCl ₂ (3) + 0.019NaCl (4) + CP (5)	
T/K	ΔH/ kJ/mol	T/K	ΔH/ kJ/mol	T/K	ΔH/ kJ/mol	T/K	ΔH/ kJ/mol
289.3	103.11	292.5	105.17	288.9	105.81	292.9	108.66
289.4	102.92	290.8	108.89	287.6	108.90	291.8	112.03
288.4	105.11	289.5	111.77	287.5	108.64	291.8	112.29
284.7	110.71	289.5	111.99	286.7	110.30	290.0	115.35
281.3	114.20	286.2	116.40	285	112.97	288.2	117.93
279.6	115.96	283.3	119.25	283.2	115.34	285.9	121.51
				281.6	116.80	282.3	125.36
				279.1	119.40		
R507 (1) + water (2)		R507 (1) + water (2) + CP (3)		R507 (1) + water (2) + 0.002CaCl ₂ (3) + 0.017NaCl (4)		R507 (1) + water (2) + 0.002CaCl ₂ (3) + 0.017NaCl (4) + CP (5)	
T/K	ΔH/ kJ/mol	T/K	ΔH/ kJ/mol	T/K	ΔH/ kJ/mol	T/K	ΔH/ kJ/mol
283.3	126.46	284.6	139.76	283.0	162.45	284.0	186.96
283.0	131.25	284.2	144.12	282.9	165.53	284.1	187.23
282.2	135.55	283.2	149.11	282.4	168.79	283.4	191.99
281.3	138.96	282.6	153.68	282.3	169.09	282.5	197.66
280.7	140.84	282.6	153.39	281.5	173.60	281.8	201.50
280.0	143.14	281.1	157.95	281.0	175.62	280.9	204.96
279.0	145.35	279.8	161.13	280.1	179.17	279.5	209.77
278.1	147.04			279.3	181.32		
277.7	147.64			277.8	185.02		
R410a (1) + water (2) + 0.05NaCl (3) + 0.05CaCl ₂ (4)		R410a (1) + water (2) + CP (3)					
T/K	ΔH/ kJ/mol	T/K	ΔH/ kJ/mol				
291.5	62.69	294.4	85.70				
289.8	65.94	293.7	89.10				
286.8	70.44	292.6	92.14				
282.3	73.83	290.3	96.01				
280.8	74.86	287.0	100.03				
275.1	76.94	283.8	102.95				
		280.9	104.62				

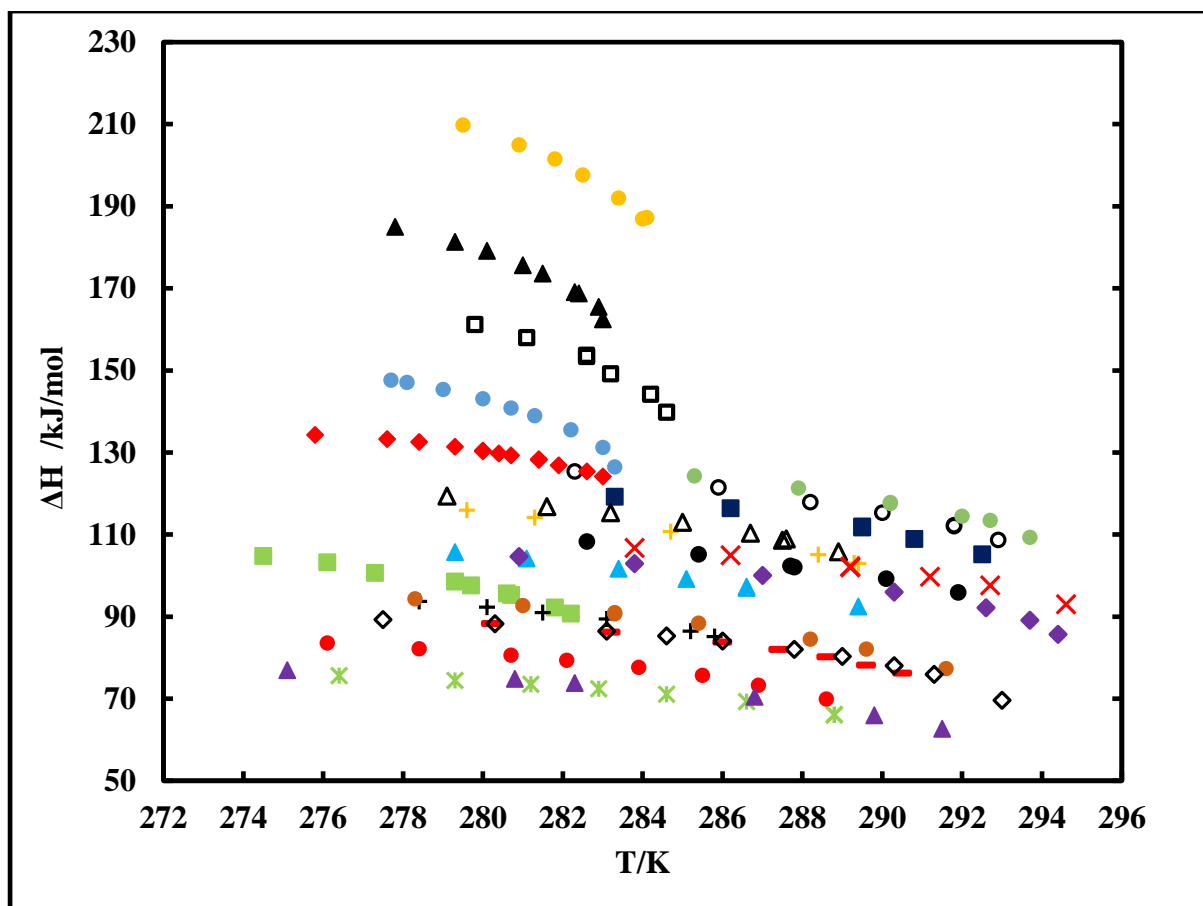


Figure 5. 17: Enthalpy of measured hydrate dissociation data in the absence and presence of single and mixed salt as well as CP: This work: \diamond , A; \blacklozenge , B; \bullet , C; $—$, D; $+$, E; \bullet , F; \bullet , G; \bullet , H; $*$, I; \times , J; \blacksquare , K; \blacktriangle , L; $+$, M; \blacksquare , N; \triangle , O; \circ , P; \bullet , Q; \square , R; \blacktriangle , S; \bullet , T; \blacktriangle , U; \blacklozenge , V

A: R410a (1) + water (2); **B:** R134a (1) + water (2); **C:** R410a (1) + water (2) + 0.1NaCl (3); **D:** R410a (1) + water (2) + 0.1NaCl (3) + CP (4); **E:** R410a (1) + water (2) + 0.2NaCl (3) + CP (4); **F:** R410a (1) + water (2) + 0.1CaCl₂ (3) + CP (4); **G:** R410a (1) + water (2) + 0.15CaCl₂ (3) + CP (4); **H:** R410a (1) + water (2) + 0.1Na₂SO₄ (3); **I:** R410a (1) + water (2) + 0.05NaCl (3) + 0.08CaCl₂ (4); **J:** R410a (1) + water (2) + 0.05NaCl (3) + 0.08CaCl₂ (4) + CP (5); **K:** R410a (1) + water (2) + 0.05NaCl (3) + 0.15CaCl₂ (4); **L:** R410a (1) + water (2) + 0.05NaCl (3) + 0.15CaCl₂ (4) + CP (5); **M:** R410a (1) + water (2) + 0.002CaCl₂ (3) + 0.017NaCl (4); **N:** R410a (1) + water (2) + 0.002CaCl₂ (3) + 0.017NaCl (4) + CP (5); **O:** R410a (1) + water (2) + 0.0013MgCl₂ (3) + 0.019NaCl (4); **P:** R410a (1) + water (2) + 0.0013MgCl₂ (3) + 0.019NaCl (4) + CP (5); **Q:** R507 (1) + water (2); **R:** R507 (1) + water (2) + CP (3); **S:** R507 (1) + water (2) + 0.002CaCl₂ (3) + 0.017NaCl (4); **T:** R507 (1) + water (2) + 0.002CaCl₂ (3) + 0.017NaCl (4) + CP (5); **U:** R410a (1) + water (2) + 0.05NaCl (3) + 0.05CaCl₂ (4); **V:** R410a (1) + water (2) + CP (3)

5.6 Kinetic measurements

The kinetics of hydrate formation rates were studied for the systems of interest. Kinetics data is essential in the hydrate reactor design. Hence, the rate of hydrate formation of R410a refrigerant was evaluated and the effect of initial pressure, initial temperature, and the degree of subcooling on the hydrate nucleation and growth rate. Only R410a was investigated because it was found that it was the suitable refrigerant for the desalination process using gas hydrate technology. Figure 5.18 shows the initial pressure, initial temperature and the degree of subcooling for R410a + water + mixed salt systems in the absence. More results are presented in Appendix E. The initial pressure and initial temperature were selected in the hydrate stability zone to ensure the formation of the clathrate hydrate.

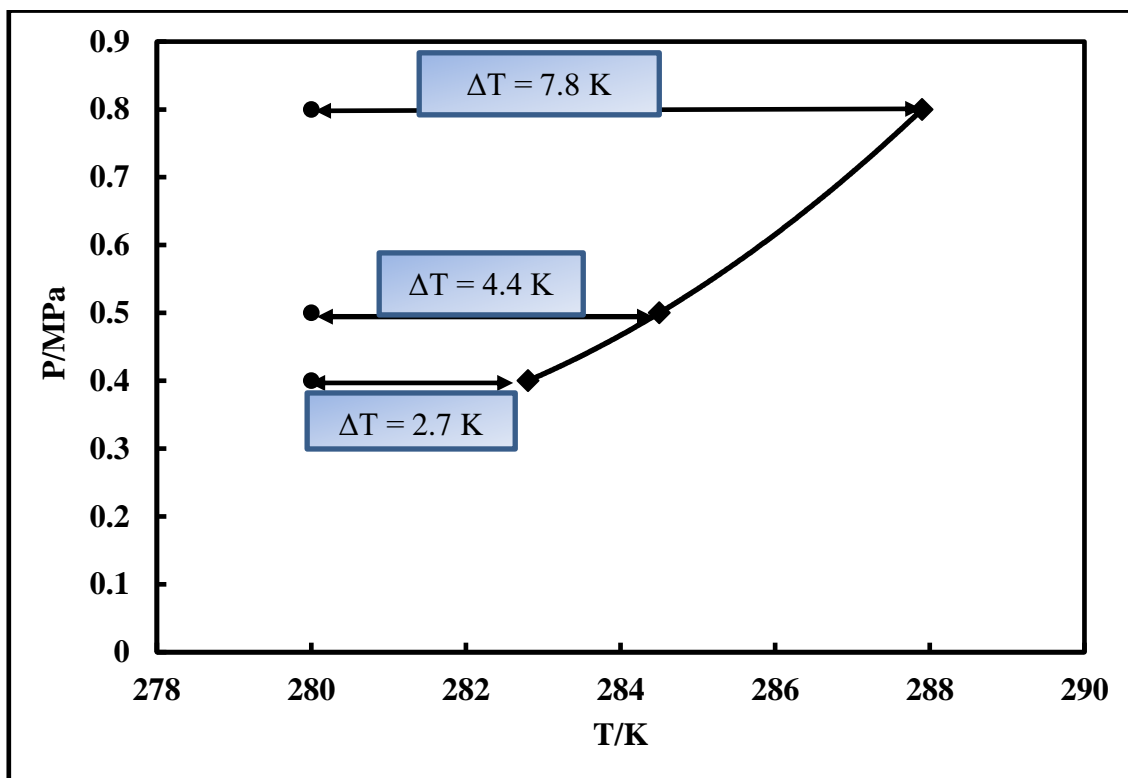


Figure 5. 18: Initial conditions and degree of subcooling for R410a (1) + water (2) + 0.013 mass fraction of MgCl₂ (3) + 0.019 mass fraction of NaCl system: This work; ●, 280.8 K; ◆, gas hydrate equilibrium conditions; Solid lines, model correlations.

Induction time is known as the time elapsed before the rapid drop in pressure as shown in Figure 5.19. This figure shows the change in pressure before and during the formation of gas hydrate. It was noted that the induction time depends on the initial temperature and pressure, because some initial pressures have shown zero induction time or no hydrate was formed as shown in Figure 5.19. It was noted that the induction time decreases as pressure increases and

at higher pressure, no hydrate is formed. Consequently, the energy consumption in a practical increases with the higher initial condition or degree of subcooling. Thus, the degree of subcooling should be considered as an economic factor.

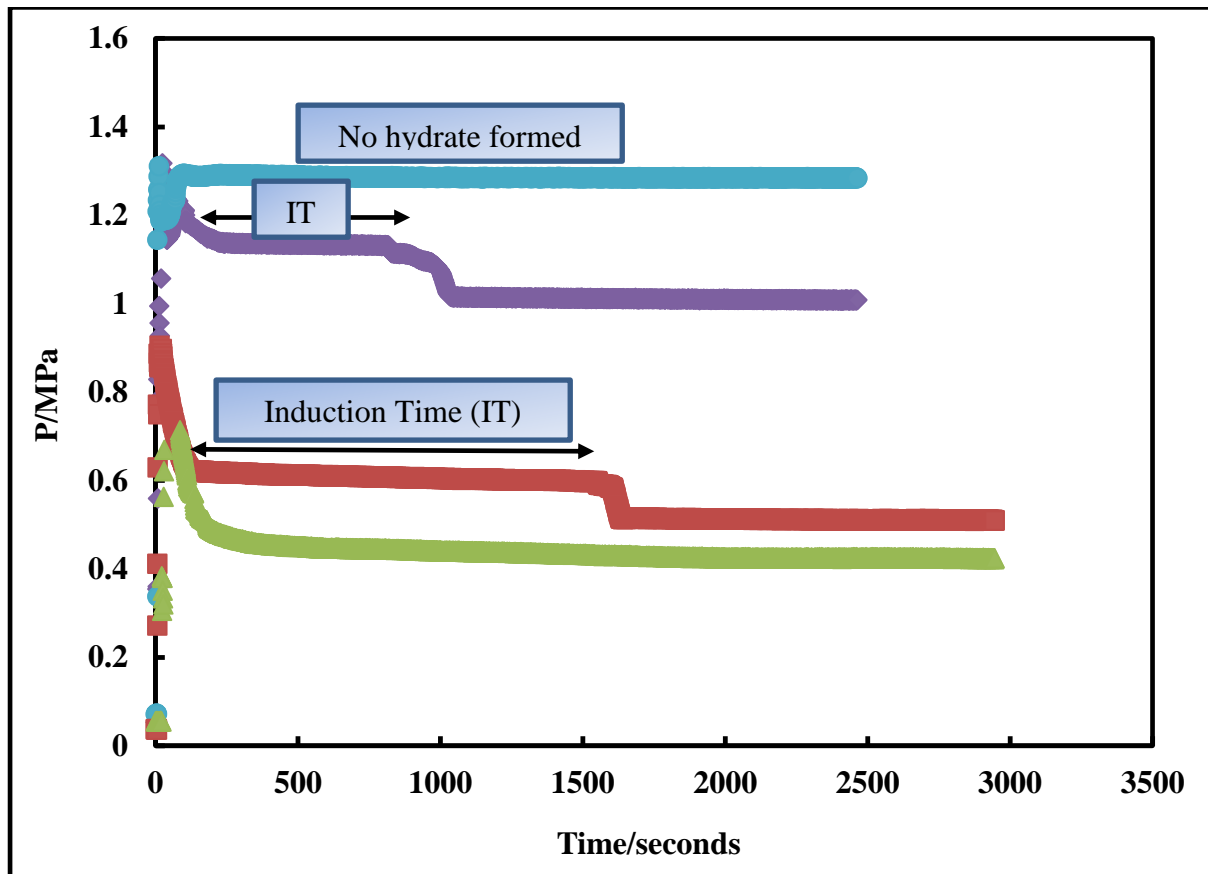


Figure 5. 19: Kinetic measurements for R410a (1) + water (2) + 0.002 mass fraction of CaCl_2 (3) + 0.017 mass fraction of NaCl (4) system at 281.8 K at the following initial pressures; \blacktriangle , 0.71 MPa; \blacksquare , 0.9 MPa, \blacklozenge , 1.23 MPa; \bullet , 1.31 MPa.

The study evaluated water to hydrate conversion and the apparent rate constant at induction time for R410a + water + mixed salts in the absence and presence of CP using the Mohammadi et al. (2014) algorithm as shown in Figure 5.20. Table 5.15 presents the conversion of water to hydrate and the apparent rate constant for the systems studied at the induction time. During the nucleation and growth, the apparent rate constant decreases to a constant value at which the hydrate formation is completed.

The hydrate nucleation and growth rate increase with an increase in pressure. However, Figure 5.19 shows the hydrate formation of R410a + water + mixed salt systems, with an increase of the pressure the rate of hydrate nucleation increases up to a particular pressure and it was

observed that no hydrate was formed at higher pressure even after a long period of time. This occurs when the refrigerant becomes a liquid. With the formation of liquid phase, the dispersion of gas molecules into the solution decreases significantly resulting in the slow nucleation of hydrate. Consequently, before gas hydrate formation takes place it is essential to ensure that no liquid refrigerant has been formed inside the equilibrium cell.

Table 5. 15: Water to hydrate conversion, apparent rate constant and induction time for studied systems^a

Studied systems	^c T ₀ /K	^d P ₀ /MPa	^e IT/min	^f WHC/mole	^g K _{app}
R410a + ^b 0.13Mg + ^b 0.19Na	281.8	0.8	0	0.87	0.019
		1.1	0	0.99	0.021
		1.4	^h n.f	-	-
	279.9	0.8	0	2.30	0.049
		0.5	0	2.87	0.062
		0.4	0	3.03	0.078
277.1	1.1	2.5	0.39	0.009	
R410a + ^b 0.13Mg + ^b 0.19Na + CP	282.8	0.8	0	0.87	0.019
		1.2	^h n.f	-	-
	280.8	0.7	0	0.26	0.006
		1.0	7.1	0.58	0.013
		1.3	^h n.f	-	-
R410a + ^b 0.02Ca + ^b 0.17Na	282.9	0.9	0	0.75	0.016
		1.1	3.5	0.99	0.021
	281.8	1.3	9.4	1.63	0.035
	280.2	0.4	0	2.87	0.061
		0.6	0	3.27	0.096
R410a + water + ^b 0.02Ca + ^b 0.17Na + CP	281.9	0.7	0	5.15	0.111
	279.9	0.6	0	1.35	0.029
		1.3	0	3.39	0.073
R410a + water	282.9	0.9	0	0.87	0.029
		1.0	0	1.72	0.037
	280.2	0.9	0	1.35	0.029
		276.8	0.5	0	3.26

^aU(T) (0.95 level of confidence) = 0.1 K, U(P) (0.95 level of confidence) = 0.0007 MPa

^bMass fraction, ^cInitial temperature, ^dInitial pressure, ^eInduction time, ^fWater hydrate conversion, ^gApperant rate constant, ^hNo hydrate formed

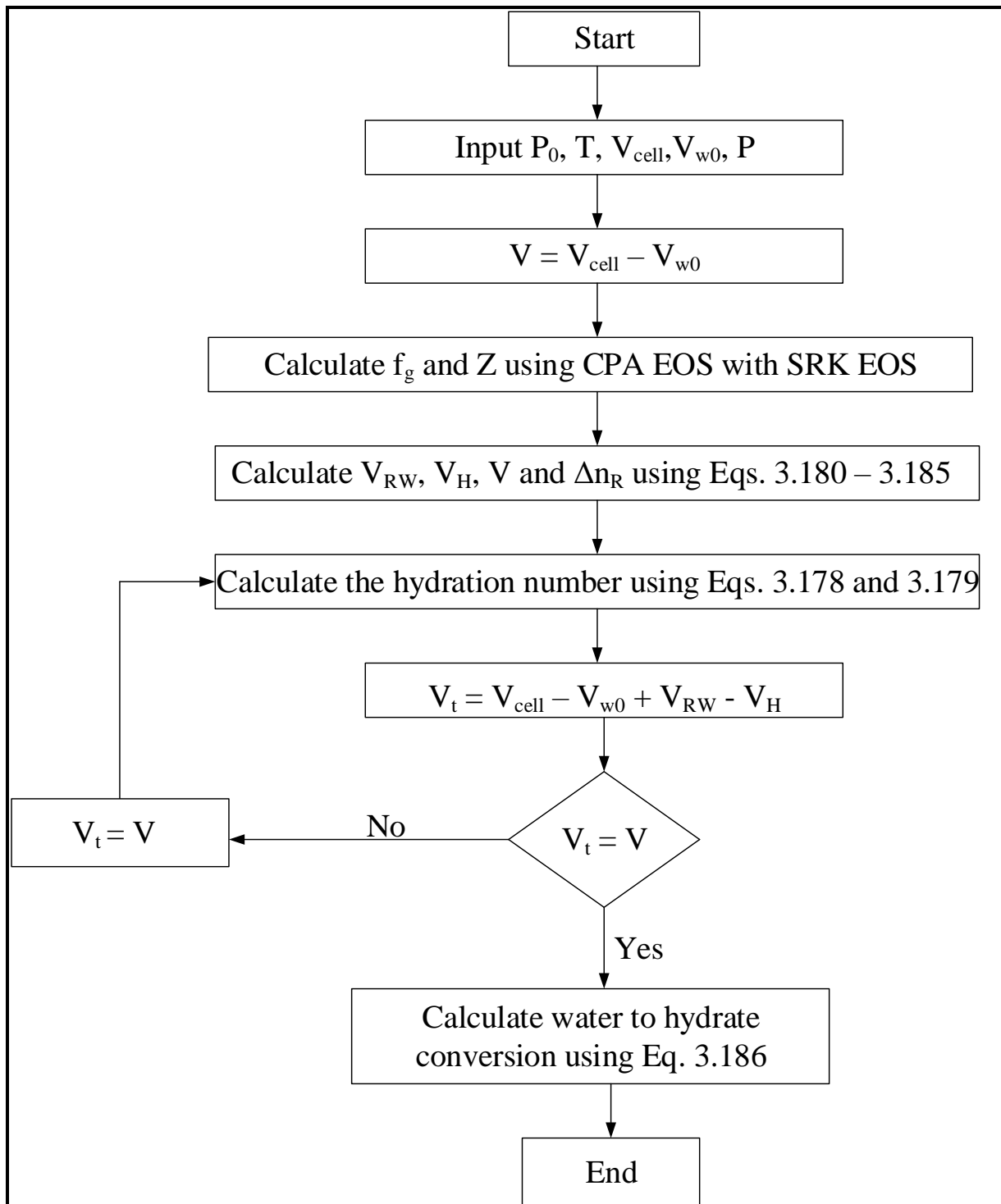


Figure 5. 20: The algorithm to calculate the water to hydrate conversion (Mohammadi et al., 2014).

5.7 Carbon dioxide + water + single salt + CP systems

CO₂ can be used as an hydrate former in water desalination or wastewater treatment, due to its chemical and physical properties (Javanmaardi and Moshefeghian, 2003; Sloan and Koh, 2008; Cha and Seol, 2013). The use of CO₂ to form hydrates in the presence of CP is attractive because it is expected that CP may reduce CO₂ hydrate dissociation pressures and increase temperatures closed to ambient conditions. A water-insoluble promoter should be added when hydrate dissociation data are below ambient conditions to move temperatures or pressures closer to ambient conditions for the convenient operation of the desalination processes. (Petticrew, 2011). In this study, CP is used to reduce dissociation pressures or raise dissociation temperatures near ambient conditions, so that CO₂ can be suitable for gas hydrate technology for the desalination process.

Mohammed and Richon, (2009) measured the ternary system for CO₂ + water + CP, the results show that CP made an impressive increase of dissociation temperatures and pressure reduction for CO₂ + water system as shown in Figure 5.21. It was noted from the results that the dissociation temperatures increase by 13.2 K and dissociation pressures decrease by 1.82 MPa compared to the system in the absence of CP. However, the increases in temperatures are still below ambient temperatures and the reduction in pressures is above atmospheric pressure, which makes CO₂ not suitable for gas hydrate technology for the desalination process. Moreover, it is important to study the effect of cyclopentane in the aqueous or saline solution in the presence of CO₂ as the hydrate former. It is recommended to investigate the suitable promoter to reduce dissociation pressures at or below atmospheric pressures.

In this study the effect of single electrolytes is investigated in the presence of CP. Gas hydrate dissociation data for CO₂ + water + {NaCl or CaCl₂ or MgCl₂} + CP systems at mass fraction ranging from (0.10 to 0.20).

The hydrate dissociation data for CO₂ + water + NaCl + CP systems were measured at a various salt mass fraction of (0.10, 0.15 and 0.20). The experimental hydrate measurements for CO₂ + water + NaCl + CP systems in the presence of CP are presented in Table 5.16 and shown in Figure 5.21. The results show that the addition of CP does not have an effect on these systems because the dissociation temperatures are similar with those measured by Dlolabhia et al., (1993) in the absence of a promoter at the same concentration, but there is slight decrease in dissociation pressures. It was noted from the results obtained by Dlolabhia et al., (1993) that

the presence of electrolytes shows an inhibition effect to shift the phase equilibrium boundary to lower dissociation temperatures.

Table 5. 16: Measured data for hydrate–liquid water–liquid promoter–vapour for the CO₂ (1) + water (2) + NaCl (3) + CP (4) system at various salt concentrations^a

^b CO ₂ (1) + water (2) + CP (3)		CO ₂ (1) + water (2) + 0.10 ^c NaCl (3) + CP (4)		CO ₂ (1) + water (2) + 0.15 ^c NaCl (3) + CP (4)		CO ₂ (1) + water (2) + 0.20 ^c NaCl (3) + CP (4)	
T/K	P/MPa	T/K	P/MPa	T/K	P/MPa	T/K	P/MPa
291.8	2.5200	276.0	3.239	271.9	2.7811	266.3	2.4461
290.7	2.0600	275.3	2.9392	270.5	2.2819	265.3	2.1074
289.1	1.5900	274.2	2.4011	269.8	2.0463	264.2	1.7872
288.1	1.2000	273.2	2.1312	268.5	1.7854	262.3	1.3381
286.9	0.9300	272.1	1.8751	266.0	1.3584		
285.3	0.6400	270.0	1.4881				
284.3	0.3500						

^aU(T) (0.95 level of confidence) = 0.1 K, U(P) (0.95 level of confidence) = 0.0007 MPa,

^b(Mohammadi and Richon, 2009), ^cValues are in mass fraction.

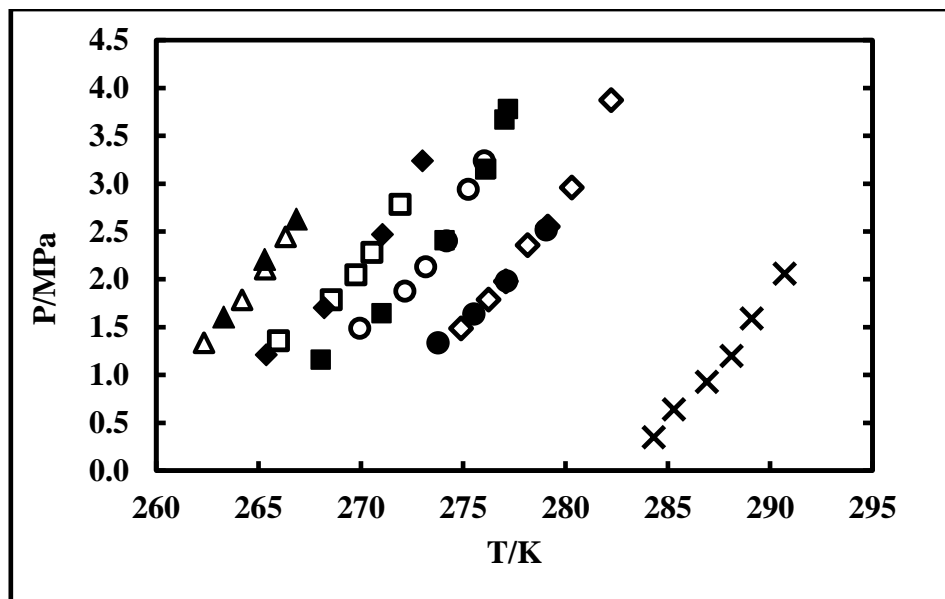


Figure 5. 21: Measured data for hydrate–liquid water–liquid promoter–vapour for the CO₂ (1) + water (2) + NaCl (3) + CP (4) system: x, Mohammed and Richon, (2009) in the presence of CP and absence of salt; •, Mohammed and Richon, (2009) in the absence of CP and salt; ■, 0.10 mass fraction in the absence of CP (Dlolahia et al., 1993); ◆, 0.15 mass fraction in the absence of CP (Dlolahia et al., 1993); ▲, 0.20 mass fraction in the absence of CP (Dlolahia et al., 1993); This work: ◇, in the absence of CP and salt; ○, 0.10 mass fraction in the presence of CP; □, 0.15 mass fraction in the presence of CP; △, 0.20 mass fraction in the presence of CP.

The CO₂ + water + CaCl₂ + CP systems were measured at salt concentrations of (0.10, 0.15 and 0.20) mass fraction. The experimental hydrate measurements for CO₂ + water + NaCl + CP systems in the presence of CP are presented in Table 5.17 and shown in Figure 5.22. It was noted that at the mass fraction of 0.10 mass fraction, the dissociation temperatures increase by 2.1 K compared to the data of Dlolabhia et al., (1993) without the addition of CP. At the mass fraction of 0.15 mass fraction, the increase of 1.6 K was noted compared to the hydrate data measured by Dlolabhia et al., (1993) in the absence of CP. There was no data found to compare at the mass fraction 0.20 mass fraction. Consequently, for this system CP made a significant increase in dissociation temperatures.

Table 5. 17: Measured data for hydrate–liquid water–liquid promoter–vapour for the CO₂ (1) + water (2) + CaCl₂ (3) + CP (4) system at various salt concentrations^a

^b CO ₂ (1) + water (2) + CP (3)		CO ₂ (1) + water (2) + 0.10 ^c CaCl ₂ (3) + CP (4)		CO ₂ (1) + water (2) + 0.15 ^c CaCl ₂ (3) + CP (4)		CO ₂ (1) + water (2) + 0.20 ^c CaCl ₂ (3) + CP (4)	
T/K	P/MPa	T/K	P/MPa	T/K	P/MPa	T/K	P/MPa
291.8	2.5200	277.2	2.7784	273.4	2.4881	267.2	2.3484
290.7	2.0600	276.4	2.4860	271.8	1.9993	264.8	1.7824
289.1	1.5900	275.2	2.0844	270.3	1.5913	263.1	1.3891
288.1	1.2000	272.9	1.6322	268.0	1.1924	261.4	1.0623
286.9	0.9300	271.6	1.3693				
285.3	0.6400	268.8	0.9660				
284.3	0.3500						

^aU(T) (0.95 level of confidence) = 0.1 K, U(P) (0.95 level of confidence) = 0.0007 MPa,

^b(Mohammadi and Richon, 2009), ^cValues are in mass fraction.

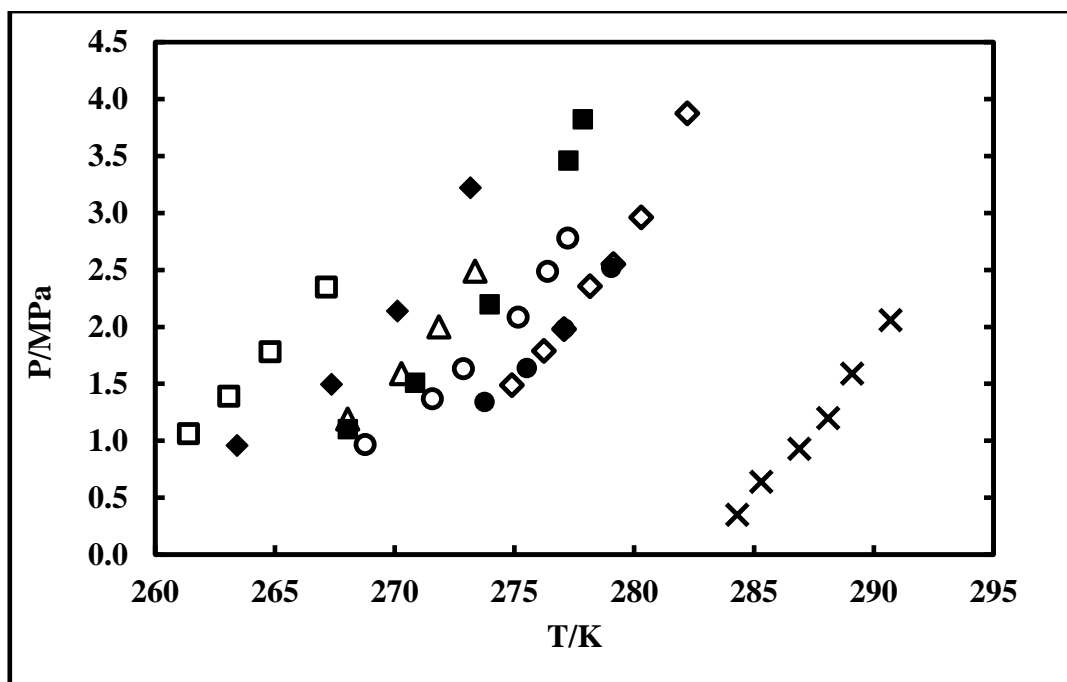


Figure 5. 22: Measured data for hydrate–liquid water–liquid promoter–vapour for the CO₂ (1) + water (2) + CaCl₂ (3) + CP (4) system: x, Mohammed and Richon, (2009) in the presence of CP and absence of salt; •, Mohammed and Richon, (2009) in the absence of CP and salt; ■, 0.10 mass fraction (Dlolabhia et al., 1993) in the absence of CP; ♦, 0.15 mass fraction (Dlolabhia et al., 1993) in the absence of CP; This work: ◇, absence of CP and salt; ○, 0.10 mass fraction in the presence of CP; △, 0.15 mass fraction in the presence of CP; □, 0.20 mass fraction in the presence of CP.

The CO₂ + water + MgCl₂ + CP systems were measured at salt concentration of (0.10 and 0.15) mass fraction. The experimental hydrate measurements for CO₂ + water + MgCl₂ + CP systems in the presence of CP are presented in Table 5.18 and shown in Figure 5.23. There was data in the literature for CO₂ + water + MgCl₂ system in the absence of CP. It is difficult to comment on the effect of CP for this particular systems. It is recommended that one has to measured this system in the absence of CP.

Table 5. 18: Measured data for hydrate–liquid water–liquid promoter–vapour for the CO₂ (1) + water (2) + MgCl₂ (3) + CP (4) system at various salt concentrations^a

^b CO ₂ (1) + water (2) + CP (3)		CO ₂ (1) + water (3) + 0.10 ^c MgCl ₂ (3) + CP (4)		CO ₂ (1) + water (2) + 0.15 ^c MgCl ₂ (3) + CP (4)	
T/K	P/MPa	T/K	P/MPa	T/K	P/MPa
291.8	2.5200	287.2	2.4193	268.6	2.0621
290.7	2.0600	286.2	1.9899	266.0	1.5255
289.1	1.5900	285.3	1.6422	263.3	1.1524
288.1	1.2000	284.3	1.3414	261.1	0.8833
286.9	0.9300	282.0	0.8133		
285.3	0.6400				
284.3	0.3500				

^aU(T) (0.95 level of confidence) = 0.1 K, U(P) (0.95 level of confidence) = 0.0007 MPa,

^b(Mohammadi and Richon, 2009), ^cValues are in mass fraction.

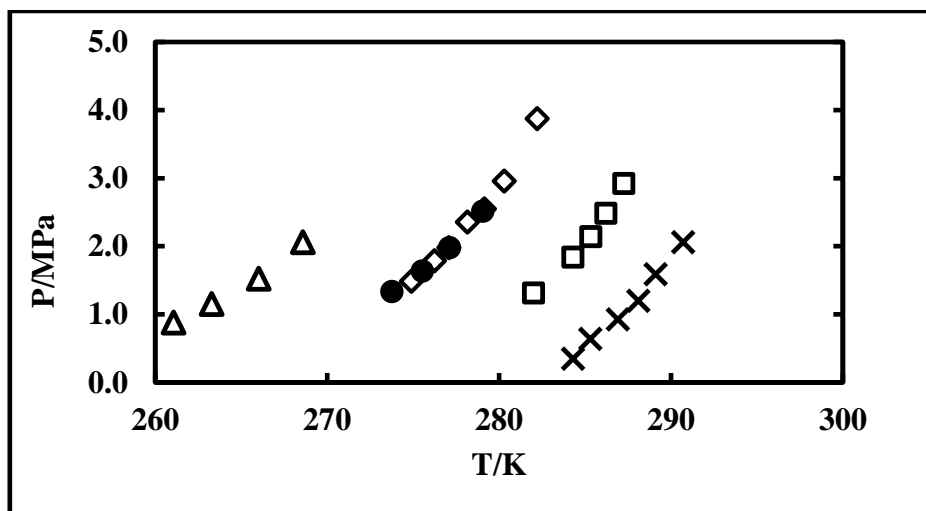


Figure 5. 23: Measured data for hydrate–liquid water–liquid promoter–vapour for the CO₂ (1) + water (2) + MgCl₂ (3) + CP (4) system: x, Mohammed and Richon, (2009) in the presence of CP and absence of salt; •, Mohammed and Richon, (2009) in the absence of CP and salt; This work: ◊, in the absence of salt and CP; ◦, 0.10 mass fraction in the presence of CP; Δ, 0.15 mass fraction in the presence of CP.

5.8 Desalination using gas hydrate technology

The gas hydrate technology is the separation technique that forms the main basis for the present study. This technology has been considered as an alternative to the existing desalination processes such as RO and MSF. One of the advantages of gas hydrate separation technology is that it operates at lower temperatures where low-quality heat can be used to dissociate the process. This technology is the endothermic process. The main challenge of this technology was to find the hydrate former that can form hydrates at ambient conditions. Most researchers

have been using hydrocarbons such as methane and, ethane as hydrate former as a result the hydrate forms at high pressure and low temperature. The following fluorinated refrigerants (R134a, R410a and R507) were investigated in previous works of this author in 2014. It was found that R134a and R507 were forming hydrate at lower pressure and temperature, only R410a was closed to ambient conditions. Then, in this study, R410a was investigated further as per recommendation was made by this author in 2014. It was also found that R410a can be utilised as a hydrate former for gas hydrate technology for the desalination process in the presence of insoluble water promoter (CP).

Consequently, the use of fluorinated refrigerant in industrial wastewater and seawater can be an advantageous because they form hydrates with water only (Eslamimanesh et al., 2011). As a result, in the desalination process, when the gas hydrates dissociation, pure/clean is produced, however, some desired concentration of salt may likely be present in water. The released refrigerant can be recycled to the hydrate reactor to form hydrates again (Chun et al., 2000; Sloan and Koh, 2008). This shows that there is no loss of refrigerant during the process, the use of gas hydrate technology has an ability to save gas (refrigerant).

The separation of electrolytes and water occurs during the formation of the gas hydrate because electrolytes do not enter to any cavities for the hydrate lattice, as fluorinated refrigerant forms hydrate with water only (Mohammadi and Richon, 2009; Eslamimanesh et al., 2011). Subsequently, the electrolytes remain at the surface of hydrate and it is easily flush with water as concentrated brine. It was assumed that there are no electrolytes ions present in the vapour phase, which means the vapour phase consists of pure refrigerant and a small amount of water.

R410a and R507 were assumed to be ideal although R410a is composed of 0.5 mass fraction difluoromethane + 0.5 mass fraction 1,1,1,2,2-pentafluoroethane and R507 is composed of 0.5 mass fraction 1,1,1-trifluoroethane + 0.5 mass fraction 1,1,1,2,2-pentafluoroethane. The R410a and R507 have larger molecules and they are forming structure II. These larger molecules cannot enter into the small cavities of their relevant gas hydrate structures when compared with CO₂. Chun et al. (2000) reported that chlorodifluoromethane (R22) molecules that can occupy large cavities of structure I.

From the results, it was noted that the measured data for R410a + water + (mixed or single electrolytes) systems cause an inhibition effect of the H–L_w–V equilibrium phase boundary to shift to lower dissociation temperatures as concentration increases. The effect of adding a small amount of promoter shows an increase of dissociation temperatures and slight decrease in dissociation pressures. This shows the effect of the insoluble water promoter (cyclopentane).

The electrolytes presence in industrial wastewater and seawater have ability to lower the fugacity of water (Kang et al., 1998). This means that the gas hydrate systems for the pure water with refrigerant are required. Lederhos et al. (1996); Kavamoddin and Varaminiam, (2013) reported that electrolytes have an effect to reduce growth and the rate of nucleation in the hydrate formation as well as the reduction of cavities in the surface occurs due to the presence of electrolytes. The inhibition effect of electrolytes in the formation of hydrate strongly depends on the ionic size and electrical charges (Park et al., 2011). The inhibition strength is directly proportional to the number of electrical charges and inversely proportional to the ionic size (Kavamoddin and Varaminiam, 2013).

5.8.1 Solubility of refrigerants

Fluorinated refrigerants such as R410a and R507 are used as hydrate formers, and they have low solubility in water as well as in aqueous electrolytes solution. Then, it is assumed that the vapour pressures of refrigerants are equal to the partial pressure of refrigerants in the aqueous solution. In the study by Eslamimanesh et al., (2011) it was assumed that the vapour phase is an ideal gas of refrigerant because to its lower solubility, and it was also assumed that the fugacity of refrigerant in the vapour phase is equal to the dissociation pressure of a gas hydrate.

5.8.2 Separation of residual by hydrate formation

The hydrate former (refrigerant) forms hydrate with water only. The impurities and concentrated brine or salt are not included from the hydrate structures. The high salinity residual water was on the surface of hydrate structures or crystals. Bradshaw et al. (2007) reported that if hydrate dissociated, the interstitial water was caused by salinity in water. Repeated steps in the hydrate formation process are required to achieve an acceptable salinity level (Bradshaw et al., 2007). The main challenge is to develop an efficient technique to separate residual interstitial brine from hydrate crystals. Cha et al. (2013) crushed hydrate from the reactor and filtered by vacuum suction for removing the interstitial water. It was found the removal efficiency for each cation was almost similar in all hydrate crystals collected after

filtration. Subsequently, the hydrate was dissociated at ambient pressure. This leads to the new proposed desalination process, which is presented later in this chapter.

Thereafter, the promoters (cyclopentane and cyclohexane) can be separated from water because they were water-immiscible. The promoter can be recycled and reused for the next hydrate formation (Cha et al., 2013). However, Englin et al. (1965) reported the solubilities of cyclopentane and cyclohexane to be 86 and 67 mg/l at 283 K, respectively. Consequently, pre-treatment and post-treatment are required for the removal of a small amount of cyclopentane and cyclohexane dissolved in the water if desalinated water requires a high water quality standard. These promoters are not harmful and does not change the taste of water.

5.9 Solubility measurement of electrolytes

Electrolytes used in this study to conduct the investigation are NaCl, CaCl₂, MgCl₂, Na₂SO₄, and CaSO₄. These electrolytes except for CaSO₄ are completely soluble in water. These electrolytes are highly corrosive. However, they play an important role as inhibiting agents (Kang et al., 1998). These electrolytes are attractive due to their availability and they are not expensive. Moreover, these electrolytes are found in seawater and industrial wastewater, which makes water sour or unsuitable for domestic and agricultural purposes.

The solubility measurements were conducted to ensure that all concentrations used to perform gas hydrate experiments were below their saturation point. Due to the interaction between the water molecules and the ions, the solubility decreases in the presence of electrolytes more than the interaction between water and the dissolved refrigerant or gas (Thomsen, 2009).

Industrial wastewater and seawater contains dissolved electrolytes at a higher concentration that makes water unsuitable for any purpose. These waters have a higher concentration of NaCl in industrial wastewater and seawater compared to CaCl₂, MgCl₂ and other salts. The solubility of salt increases as the temperature increases as shown in Figures 5.24 except CaSO₄ solubility that increase from 273 K to 308 K then starts to decrease as temperature increases up to 328 K as presented in Figure 5.25. In this study, the aqueous solutions are prepared at 298.2 K, consequently, all conducted experiments, and the solubility is less than the solubility of that particular salt at 298.2 K. Table 5.19 presents the measured concentration compared to the literature concentration at 298.2 K. The measured solubility data are tabulated in Tables 5.20 to 5.22.

Table 5. 19: Comparison of solubility of measured salt and at 298.2 K

Salt	Measured concentration	^a Concentration at 298 K	Deviation
	(g/100g)	(g/100g)	
NaCl	36.01	36.02	0.01
CaCl ₂	83.92	84.22	0.30
MgCl ₂	55.04	55.07	0.03
Na ₂ SO ₄	28.16	28.18	0.02
CaSO ₄	0.26	0.26	0.00

^aNIST**Table 5. 20: Solubility data for sodium sulphate and sodium chloride**

T/K	Sodium sulphate			Sodium chloride		
	Measured g/100g	NIST g/100g	Difference	Measured g/100g	NIST g/100g	Deviation
273.2	4.494	4.500	0.006	35.656	35.650	0.006
278.2	6.632			35.694		
283.2	9.120	9.100	0.020	35.714	35.720	0.006
288.2	12.998			35.782		
293.2	19.515	19.500	0.015	35.887	35.890	0.003
298.2	28.166			36.011	36.020	0.009
303.2	40.028	40.080	0.052	36.155	36.110	0.045
308.2	44.936			36.272		
313.2	48.800	48.800	0.000	36.377	36.370	0.007
318.2	48.556			36.457		
323.2	47.483			36.541	36.460	0.081

Table 5. 21: Solubility data for magnesium chloride and calcium chloride

T/K	Magnesium chloride			Calcium chloride		
	Measured g/100g	NIST g/100g	Difference	Measured g/100g	NIST g/100g	Deviation
273.2	52.134	52.100	0.034	59.484	59.500	0.016
278.2	52.459			61.367		
283.2	53.372	53.600	-0.228	64.697	64.700	0.003
288.2	53.802			69.572		
293.2	54.532	54.600	-0.068	74.594	74.500	0.094
298.2	55.043			83.915		
303.2	55.844	55.800	0.044	100.000	100.000	0.000
308.2	56.874			113.607		
313.2	57.493	57.500	-0.007	123.025	123.000	0.025
318.2	58.659			130.560		
323.2	59.639	59.600	0.039	133.950	134.000	0.050

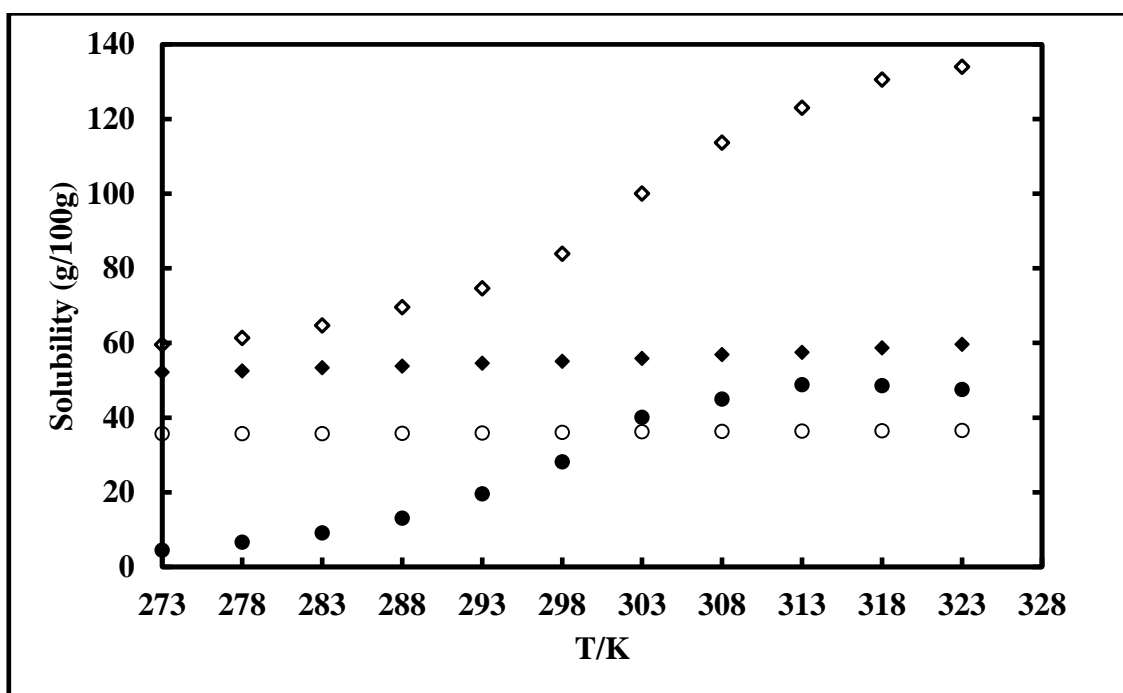


Figure 5. 24: Solubility data for measured salts: This work: ○, NaCl; ◇, CaCl₂; ◆, MgCl₂; ●, Na₂SO₄

Table 5. 22: Solubility data for calcium sulphate

Calcium sulphate			
T/K	Measured g/100g	NIST g/100g	Deviation
273.2	0.243	0.243	0.000
278.2	0.243		
283.2	0.247	0.244	0.003
288.2	0.252		
293.2	0.255	0.255	0.000
298.2	0.261		
303.2	0.263	0.264	0.001
308.2	0.265		
313.2	0.264	0.265	0.001
318.2	0.257		
323.2	0.251		

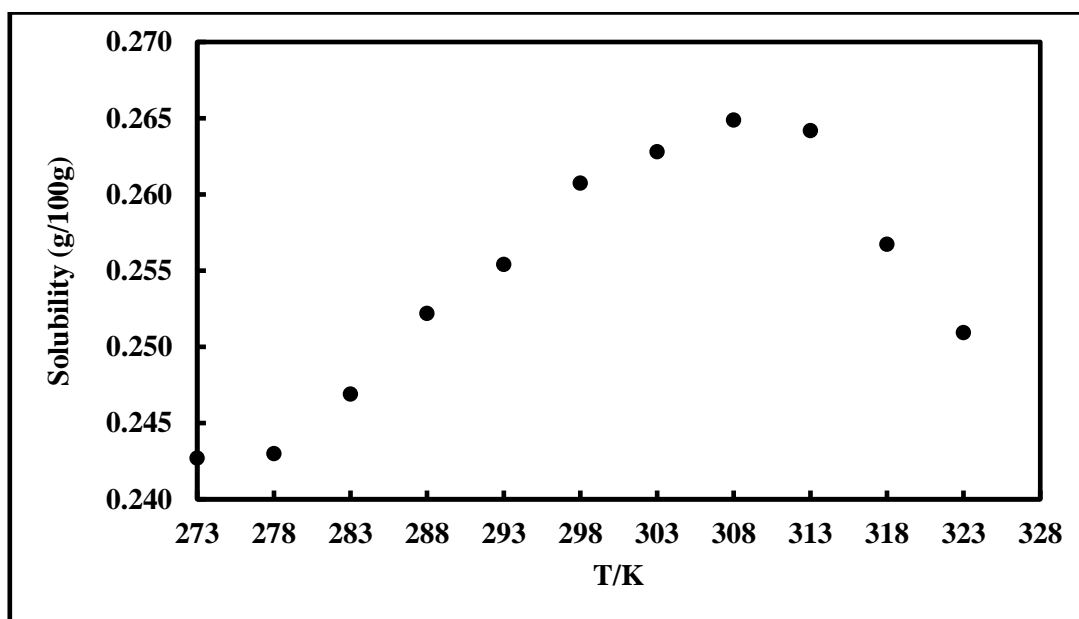


Figure 5. 25: Solubility data for calcium sulphate

5.10 Hydrate Electrolyte – Cubic Plus Association (HE-CPA) model discussion

The development model used in this study was described in detail in Chapter 3. HE-CPA model describes the properties and the behaviour of electrolyte solutions to utilise gas hydrate technology in the purification of industrial wastewater and seawater. In this study, three models were combined to form one model to be used for the optimization of water desalination employing gas hydrate technology, namely, the van der Waals and Platteeuw, Debye–Hückel (DH) and CPA Equation of State (EoS). These combination contributions were developed from electrolyte–CPA (e-CPA) equation of state of Maribo-Mogensen, (2014), consequently, the newly developed model is namely, Hydrate Electrolyte–Cubic Plus Association (HE–CPA) equation of state and it has the following contributions terms:

$$A^{HE-CPA} = A^{CPA} + A^{DH} + A^{Hydrate} \quad (5.1)$$

In the HE–CPA equation of state, the solid solution theory of van der Waals and Platteeuw, (1959) was used to model the hydrate phase, and later this model, which was adapted by Eslamimanesh et al. (2011), was used in this study. The electrolytes aqueous systems were modelled using Debye–Hückel, (1923), and the CPA equation of state was used to model the liquid or vapour phase (Kontogeorgis et al., 1996). The CPA equation of system consists of Soave-Redlich-Kwong (SRK) (Soave, 1972) equation of state with association term, and it is used to calculate the fugacity of the liquid. The SRK model accounts for the physical interaction contribution between the components.

The association term in the CPA equation of state takes into account the specific site-site interaction because of hydrogen bonding. According to Haghghi et al. (2009), there no combining rules are required for associating energy and volume for refrigerant. Only the binary interaction (k_{ij}) can be adjustable. Wie et al. (1991) indicated that in the cluster of liquid water only three sites are bonded per molecules. Then, water can be treated with the 3B association scheme. All water sites were presented in Table 3.5 in Chapter 3. The four-site (4C) association scheme is used for highly hydrogen-bonded substances, including water and glycols (Kontogeorgis and Folas, 2010). It was found that 4C association scheme provides good results compared to 3B association scheme (Kontogeorgis and Folas, 2010). Consequently, 4C association scheme was chosen to be in this study because water is the only associating component, which is called as self-association.

The combination contribution was used to model the measured hydrate dissociation data for single and mixed electrolytes in the presence of a fluorinated refrigerant as hydrate former and the promoter as well as a system without salt. A computational algorithm diagram for the HE-CPA is presented in Figure 5.26. The Matlab tool was used to program the code for modelling as present in the algorithm diagram.

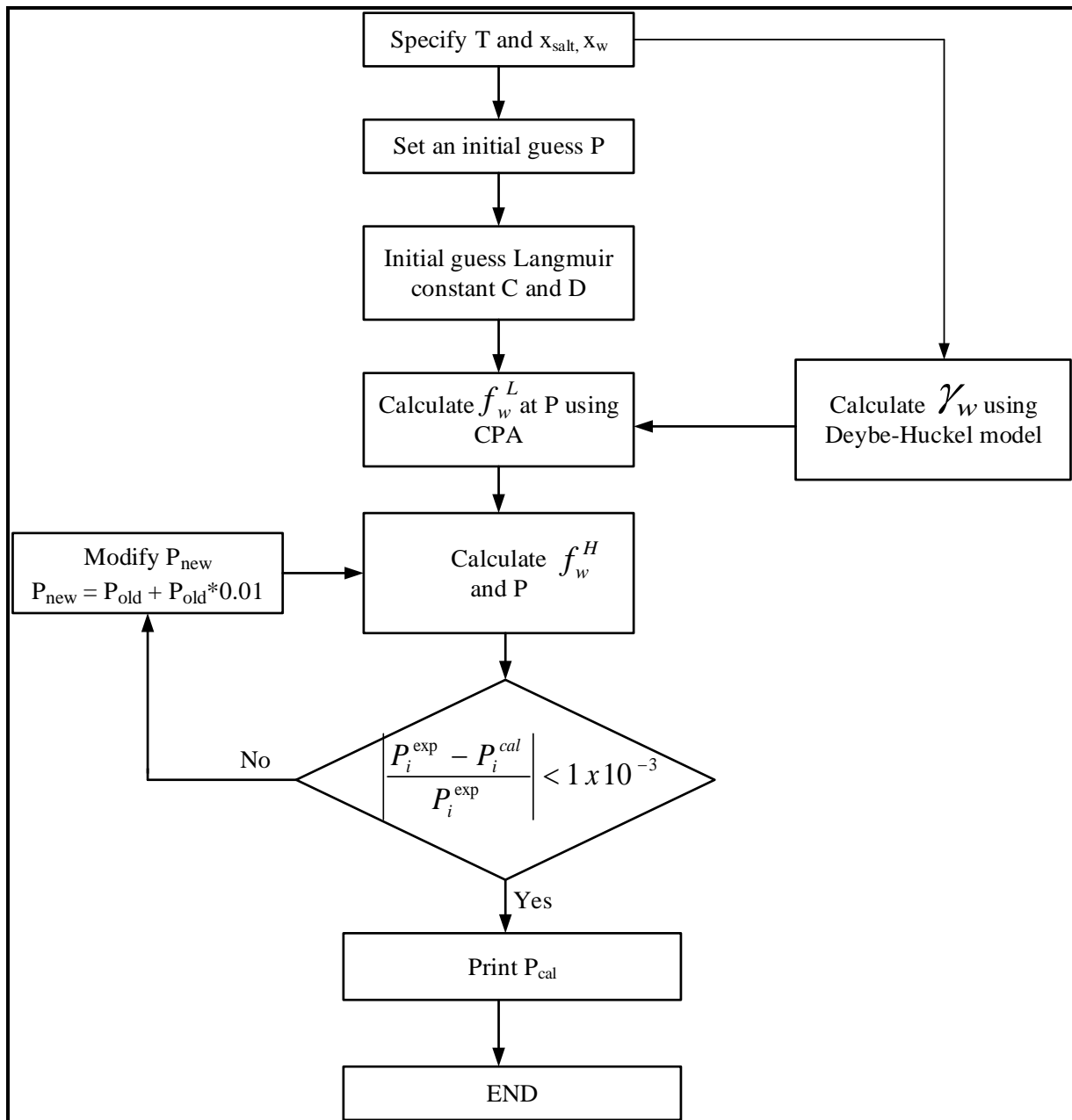


Figure 5. 26: Computational algorithm flow diagram

5.10.1 Fugacity calculation

The fugacity calculation of all refrigerants used in this study was calculated in same manner as that of water. Refrigerants are non-associating components, consequently, the energy and volume cross association between refrigerant molecules is equal to zero. The energy and volume association parameters were used only for associating component, which is water. These parameters were used together with the three additional parameters in the SRK term (a_o , b , c_1). Five parameters are obtained by fitting vapour pressure and liquid density data or

calculated from critical temperature and pressure as well as an acentric factor (Kontogeorgis and Folas, 2010). In this study, only water is associating in the solution, therefore referred to as self-association. In the case of different species associated, it is called cross-association (Kontogeorgis and Folas, 2010). The simple layout procedure for calculating fugacity of water or refrigerant was presented in Chapter 3.

The one-fluid van der Waals classical mixing rules were employed in the physical term (SRK) for the energy and co-volume parameters. The interaction parameter k_{ij} is for mixtures only self-associating compounds include alcohol, water, glycol or acid with n-alkanes (Kontogeorgis and Folas, 2010). In this study, the interaction parameters k_{ij} is equal to zero since the mixture has one self-associating and one inert. The values of k_{ij} for mixtures are presented on the website at www.wiley.com/go/Kontogeorgis on Appendix B.

Carbon dioxide is forming structure I and the refrigerant (R410a and R507) is forming structure II, consequently, Equation 3.171 and 3.172 in Chapter 3 are used to obtain Langmuir constant. HE-CPA model is more flexible because it can model systems with very low salt concentration and high concentration. The model results are strongly agreeing with the measured hydrate dissociation data at all concentration range, which demonstrate the reliability and ability of the model to describe the hydrate phase behaviour.

5.11 Modelling Results

This researcher and Akiya et al., (1999) measured the hydrate dissociation data for (R134a or R410a) + water systems as test systems. These known data were used to test the developed HE-CPA equation of state that is working correctly. For {R134a and R410a} + water systems show that the model result strongly agreed with the experimental data as shown in Figures 5.27 and 5.28. Furthermore, this model was tested using R152a + water system of Liang et al., (2001) and R507 + water system measured by this author in the MSc program in 2014. This was done to ensure that the model provides or predicts reliable data and gives confidence to use this model for the new systems of interest in this study. The model results were in good agreement with the measured data as shown in Figures 5.29 and 5.30. Table 5.23 presents the temperature and a pressure range for (R134a, R410a and R507) + water systems. The model parameters were presented and discussed later in this chapter. The absolute average deviation (AAD) were calculated for these systems and it is presented in Appendix C. It was shown that

the error is less than 1%, this is an acceptable error. Consequently, the obtained result shows that the model fits very well with the experimental hydrate dissociation data.

Table 5. 23: Temperature and pressure ranges for hydrate dissociation data for (R134a, R410a, R152a and R507) + water systems

Hydrate systems	No. points	T (K)	P (MPa)
^{a,b} R134a + water	8	275.8 to 283.0	0.0916 to 0.4047
^a R152a + water	11	273.9 to 288.2	0.0440 to 0.4440
^{b,c} R410a + water	10	277.5 to 293.0	0.1788 to 1.4213
^b R507 + water	9	277.7 to 283.3	0.2212 to 0.8733

^aLiang et al. (2001), ^bNgema et al. (2014), ^cAkiya et al. (1999)

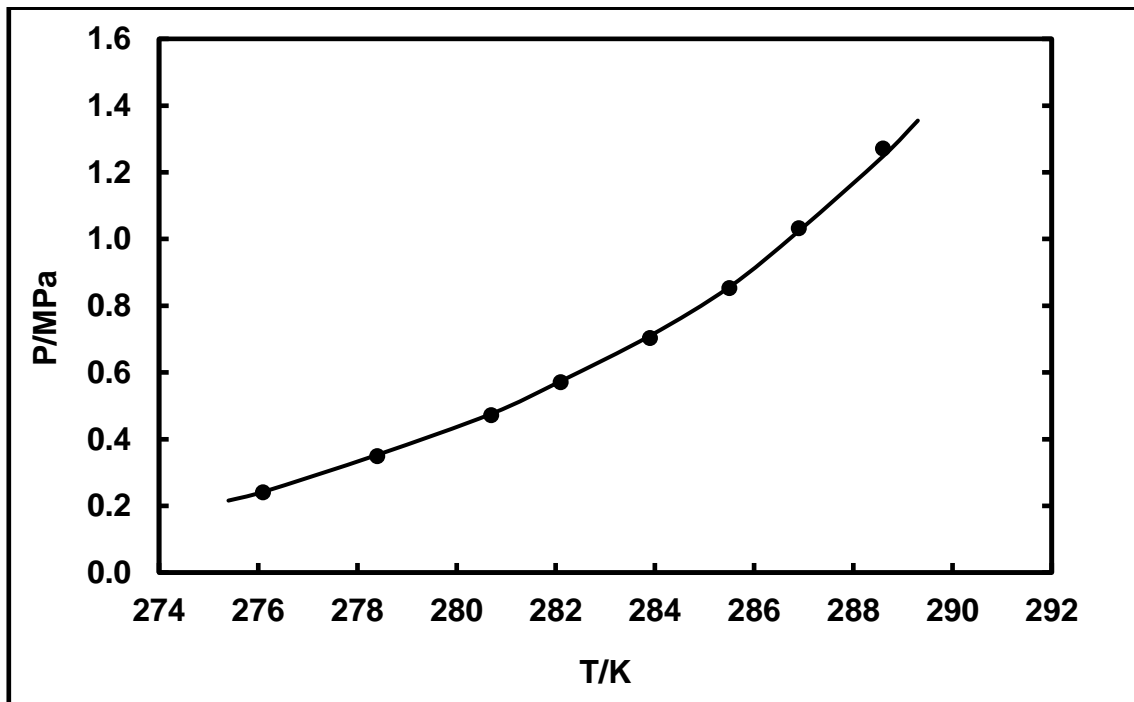


Figure 5. 27: Measured and estimated data for hydrate–liquid water–vapour for the R134a (1) + water (2) test system: symbols represent experimental data: ●, absence of salt; —, model results

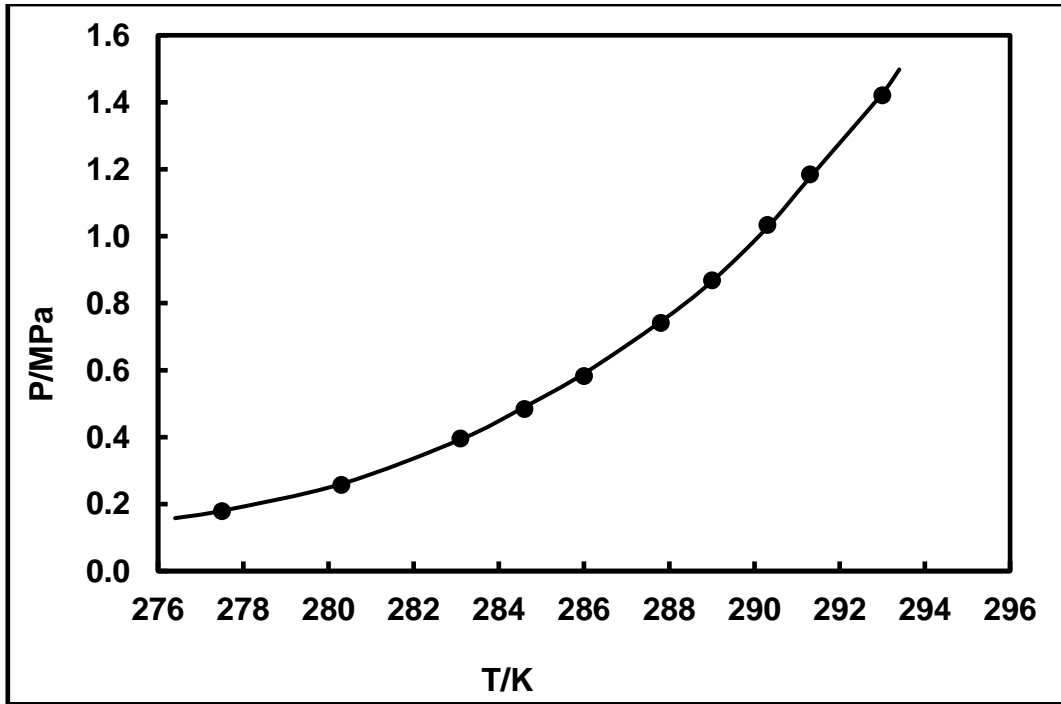


Figure 5. 28: Measured and estimated data for hydrate–liquid water–vapour for the R410a (1) + water (2) test system: symbols represent experimental data: ●, absence of salt; —, model results.

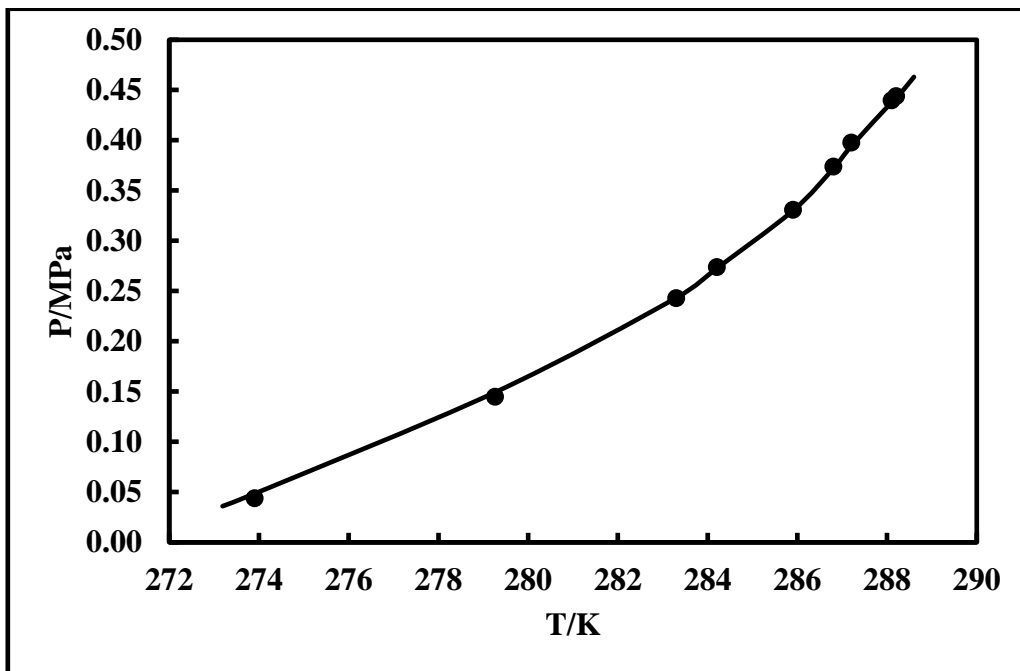


Figure 5. 29: Measured and estimated data for hydrate–liquid water–vapour for the R152a (1) + water (2) test system: symbols represent experimental data: ●, absence of salt (Liang et al., 2001); —, model results

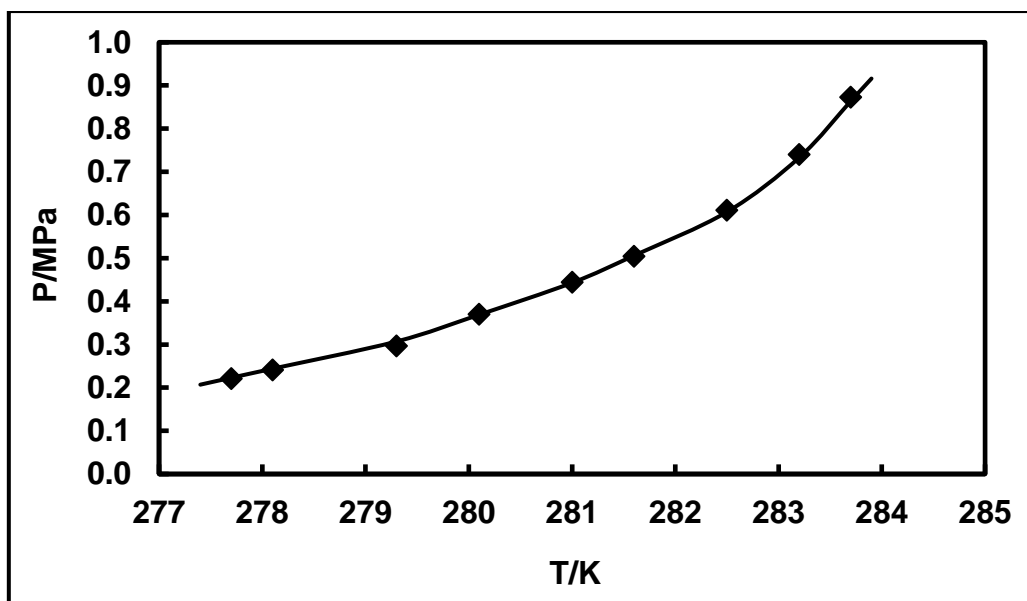


Figure 5. 30: Measured and estimated data for hydrate–liquid water–vapour for the R507 (1) + water (2) system: symbols represent experimental data: \blacklozenge , Ngema et al., (2014) in the absence of salt; —, model results.

5.11.1 Refrigerant + water + CP systems

The new ternary systems comprising for (R410a or R507) + water + CP were modelled using a HE–CPA equation of state. Table 5.24 presents the temperature and a pressure range for (R410a and R507) + water systems in the presence of CP. The model results were found to be strongly consistent with the measured hydrate dissociation data shown in Figures 5.31 and 5.32 in the absence and presence of CP. The model parameters were presented and discussed later in this chapter. The absolute average deviation (AAD) were calculated for these systems and it is presented in Appendix C. It was shown that the error is less than 1%, this is an acceptable error. Consequently, the obtained result shows that the model fit consistently with the measured hydrate dissociation data.

Table 5. 24: Temperature and pressure ranges for hydrate dissociation data in the presence of CP

Hydrate systems	No. points	T (K)	P (MPa)
^{a,b} R410a + water	10	277.5 to 293.0	0.1788 to 1.4213
^c R410a + water + CP	7	280.9 to 294.4	0.1588 to 1.3852
^b R507 + water	9	277.7 to 283.3	0.2212 to 0.8733
^c R507 + water + CP	7	279.8 to 284.6	0.2489 to 0.8580

^aLiang et al., (2001), ^bNgema et al., (2014), ^cThis work

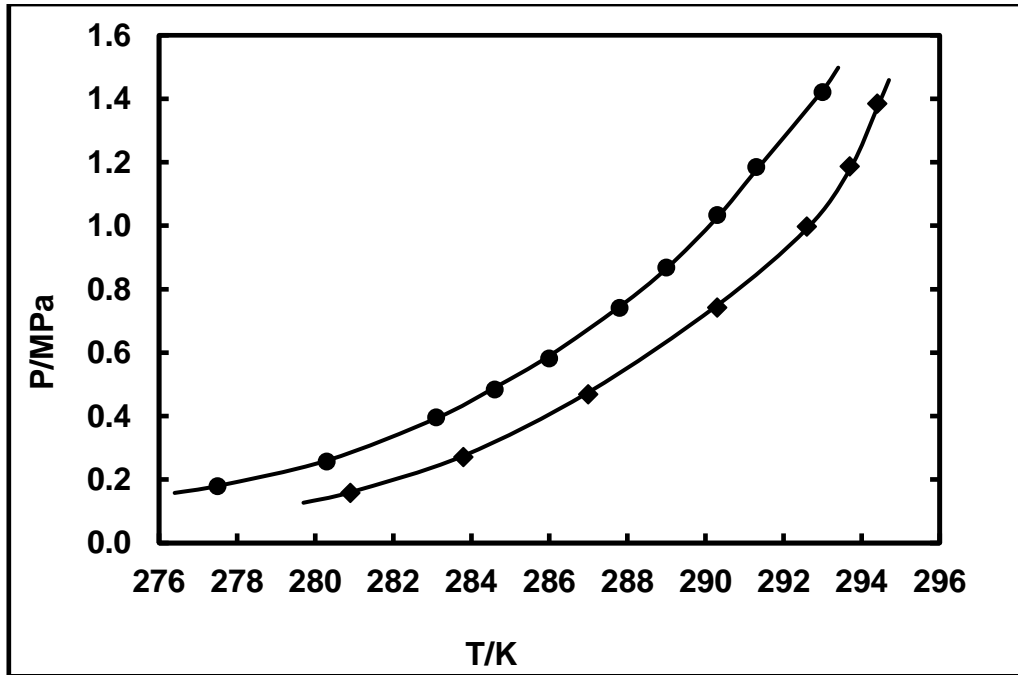


Figure 5. 31: Measured and estimated data for hydrate–liquid water–liquid promoter–vapour for the R410a (1) + water (2) in the absence and presence of CP (3) systems: symbols represent experimental data: ●, Ngema et al., (2014) in the absence of CP; This work: ◆, presence of CP; —, model results.

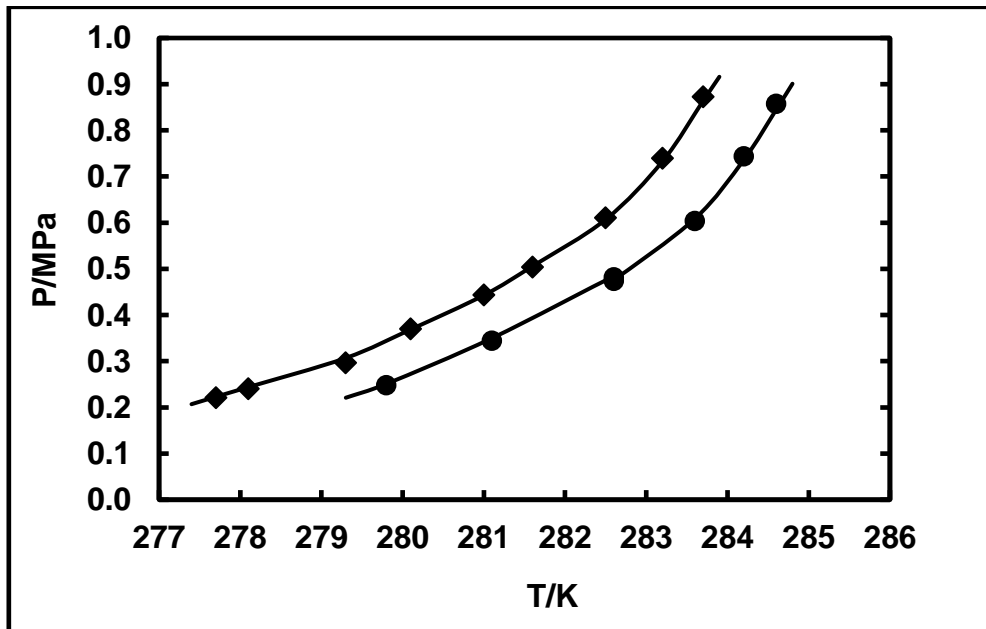


Figure 5. 32: Measured and estimated data for hydrate–liquid water–liquid promoter–vapour for the R507 (1) + water (2) in the absence and presence of CP (3) system: symbols represent experimental data: ◆, Ngema et al., (2014) in the absence of CP; This work: ●, in the presence of CP; —, model results.

5.11.2 Refrigerant + water + single salts in the presence of CP

Hydrate dissociation data for R410a + water + {NaCl or CaCl₂} + CP systems were measured at high salt concentrations of (0.10, 0.15 and 0.20) mass fraction in the temperature and pressure range that are presented in Table 5.25. The R410a + water + Na₂SO₄ system was measured at a salt concentration of 0.10 mass fraction in the temperature and pressure range presented in Table 5.25.

The experimental data for R410a + water + {NaCl or CaCl₂ or Na₂SO₄} + CP are modelled using a HE-CPA equation of state as shown in Figures 5.33 to 5.35. It was assumed that there is no ion present in the vapour phase and the electrolyte does not enter hydrate phase. The model results strongly agreed with measured hydrate dissociation data for R410 + water + {NaCl or CaCl₂}. The results obtained show that HE-CPA can be used to optimize a desalination process at industrial wastewater. The absolute average deviation (AAD) were calculated for these systems and it is presented in Appendix C. It was shown that the error is less than 1%, this is an acceptable error. Consequently, the obtained result shows that the model fit consistently with the measured hydrate dissociation data.

Table 5. 25: Temperature and pressure ranges investigated for hydrate dissociation data in the absence and presence of CP at various salt concentration (w_i = mass fraction)

Hydrate systems	Salt	w_i (mass fraction)	No. points	T (K)	P (MPa)
^a R410a + water	NaCl	0.10	8	276.1 to 288.6	0.2399 to 1.2706
R410a + water + CP	NaCl	0.10	7	280.2 to 290.5	0.2869 to 1.1791
R410a + water + CP	NaCl	0.20	7	278.4 to 285.8	0.2860 to 0.8790
R410a + water + CP	CaCl ₂	0.10	7	281.5 to 292.3	0.2148 to 1.0561
R410a + water + CP	CaCl ₂	0.15	6	279.9 to 289.9	0.2178 to 1.0561
R410a + water	Na ₂ SO ₄	0.10	7	278.3 to 291.6	0.1997 to 1.3733

^aNgema et al. (2014)

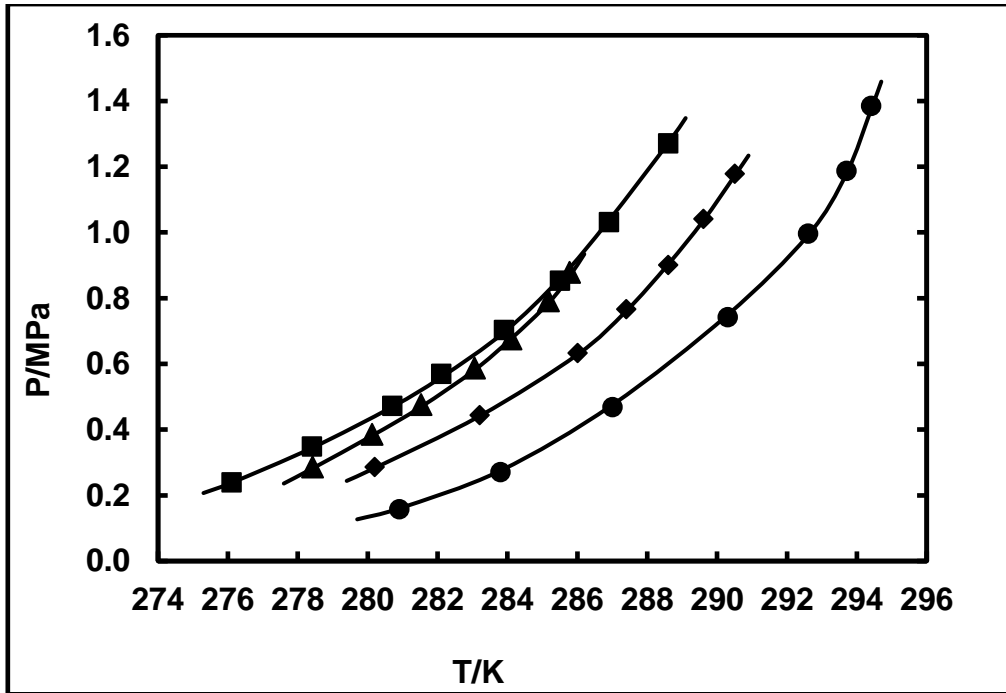


Figure 5. 33: Measured and estimated data for hydrate–liquid water–liquid promoter–vapour for the R410a (1) + water (2) + NaCl (3) + CP (4) system: symbols represent experimental data: ■, Ngema et al., (2014); This work: ●, absence of salt + CP; ◆, 0.10 mass fraction + CP; ▲, 0.20 mass fraction + CP; —, model results

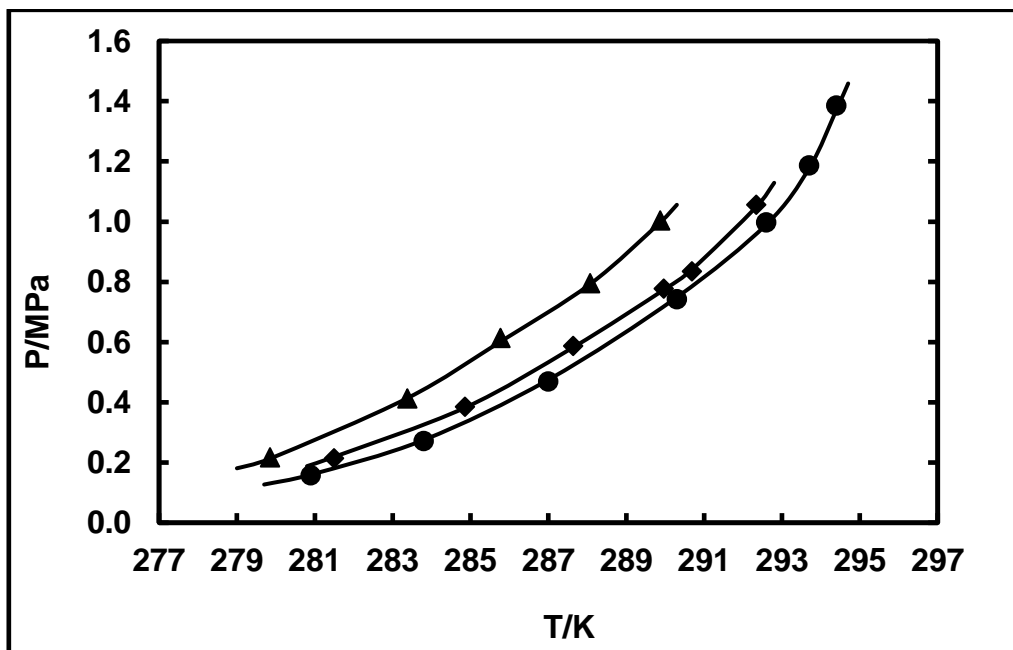


Figure 5. 34: Measured and estimated data for hydrate–liquid water–liquid promoter–vapour for the R410a (1) + water (2) + CaCl₂ (3) + CP (4) system: symbols represent experimental data: This work: ◆, absence of salt + CP; ●, 0.10 mass fraction + CP; ▲, 0.15 mass fraction + CP; —, model results.

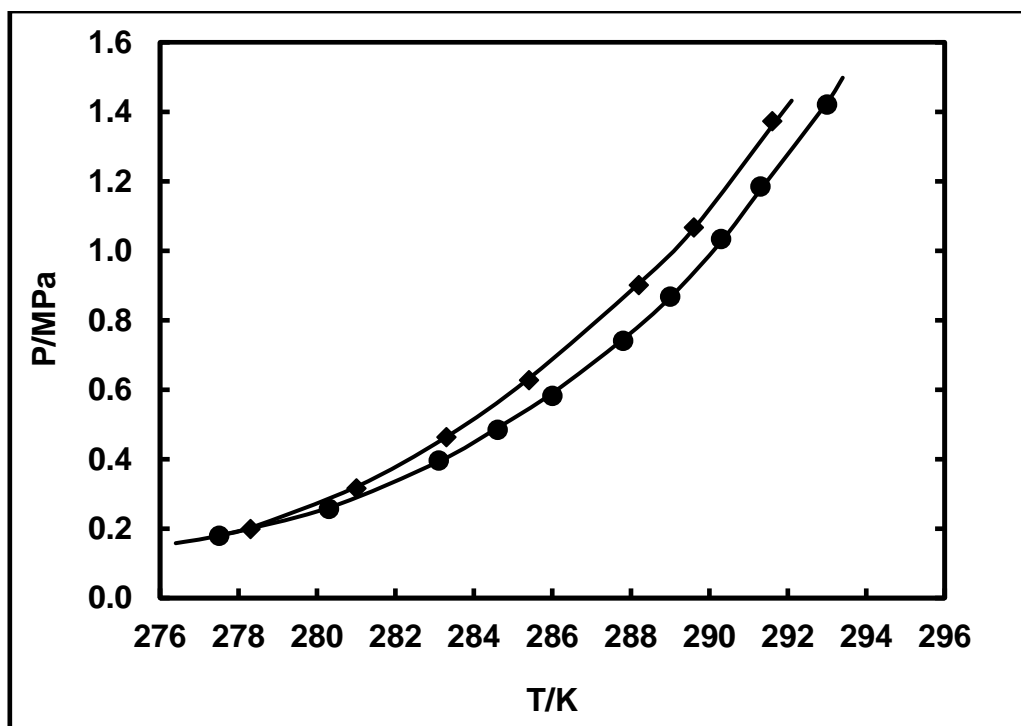


Figure 5. 35: Measured and estimated data for hydrate–liquid water–vapour for the R410a (1) + water (2) + Na₂SO₄ (3) system: symbols represent experimental data: ●, Akiya et al., (1999) in the absence of salt; This work in the presence of salt: ◆, 0.10 mass fraction; —, model results

5.11.3 Refrigerant + water + mixed salts in the presence of CP

The experimental hydrate dissociation data for R410a + water 0.02 mass fraction CaCl₂ and 0.17 mass fraction NaCl; R410a + water + 0.13 mass fraction MgCl₂ + 0.19 mass fraction NaCl and R507 + water 0.02 mass fraction CaCl₂ and 0.17 mass fraction NaCl systems in the absence and presence of CP. Table 5.26 presents the concentration of mixed electrolytes, temperature and pressure range for undertaken gas hydrate measurements for the industrial wastewater concentrations of NaCl, MgCl₂ and CaCl₂ systems. The experimental hydrate dissociation data for these system were modelled using a HE–CPA equation of state. The modelled results strongly agreed with the measured data as shown in Figures 5.36 to 5.38. It was revealed that the HE–CPA equation of state can model very well systems with lower concentrations. The absolute average deviation (AAD) were calculated for these systems and it is presented in Appendix C. It was shown that the error is less than 1%, this is an acceptable error. Consequently, the obtained result shows that the model fit consistently with the measured hydrate dissociation data.

Table 5. 26: Temperature and pressure ranges investigated for gas hydrate measurements in the absence and presence of CP at various salt concentration ($w_i =$ mass fraction)

Hydrate systems (salt conc. = mass fractions)	No. points	T (K)	P (MPa)
R410a + water + 0.002 CaCl ₂ + 0.017 NaCl	7	279.6 to 289.4	0.2500 to 1.0197
R410a + water + 0.002 CaCl ₂ + 0.017 NaCl + CP	6	283.3 to 292.5	0.2993 to 1.1193
R410a + water + 0.013 MgCl ₂ + 0.019 NaCl	8	279.1 to 288.9	0.2446 to 1.0183
R410a + water + 0.013 MgCl ₂ + 0.019 NaCl + CP	7	282.3 to 292.9	0.2381 to 1.1693
R507 + water + 0.002 CaCl ₂ + 0.017 NaCl	9	277.8 to 283.2	0.2503 to 0.8311
R507 + water + 0.002 CaCl ₂ + 0.017 NaCl + CP	7	279.5 to 284.1	0.2483 to 0.7783

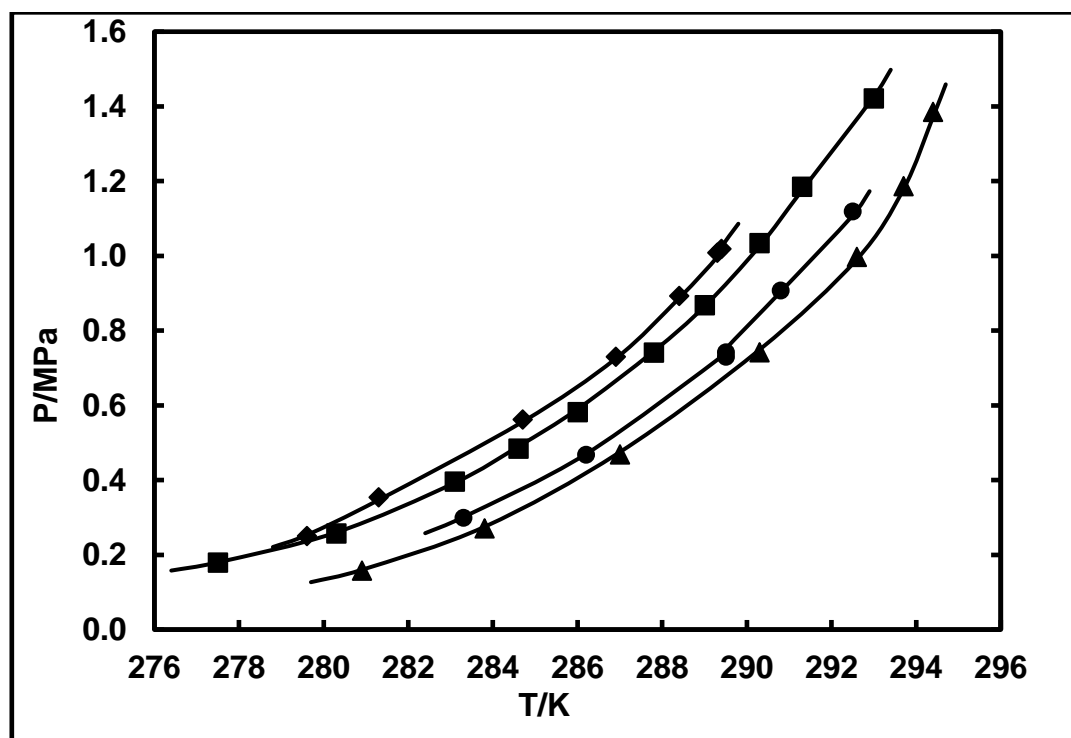


Figure 5. 36: Measured and estimated data for hydrate–liquid water–liquid promoter–vapour for the R410a (1) + water (2) + 0.0020 mass fraction of CaCl₂ (3) + 0.017 mass fraction of NaCl (4) + CP (5) systems: Symbols represent experimental data: ■, Akiya et al., (1999); This work: ◆, mixed salt in the absence of CP; ●, mixed salt in the presence of CP; ▲, water + CP; —, model results.

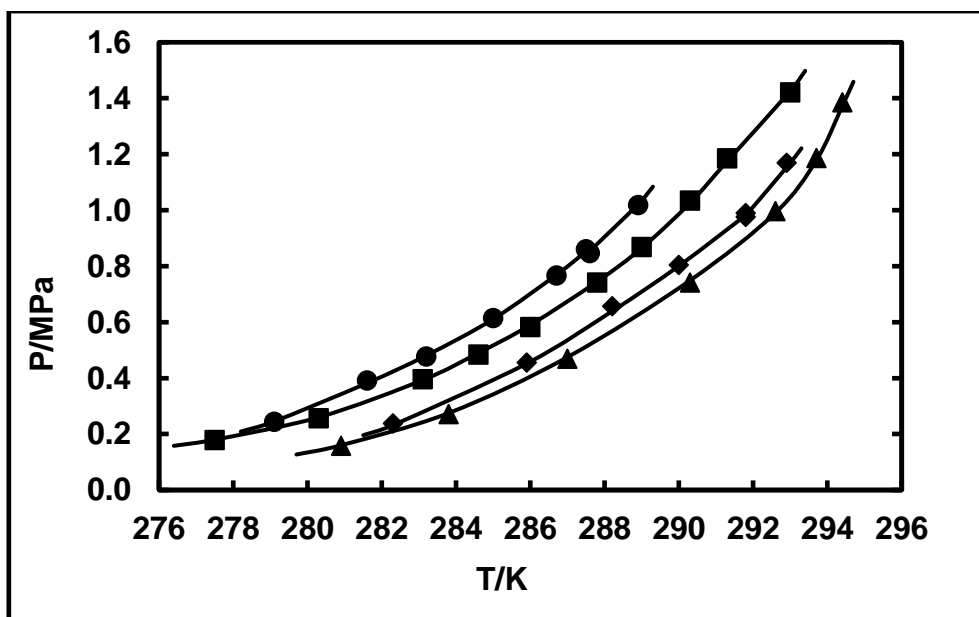


Figure 5. 37: Measured and estimated data for hydrate–liquid water–liquid promoter–vapour for the R410a (1) + water (2) + 0.013 mass fraction of MgCl_2 (3) + 0.019 mass fraction of NaCl (4) + CP (5) system: Symbols represent experimental data: ■, Ngema et al. (2014) in the absence of CP; This work: ●, mixed salt in the absence of CP; ◆, mixed salt in the presence of CP; ▲, R410a in the presence of CP; —, model results.

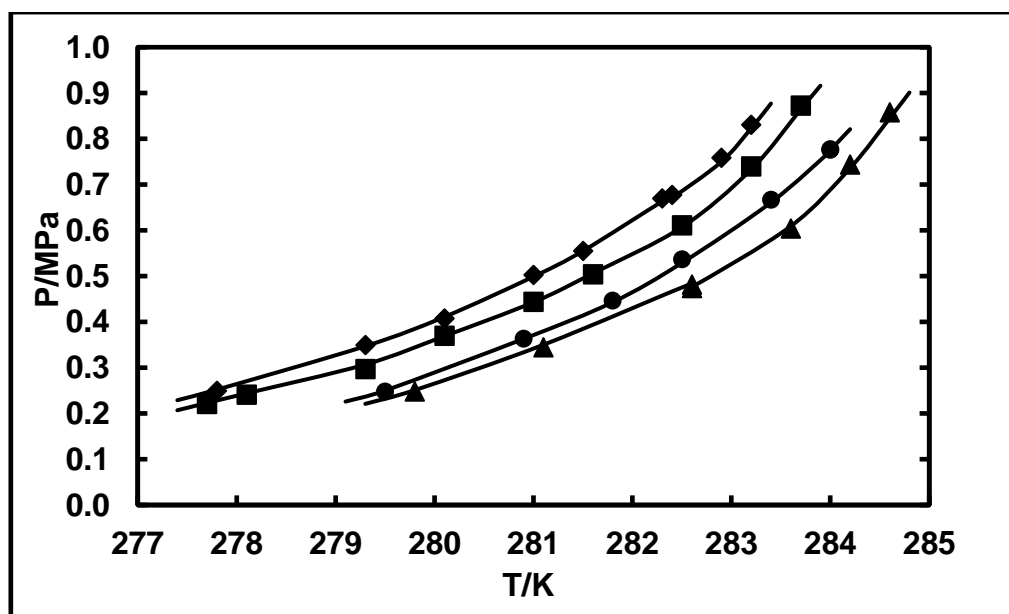


Figure 5. 38: Measured and estimated data for hydrate–liquid water–liquid promoter–vapour for the R507 (1) + water (2) + 0.0020 mass fraction of CaCl_2 (3) + 0.017 mass fraction of NaCl (4) + CP (5) system: Symbols represent experimental data: ■, Ngema et al. (2014); This work: ◆, mixed salt in the absence of CP; ●, mixed salt in the presence of CP; ▲, R507 + water + CP; —, model results.

5.11.4 R410a high concentration of salt

The experimental hydrate dissociation data for R410a + water 0.08 mass fraction CaCl_2 and 0.05 mass fraction NaCl and R410a + water + 0.05 mass fraction NaCl + 0.15 mass fraction CaCl_2 systems in the absence and presence of CP. Table 5.27 presents temperature and pressure range for undertaken gas hydrate measurements for the higher concentrations of NaCl and CaCl_2 systems. The experimental hydrate dissociation data for these system were modelled using a HE-CPA equation of state. The modelled results strongly agreed with the measured data as shown in Figures 5.39 and 5.40. It was revealed that the HE-CPA equation of state can model very well systems with low and high concentrations over a range of temperature. The absolute average deviation (AAD) were calculated for these systems and it is presented in Appendix C. It was shown that the error is less than 1%, this is an acceptable error. Consequently, the obtained result shows that the model fit consistently with the measured hydrate dissociation data. Table 5. 27: Temperature and pressure ranges investigated for gas hydrate measurements in the absence and presence of CP at various salt concentration (w_i = mass fraction)

Hydrate systems (salt in mass fractions)	No. points	T (K)	P (MPa)
R410a + water + 0.08 CaCl_2 + 0.05 NaCl	8	276.4 to 288.8	0.2498 to 1.0676
R410a + water + 0.08 CaCl_2 + 0.05 NaCl + CP	7	280.6 to 291.7	0.1919 to 1.0992
R410a + water + 0.15 CaCl_2 + 0.05 NaCl	9	274.5 to 282.1	0.2796 to 1.0744
R410a + water + 0.15 CaCl_2 + 0.05 NaCl + CP	7	278.1 to 289.4	0.2041 to 1.0413

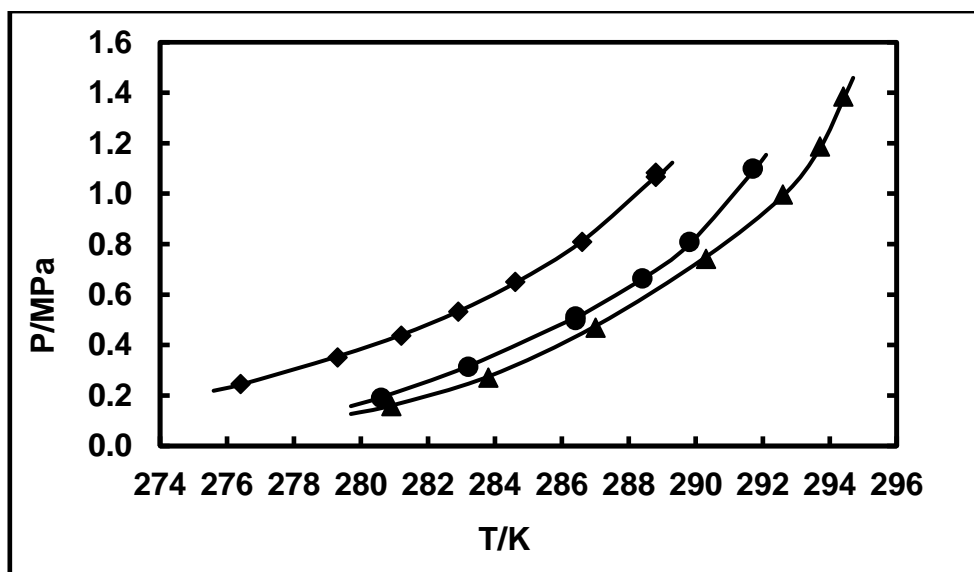


Figure 5. 39. Measured and estimated data for hydrate–liquid water–liquid promoter–vapour for the R410a (1) + water (2) + 0.08 mass fraction of CaCl₂ (3) + 0.05 mass fraction of NaCl (4) + CP (5) system: Symbols represent experimental data: This work: ▲, R410a in the presence of CP; ◆, mixed salt in the absence of CP; ●, mixed salt in the presence of CP; —, model results.

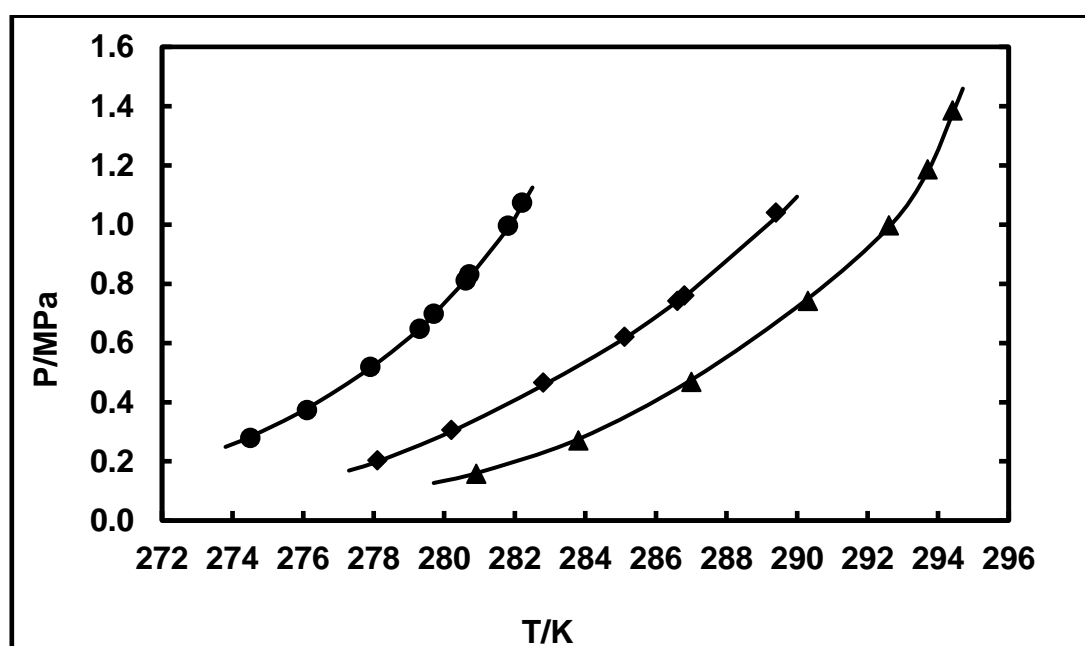


Figure 5. 40: Measured and estimated data for hydrate–liquid water–liquid promoter–vapour for the R410a (1) + water (2) + 0.15 mass fraction of CaCl₂ (3) + 0.05 mass fraction of NaCl (4) + CP (5) system: Symbols represent experimental data: This work: ▲, R410a in the presence of CP; ●, mixed salt in the absence of CP; ◆, mixed salt in the presence of CP; —, model results.

5.11.5 Model parameters

The measured systems for (R134a, R152a, R410a and R507) + water + single or mixed salt in the absence or presence of CP were modelled using a combination of various contributions in order to completely develop a HE–CPA equation of state as presented in Equation 5.1. The modelling of the electrolyte systems is based on the assumptions that no ions are present in the vapour phase and electrolyte does not enter the hydrate phase.

Tables 5.28 presents the Langmuir constant parameters (*c* and *d*) obtain by Eslamimanesh et al., (2011) for refrigerant (R134a, R152a, R410a and R507) + water systems were achieved by using Equation 3.172 in Chapter 3, then, the obtained Langmuir constant parameters were regressed using the measured hydrate dissociation data in the presence of single and mixed electrolyte as well as CP. Equation 3.172 was selected to determine parameters for R134a, R152a, R410a and R507 because these fluorinated refrigerants have large molecules, thus, they cannot enter the small cavities of their applicable gas hydrate structures. The constant parameters were determined based on the assumption that R410a and R507 are pure gases. In the case of HE–CPA model, it is revealed that the model results provide an adequate illustration of the measured hydrate dissociation data.

Table 5. 28: Regressed Langmuir constants parameters used in this study

Hydrate systems	<i>c</i> (K.MPa ⁻¹)	<i>d</i> (K)	^a AAD
^b R134a + water	5.70 x 10 ⁻³	4908.75	5.30
^b R152a + water	9.34 x 10 ⁻²	4241.71	2.40
^c R410a + water	4.75 x 10 ⁻³	5969.68	0.79
^c R507 + water	4.50 x 10 ⁻⁴	6233.08	0.83

$${}^a AAD(\%) = \frac{100}{N} \sum_i \frac{|P_i^{cal} - P_i^{exp}|}{P_i^{exp}}, \quad {}^b \text{Eslamimanesh et al. (2011)} \quad {}^c \text{Ngema et al. (2014)}$$

5.12 Carbon dioxide system

5.12.1 CO₂ + water + single salt in the presence of CP

Table 5.29 presents the temperature, pressure and mass fraction ranges for CO₂ hydrate measurements. The measured systems are modelled using a HE–CPA equation of state as present in Equation 5.1. HE–CPA equation of state was first tested using known systems for CO₂ + water + CP from Mohammed and Richon, (2009). The results were agreed well with experimental data. Subsequently, the HE–CPA equation of state was utilised to model the hydrate measurements for CO₂ + water + single electrolyte + CP. The obtained results show a satisfactory agreement with measured data and model data as shown in Figures 5.41 to 5.43. The absolute average deviation (AAD) were calculated for these systems and it is presented in Appendix C. It was shown that the error is less than 1%, this is an acceptable error. Consequently, the obtained results shows that the consistent fits of the model with the measured hydrate dissociation data.

Table 5. 29: Temperature and pressure ranges investigated for gas hydrate measurements

Hydrate former	No. of points	T/K	P/MPa
^a CO ₂ + water	5	273.6 to 282.2	1.3400 to 3.8756
^b CO ₂ + water + CP	6	284.3 to 290.7	0.3500 to 2.0600
CO ₂ + water + 0.10 NaCl + CP	5	270.0 to 276.0	1.4881 to 3.2390
CO ₂ + water + 0.15 NaCl + CP	5	266.0 to 271.9	1.3584 to 2.7811
CO ₂ + water + 0.20 NaCl + CP	4	262.3 to 266.3	1.3381 to 2.4461
CO ₂ + water + 0.10 CaCl ₂ + CP	6	268.8 to 277.2	0.9660 to 2.7784
CO ₂ + water + 0.15 CaCl ₂ + CP	4	268.0 to 273.4	1.1924 to 2.4881
CO ₂ + water + 0.20 CaCl ₂ + CP	4	261.4 to 267.2	1.0623 to 2.3484
CO ₂ + water + 0.10 MgCl ₂ + CP	5	282.0 to 287.2	0.8133 to 2.4193
CO ₂ + water + 0.15 MgCl ₂ + CP	4	261.1 to 268.6	0.8833 to 2.0621

^aDlolabhia et al., (1993); ^bMohammadi and Richon (2009)

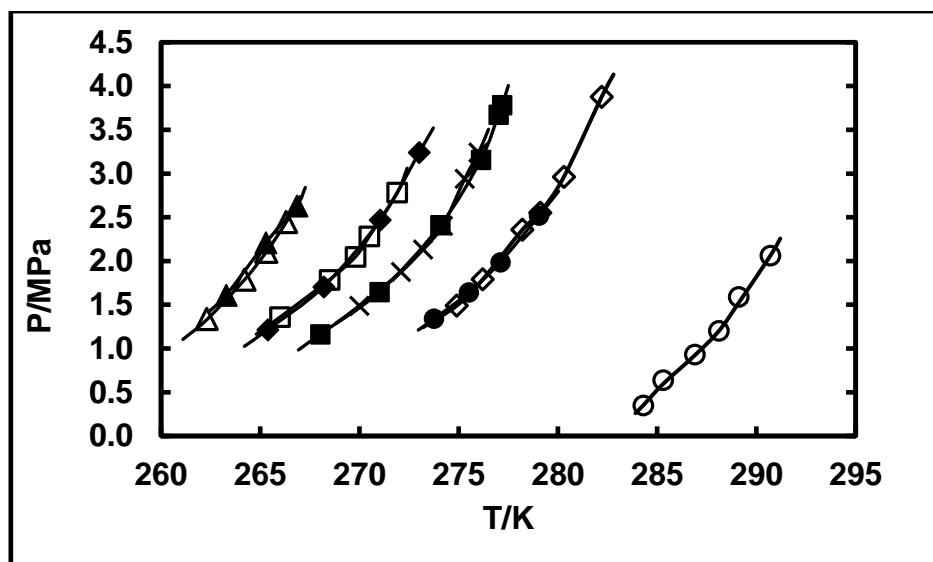


Figure 5. 41: Measured and estimated data for hydrate–liquid water–liquid promoter–vapour for the CO₂ (1) + water (2) + NaCl (3) + CP (4) system: Symbols represent experimental condition: x, Mohammed and Richon, (2009) in the presence of CP and absence of salt; ●, Mohammed and Richon, (2009) in the absence of CP and salt; ■, 0.10 mass fraction in the absence of CP (Dlolabhia et al., 1993); ◆, 0.15 mass fraction in the absence of CP (Dlolabhia et al., 1993); ▲, 0.20 mass fraction in the absence of CP (Dlolabhia et al., 1993); This work: ◇, in the absence of CP and salt; ○, 0.10 mass fraction in the presence of CP; □, 0.15 mass fraction in the presence of CP; △, 0.20 mass fraction in the presence of CP; —, model results.

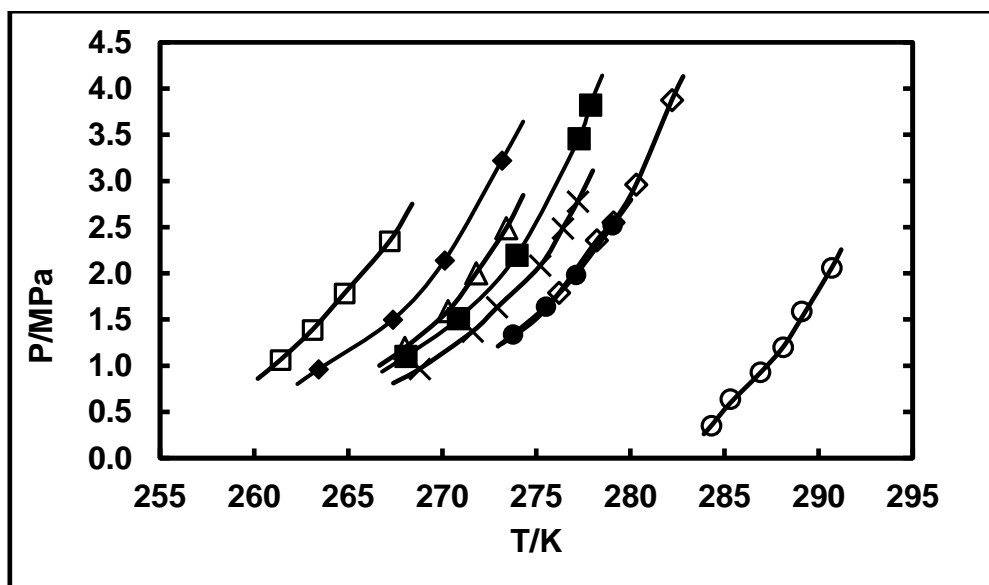


Figure 5. 42: Measured and estimated data for hydrate–liquid water–liquid promoter–vapour for the CO₂ (1) + water (2) + CaCl₂ (3) + CP (4) system: Symbols represent experimental condition: x, Mohammed and Richon, (2009) in the presence of CP and absence of salt; ●, Mohammed and Richon, (2009) in the absence of CP and salt; ■, 0.10 mass fraction (Dlolabhia et al., 1993) in the absence of CP; ◆, 0.15 mass fraction (Dlolabhia et al., 1993) in the absence of CP; This work: ◇, absence of CP and salt; ○, 0.10 mass fraction in the presence of CP; △, 0.15 mass fraction in the presence of CP; □, 0.20 mass fraction in the presence of CP; —, model results.

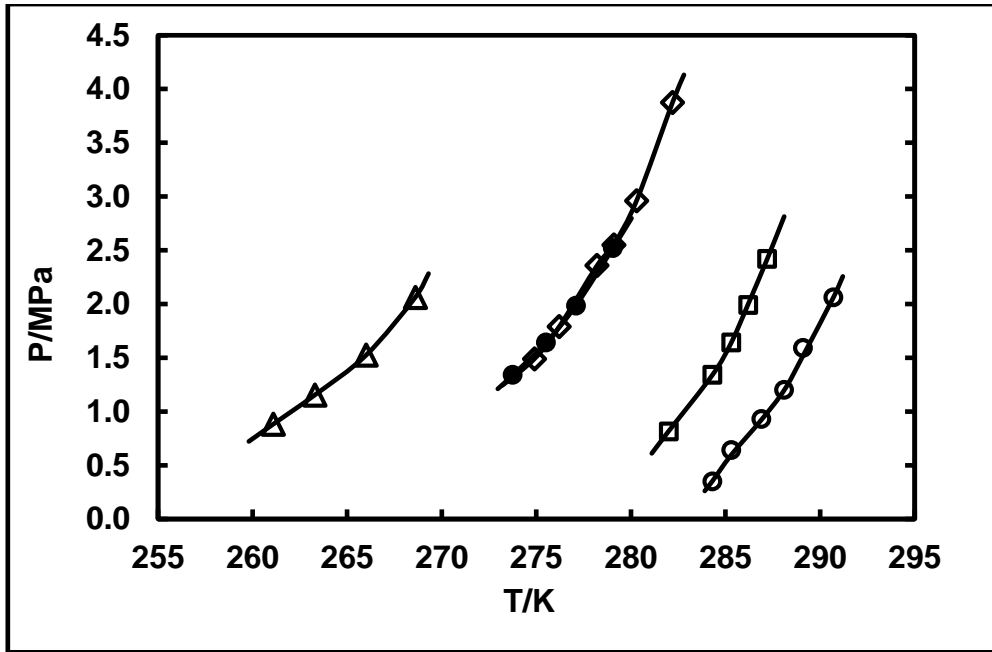


Figure 5. 43: Measured and estimated data for hydrate–liquid water–liquid promoter–vapour for the CO₂ (1) + water (2) + MgCl₂ (3) + CP (4) system: Symbols represent experimental condition: x, Mohammed and Richon, (2009) in the presence of CP and absence of salt; ●, Mohammed and Richon, (2009) in the absence of CP and salt; This work: ◇, in the absence of salt and CP; ○, 0.10 mass fraction in the presence of CP; Δ, 0.15 mass fraction in the presence of CP; —, model results.

Table 5.30 presents the Langmuir constant parameters (*a*, *b*, *c* and *d*) which were attained using Equation 3.171 in Chapter 3 in the absence of single electrolytes and presence of CP. In this research, the Langmuir constants parameters for guest molecule interaction with each type of cavity was calculated using Equation 3.171 for a small cavity pentagonal dodecahedral (sI), because CO₂ forms structure I (sI) hydrate as mentioned by Circone et al., (2003). Afterward, the parameters were regressed to obtain final Langmuir constant parameters in the absence and presence of electrolyte aqueous solutions.

Table 5. 30: Regressed Langmuir constants parameters for the CO₂ (1) + water (2) system (Parrish and Prausnitz, 1972).

Hydrate system s	$a_{small}/K.MPa^{-1}$	b_{small}/K	$A_{large}/K.MPa^{-1}$	B_{large}/K
^a CO ₂ + water	1.1979×10^{-3}	2.8605×10^{-3}	8.5070×10^{-3}	3.2779×10^3

CHAPTER 6

CONCEPTUAL DESIGN FOR DESALINATION PROCESS

This chapter presents the proposed hydrate desalination process for the purification of seawater and industrial wastewater. The design of the proposed process was conducted at a high level where only a hydrate reactor, separator and compressor were designed. Hydrate desalination involves the phase change from liquid to solid by employing a suitable hydrate former whereby excluding salts from seawater or wastewater. The hydrate reactor was designed at moderated pressure due to the limitation of lower pressure of fluorinated refrirant hydrate former, which is suitable to oprate at ambient conditions. Subsequently, the economic feasibility study was conducted for this process.

6.1 Proposed hydrate desalination process

Parker in 1942 first proposed the clathrate hydrate or gas hydrate desalination process for seawater desalination. This process is similar to the freezing desalination process (Englezos, 1994). In the gas hydrate process, the water molecule creates a structured cage around the hydrate former at the appropriate temperature and pressure (Englezos, 1993). Once the hydrate is being formed, it excludes the dissolved ion and salts from the hydrate crystals (Barduhn et al., 1962). Subsequently, the hydrate crystals can be separated easily from a brine solution using a solid-liquid separator. Then, the hydrate crystals are dissociated into fresh water and hydrate former is released by heat stimulation or pressure reduction. Some researchers conducted the performance of hydrate former candidates, which include propane, carbon dioxide, refrigerant, methane and cyclopentane for seawater desalination process (He et al., 2018). Consequently, in this study, fluorinated refrigerant and cyclopentane were used in a proposed hydrate desalination process as hydrate former and promoter, respectively.

Figure 6.1 presents a proposed process flow diagram for the hydrate desalination process for the purification of industrial wastewater and seawater using gas hydrate technology. This process is the modification of the process presented by Sangwai et al., (2013). Industrial wastewater or seawater is pumped from the reservoir passing through the heat exchanger into the hydrate reactor. The purpose of the heat exchanger is to decrease the temperature near the

hydrate formation temperature. When the high level of water is reached in the hydrate reactor, then the fluorinated refrigerant is pressurized through the nozzle at high pressure from the gas cylinder via regulating valve. Once the desired pressure is achieved inside the reactor, then the valve can be closed. Refrigerant absorption is allowed to take place by agitating the content inside the hydrate reactor. The homogenous mixture can be achieved in the hydrate reactor by higher agitation speed. The temperature must be stable outside hydrate formation region. The reactor temperature is maintained or controlled by the chilled fluid flowing in the jacket. The reactor consists of a jacket where a chilled fluid circulates through the pump and the chiller unit. The chilled fluid further decreases the temperature of the content inside the reactor until the hydrate is being formed. Once the hydrate is being formed, the hydrate crystal can be crushed, subsequently, it is transferred into the horizontal filter belt by a pellet pusher as shown in Figure 6.4. The crushed hydrate crystals can be washed in the spray separator using chilled water, the concentrate filtrate (concentrated brine) come from underneath of the filter belt via suction boxes, while the washed and dried hydrate crystals are transferred into the decomposer. The temperature is higher at the decomposer in order to dissociate hydrate crystals, once hydrate crystal dissociate the purified water can be collected at the bottom of the decomposer and the released refrigerant can be compressed in the compressor to increase pressure to the desired value of 1600 kPa. The pressurized refrigerant can be stored in the gas storage tank, ready to be introduced into the hydrate reactor to form the hydrate again.

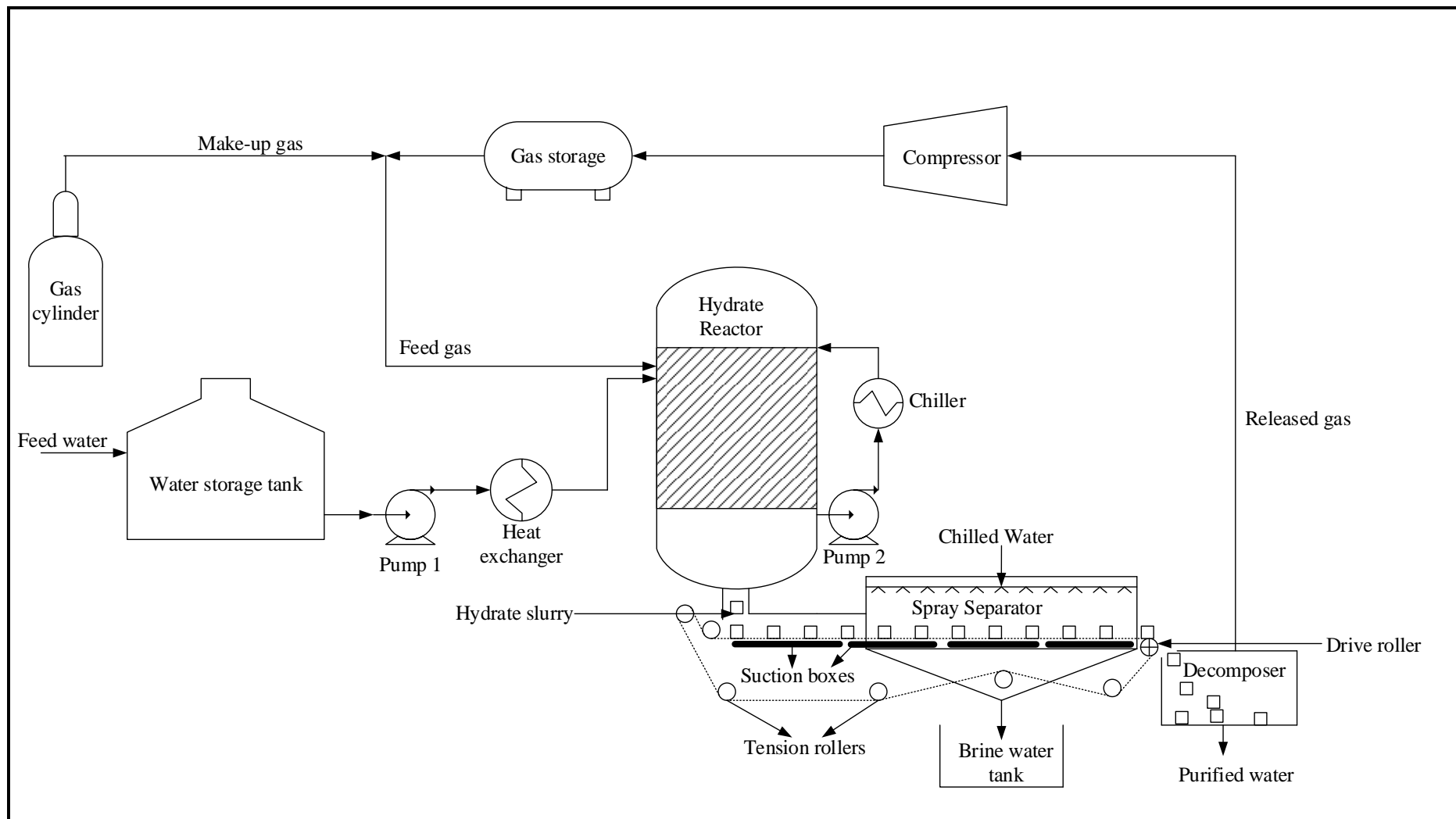


Figure 6.1: Proposed hydrate desalination process

6.2 Hydrate reactor design

A hydrate reactor is a continuous stirred tank reactor (CSTR) reactor type. This type of reactor is commonly used in industrial processing in a continuous operation (Folger, 2006). It is designed for liquid phase reaction or gas-liquid mixtures. It is designed to operate at steady-state and it is considered to be a perfect homogenous mixing. This type of reactor is not time dependent, the concentration or the reaction rate inside the reactor or position is temperature dependent. The content inside is homogenous at every point because the temperature and concentration are the same everywhere in the reactor tank, and they are identical at the exit point. In this study, the CSTR is designed for gas-liquid mixing as shown in Figure 6.2. It consists of impellers for stirring, the type of gas injection device and jacketed for cooling. It is cylindrical, vertical oriented with a rotating mechanical stirrer inserted into the hydrate reactor as shown in Figure 6.2. The impellers are fixed onto the stirrer shaft that is driven by a mechanical motor. The CSTR is equipped with baffles on its inside wall. The hydrate former (refrigerant) is bubbled into the reactor vessel from the gas injection device. A coolant jacket for continuously cooling its content sheaths the hydrate reactor.

The heat transfer from the content inside a reactor to the coolant flowing in the external jacket of the reactor vessel includes three heat transfer processes (Mori, 2015):

- The convection heat transfer from the aqueous solution to the surface wall of the reactor
- The conduction heat transfer across the wall
- Lastly, the convection heat transfer from the outside surface of the wall to the flowing coolant.

This study focuses on the first heat transfer by convection that directly depends on reactor size and the power of the stirrer mechanism. It is assumed that the content inside the reactor is a single phase of a Newtonian liquid, then any multi-phase effects on the stirrer-induced flow is neglected. Thus, the discussion is not based on how hydrate former bubbles into an aqueous solution, the slugs are very densely dispersed in the content and a dense slurry of formed hydrate crystals occupies the aqueous mixture.

Several researchers have reported on heat transfer between the reactor vessel wall and the content stirred inside the reactor (Mori, 2015). The following correlation is widely used for calculating inside heat transfer coefficient, h_i

$$h_i = \frac{Nu k_l}{D} \quad (6.1)$$

$$Nu = C Re^{2/3} Pr^{1/3} \quad (6.2)$$

where k_l is liquid thermal conductivity, D is the inside diameter of reactor vessel, Nu is Nusselt number, Re is Reynolds number, Pr is the Prandtl number and C is the lead constant that range from 0.3 to 1.2 depending on the geometric details of the reactor vessel and impeller (Mori, 2015). Most of the design equations are presented in Appendix D. Table 6.1 presents the hydrate reactor design specification for the proposed desalination process in Figure 6.1.

Table 6.1: Design specification of the reactor

Parameters	Values	Units
Design temperature	298	K
Design pressure	10000	kPa
Reactor diameter	0.9	m
Reactor height	1.6	m
Volume	1.12	m ³
Conversion	0.8	-
Impeller diameter	0.3	m
Power required	7.9	kW

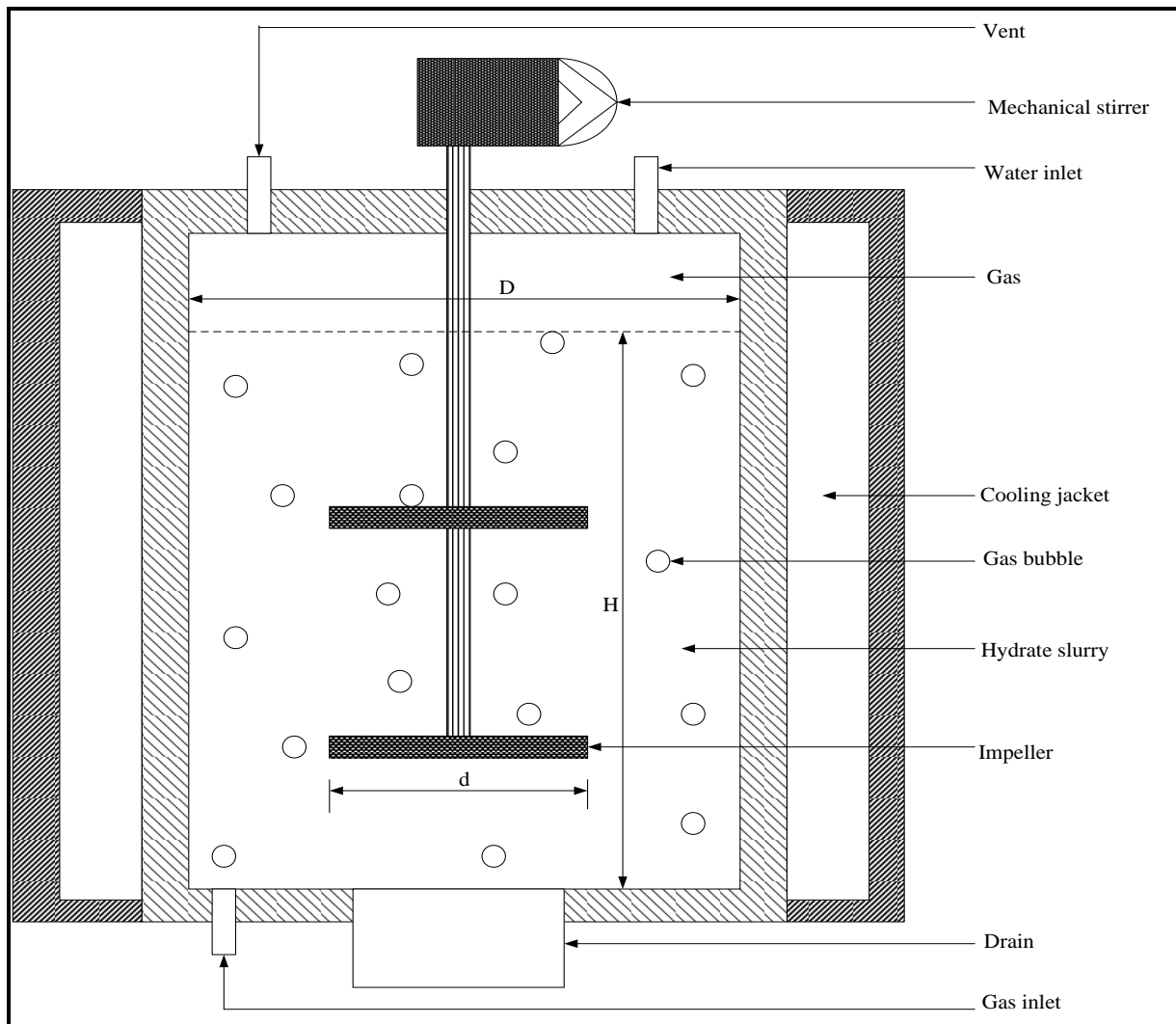


Figure 6.2: The design reactor

6.3 Horizontal belt filter separation design

The horizontal belt filter is a gravity method for separation, the hydrate slurry was fed on top of the belt. It has a large filtration area, and several advantages compared to others filters such as drum and disc filters. The filter was made up of several suction boxes over which is fitted a continuous belt filter (Tarleton and Wakeman, 2007). As the filter belt moves over the suction boxes, the low pressure below atmospheric pressure was applied to draw water from suspension and form a dry hydrate slurry as shown in Figure 6.3. This is how the separation takes place on the horizontal belt filter. The speed of the belt can be adjusted in order to provide sufficient time for dewatering a hydrate slurry. The limitations of belt filter is not suitable to handle very fine and particles, slow filtering suspensions (Tarleton and Wakeman, 2007). This limitation leads to poor separation and produces wet slurry as the final product.

The belt filters were washed to ensure that there is no clogging in pores. The washing can be done either singly or in a combination of the following:

- Co – current – the simplest displacement wash with one large volume of wash liquor.
- Counter-current – often a smaller volume of wash liquor passing through the slurry several times in the opposite direction to the slurry direction.
- Reflux – circulation of a large volume of wash liquor over the zone with a small bleed off and fresh wash liquor make-up.
- Reslurry – breaking up of the filter slurry with sprays over a zone without vacuum, then followed by a vacuum zone.

In this study, the horizontal belt filter cycle is used to separate hydrate crystals and salinity that was at the surface of hydrate crystals by using chilled water. The purpose of using chilled water was to keep hydrate crystals at the solid phase before dissociation takes place. The horizontal belt filter is an endless perforated cloth, which was driven by rollers over suction boxes as shown in Figure 6.3 It consists of a sequence of evacuated suction boxes. The hydrate slurry was introduced from one end of the filter and processed at constant pressure that was less atmospheric (vacuum). The nozzles sprayed chilled water over the hydrate crystal to remove salinity at the surface. The saline water is drawn via suction boxes to the brine storage tank. The hydrate crystal with zero salinity after the washing process is transferred to the decomposer where the dissociation takes place as shown in Figure 6.1. The separation consists of three stages that include filtrate, washing and deliquoring phase.

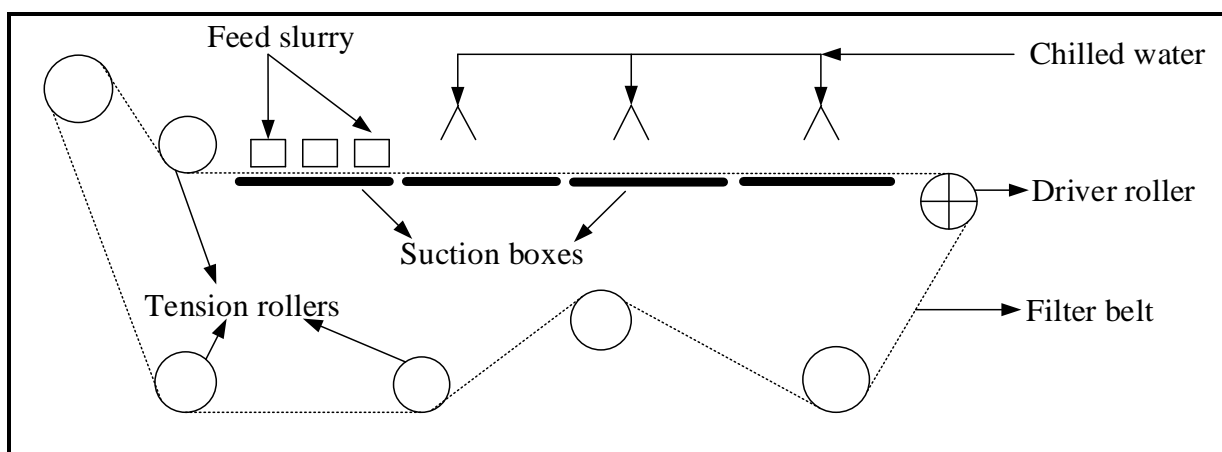


Figure 6.3: Horizontal belt filter

The detailed design procedure for the horizontal belt filter can be found in Tarleton and Wakeman, (2007). Some design equations and the table of results for filtrate, washing and deliquoring phase are presented in the Appendix D. The assumed length and width of the belt filter for the calculation are 9 m and 2 m respectively. The applied pressure at suction is 50 kPa. The cumulative volume is changes with time as the separation process takes place. The filtration is 15 seconds, the washing is 45 seconds and deliquoring is 30 seconds. The total cycle time is 90 seconds.

6.4 Compressor design

A compressor is an equipment that is reliable for a wide operating range. It is used to handle compressible fluid like air, gases and vapours. A centrifugal compressor is essentially a variable capacity, constant pressure machine. It consists of an impeller with a series of curved radial vanes, inducer, diffuser and volute. The gas (refrigerant) released by decomposer at a lower pressure is drawn by the impeller eye, and it is whirled round at high rotational speed by the vanes on the impeller. Then, the static pressure of the gas increases from the eye to the tip of the impeller in order to produce the centripetal force on the air. The gas leaves the impeller tip, and it passes through the diffuser passages, which convert the kinetic energy to increase in enthalpy, subsequently, the pressure of the gas increases to the desired pressure. The volute is used for flow collection and for directing the fluid to the pipe. A centrifugal compressor has the following advantages:

- High degree of balancing;
- Pulsation free delivery;
- Obviates the use of surge tank receivers;
- Easy maintenance;
- Best suited for part load operations;
- Lower noise level;
- Compact.

6.4.1 Sizing and selection

Figure 6.4 presents various compressor types that can be selected for design, these types are not discussed in detail compared to the centrifugal compressor. Some factors that are considered in selecting a suitable compressor type (Brown and Lewis, 1995):

Volume flow: centrifugal compressors handle volume flows higher than the reciprocating compressor and positive displacement, and lower than the axial flow type.

Pressure ratio and head: Centrifugal compressor is dynamic rather than positive displacement compressor, and produce head rather than pressure ratio as in a positive displacement compressor. The head is a function of the molecular weight of the gas. The head calculation method is presented in the Appendix D.

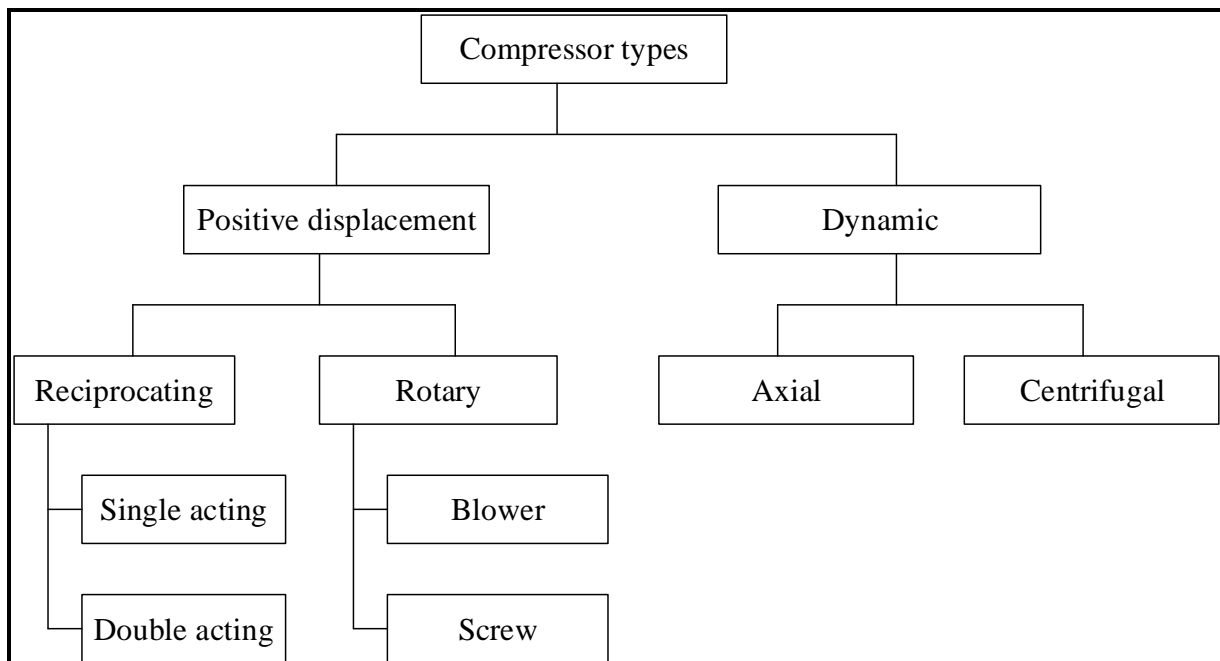


Figure 6.4: Compressor types based on operating principles (Bloch, 2006)

Brown and Lewis, 1995, discuss other factors such as volume flow variation, controls and cost, critically of service and efficiency in detail. There are two methods used for compressor design – the N-method and Mollier method (Bloch, 2006). The N-methods, which is presented in Appendix D was used in thi study.

The centrifugal compressor was designed to increase the outlet pressure (P_2) of gas (refrigerant) to the desired value of 1600 kPa. The intercooler is not needed because the calculated outlet temperature (T_2) was 402.73 Kwas less than 478.20 K (Bloch, 2006). Table 6.2 presents the design specification of the centrifugal compressor. For gas such as refrigerant, Brown and Lewis, (1995) recommend the material of construction to be an austinetic stainless steel due to

its strength as well as considering the properties of the gas. Moreover, the impeller design and design assessment as well as design procedure for centrifugal compressors are found elsewhere in Zahed and Bayomi, (2014).

Table 6.2: Design specification of the centrifugal compressor

Parameters	Values	Units
Inlet pressure	300	kPa
Discharge pressure	1600	kPa
Mass flowrate	6.6	kg/min
Specific volume (inlet)	0.11	m ³ /kg
Volumetric flowrate	44.17	m ³ /h
Overall head	65344.08	Nm/kg
Temperature, T ₂	402.73	K
No intercooler is needed, T ₂	< 478.15	K
Frame size	29	M
Nominal polytropic efficiency	0.78	
Nominal speed	11500	r/min
Actual number of stages	2	
Impeller diameter	459	mm
Speed required	12050.27	r/min
Power required	9.4	kW

6.5 Economic feasibility study

Generally, there are two types of equipment costs which known as capital costs and operation costs. Capital costs are the cost associated with initial of purchasing or building equipment that is used in the process, such hydrate reactor, pumps, compressor, separator, piping and fittings, control valves, electrical systems and structural work for support. Operating costs are the cost of day to day operation of equipment which includes raw material, pumping, labour, maintenance, heating and cooling, (Solen and Harb, 2005). This study is focused on capital costs because it includes costs associated with design of hydrate reactor, horizontal filter belt separator and compressor. The cost for piping, construction, heat exchanger, chiller unit, storage tanks, pumps and gas cylinders are not included in this study.

6.5.1 The capital cost

The cost associated with the construction and maintenance of a gas hydrate desalination process is affected by the following variables (Barron and Wrobel, 1985):

- Plant capacity
- Hydrate formation and dissociation temperatures of the hydrate crystal or slurry
- Viscosity of the mother liquor from which the component is being crystallized
- Latent heat of fusion for the material being crystallized
- Material of construction requirements.

The capital costs associated with the construction of the gas hydrate desalination process can be determined using the following equation:

$$\text{Capital cost (\$)} = (\text{Base cost})(F_s)(F_t)(F_v)(F_{hf})(F_{mat}) \quad (6.3)$$

where F_s is the size factor, F_t is the temperature, F_v is the viscosity factor, F_{hf} is the latent heat factor and F_{mat} is the material of construction factor. The base cost had to be converted into its present-day monetary value. The base cost can be determined using the latest price indexing

$$\text{Base cost (\$)} = \text{past price} \times \left(\frac{\text{present day CEPCI}}{\text{past CEPCI}} \right) \quad (6.4)$$

Since the hydrate is being formed at low temperatures, then the material of the construction factor can be on material corrosion at low temperatures. Therefore, Table 6.3 presents the cost factors of the material.

Table 6.3: Material of construction cost factors (Barron and Wrobel, 1985)

Material	Material of construction factor
Carbon steel	0.60
Line carbon steel	0.70
316 Stainless steel	1.00

6.5.2 Operation and maintenance costs

The operation and maintenance costs associated with the operation of the hydrate desalination process are determined using the following equation

$$\text{Operations and maintenance costs (\$)} = L + E + M + A \quad (6.5)$$

$$L = (\text{average labour rate})(C_s)(\text{overhead rate}) \quad (6.6)$$

$$E = (\text{Local energy cost})(C_t)(7.20) \quad (6.7)$$

$$M = (0.035)(\text{capital cost})(\text{annual hydrate production rate})^{-1} \quad (6.8)$$

$$A = (\text{amortized capital cost})(\text{annual hydrate production rate})^{-1} \quad (6.9)$$

where C_s is the size-labour cost factor and C_t is the energy temperature cost factor

In this study, the purchase cost of the selected individual equipment that make up the hydrate process are hydrate reactor, filter belt separator and compressor. The material of construction of these units is assumed at 316 stainless steel, which is based on year 2017. The Marshall & Swift Equipment Cost Index (M&S Index) reflects the current average cost for equipment for 2017, which is inserted into the cost correlations to determine the capital costs (Chemical Engineering Essential for the CPI Professional, February 2017). Table 6.4 presents the cost of the selected equipment.

$$\text{Hydrate Reactor Cost (\$)} = \left(\frac{M \& S}{556.8} \right) (47.0 * V^{0.61}) \quad (6.10)$$

where V is the hydrate reactor volume in gallons

$$\text{Horizontal Filter Belt Separator (\$)} = \left(\frac{M \& S}{556.8} \right) (47.0 * Q^{0.61}) \quad (6.11)$$

where Q is the volumetric flowrate in gal/min

$$Compressor (\$) = \left(\frac{M \& S}{556.8} \right) (47.0 * P^{0.61}) \quad (6.12)$$

where P is the power required in Btu/h

Table 6.4: Cost of the designed selected equipment

Equipment	Cost (\$)
Hydrate reactor	1824.51
Horizontal filter belt separator	288.09
Centrifugal compressor	1849.51

Since the costing of the proposed hydrate desalination process is based on three units only, it makes difficult to compare to the capital cost for other hydrate separation processes. The reason is that the capital cost of other hydrate separation processes such as freezing process includes construction, piping and fitting, pumps, etc. Nevertheless, researcher shows that gas hydrate technology for desalination is more economical compared to the traditional desalination processes. Furthermore, it is recommended that one has to do a full capital cost of the proposed hydrate desalination process and compare it to other hydrate separation processes.

CHAPTER 7

CONCLUSIONS

Gas hydrate dissociation data were measured for ternary systems comprising of fluorinated refrigerant (R410a or R507) + water in the presence of CP. It was revealed that the presence of CP shows impressive results by shifting hydrate dissociation temperatures to higher temperatures. The result for R507 + water + CP system shows an increase in hydrate dissociation temperatures but the hydrate dissociation temperatures were still far below ambient temperatures. Consequently, R507 is not suitable for gas hydrate technology for desalination process. Despite this, measured hydrate dissociation pressures were found below atmospheric pressures, which is good for gas hydrate technology for the desalination process.

In this study, gas hydrate dissociation data for R410a + water + (NaCl, MgCl₂, CaCl₂, and Na₂SO₄) systems were measured at various salt concentrations in the absence and the presence of CP. The measured concentrations ranged between (0.10 to 0.20) in mass fraction. All measured concentrations were below their solubility at 298.2 K. It was also noted that the equilibrium phase boundary shifts to lower temperatures as salt concentration increases to 0.20 mass fraction. The results show that R410a can be employed as a hydrate former, because it enables the elimination of electrolytes, even at high concentration of 0.20 mass fraction.

Experimental gas hydrate dissociation data for {R410a or R507} + water + mixed electrolytes (NaCl, CaCl₂, and MgCl₂) systems were measured at maximum concentrations of electrolytes at industrial wastewater treatment plant as indicated in Table 2.6 in Chapter 2. The selected maximum concentration covers the electrolytes concentrations in seawater as tabulated in Chapter 2 in Table 2.7. The measurements were conducted in the absence and the presence of CP. It was found that R410a systems were closed to ambient conditions, which bring evidence that this refrigerant is the best hydrate former for gas hydrate desalination process. Furthermore, the hydrate dissociation data were measured at a higher concentration than industrial wastewater concentration, because the salt concentrations may increase way above the targeted. Secondly, it is necessary to check that the gas hydrate can be formed at higher concentration where no precipitate formed in the mixed salts. In this study, gas hydrate dissociation data for R410a + water + mixed electrolytes (NaCl and CaCl₂) systems were measured at higher concentrations range of (0.05 to 0.15) mass fraction of electrolytes. The

results were impressive, showing that CP and R410a can be utilised for application in gas hydrate technology for the desalination processes at ambient conditions. A water-insoluble promoter (CP) shows an impressive result to shift the H–L_w–V equilibrium phase boundary closer to ambient conditions by increasing the dissociation temperatures.

Enthalpy of hydrate dissociation for R410a, R507 and R134a measured systems were evaluated. It was observed that R507 systems have high enthalpy compared to R134a and R410a systems. It was noted that the measured dissociation temperatures for R507 hydrate systems are lower than R410a, which means more energy is required for R507. Consequently, it is not a suitable hydrate former for hydrate process as well as R134a for the same reasons.

The kinetics measurements were conducted for R410a systems only for both single and mixed salt in the absence and the presence of CP. The rate of hydrate formation of R410a refrigerant was evaluated and the effect of initial pressure, initial temperature, and the degree of subcooling on the hydrate nucleation and growth rate. Only R410a was investigated, where it was found that it was a suitable refrigerant for desalination process using gas hydrate technology. The moles of R410a were consumed, and the apparent rate constant at induction time was evaluated.

Moreover, in this study, the hydrate dissociation data for CO₂ + water + {NaCl or CaCl₂ or MgCl₂} + CP systems were measured at mass fraction range from (0.10 to 0.20) mass fraction. However, the increases in temperatures are still below that of ambient temperatures and the reduction in pressures is above atmospheric pressure, making CO₂ unsuitable for gas hydrate technology for the desalination process.

The developed model used in this study was well described in detail in Chapter 3. The HE-CPA model describes the properties and the behaviour of electrolyte solutions in utilising gas hydrate technology in the purification of industrial wastewater and seawater. In this study, three models were combined to form one model to be used for the optimisation of water desalination by means of gas hydrate technology, namely, the van der Waals and Platteeuw, Debye–Hückel (DH) and CPA Equation of State (EoS) models. These combination contributions were developed from electrolyte–CPA (e-CPA) equation of state by Maribo-Mogensen, (2014). Consequently, a newly developed model was named the Hydrate Electrolyte–Cubic Plus Association (HE–CPA) equation of state, where Equation 3.173 shows all contributions terms involved.

In the HE–CPA equation of state, the solid solution theory of Van der Waals and Platteeuw, (1959) was used to model the hydrate phase. Later, Eslamimanesh et al. (2011), which was used in this study, adapted this model. The electrolytes aqueous systems were modeled using Deybe–Hückel, (1923), and CPA equation of state of Kontogeorgis et al., (1996) was used to model liquid or vapour phase. All experimental hydrate dissociation data in the absence and the presence of CP were satisfactorily correlated with a developed HE–CPA equation of state. Consequently, this model can be easily used, and may be employed for the application of gas hydrate technology for desalination processes at ambient conditions.

The hydrate desalination process was proposed to purify industrial wastewater and seawater. The proposed process is shown in Figure 5.43. From the proposed process only three major units were designed, which include hydrate reactor, separator (horizontal belt filter) and compressor. Even the economic study was conducted on these units or equipment. It was found that desalination using gas hydrate technology is more economical when compared to the traditional desalination processes such as RO, MSF etc. Consequently, desalination by using gas hydrate technology can be implemented on a large scale for the treatment of saline waters.

CHAPTER 8

FUTURE WORK

Experimental hydrate dissociation data for the selected systems to complete this study were conducted successfully. Further to this, an investigation is required for hydrate measurements for refrigerant (R410a) + sample of seawater and industrial wastewater in the absence and in the presence of CP. The reason for this is that the designed hydrate desalination process will be treating seawater and industrial wastewater, rather than synthetic water. Some hydrate measurements can be conducted in the mixed of three salts at different concentrations. It is recommended to conduct hydrate measurements in the pilot plant. The kinetics of hydrate measurements for R410a with seawater and industrial wastewater systems must be conducted in the absence and the presence of CP.

All measured hydrate dissociation data were model using the developed HE–CPA equation of state. It is recommended that HE–CPA equation of state can be optimised by using the combination of Deybe–Hückel and UNIQUAC model to cover all types of interactions in aqueous solution such as short and middle-range interactions. Some research is required to fine-tune kinetic hydrate parameters since the systems are comprising of the mixed electrolytes and cyclopentane.

In the proposed hydrate desalination process, only three units were designed which include hydrate reactor, separator and compressor. It was recommended that one must design all equipment included in the proposed desalination process. Furthermore, it is recommended that one conduct a full capital cost analysis of the proposed hydrate desalination process, and compare this to other separation processes. Consequently, one has to propose the location of the plant near the sea or ocean in South Africa since the process is based on seawater treatment. This can lead to reducing the cost involved in pumping water from the sea.

REFERENCES

- Abrams, D. S., Prausnitz, J. M., (1975), "Statistical thermodynamics of liquid mixtures: A new expression for the excess Gibbs energy of partly or completely miscible systems". *AIChE J*, 21(1), 116–128
- Acosta, H.Y., Bishnoi, P.B., Clarke, M.A., (2010), "Experimental measurements of the thermodynamic equilibrium conditions of tetra-n-butylammonium bromide semiclathrates formed from synthetic landfill gases". *J. Chem. Eng. Data*, 56, 69–73
- Adisasmito, S., Franck, R. J., Sloan, E. D., (1991), "Hydrates of carbon dioxide and methane mixtures". *J. Chem. Eng. Data*, 36, 68–71
- Adisasmito, S., Sloan, E. D., (1992), "Hydrates of hydrocarbon gases containing carbon dioxide". *J. Chem. Eng. Data*, 37, 343–348
- Akiya, T., Shimazaki, T., Oowa, M., Matsuo, M., Yoshida, Y., (1999), "Formation conditions of gas between HFC alternative refrigerants and water". *Intern. J. Thermophy*, 20, 1753 – 1763
- Aliev, A. M., Yusifov, R. Y., Tairov, A. Z., Sarydzhanov, A. A., Mirzoeva, R. Y., Yusifov, Y. G., (2011), "Mathematical modeling of seawater desalination by the gas hydrate method". *Theor. Found. Chem. Eng*, 45, 185–189
- Anderko, A., Wang, P., Rafal, M., (2002), "Electrolyte solutions: From thermodynamic and transport property models to the simulation of industrial processes". *Fluid Phase Equilib*, 194, 132–142
- Aspen Plus Version V7.3., (2011), "Aspen Technology Inc."
- Atik, Z., Windmeier, C., Oellrich, L. R., (2010), "Experimental and theoretical study on gas hydrate phase equilibria in seawater". *J. Chem. Eng. Data*, 55, 804–807

Attard, P., (1993), “Asymptotic analysis of primitive model electrolytes and the electrolytes and the electrical double layer”. *Phys Review E*, 48 (5), 3604 – 3621.

Austgen, D. M., Rochelle, G. T., Peng, X., Chen, C. C., (1989), “Model of vapour-liquid equilibria for aqueous acid gas-alkanolamine systems using the electrolyte-NRTL equation”. *Ind. Eng. Chem. Res*, 28(7), 1060–1073

Babae, S., Hashemi, H., Javanmardi, J., Eslamimanesh, A., Mohammadi, A. H., (2012), “Thermodynamic model for prediction of phase equilibria of clathrate hydrates of hydrogen with different alkanes, alkenes, alkynes, cycloalkanes or cycloalkenes”. *Fluid Phase Equilib*, 336, 71–78

Babae, S., Hashemi, H., Mohammadi, A. H., Naidoo, P., Ramjugernath, D., (2015), “Kinetic and thermodynamic behavior of CF₄ clathrate hydrates”. *J. Chem. Thermodyn*, 81, 52–59

Bakker, R. J., (1997), “Gas: Computers programs to calculate fluid inclusion V-x properties using gas melting points temperature”. *Computer and Geosci*, 23, 1–18

Barduhn, A. J., Towlson, H. E., Hu, Y. C., (1962), “The properties of some new gas hydrates and their use in demineralizing sea water”. *AIChE J.* 8, 176–183

Barduhn, A. J., (1967), “Desalination by crystallization processes”. *Chem. Eng. Prog.* 63, 98–103

Barduhn, A. J., (1968), “The state of the crystallization processes for desalting saline waters”. *Desalination*, 5, 173–184

Barron, T. S., Wrobel, P. J., (1985), “Separation process economics”. Houston

Beltrán, J. G., Servio, P., (2008), “Equilibrium studies for the system methane + carbon dioxide + neohexane + water”. *J. Chem. Eng. Data*, 53, 1745–1749

Bloch, H. P., (2006), “A practical guide to compressor technology”. Second Edition, John Wiley & Sons, Inc.

Born, M., (1920), “Volume and the ionic hydration”. *Z. Phys*, 1, 45–68

Bradshaw, R. W., Greathouse, J. A., Cygan, R. T., Simmons, B. A., Dedrick, D. E., Majzoub, E. H., (2008), “Desalination Utilizing Gas Hydrates (LDRD Final Report)”, Sandia National Laboratories: Albuquerque, NM, Livermore

Brown, R. N., Lewis, R. A., (1995), “Centrifugal compressor application sizing, selection and modelling”. *ISESCO J. Sci. Technol*, 12, 195–201

Brinchi, L., Castellani, B., Cotana, F., Filipponi, M., Rossi, F., Savelli, G., (2011), “Investigation on a novel reactor for gas hydrate production” *Proceedings of the 7th International Conference on Gas Hydrate (ICGH 2011)*, Edinburgh, Scotland, United Kingdom, July 17–21

Cakmakci, M., Kayaalp, N., Koyuncu, I., (2008), “Desalination of produced water from oil production fields by membrane processes”. *Desalination*, 222, 176–186

Calm, J. E., (2008), “Properties and efficiencies of R-410A, R-421A, R-422B and R-422D compared to R-22”. *Refrigerant Management Services*, 1–14

Carroll, J. J., (2003), “Natural gas hydrates: A guide for engineers”. Gulf Professional Publishing, London, New York, Oxford

Castellania, B., Fillipponib, M., Rinaldia, S., Rossib, F., (2012), “Capture of carbon dioxide using gas hydrate technology”: *The 25th International Conference on efficiency, Cost, Optimization and Environmental Impact of Energy Systems*, Perugia, Italy, June 26–29

Cha, J-H., Seol, Y., (2013), “Increasing gas hydrate formation temperature for desalination of high salinity produced water with secondary guests”. *Sustain. Chem. Eng*, 1, 1218–1224

Chapoy, A., (2004), "Phase behavior in water\hydrocarbon mixtures involved in gas production", PhD Thesis, Department of Chemical Engineering, Ecole des Mines de Paris.

Chapoy, A., Gholinezhad, J., Tohidi, B., (2010), "Experimental clathrate dissociations for the hydrogen + water and hydrogen + tetrabutylammonium bromide + water systems". *J. Chem. Eng. Data*, 45, 5323–5327

Chapoy, A., Haghghi, H., Burgass, R., Tohidi, B., (2010), "Gas hydrates in low water content gases: Experimental measurement and modelling using the CPA equation of state". *Fluid Phase Equilib*, 296, 9–14

Chemical engineering essentials for the CPI professional, February 2017

Chen, Z-Y., Li, Q-P., Yan, Z-Y., Yan, K-F., Zeng, Z-Y., Li, X-S., (2010), "Phase equilibrium and dissociation enthalpies for cyclopentane + methane hydrate in NaCl aqueous solution". *J. Chem. Eng. Data*, 55, 4444–4449

Chen, G-J., Guo, T-M., (1998), "A new approach to gas hydrate modeling". *Chem. Eng. J*, 71, 145–151

Chen, C. C., Evans, L. B., (1986), "A local composition model for the excess Gibbs energy of aqueous electrolyte systems". *AIChE J*, 32(3), 444 – 454

Chun, M-K., Lee, H., Ryu, B. J., (2000), "Phase equilibria of R22 (CHClF₂) hydrate systems in the presence of NaCl, KCl and MgCl₂". *J. Chem. Eng. Data*, 45, 1150–1153

Clarke, M. A., Majumdar, A., Bishnoi, P. R., (2004), "Experimental investigation of carbon dioxide hydrate formation conditions in the presence of KNO₃, MgSO₄ and CuSO₄". *J. Chem. Eng. Data*, 49, 1436–1439

Colten, S. L., Lin, F. S., Tsao, T. C., Stern, S. A., Barduhn, A. J., (1972), "Hydrolysis losses in the hydrate desalination process: Rate measurements and economic analysis". *Desalination*, 11, 31–59

Copeman, T. W., Stein, F. P., (1987), “A perturbed hard-sphere equation of state for solutions containing an electrolyte”. *Fluid Phase Equilib*, 35(1), 165–187

Corack, D., Barth, T., Hoiland, S., Skodvin, T., Larsen, R., Skjetne, T., (2011), “Effect of subcooling and amount of hydrate former on formation of cyclopentane hydrate in brine.” *Desalination*, 278, 268–274

Crabtree, M., Eslinger, D., Flechter, P., Miller, M., Johnson, A., King, G., (1999), “Fighting scale-removal and prevention”. *Oilfield Review*, 11(3), 30–45

Dalmacija, B., Karalovic, E., Tamas, Z., Miskovic, D., (1996), “Purification of high salinity wastewater by activated sludge process”. *Water Research*, 30 (2), 295–298

Daraboina, N., Linga, P., Ripmeester, J., Walker, V. K., Englezos, P., (2011), “Natural gas hydrate formation and decomposition in the presence of kinetic inhibitor. 2. Stirred reactor experiments”. *Energy Fuels*, 25, 4384–4391

Daraboina, N., Malmos, C., von Solms, N., (2013), “Synergistic kinetic inhibition of natural gas hydrate formation”. *Fuel*, 108, 749 – 757

Daraboina, N., von Solms, N., (2014), “The combined effect of thermodynamic promoters tetrahydrofuran and cyclopentane on the kinetics of flue gas hydrate formation”. *J. Chem. Eng. Data*, 60, (2), 274–251

Daubert, T. E., Danner, R. P., (1985), “DIPPR data compilation tables of properties pure compounds”. *AIChE*, New York

Davis, U. C., (2014), “Solubility of salts/solubility equilibria”. Chemwiki, 1–29

Davies, S. R., Selim, M. S., Sloan, E. D., Bollavaram, P., Peters, D. J., (2006), “Hydrate plug dissociation”. *AIChE J*, 52, 4016–4027

Delahaye, A., Fournaison, L., Marinhas, S., Chatti, I., (2006), "Effect of THF on equilibrium pressure dissociation enthalpy of CO₂ hydrates applied to secondary refrigeration". *Ind. Eng. Chem. Res.*, 45, 391–97

Derawi, S. O., Kontogeorgis, G. M., Michelsen, M. L., Stenby, E. H., (2003), "Extension of the Cubic-Plus-Association equation of state to glycol-water cross associating systems". *Ind. Eng. Chem. Res.*, 42, 1470 – 1478

Deschamps, J., Dalmazzone, D., (2010), "Hydrogen storage in semiclathrate hydrates of tetrabutyl ammonium chloride and tetrabutyl phosphonium bromide". *J. Chem. Eng. Data*, 55, 3395–3399

Deybe, P., Hückel, E., (1923), "Zur Theorie der Elektrolyte". *Z. Phys.*, 24, 179–207

Dholabhai, P. D., Kalogerakis, N., Bishnoi, P. R., (1993), "Equilibrium conditions for carbon dioxide formation in aqueous electrolytes solutions". *J. Chem. Eng. Data*, 38, 650–654

Dholabhai, P. D., Parent, J. S., Bishoi, P. R., (1996), "Carbon dioxide hydrate equilibrium conditions in aqueous solutions containing electrolytes and methanol using a new apparatus". *Ind. Eng. Chem. Res.*, 35, 819–823

Diamond, L. W., (1994), "Sanility of multivolatile fluid inclusions determined from gas hydrate stability". *Geochim. Cosmochim. Acta*, 58, 19–41

Diaz, M., Boyd, K. G., Grigson, S. J. W., Burgess, J. G., (2002), "Biodegradation of crude oil across a wide range of salinities by an extremely halotolerant bacterial consortium MPD-M, immobilized onto polypropylene fibers". *Biotech. Bioeng.*, 79, (2), 145–153

Döring, R., Buchwald, H., Hellmann, J., (1997), "Results of experimental and theoretical studies of the azeotropic refrigerant R507". *Int. J. Refrig.*, 20, (2), 78–84

Duan, D., Sun, R., (2006), "A model to predict phase equilibrium of CH₄ and CO₂ clathrate in aqueous electrolyte solutions". *American Mineralogist*, 91, 1346–1354

DuPlessis, J. A., Burger, A. J., Swartz, C. D., Museev, N., (2006), “A Desalination guide for South African Municipal Engineers”, *Water Res Comm*, Department of Water Affairs and forestry

DuQuesnay, J. R., Posada, M. C. D., Beltran, J. G., (2016), “Novel gas hydrate reactor design: 3-in-1 assessment of phase equilibria, morphology and kinetics”. *Fluid Phase Equilibria*, 413, 148–157

El-Dessouky, H. T., Ettouney, H. M., (2008), “Fundamentals of salt water desalination”. Elsevier Science: Amsterdam, Netherlands

Eslamimanesh, A., Mohammadi, A. H., Richon, D., (2011), “Thermodynamic model for predicting phase equilibria of simple gas hydrates of refrigerants”. *Chem. Eng. Sci.* 66, 5439–5445

Eslamimanesh, A., Gharagheizi, F., M., Mohammadi, A. H., Richon, D., (2011), “Phase equilibrium modelling of structure H clathrate hydrates of methane + water “insoluble” hydrocarbon promoter using QSPR molecular approach”. *J. Chem. Eng. Data*, 56, 3775–3793

Eslamimanesh, A., Gharagheizi, F., Illbeigi, M., Mohammadi, A. H., Fazlali, A., Richon, D., (2012), “Phase equilibrium modelling of clathrate hydrates of methane, carbon dioxide, nitrogen, and hydrogen + water soluble organic promoters using support vector machine algorithm”. *Fluid Phase Equilib*, 316, 34–45

Eslamimanesh, A., Mohammadi, A. H., Richon, D., Naidoo, P., Ramjugernath, D., (2012), “Application of gas hydrate formation in separation processes: A review of experimental studies”. *J. Chem. Thermodyn*, 46, 62–71

Englezos, P., Kalogerakis, N., Dholabhai, P. D., Bishnoi, P. R., (1987), “Kinetics of formation of methane and ethane gas hydrates”. *Chem. Eng. Sci.* 42, 2647–2658

Englezos, P., Bishnoi, P. R., (1991), “Experimental study on the equilibrium ethane hydrate formation conditions in aqueous electrolyte solutions”. *Ind. Eng. Chem. Res*, 30, 1655–1659

- Englezos, P., (1992), "Computation of the incipient equilibrium carbon dioxide hydrate formation condition in aqueous solutions". *Ind. Eng. Chem. Res*, 31, 2232–2237
- Englezos, P., Ngan, Y. T., (1993), "Incipient equilibrium data for propane hydrate formation in aqueous solutions of NaCl, KCl, and CaCl₂", *J. Chem. Eng. Data*, 38, 250–253
- Englezos, P., (1993), "Reviews gas hydrates". *Ind. Eng. Chem. Res*, 32, 1251–1274
- Fakharian, S., Ganji, H., Naderifar, A., (2017), "Saline produced water treatment using gas hydrates". *J. Environ, Chem. Eng*, 5, 4269–4273
- Fan, S., Li, S., Wang, J., Lang, X., Wang, Y., (2009), "Efficient capture of CO₂ from simulated flue gas by formation of TBAB or TBAF semiclathrate hydrates". *Energy and Fuels*, 23, 4202–4208
- Folger, H. S., (2006). "Elements of chemical reaction engineering" Fourth Edition, Prentice Hall
- Folas, G. K., (2006), "Modelling of complex mixtures containing hydrogen bonding molecules". PhD Thesis, Center for Energy Resources Engineering, Department of Chemical Engineering, Technical University of Denmark, Denmark
- Fournaison, L., Delahaye, A., Chatti, I., (2004), "CO₂ hydrates on refrigeration processes". *Ind. Eng. Chem. Res*, 43, 6521–6526
- Fürst, W., Renon, H., (1993), "Representation of excess properties of electrolyte solutions using a new equation of state". *AIChE. J*, 39 (2), 335–343
- Garcia-Rodriguez, L., (2003), "Renewable energy applications in desalination: state of the art". *Solar Energy*, 75, 381–393
- Gmehling, J., Kolbe, B., Kleiber, M., Rarey, J., (2012), "Chemical thermodynamics for process simulation", Wiley-VCH Verlag GmbH & Co. KGaA

Gou, Y., Fan, S., Gou, K., Chen, Y., (2002), "Storage capacity of methane in hydrate using calcium hypochlorite as additive. In Proceedings of the 4th International Conference on Natural Gas Hydrate". *Yokohama, Japan*, 1040-3

Gou, Y. K., Fan, S. S, Gou, K. H., Chen, Y., (2000), "Storage capacity of methane in hydrate using calcium hypochlorite as additive. In Proceedings of the 4th International Conference on Natural Gas Hydrate". *Yokohama, Japan*, P-1040

Gudmundsson, J. S., Parlaktuna, M., Levik, O. I., Andersson, V., (2000), "Laboratory for continuous production of natural gas hydrates". *Ann. N.Y. Acad. Sci*, 912, 851–858

Guo, T-M., Qiu, J-H., (1998), "Kinetics of methane hydrate formation in pure water and inhibitor containing systems". High Pressure Fluid Phase Behavior and Property Research Laboratory, 490–497

Gupta, K., (1968), "Solubility of calcium sulphate dihydrate in hydrochloric acid solutions". *J. App. Chem*, 18 (12), 49–51

Gutierrez, E., (2010), "Design and analysis of a centrifugal compressor for a simple cycle gas turbine engine" ANYS South American conference and ESSS users meeting

Haghighi, H., Chapoy, A., Tohidi, B., (2008), "Freezing point depression of electrolyte solutions: Experimental measurements and modeling using the Cubic-Plus-Association Equation of state". *Ind. Eng. Chem. Res*, 47, 3983–3989

Haghighi, H., Chapoy, A., Tohidi, B., (2009), "Methane and water phase equilibria in the presence of single and mixed electrolyte solutions using the Cubic-Plus-Association Equation of state". *Oil and Gas Sci. Techn*, 64 (2), 141–154

Han, S., Shin, J-Y., Rhee, Y-W., Kang, S-P., (2014), "Enhanced efficiency of salt removal from brine for cyclopentan hydrates by washing, centrifuging, and sweating". *Desalination*, 354, 17–22

Han, S., Rhee, Y-W., Kang, S-P., (2014), “Investigation of salt removal using cyclopentan hydrate formation and washing treatment for seawater desalination”. *Desalination*, 404, 132–137

Hao, W., Wang, J., Fan, S., Hao, W., (2008), “Evaluation and analysis method for natural gas hydrate storage and transportation processes”. *Energy Convers. Manage*, 49, 2546–2553

Hartono, A., Kim, I., (2004), “Calculation of vapour-liquid equilibria for methanol-water using Cubic-Plus-Association equation of state: Project work in the subject KP8108”, Advanced Thermodynamics, NTNU

Hashemi, H., (2015), “Application of gas hydrates in cold storage technology: experiment study and thermodynamic modelling”. PhD Thesis, Chemical Engineering Department, University of KwaZulu-Natal, South Africa, Durban

Hashimoto, S., Miyauchi, H., Inoue, Y., Ohgaki, K., (2010), “Thermodynamic and raman spectroscopic studies on difluoromethane (HFC-32) + water binary system”. *J. Chem. Eng. Data*, 55, 2764–2768

He, T., Nair, S. K., Bavu, P., Linga, P., Karimi, I., (2018), “A novel conceptual design of hydrate base desalination (HyDesal) process by utilizing LNG cold energy”, *App. Energy*, 222, 13–24

Herslund, P. J., (2013), “Thermodynamic and process modelling of gas hydrate systems in CO₂ capture processes”. Phd Thesis, Technical University of Denmark, Denmark

Herzog, S., Gross, J., Arlt, W., (2010), “Equation of state for aqueous electrolyte systems based on the semirestricted non-primitive mean spherical approximation”. *Fluid Phase Equilib*, 297(1), 23–33

Hong, H., Pooladi-Darvish, M., Bishnoi, P. R., (2003), “Analytical modelling of gas production from hydrates in porous media”. *J. Can. Petrol. Technol*, 42, 45–56

Horiguchi, K., Watanabe, S., Moriya, H., Nakai, S., Yoshimitsu, A., Taoda, A., (2011), “Completion of natural gas hydrate (NGH) overland transportation demonstration project”. In *Proceedings of the 5th International Conference on Gas Hydrate*, Edinburgh, Scotland, UK, July 17–21

Hsieh, M-K., Yen, Y-T., Chen, Y-P., Chen, P-C., Lin, S-T., Chen, L-J., (2012), “Predictive method for the change in equilibrium conditions of gas hydrates with addition of inhibitors and electrolytes”, *Ind. Eng. Chem. Res.*, 51, 2456–2469

Huang, C. P., Fennema, O., Poweri, W. D., (1966), “Gas hydrates in aqueous-organic systems: II. Concentration by gas hydrate formation”. *Cryobiology*, 2, 240–245

Huang, S. H., Radosz, M., (1990), “Equation of state for small, large, polydisperse and associating molecules”. *Ind. Eng. Chem. Res.*, 29, 2284–2294

Ida, H., Kolda, K., (2004), “Highly efficient natural gas hydrate production technology”. *JFE Gihō*, 6, 76–80

Ilani-Kashkouli, P., Babaei, S., Gharagheizi, F., Hashemi, H., Mohammadi, A. H., Ramjugernath, D., (2013), “An assessment test for phase equilibrium data of water soluble and insoluble clathrate hydrate formers”. *Fluid Phase Equilib.*, 360, 68–76

Illbeigi, M., Fazlali, A., Mohammadi, A. H., (2011), “Thermodynamic model for the prediction of equilibrium conditions of clathrate hydrates of methane + water-soluble or – insoluble hydrate former”, *Ind. Eng. Chem. Res.*, 50, 9437–9450

Isobe, F., Mori, Y. H., (1992), “Formation of hydrate or ice by direct-contact evaporation of CFC alternatives”. *Intern. J. Refrig.*, 15(3), 137–142

Iwasaki, T., Katoh, Y., Nagamori, S., Takahashi, S., Oya, N., (2005), “Continuous natural gas hydrate pellet production (NGHP) by process development unit (PDU)”. In *Proceedings of the 5th International Conference on Gas Hydrate*, Trondheim, Norway, June 16–25

- Javanmardi, J., Moshefeghian, M., Maddox, R. N., (1998), "A simple method for predicting gas hydrate forming conditions in aqueous mixed electrolyte solutions", *Energy and Fuels*, 12, 219–222
- Javanmardi, J., Moshefeghian, M., (2003), "Energy consumption and economic evaluation of water desalination by hydrate phenomenon". *Appl. Therm. Eng*, 23, 845–857
- Javanmardi, J., Moshefeghian, M., (2004), "Experimental measurement and modeling of R22 (CHClF₂) hydrates in mixtures of acetone + water". *J. Chem. Eng. Data*, 49, 886–889
- Javanmardi, J., Nasrifar, K., Najibi, S.H., Moshefeghian, M., (2005), "Economic evaluation of natural gas hydrate as an alternative for natural gas transportation". *Appl. Therm. Eng*, 25, 1708–1723
- Jin, G., Donohue, M. D., (1988a), "An equation of state for electrolyte solutions. 1. Aqueous systems containing strong electrolytes". *Ind. Eng. Chem. Res*, 27(6), 1073–1084
- Jin, G., Donohue, M. D., (1988b), "An equation of state for electrolyte solutions. 2. Single volatile weak electrolytes in water". *Ind. Eng. Chem. Res*, 27(9), 1737–1743
- Kalogirou, S. A., (2005), "Seawater desalination using renewable energy sources". *Progr. Energ. Comb. Sci*, 31, 242–281
- Kamata, Y., Oyama, H., Shimada, W., Ebinuma, T., Takeya, S., Uchida, T., Nagao, J., Narita, H., (2004), "Gas separation method using tetra-n-butyl ammonium bromide semi-clathrate hydrate". *Jap. J. App. Phys*, 43, 362–365
- Kang, S-P., Chun, M-K., Lee, H., (1998), "Phase equilibria of methane and carbon dioxide hydrates in the aqueous MgCl₂ solutions". *Fluid Phase Equilib*, 147, 229–238
- Kang, S-P., Lee, H., Lee, C.S., Sung, W.M., (2001), "Hydrate phase equilibria of guest mixtures containing CO₂, N₂ and tetrahydrofuran". *Fluid Phase Equilib*, 85, 101–109

- Karaaslan, U., Uluneye, E., Parlaktuma, M., (2002), "Effect of an anionic surfactant on different type of hydrate structure". *J. Petro. Sci. Eng*, 35, 49–57
- Karamoddin, M., Varaminian, F., (2013), "Experimental measurement of phase equilibrium for gas hydrates of refrigerants and thermodynamic modeling by SRK, VPT and CPA EoSs". *J. Chem. Thermodyn*, 65, 213–219
- Karamoddin, M., Varaminian, F., (2013). "Water desalination using R141b gas hydrate formation". *Desalin and Water Treatment*, 1–7
- Karamoddin, M., Varaminian, F., (2016), "Water purification by freezing and gas hydrate processes and removal of dissolved minerals (Na^+ , K^+ , Mg^{2+} , Ca^{2+})". *J. Mol. Liq*, 223, 1021–1031
- Kargi, F., Dincer, A. R., (2000), "Use of halophilic bacteria in biological treatment of saline wastewater by fed-batch operation". *Water Environ. Res*, 72, 170–174
- Kashchiev, D., Firoozabadi, A., (2003), "Induction time in crystallization of gas hydrates". *J. Crystal Growth*, 250, 499–515
- Khawajia, A. D., Kutubkhanaha, I. K., Wie, J-M., (2008), "Advances in seawater desalination technologies". *Desalination*, 221, 47–69
- Khokhar, A. A., Gudmundsson, J. S., Sloan, E. D., (1998), "Gas storage in structure H hydrates". *Fluid Phase Equilib*, 150, 383–392
- Klauda, J. B., Sandler, S. I., (2003), "Phase behavior of gas hydrates: a model and multiple gas component hydrates". *Chem. Eng. Sci.* 58, 27–41
- Knox, W. G., Hess, M., Jones, G. E., Smith, H. B., (1961), "The hydrate process" *Chem. Eng. Prog*, 57(2), 66–77

Komastu, H., Yoshioka, H., Ota, M., Sato, Y., Watanabe, M., Smith, R. L., Peters, C. J., (2010), “Phase equilibrium measurements of hydrogen-tetrahydrofuran and hydrogen – cyclopentane binary clathrate hydrate systems”. *J. Chem Eng. Data*, 55, 2214–2218

Kontogeorgis, G. M., Voutas, E. C., Yakoumis, I. V., Tassios, D. P., (1996), “An equation of state for associating fluids”. *Ind. Eng. Chem. Res.* 35, 4310–4318

Kontogeorgis, G. M., Yakoumis, I. V., Meijer, H., Hendriks, E., Moorwood, T., (1999), “Multicomponent phase equilibrium calculations for water-methanol-alkane mixtures”. *Fluid Phase Equilib*, 158–160, 201–209

Kontogeorgis, G. M., Gani, R., (2004), “Computer aided property estimation for process and product design”. Amsterdam – Boston, Elsevier

Kontogeorgis, G. M., Michelsen, M. L., Folas, G. K., Derewi, S., von Solms, N., Stenby, E. H., (2006), “Ten years with the CPA (Cubic-Plus-Association) equation of state. Part 1. Pure compounds and self-associating systems”. *Ind. Eng. Chem. Res.* 45, 4869–4878

Kontogeorgis, G. M., Michelsen, M. L., Folas, G. K., Derewi, S., von Solms, N., Stenby, E. H., (2006), “Ten years with the CPA (Cubic-Plus-Association) equation of state. Part 2. Cross-associating and multicomponent systems”. *Ind. Eng. Chem. Res.* 45, 4869–4878

Kontogeorgis, G. M., Folas, G. K., (2010), “Thermodynamic models for industrial applications: From classical and advanced mixing rules to association theories”, WILEY, Ltd, Publication

Koren, A., Nadav, N., (1994), “Mechanical vapour compression to treat oil field produced water”. *Desalination*, 98, 41–48

Kubota, H., Shimizu, K., Tanaka, Y., Makita, T., (1984), “Thermodynamics properties of R13 (CClF₃), R23 (CHF₃), R152a (C₂H₄F₂) and propane hydrates for desalination of sea water”. *J. Chem. Eng. Jap.* 17, (4), 423–429

Lalla, D., Galt, K., (2011), “Impact of various cooling technologies on effluent production and achievement of zero liquid effluent discharge within Eskom”. 1–19

Lalla, D., Raman, D., Hofmann, J., (2014), “Eskom holdings SOC LTD Tutuka power station brine concentration plant, 1–9

Langmuir, I., (1916), “The constitution and fundamental properties of solids and liquids”. *J. Am. Chem. Soc.*, 38, (11), 2221–2295

Lederhos, J. P., Long, J. P., Sum, R. L., Christiansen, E. D., Sloan, E. D., (1996), “Effective kinetic inhibitors for natural gas hydrates”. *Chem. Eng. Sci.* 51(8), 1222–1229

Lee, J. D., (2011), “A new apparatus for seawater desalination by gas hydrate process and removal characteristics of dissolved minerals”. *Korea Institute of Industrial Technology (KITECH), 2nd Korea-Japan R&D Collaboration Day*

Lee, S., Lee, Y., Park, S., Seo, Y., (2010), “Phase equilibria of semiclathrate hydrate for nitrogen in the presence of tetra-n-butyl ammonium bromide and fluoride”. *J. Chem. Eng. Data*, 55, 5883–5886

Lei, Z., Chen, B., Ding, Z., (2005), “Special distillation process”. Elsevier

Lewis, A., Nathoo, J., Reddy, T., Randall, D., Zibi, L., Jivanji, R., (2010), “Novel technology for recovery of water and solid salts from hypersaline brines: Eutectic freeze crystallization”, *Water Research Commission*, 1–82

Lewis, G. N., Randall, M., (1921), “The activity coefficient of strong electrolytes”, *J. Am. Chem. Soc.*, 43, 1112–1154

Li, J., Polka, H. M., Gmehling, J., (1994), “A g^E model for single and mixed solvent electrolyte systems: 1. Model and results for strong electrolytes”. *Fluid Phase Equilib*, 94, 89–114

- Li, M-Y., Wang, S-S., Jiang, B., (2001), “Generalized LIQAUC model for single and mixed solvent strong electrolyte systems”. *J. AIChE*, 57, 2535–2546
- Li, J., Topphoff, M., Fischer, K., Gmehling, J., (2001), “Prediction of gas solubilities in aqueous electrolytes systems using the predictive Soave–Redlich–Kwong model”. *Ind. Eng. Chem. Res.*, 40, 3703–3710
- Li, J., Gou, K., Liang, D., Wang, R., (2004), “Experiments on fast nucleation and growth of HCFC141b gas hydrate in static water columns”. *Intern. J. Refrig.* 27, 932–939
- Li, X.S., Xia, Z.M., Chen, Z.Y., Yan, K.F., Li, G., Wu, H.J., (2009), “Equilibrium hydrate formation conditions for the mixture of CO₂ + H₂ + tetrabutylammonium bromide”. *J. Chem. Eng. Data*, 55, 2180–2184
- Li, S., Fan, S., Wang, J., Lang, X., Wang, Y., (2010), “Semiclathrate hydrate phase equilibria for CO₂ in the presence of tetra-n-butyl ammonium halide (bromide, chloride or fluoride)”. *J. Chem. Eng. Data*, 55, 3212–3215
- Li, S., Fan, S., Wang, J., Lang, X., Wang, Y., (2010), “Clathrate hydrate capture of CO₂ from simulated flue gas with cyclopentane/water emulsion”. *Chinese J. Chem. Eng.*, 18, 202–206
- Liang, D., Guo, K., Wang, R., Fan, S., (2001), “Hydrate equilibrium data of 1,1,1,2-tetrafluoroethane (HFC-134a), 1,1,-dichloro-1-fluoroethane (HCFC-141b) and 1,1-difluoroethane (HFC-152a)”. *Fluid Phase Equilib*, 187-188, 61–70
- Lin, W., Chen, G. J., Sun, C. Y., Guo, X. Q., Wu, Z. K., Liang, M. Y., (2004), “ Effect of surfactant on the formation and dissociation kinetic behavior of methane hydrate”. *Chem. Eng. Sci.*, 59, 4449–4455
- Lin, Y., Kate, A., Mooijer, M., Delgado, J., Fosbol, P. L., Thomsen, K., (2010), “Comparison of activity coefficient models for electrolytes systems”. *AIChE J*, 56(5), 1334–1351

Linga, P., Adeyemo, A., Englezos, P., (2007), “Medium-pressure clathrate hydrate/membrane hybrid process for postcombustion capture of carbon of carbon dioxide”. *Environ. Sci. Tech*, 42, 315–320

Link, D. D., Ladner, E. P., Elsen, H. A., Taylor, C. E., (2003), “Formation and dissociation studies for optimizing the uptake of methane by methane hydrates”. *Fluid Phase Equilib*, 211, 1–10

Liu, Z., Wang, W., Li, Y., (2005), “An equation of state for electrolyte solutions by a combination of low-density expansion of non-primitive mean spherical approximation and statistical associating fluid theory”. *Fluid Phase Equilib*, 227(2), 147–156

Liu, Y., Harvey, A. H., Prausnitz, J. M., (1989), “Thermodynamics of concentrated electrolyte solutions”. *Chem. Eng. Comm*, 77(1), 43–66

Llano-Restrepo, M., Champan, W. G., (1994), “Monte Carlo simulation of the structural properties of concentrated aqueous alkali halide solutions at 25A⁰C using a simple civilized model”. *J. Chem. Phys*, 100, 8321–8329

Lu, H., Matsumoto, R., Tsuji, Y., Oda, H., (2001), “Anion plays a more important role than cation in affecting gas hydrate stability in electrolyte solution? – a recognition from experimental results”. *Fluid Phase Equilib*, 178, 225–232

Lungstrøm, C., Michelsen, M. L., Kontogeorgis, G. M., Pedersen, K. S., Sørensen, H., (2006), “Comparison of the SRK and CPA equations of state for physical properties of water and methanol”. *Fluid Phase Equilib*, 247, 149–157

Lv, Y-L., Wang, S-S., Sun, C-Y., Gong, J., Chen, G-J., (2017), “Desalination by forming hydrate from brine in cyclopentane dispersion system”. *Desalination*, 413, 217–222

Macedo, A. A., Skovborg, P., Rasmussen, P., (1990), “Calculation of phase equilibria for solutions of strong electrolytes in solvent-water mixtures”. *Chem. Eng. Sci*, 45 (4), 875–882

Mackay, E., Jordan, M., Feasey, N., Shah, D., Kumar, P., Ali, S., (2005), "Integrated risk analysis for scale management in deepwater developments". *Old Prod. Facil*, 20(2), 138–154

Madri, Y., Rich, A., Mangin, D., Abderafi, S., Bebon, C., Semlali, N., Klein, J-P., Bounahmidi, T., Bouhaouss, A., (2011), "Parametric study of the sweating step in the seawater desalination process by indirect freezing". *Desalination*, 269, 142–147

Maeda, K., Katsure, Y., Asakuma, Y., Fukui, K., (2008), "Concentration of NaCl in aqueous solution by chlorodifluoromethane (R22) gas hydrate". *Chem. Eng. Process.* 47, 2281–2286

Makogon, Y. F., (1981), "Hydrates of natural gas". Tulsa, Oklahoma, USA, Penwell Books

Makogon, T. Y., Sloan, E. D., (1994), "Phase Equilibrium for Methane Hydrate from 190 to 262 K". *J. Chem. Eng. Data*, 39, 351–353

Makino, T., Yamamoto, T., Nagata, K., Sakamoto, H., Hashimoto, S., Sugahara, T., Ohgaki, K., (2009), "Thermodynamic stabilities of tetra-n-butyl ammonium chloride + H₂, N₂, CH₄, CO₂, or C₂H₆ semi-clathrate hydrate systems". *J. Chem. Eng. Data*, 55, 839–841

Mali, G. A., Chapoy, A., Tohidi, B., (2018), "Investigation into the effect of cooling on the kinetics of hydrate formation". *J. Chem, Thermodyn*, 117, 91–96

Mandal, A., Laik, S., (2004), "Effect of the promoter on gas hydrate formation and dissociation". *Energy and Fuels*, 22, 2527–2532

Maribo-Mogensen, B., (2014), "Development of an electrolyte CPA equation of state for applications in the petroleum and chemical industries", PhD Thesis, Center for Energy Resources Engineering, Department of Chemical and Biochemical Engineering, Technical University of Denmark, Denmark

Masoudi, R., Tohidi, B., (2004), "On modeling gas hydrate inhibition by salts and organic inhibitors". *J. Petrol. Sci. Eng.* 74, 132–137

Mayoufi, N., Dalmazzone, D., Fürst, W., Delahaye, A., Fournaison, I., (2009), “CO₂ enclathration in hydrates of peralkyl-(ammonium/phosphonium) salts: stability conditions and dissociation enthalpies”. *J. Chem. Eng. Data*, 55, 1271–1275

McCormack, R. A., Andersen, R. K., (1995), “*Clathrate Desalination Plants Preliminary Research Study*”; Water Treatment Technology Program Report No.5; Thermal Energy Storage, Inc.: San Diego, CA

McCormack, A. J., Niblock, G. A., (1998), “*Build and operate a Clathrate Desalination Pilot Plant*”; Water Treatment Technology Program Report No. 31; Thermal Energy Storage, Inc.: San Diego, CA

Mehdi, S. M., Davood, R., Cyrus, G., Vahid, T., Ghazaleh, K., (2007), “Prediction of hydrate formation for the systems containing single and mixed electrolytes solutions”. *Iran, J. Chem. Chem. Eng*, 26(1), 35–45

Mendez, A., Gasco, G., (2005), “Optimization of water desalination using carbon based adsorbents”. *Desalination*, 183, 249–255

Menten, P. D., Parrish, W. R., Sloan, E. D., (1981), “Effect of inhibitors on hydrate formation”. *Ind. Eng. Chem. Process Des. Dev.*, 20, (2), 399–401

Michelsen, M. L., Hendriks, E. M., (2001), “Physical properties from association models”, *Fluid Phase Equilib*, 180, 165–174

Michelsen, M. L., Mollerup, J. M., (2007), “Thermodynamics models: Fundamentals and computational aspects” Second Edition, Tie-Line Publication

Miller, J. E., (2003), “Review of water resources and desalination technologies”. *SAND REPORT*. Unlimited Release.

Mohammadi, A., Manteghian, M., Haghtalab, A., Mohammadi, A. H., Rahmati-Abkenar, M., (2014), “Kinetic study of carbon dioxide hydrate formation in presence of silver nanoparticles and SDS”. *Chem. Eng. J*, 237, 387–395

Mohammadi, A. H., Eslamimanesh, A., Belandria, V., Richon, D., (2011), “Phase equilibria of semi-gas hydrates of CO₂, N₂, CH₄ or H₂ + tetra-n-butylammonium bromide aqueous solution”. *J. Chem. Eng. Data*, 56, 3855–3865

Mohammadi, A. H., Richon, D., (2011), “Phase equilibria of binary clathrate hydrates of nitrogen + cyclopentane/cyclohexane/methyl cyclohexane and ethane + cyclopentane /cyclohexane/methyl cyclohexane”, *Chem. Eng. Sci*, 66, 4936–4940

Mohammadi, A. H., Richon, D., (2010), “Phase equilibria of methane hydrates in the presence of methanol and/or ethylene glycol aqueous solution”. *Ind. Eng. Chem. Res*, 49, 925–928

Mohammadi, A. H., Richon, D., (2010), “Equilibrium data of methyl cyclohexane + hydrogen sulfide and methyl cyclohexane + methane clathrate hydrates”. *J. Chem. Eng. Data*, 55, 566–569

Mohammadi, A. H., Richon, D., (2010), “Clathrate hydrate dissociation conditions for the methane + cycloheptane/cyclooctane + water and carbon dioxide + cycloheptane /cyclooctane + water systems”. *Chem. Eng. Sci*, 65, 3356–3361

Mohammadi, A. H., Richon, D., (2010), “Clathrate hydrates of cyclohexane + hydrogen sulfide and cyclohexane + methane: Experimental measurements of dissociation conditions”. *J. Chem. Eng. Data*, 55, 1053–1055

Mohammadi, A. H., Belandria, V., Richon, D., (2009), “Can toluene or xylene form clathrate hydrates?”. *Ind. Eng. Chem. Res*, 48, 5916–5918

Mohammadi, A. H., Richon, D., (2009), “Phase equilibria of clathrate hydrates of cyclopentane + hydrogen sulfide and cyclopentane + methane”. *Ind. Eng. Chem. Res*, 48, 9045–9048

Mohammadi, A. H., Richon, D., (2009), "Phase equilibria of clathrate hydrates of methyl cyclopentane, methyl cyclohexane, cyclopentane or cyclohexane + carbon dioxide". *Chem. Eng. Sci.*, 64, 5319–5322

Mohammadi, A. H., Richon, D., (2009), "Equilibrium data of carbonyl sulfide and hydrogen sulfide gas hydrates". *J. Chem. Eng. Data*, 54, 2338–2340

Mohammadi, A. H., Richon, D., (2009), "Methane hydrate phase equilibrium in the presence of salt (NaCl, KCl, or CaCl₂) + ethylene glycol or salt (NaCl, KCl, or CaCl₂) + methanol aqueous solution: Experimental determination of dissociation condition". *J. Chem. Thermodyn.*, 41, 1374–1377

Mohammadi, A. H., Afzal, W., Richon, D., (2008), "Gas hydrate of methane, ethane, propane and carbon dioxide in the presence of single NaCl, KCl and CaCl₂ aqueous solutions: Experimental measurements and predictions of dissociation conditions". *J. Chem. Thermodyn.* 40, 1693–1697

Mohammadi, A. H., Chapoy, A., Tohidi, B., Richon, D., (2004), "A semi-empirical approach for estimating the water content of natural gases". *Ind. Eng. Chem. Res.*, 43, 7137–7147.

Mohs, A., Gmehling, J., (2013), "A revised LIQUAC and LIFAC model (LIQUAC*/LIFAC*) for the prediction of properties of electrolyte containing solutions". *Fluid Phase Equilib*, 337, 311–322

Mooijer van den Heuvel, M. M, Witteman, R., Peters, C. J., (2001), "Phase behavior of gas hydrates of carbon dioxide in the presence of tetrahydropyran, cyclobutanone, cyclohexane and methylcyclohexane". *Fluid Phase Equilib*, 182, 97–110

Mooijer van den Heuvel, M. M, Peters, C. J., de Swaan Arons, J., (2000), "Influence of water insoluble organic components on the gas hydrate equilibrium conditions of methane". *Fluid Phase Equilib*, 172, 73–91

Mori, Y. H., (2015), "On the scale-up of gas hydrate forming reactors: The case of gas dispersion type reactors". *Energies*, 8, 1317–1335

Mori, Y. H., (2003), “Recent advances in hydrate-based technologies for natural gas storage – A review”. *J. Chem. Ind. Eng*, 54, 1–17

Myerson, A. S., (2000), “Handbook of industrial crystallization” Edition, Wiley: Hoboken, NJ, USA

Myers, J. A., Sandler, S. I., Wood, R. H., (2002), “An equation of state for electrolyte solutions covering wide ranges of temperature, pressure and composition”. *Ind. Eng. Chem. Res*, 41(13), 3282–3297

Najibi, H., Chapoy, A., Haghghi, H., Tohidi, B., (2009), “Experimental determination and prediction of methane hydrate stability in alcohols and electrolyte solutions”. *Fluid Phase Equilib*, 275, 127–131

Nasrifar, K., Moshfeghian, M., Maddox, R. N., (1998), “Prediction of equilibrium conditions for gas hydrate formation in the mixtures of both electrolytes and alcohol”. *Fluid Phase Equilib*, 146, 1–13

Natarajan, V., Bishnoi, P. R., Kalogerakis, N., (1994), “Induction phenomena in gas hydrate nucleation”. *Chem. Eng. Sci*, 49, 2075–2087

Nauman, E. B., (2008), “Chemical reactor design, optimization and scale-up”. Second Edition, Wiley: Hoboken, NJ, USA

Ng, H-J., Robison, D. B., (1976), “The measurement and prediction of hydrate formation in liquid hydrocarbon-water systems”. *Ind. Eng. Chem. Fundam*, 15 (4), 293–298

Ngan, Y. T., Englezos, P., (1996), “Concentration of mechanical pulp mill effluents and NaCl solutions through propane hydrate formation”. *Ind. Eng. Chem. Res*, 35, 1894–1900

Ngema, P. T., Petticrew, C., Naidoo, P., Mohammadi, A. H., Ramjugernath, D., (2014), “Experimental measurements and thermodynamic modelling of the dissociation conditions of clathrate hydrates for (refrigerant + NaCl + water) systems.” *J. Chem. Eng. Data*, 59 (2), 466–475

Ngema, P. T., (2014), “The use of fluorinated refrigerants in the application of gas hydrates for desalination”, MSc Thesis, University of KwaZulu-Natal, Department of Chemical Engineering, Durban, South Africa

Nikbakht, F., Izadpanah, A. A., Varaminian, F., (2011), “Modelling of hydrate formation conditions for refrigerant R134a, R141b and R152a using CPA equation of state and obtaining the Kihara potential parameters for these refrigerants”. *Proceeding of the 7th International Conference on Gas Hydrate (ICGH 2011)*, Edinburgh, Scotland, United Kingdom

Ohgaki, K., Takano, K., Moritoki, M., (1994), “Exploitation of CH₄ hydrates under the Nankai Trough in combination with CO₂ storage”. *Kagaku Kogaku Ronbunshu*, 20, 121–123

Okutani, K., Kuwabara, Y., Mori, Y. H., (2008), “Surfactant effects on hydrate formation in an unstirred gas/liquid system: An experimental study using methane and sodium alkyl sulfates”. *Chem. Eng. Sci.* 63, 183–194

Oshima, M., Shimada, W., Hashimoto, S., Tani, A., Ohgaki, K., (2010), “Memory effect on semi-clathrate hydrate formation: a case study of tetragonal tetra-n-butyl ammonium bromide hydrate”. *Chem. Eng. Sci.* 65, 5442–5446

Østergaard, K. K., Tohodi, B., Danesh, A., Burgass, R. W., Todd, A. C., Bartex, T., (2000), “A novel approach for oil and gas separation by using gas hydrate technology”. *Ann. NY Acad. Sci.* 832–842

Østergaard, K. K., Masoudi, R., Tohodi, B., Danesh, A., Todd, A. C., (2005). “A general correlation for predicting the suppression of hydrate dissociation temperature in the presence of thermodynamic inhibitors”. *J. Petrol. Sci. Eng.* 48, 70–80

Papadimitriou, N. I., Tsimpanogiannis, I. N., Stubos, A. K., Martin, A., Rovetto, L. J., Florusse, L., Peters, C. J., (2011), “Experimental and computational investigation of the sII binary He – THF hydrate”, *J. Phys. Chem. B*, 115, 1411–1415

Paricaud, P., (2011), “Modelling the dissociation conditions of salts hydrates and gas semiclathrate hydrates: Application to lithium bromide, hydrogen iodide and tetra-n-butylammonium bromide + carbon dioxide systems”, *J. Phys. Chem. B*, 115, 288–299

Park, K., Hong, S. Y., Lee, J. W., Kang, K. C., Lee, Y. C., Ha, M-G., Lee, J. D., (2011), “A new apparatus for seawater desalination by gas hydrate process and removal characteristics of dissolved minerals”. *Desalination*, 274, 91–96

Parker, A., (1942), “Potable water from seawater”. *Nature*, 149, 184–186

Parrish, W. R., Prausnitz, J. M., (1972), "Dissociation pressures of gas hydrates formed by gas mixtures". *Ind. Eng. Chem.* 11(1), 26–35

Peng, D. Y., Robinson, D. B., (1979), “A new two constant equation of state”. *Ind. Eng. Chem. Fundam*, 15, 59–64

Peters, M. S., Timmerhaus, K. D., West, R. E., (2003), “Plant Design and Economics for Chemical Engineers”. Fifth Edition, McGraw-Hill

Petticrew, C., (2011), “An investigation into the use of fluorinated hydrating agents in the desalination of industrial wastewater”. MSc Thesis in Chemical Engineering, University of KwaZulu-Natal, South Africa

Pitzer, K. S., (1973), “Thermodynamic of electrolytes. I. Theoretical basis and general equations”. *J. Phys. Chem*, 77(2), 268–277

Pitzer, K. S., Simonson, J. M., (1986), “Thermodynamics of multicomponent, miscible, ionic systems: theory and equations”. *J. Phy. Chem*, 90(13), 3005–3009

Planche, H., Renon, H., (1981), “Mean spherical approximation applied to a simple but non-primitive model of interaction for electrolyte solutions and polar substances”. *J. Phys. Chem*, 85 (25), 3924–3929

- Polka, H. M., Li, J., Gmehling, J., (1994), “A g^E model for single and mixed solvent electrolyte systems: 2. Results and comparison with other models”. *Fluid Phase Equilib*, 94, 115–127
- Porteous, A., (1983), “Desalination Technology developments and practise”, Applied Science Publishers, London and New York
- Raatschen, W., Harvey, A. H., Prausnitz, J. M., (1987), “Equation of state for solutions of electrolytes in mixed solvent”. *Fluid Phase Equilib*, 38(1), 19–38
- Ramjugernath, D., (2000), “High pressure phase equilibrium studies”. PhD Thesis, Chemical Engineering, University of KwaZulu-Natal, Durban, South Africa
- Rautenbach, R., Seide, A., (1978), “Technical problems and economics of hydrate-processes”. *Proceeding 6th International Symposia Fresh Water from Sea*, 4, 43–51
- Ripmeester, J. A., Tse, J. S., Rateliffe, C. I., (1987), “A clathrate hydrate of carbon monoxide”. *Nature*, 328, 469–478
- Ripmeester, J. A., Rateliffe, C. I., McLaurin, G. E., (1991), “The role of heavier hydrocarbon in hydrate formation. AIChE Spring Meeting Session 44, *Hydrates in Gas Industry*
- Robinson, R. R. A., Stokes, R. R. H., (1970), “Electrolyte solution” Dover Publication
- Rodionova, T., Komarov, V., Villevald, G., Aladko, I., Karpova, T., Manakov, A., (2010), “Calorimetric, structural studies of tetrabutylammonium chloride ionic clathrate hydrates”. *J. Phys. Chem. B*, 114, 11838–11846
- Rogers, R., Zhang, G., Dearman, J., Woods, C., (2007), “Investigations into surfactant/gas hydrate relationship”. *J. Petrol. Sci. Eng*, 56, 82–88
- Roosta, H., Khosharay, S., Varaminian, F., (2013), “Experimental study of methane hydrate formation kinetics with or without additives and modeling based on chemical affinity”. *Energy Conv. Man*, 76, 499–505

Sabil, K. B. M., (2009), “Phase behaviour thermodynamics and kinetics of gas hydrate systems of carbon dioxide in presence of tetrahydrofuran and electrolytes”. MSc Thesis, University Sains Malaysia, Malaysia

Sabil, K. M., Duarte, A. R. C., Zevenbergen, J., Ahmad, M. M., Yusup, S., Omar, A. A., Peters, C. J., (2010), “Kinetic of formation for single carbon dioxide and mixed carbon dioxide and tetrahydrofuran hydrates in water and sodium chloride aqueous solution”, *Inter. J. Green Gas Contr*, 4, 798–805

Sabil, K. M., Witkamp, G-J., Peters, C. J., (2010), “Phase equilibria in ternary (carbon dioxide + tetrahydrofuran + water) system in hydrate-forming region: Effects of carbon dioxide concentration and the occurrence of pseudo-retrograde hydrate phenomenon”, *J. Chem. Thermody*, 42, 8–16

Sahu, P., Krishnaswamy, S., Ponnani, K., Pande, N. K., (2018), “A thermodynamic approach to selection of suitable hydrate formers for seawater desalination”. *Desalination*, 436, 144–151

Sarshar, M., Sharafi, A. H., (2010), “Simultaneous water desalination and CO₂ capturing by hydrate formation”. *1st International Conference on Water and Wastewater Treatment*, Isfahan, Iran, 21–22

Seo, Y., Lee, H., (2001), “A new hydrate-based recovery process for removing chlorinated hydrocarbons from aqueous solutions”. *Environ. Sci. Technol*, 35, 3386–3390

Sharifi, H., Ripmeester, J., Walker, V. K., Englezos, P., (2014), “Kinetic inhibition of natural gas hydrates in saline solutions and heptane”. *Fuel*, 117, 109–117

Shin, K., Kim, Y., Strobel, T.A., Prasad, P.S.R., Sugahara, T., Lee, H., Sloan, E.D., Sum, A.K., Koh, C.A., (2009), “Tetra-n-butylammonium borohydride semiclathrate: a hybrid material for hydrogen storage”. *J. Phys. Chem. A*, 113, 6415–6418

Shouzhi, Y. I., Yuanyuan, J. I. A., Peisheng, M. A., (2005), "Estimation of acentric factor of organic compounds with corresponding states group contribution method", *Chin. J. Chem. Eng.* 13(5), 709–712

Sinnott, R. K., (2005), "Coulson and Richardson's Chemical Engineering Volume 6: Chemical Engineering Design". 4th Edition, Butterworth-Heinemann, Oxford

Sloan, E. D., Koh, C. A., (2008), "Gas hydrates of natural gases" Third Edition, CRC Press, Taylor & Francis Group, London, New York

Skovborg, P., Ng, H., Rasmussen, P., (1993), "Measurement of induction times for the formation of methane and ethane gas hydrates". *Chem. Eng. Sci.* 48, 445–453

Smythe, G., Matelli, G., Bradford, M., Rocha, C., (2006), "Biological treatment of salty wastewater". *Environ. Prog. Sust. Energy*, 16 (3), 179–183

Soave, G., (1972), "Equilibrium constant from a modified Redlich-Kwong equation of state". *Chem. Eng. Sci.* 27(6), 1197–1203

Solen, K. A., Harb, J. N., (2005), *Chemical process: Fundamental and design*, 4th Edition, McGraw Hill, Boston

Solms, N. V., Michelsen, M. L., Passos, C. P., Derawi, S. O., Kontogeorgis, G. M., (2006), "Investigating models for associating fluids using spectroscopy". *Ind. Eng. Chem. Res.* 45, 5368–5374

Song, Y., Chen, C. C., (2009), "Symmetric electrolyte nonrandom two-liquid activity coefficient model". *Ind. Eng. Chem. Res.* 48(16), 7788–7797

Spiegler, K. S., (1966), *Principles of Desalination*, Academic press, New York and London

Strobel, T. A., Koh, C. A., Sloan, E. D., (2000), "Hydrogen storage properties of clathrate hydrate materials", *Fluid Phase Equilib.* 261, 382–389

Strobel, T. A., Koh, C. A., Sloan, E. D., (2009), “Thermodynamic predictions of various tetrahydrofuran and hydrogen clathrate hydrates”, *Fluid Phase Equilib*, 280, 61–67

Strobel, T. A., Hester, K.C., Koh, C. A., Sum, A.K., Sloan, E. D., (2009), “Properties of the clathrates of hydrogen and developments in their applicability for hydrogen storage”. *Chem. Phys Letters*, 478, 97–108

Sugahara, T., Haag, J.C., Warntjes, A.A., Prasad, P.S.R., Sloan, E.D., Koh, C.A., Sum, A.K., (2010), “Large-cage occupancies of hydrogen in binary clathrate hydrates dependent on pressure and guest concentrations”. *J. Phys. Chem C*, 114, 15218–15222

Sugi, J., Saito, S., (1967), “Concentration and demineralization of sea water by hydrate process,” *Desalination*, 3, 27–31

Sum, A.K., Koh, C.A., Sloan, E.D., (2009), “Clathrate hydrates: from laboratory science to engineering practice”. *Ind. Eng. Chem. Res*, 48, 7457–7465

Sun, C., Li, W., Yang, X., Li, F., Yuan, Q., Mu, I., Chen, J., Liu, B., Chen, G., (2011), “Progress in research of gas hydrate”. *Chin. J. Chem. Eng*, 19, 151–162

Sun, Z.G., Sun, L., (2010), “Equilibrium conditions of semi-clathrate hydrate dissociation for methane + tetra-n-butyl ammonium bromide”. *J. Chem. Eng. Data*, 55, 3538–3541

Sun, Z., Wang, R., Ma, R., Guo, K., Fan, S., (2003), “Natural gas storage in hydrates with the presence of promoters”. *Energy Convers. Manage*, 44, 2733–2740

Sun, Z-G., Fan, S-S., Guo, K-H., Shi, L., Cuo, Y-K., Wang, R. Z., (2002), “Gas hydrate phase equilibrium data of cyclopentane and cyclohexane”. *J. Chem. Eng. Data*, 47, 313–315

Tarleton, E. S., Wakeman, R. J., (2007), “Solid/liquid separation: Equipment selection and process design”. Elsevier

Thomsen, K., Rasmussen, P., Gani, R., (1996), “Correlation and prediction of thermal properties and phase behaviour for a class of aqueous electrolyte systems”. *Chem. Eng. Sci.*, 51(14), 3675–3683

Thomsen, K., Rasmussen, P., (1999), “Modelling of vapour-liquid-solid equilibrium in gas-aqueous electrolyte systems”. *Chem. Eng. Sci.*, 54(12), 1787–1802

Thomsen, K., (2009), “Electrolyte solutions: Thermodynamics, crystallization, separation methods”. Technical University of Denmark, Department of Chemical Engineering, Denmark

Tohidi, B., Danesh, A., Todd, A. C., (1995), “Modelling single and mixed electrolyte solutions and its applications to gas hydrates”. *Instit. of Chem. Eng.*, 71, 464–471

Tohidi, B., Burgrass, R. W., Danesh, A., Østergaard, K. K., Todd, A. C., (2000), “Improving the accuracy of gas hydrate dissociation point measurement”. *Ann. N. Y. Acad. Sci.*, 912, 924–931

Tohidi, B., Danesh, A., Todd, A. C., Burgrass, R. W., (1997), “Hydrate-free zone for synthetic and real reservoir fluids in the presence of saline water”. *Chem Eng. Sci.* 52 (19), 3257–3263

Tohidi, B., Danesh, A., Todd, A. C., Burgrass, R. W., Østergaard, K. K., (1997), “Equilibrium data and thermodynamic modeling of cyclopentane and neopentane hydrates”. *Fluid Phase Equilib*, 138, 241–250

Tohidi-Kalorazi, B., (1995), “Gas hydrate equilibria in the presence of electrolyte solutions”. PhD Thesis, Department of Petroleum Engineering, Heriot-watt University, Edinburgh, UK.

Trueba, A. T., Rovetto, L. J., Florusse, L. J., Kroon, M. C., Peters, C. J., (2011), “Phase equilibrium measurements of structure II clathrate hydrates of hydrogen with various promoters”. *Fluid Phase Equilib*, 307, 6–10

Turton, R., Bailie, R. C., Whiting, W. B., Shaeiwitz, J. A., Bhattacharyya, D., (2012), *Analysis, synthesis, and design of chemical process*, Fourth Edition, Prentice Hall

Valderrama, J. O., 1990, "A generalized Patel-Teja equation of state for polar and nonpolar fluids and their mixtures". *J. Chem. Eng. Jap*, 23, 87–91

Voutsas, E. C., Yakoumis, I. V., Tassios, D. P., (1999), "Prediction of phase equilibria in water/alcohol/alkane systems". *Fluid Phase Equilib*. 158-160, 151–159

Voutsas, E. C., Boulougouris, G. C., Economou, I. G., Tassios, D. P., (2000), "Water/hydrocarbon phase equilibria using the thermodynamic perturbation theory". *Ind. Eng. Chem. Res*, 39, 797–808

Vysniauskas, A., Bishnoi, P. R., (1983), "A kinetic study of methane hydrate formation". *Chem. Eng. Sci*, 38, 1061–1072

Wade, N. M., (2001), "Distillation plant development and cost update". *Desalination*, 136, 3–12

Wagner, L., (2007), "Water desalination – Tap into the liquid gold". *Mora Ass. Ltd*, 1–8

Wakeman, R. J., Tarleton, E. S., (2005), "Solid/liquid separation: Scale-up of industrial equipment". Elsevier Advanced Technology

Wakeman, R. J., Tarleton, E. S., (1999), "Filtration: Equipment selection modelling and process simulation". First Edition, Elsevier Advanced Technology

Walas, S. M., (1985), "Phase equilibria in chemical engineering" Butterworth Publishers, Boston, London

Walas, S. M., (1990), "Chemical Process equipment: Selection and design". Butterworth-Heinemann

Wang, P., Anderko, A., Young, R. D., (2002), "A speciation-based model for mixed-solvent electrolytes systems". *Fluid Phase Equilib*, 203(1), 141–176

- Wang, P., Springer, R. D., Anderko, A., Young, R. D., (2004), "Modelling phase equilibria and speciation in mixed-solvent electrolytes systems". *Fluid Phase Equilib*, 222, 11–17
- Wang, P., Anderko, A., Springer, R. D., Young, R. D., (2006), "Modelling phase equilibria and speciation in mixed-solvent electrolytes systems: II. Liquid-liquid equilibria and properties of associating electrolyte solutions". *J. Mol. Liq*, 125(1), 37–44
- Wang, P., Kosinski, J. J., Lencka, M. M., Anderko, A., Springer, R. D., (2013), "Thermodynamic modelling of boric acid and selected metal borate systems". *Pure App. Chem*, 85(11), 2117–2144
- Wichterle, K., (1994), "Heat transfer in agitated vessels". *Chem. Eng. Sci*, 49 (9), 1480–1483
- Williams, P. M., Ahmad, M., Connolly, B. S., (2013), "Freeze desalination: An assessment of an ice maker machine for desalting brines". *Desalination*, 308, 219–224
- Woolard, C. R., Irvine, R. L., (1994), "Biological treatment of hypersaline wastewater by a biofilm of halophilic bacteria". *Water Environ. Res*, 66, 230–235
- Woolard, C. R., Irvine, R. L., (1995), "Treatment of hypersaline wastewater in the sequencing batch reactor". *Water Res*, 29, 1159–1167
- Yang, S. O., Yang, I. M., Lee, C. S., (2000), "Measurement and prediction of phase equilibria for water + CO₂ in hydrate forming conditions". *Fluid Phase Equilib*, 175, 75–89.
- Yang, S. O., Cho, S. H., Lee, H., Lee, C. S., (2001), "Measurement and prediction of phase equilibria for water + methane in hydrate forming conditions". *Fluid Phase Equilib*, 185, 53–83
- Yin, Z., Khurama, M., Tan, H. K., Linga, P., (2018), "A review of gas hydrate growth kinetic models". *Chem. Eng. J*, 342, 9–29

Yoslim, J., Linga, P., Engelos, P., (2010), “Enhanced growth of methane-propane clathrate hydrate crystals with sodium dodecyl sulfate, sodium tetradecyl sulfate, and sodium hexadecyl sulfate surfactants”. *J. Cryst. Growth*, 313, 68–80

Younos, T., (2005), “The economics of desalination”. *J. Contemp. Water Res. Edu*, Issued 132, 39–45

Younos, T., Tulou, K. E., (2005), “Overview of desalination techniques”. *J. Contemp. Water Res. Edu*, Issued 132, 3–10

Zahed, A. H., Bayomi, N. N., (2014), “Design procedure of centrifugal compressors”. *ISESCO J. Sci. Technol*, 10 (17), 77–91

Zemaitis, J. F., Clark, D. M., Rafal, M., Scriven, N. C., (1986), “Handbook of aqueous electrolytes thermodynamics”. DIPR/AIChE, New-York

Zhang, J., Lee, S., Lee, J. W., (2007), “Kinetics of methane hydrate formation from SDS solution”. *Ind. Eng. Chem. Res*, 46, 6353–6359

Zhang, J., Yedlapadi, P., Lee, J. W., (2009), “Thermodynamic analysis of hydrate-based pre-combustion capture of CO₂”. *Chem. Eng. Sci*, 64, 4732–4736

Zhao, W-L., Zhong, D-L., Yang, C., (2016), “Prediction of phase equilibrium conditions for gas hydrates formed in the presence of cyclopentane or cyclohexane”. *Fluid Phase Equilibria*, 427, 82–89

Zheng, J-N., Yang, M-J., Lui, Y., Wang, D-Y., Song, Y-C., (2017), “Effects of cyclopentane on CO₂ hydrate formation and dissociation as a co-guest for desalination”. *J. Chem. Thermodyn*, 104, 9–15

Zhong, Y., Rogers, R. E., (2000), “Surfactant effects on gas hydrate formation”. *Chem. Eng. Sci*, 55, 4175–4187

APPENDIX A: CALIBRATION AND UNCERTAINTIES

A.1 Calibrations

Temperature calibrations

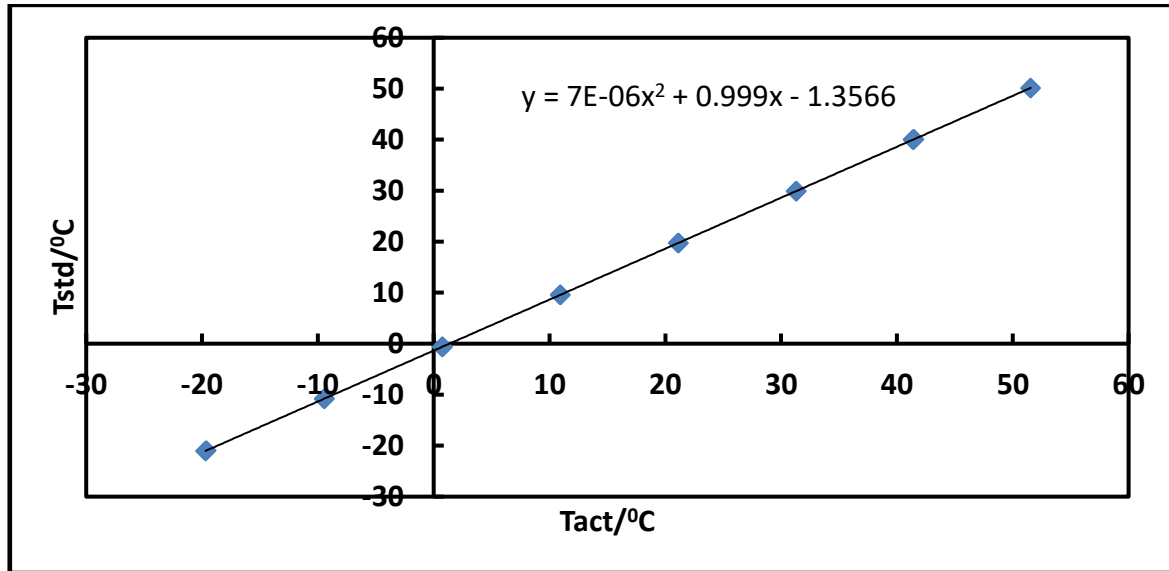


Figure A1. 1: Calibration temperature curve for T_{std} against T_{exp} for the isochoric pressure cell: T_{exp} is the experimental temperature and T_{std} is the standard probe from WIKA

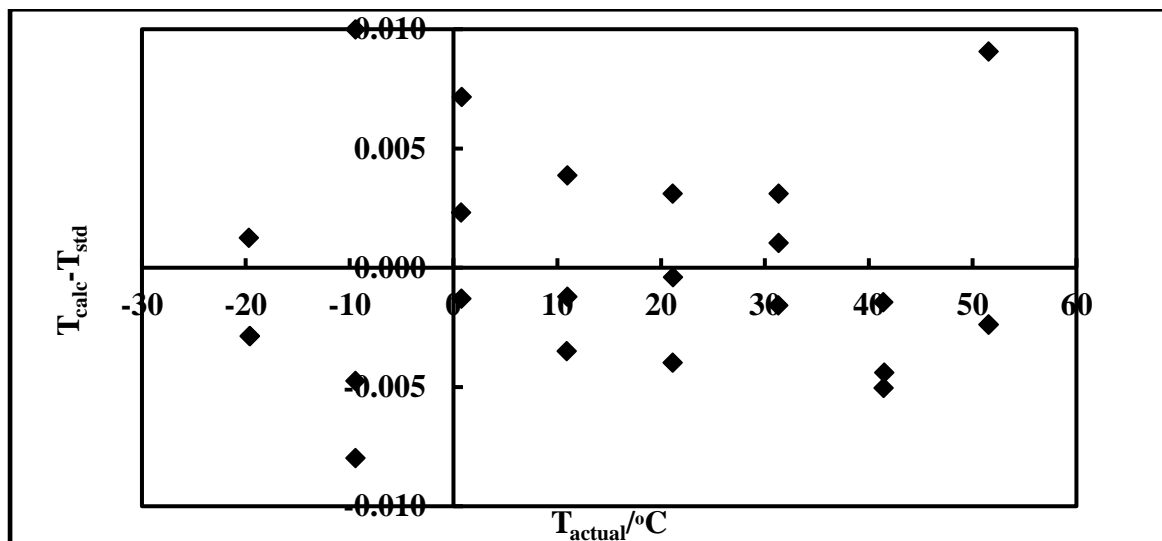


Figure A1. 2: Deviation for temperature sensor (Pt-100) for isochoric pressure cell: T_{act} is the calculated temperature using equation obtained in Figure A1.1

Pressure calibrations

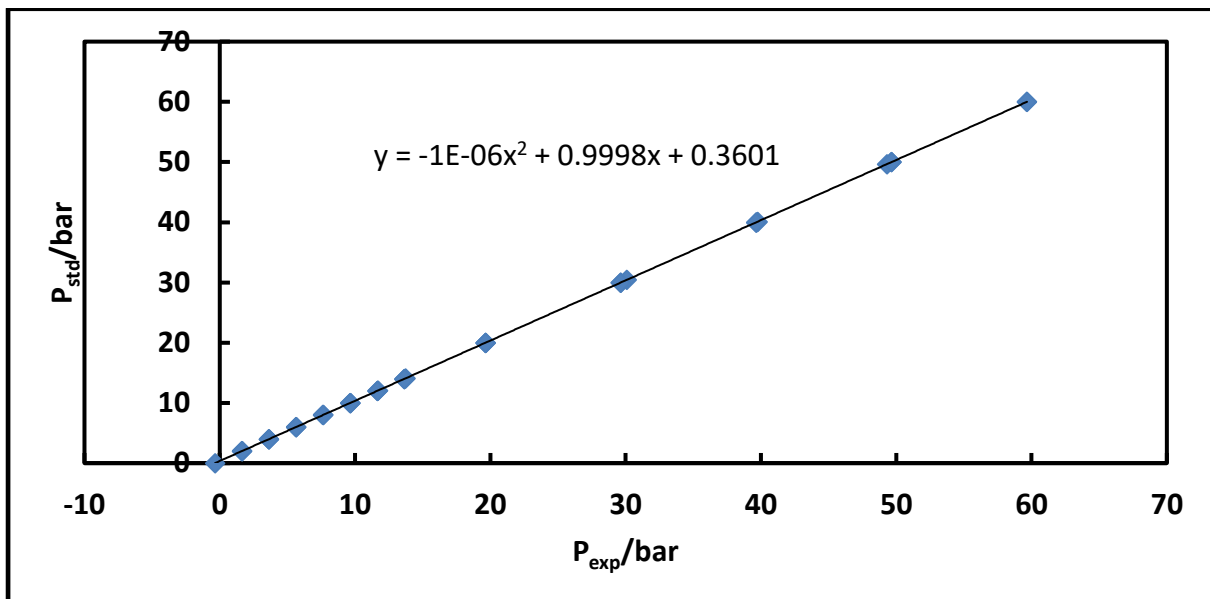


Figure A1. 3: Calibration for pressure transmitter curve range (0–60 bar) for P_{std} against P_{exp} for the isochoric pressure cell: P_{exp} is the experimental temperature and P_{std} is the standard transmitter from WIKA

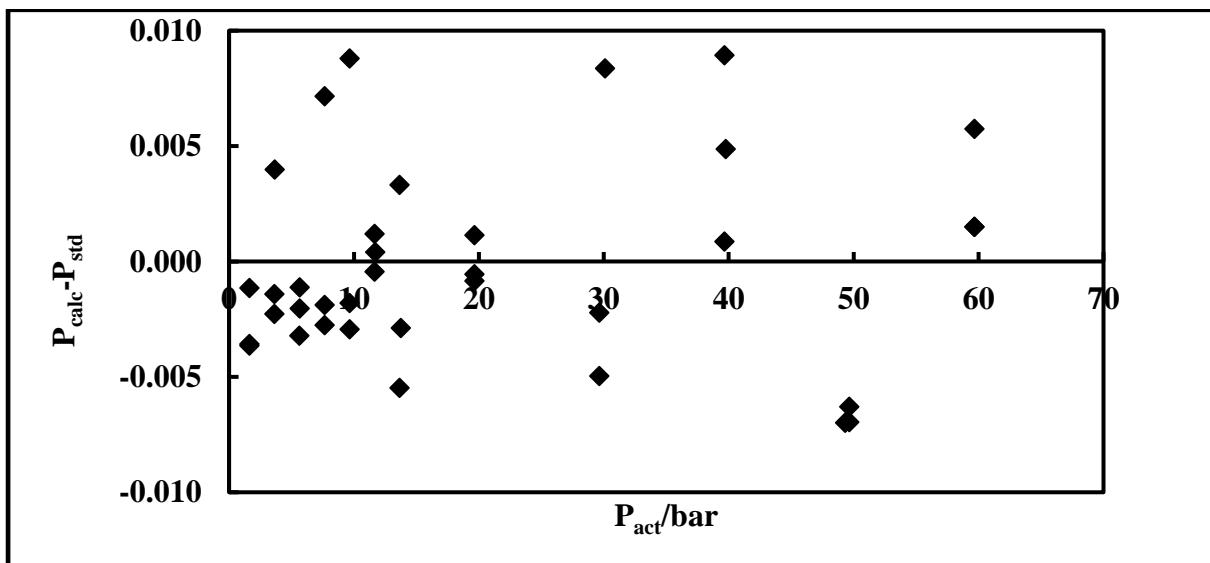


Figure A1. 4: Deviation for pressure transmitter sensor for isochoric pressure cell: P_{act} is the calculated pressure using equation obtained in Figure A1.3

A.2 NIST uncertainty determinations

Estimation of uncertainty for temperature and pressure

It is of utmost important to report the uncertainties of temperature and pressure before the presentation of original results of experimental data. This calculates an interval within the true value of measurement, which had a high possibility of residing. The error was not the same as uncertainty, the error was the upper and lower limits of difference in calculated values and experimental values. It was used to calculate the uncertainty. Taylor and Kuyatt, (1994) reported only uncertainty, according to NIST measurement results and the error was not reported. Accurate and reliable experimental data are subjected into the lowest uncertainties, for either temperature or pressure which cannot be ignored in the calculations.

The objective function represent for θ an interval if uncertainty that was a combination of all possible sources of uncertainties. This was referred as the combined standard uncertainty $u_c(\theta)$

$$u_c(\theta) = \pm \sqrt{\sum_i u_i(\theta)^2} \quad (\text{A2.1})$$

where $u_i(\theta)$ is representing any source of uncertainty such as errors of T and P from calibration curves or standard deviation from averaging repeated recording values. Uncertainties in temperature and pressure come from calibration curves and repeatability of readings for Pt-100 probe and single pressure transducer. The use of $u_i(\theta)$ was expressed in terms of temperature but it can be interchanged with pressure. The combined standard uncertainty for temperature was expressed as

$$u_c(T) = \pm \sqrt{u_{calib}(T)^2 + u_{rep}(T)^2} \quad (\text{A2.2})$$

where subscripts *calib* and *rep* represent the calibration and repeatability, respectively. The error from the temperature calibration curves or polynomial equation was shown in Figure 6.3 with a value of ± 0.09 K. One assumed that the temperature is equally to fall anywhere between the upper and lower limits of calibration such that a uniform or rectangular distribution was

followed. In this study, uncertainties based on this prescribed distribution was referred as a type B calculation (random uncertainty), and it was expressed for a rectangular distribution as

$$u_{calib}(T) = \frac{b}{\sqrt{3}} \quad (A2.3)$$

where b is the half-width between the upper and lower limits, i.e. $b = \pm 0.07$ K in this study. Therefore, b is called an *error* in temperature. The Gaussian distribution (type A which is systematic uncertainty) was not use in this study, only for calibrations range of temperature and pressure has to be taken in consideration. However, consider during an experiment regardless the temperature remains repeated constant at the time of recording the final value or sampling. The average of repeated of final reading results in a mean \bar{T} with a standard deviation, σ . This can be used to calculate an uncertainty due to repeatability of the measurements. It was expressed as

$$u_{rep}(T) = \frac{\sigma}{\sqrt{n}} \quad (A2.4)$$

Reporting of uncertainties

A coverage factor k was taken into account for the final calculation of the combined standard uncertainties. This was known as *expanding uncertainty* $U(\theta) = k u_c(\theta)$. The coverage factor plays an important role to compensate confidence level by expanding the uncertainty interval, for $k > 1$

$$\theta_{final} = \theta_{measured} \pm k u_c(\theta) \quad (A2.5)$$

A value of $k = 2$ gives an approximate 95% confidence level on the uncertainty level for the distribution errors of a Gaussain (type A) distribution. In this study, $u_c(\theta)$ represent systematic distribution (type A) and rectangular distribution (type B). According to Taylor and Kuyatt, (1994) the level of 98% confidence for a rectangular distribution was given by a value of $k = 1.65$. In this study, a value of $k = 2$ was used for standard practice. Therefore, a rectangular distribution gives at least a 98% confidence level in overall.

APPENDIX B: PARAMETERS

Table B1. 1: Constant parameters (Gmehling et al., 2012)

Symbols	Description	Value	Units
a	Ion size parameter	$3.5 - 6.2 \times 10^{-10}$	m
e	Electronic charge	1.60206×10^{-19}	C
k	Boltzmanns constant	1.381×10^{-23}	J.K ⁻¹
N _A	Avogadro's number	6.023×10^{23}	
R	Universal gas constant	8.314	J.mol ⁻¹ K ⁻¹
r	Ionic radius	3×10^{-10}	m
ε ₀	Permittivity in vacuum	8.08542×10^{-12}	C ² J ⁻¹ m ⁻¹

Table B1. 2: Relative dielectric constant of selected solvents at T = 298.15 K (Gmehling et al., 2012)

Solvent	ε _r
Water	78.54
Nitromethane	38.00
Nitrobenzene	34.82
Methanol	32.63
Ethanol	24.35
1-Propanol	20.33
2-Propanol	19.40
1-Butanol	17.43
2-Butanol	16.70
Acetone	20.56
Acetic acid	6.25
Diethyl ether	4.33
Benzene	2.27
Cyclohexane	2.02

Table B1. 3: The charge of electrolytes (Gmehling et al., 2012)

Charge	Value of Z
Na ⁺	+1
Cl ⁻	-1
Ca ²⁺	+2
SO ₄ ²⁻	-2
Mg ²⁺	+2
CO ₃ ⁻	-1
K ⁺	+1

Table B1. 4: Selected interaction parameters for the MR term (Li et al., 1994)

Component <i>i</i>	Component <i>j</i>	<i>a_{ij}</i> (K)	<i>a_{ji}</i> (K)	<i>b_{ij}</i>	<i>c_{ij}</i>
H ₂ O	Na ⁺	219.4	-299.4	-7.432	1.576
H ₂ O	Ca ²⁺	1137.0	-759.9	-19.84	3.149
H ₂ O	Cl ⁻	22.93	159.1	7.387	-1.576
H ₂ O	SO ₄ ²⁻	-364.0	789.4	14.28	-3.151
H ₂ O	Mg ²⁺	663.3	-679.3	-	3.155
Na ⁺	Cl ⁻	89.17	-483.7	0.1925	0.1165
Na ⁺	SO ₄ ²⁻	269.3	-919.3	0.06311	0.3924
Ca ²⁺	Cl ⁻	339.0	-	0.4088	-0.2575
Mg ²⁺	Cl ⁻	-199.8	-644.6	0.3565	1.985

Table B1. 5: Impeller diameter (Bloch, 2006)

Frame	Diameter (in)	Frame	Diameter (mm)
22	13.65	22	347
26	16.26	26	413
31	19.25	31	489
37	22.575	37	581
44	27.25	44	692
53	32.60	53	826
62	38.50	62	978
74	45.60	74	1158
88	54.26	88	1378

Table B1. 6: M-Line and MB-Line frame data (Bloch, 2006)

Frame	Nominal flow Range (m ³ /h)	Nominal Max No. of casing stages	Max casing pressure (bar)	Nominal speed (r/min)	Nominal polytropic efficiency	Nominal H/N ² (per stage)	Maximum Q/N
29M	1275 – 18140	10	52	11500	0.78	2.25 x 10 ⁻⁴	1.403
38M	10200 – 37880	9	43	7725	0.79	4.55 x 10 ⁻⁴	4.84
46M	27200 – 57750	9	43	5300	0.80	5.54 x 10 ⁻⁴	9.17
60M	42500 – 98550	8	23	4700	0.81	11.55 x 10 ⁻⁴	20.97
70M	85000 – 142700	8	23	4200	0.81	17.01 x 10 ⁻⁴	33.98
88M	119000 – 229400	8	23	3160	0.81	27.3 x 10 ⁻⁴	72.6
103M	186900 – 272000	8	3	2800	0.82	34.8 x 10 ⁻⁴	97.0
110M	237900 – 323000	8	3	2600	0.82	40.2 x 10 ⁻⁴	124.0
10MB	150 – 2700	12	690	18900	0.77	8.0 x 10 ⁻⁴	0.14
15MB	340 – 4000	12	690	15300	0.77	10.8 x 10 ⁻⁴	0.26
20MB	550 – 6120	12	690	12400	0.77	18.6 x 10 ⁻⁴	0.49
25MB	650 – 9346	12	690	10000	0.78	28.5 x 10 ⁻⁴	0.94
32MB	3400 – 13600	10	690	8300	0.78	4.2 x 10 ⁻⁴	1.64
38MB	10200 – 37380	9	103	7725	0.79	4.56 x 10 ⁻⁴	4.84
46MB	27200 – 57750	9	83	6300	0.79	6.84 x 10 ⁻⁴	9.17
60MB	42500 – 98550	8	55	4700	0.80	11.55 x 10 ⁻⁴	20.97
70MB	8500 – 142700	8	55	4200	0.80	17.01 x 10 ⁻⁴	33.98

Table B1. 7: Nominal Ψ (Bloch, 2006)

MW	Ψ	MW	Ψ
6	0.45	44	0.50
18	0.46	71	0.51
29	0.48		

APPENDIX C: MEASURED AND CALCULATED HYDRATE DISSOCIATION DATA WITH THEIR AAD

Table C1. 1. Measured and calculated data for hydrate–liquid water–liquid promoter–vapour for the R410a (1) + water (2) + NaCl (3) + CP (4) system at various salt concentrations^a

R410a (1) + water (2) + CP (3)				^b R410a (1) + water (2) + 0.10 ^c				R410a (1) + water (2) + 0.10 ^b				R410a (1) + water (2) + 0.20 ^b			
				NaCl (3)				NaCl (3) + CP (4)				NaCl (3) + CP (4)			
T/K	P ^{exp}	P ^{cal}	AAD	T/K	P ^{exp}	P ^{cal}	AAD	T/K	P ^{exp}	P ^{cal}	AAD	T/K	P ^{exp}	P ^{cal}	AAD
294.4	1.3852	1.3726	0.0091	288.6	1.2706	1.2718	0.0010	290.5	1.1791	1.1648	0.0122	285.8	0.8790	0.8666	0.0141
293.7	1.1877	1.1784	0.0078	286.9	1.0315	1.0478	0.0158	289.6	1.0413	1.0354	0.0057	285.2	0.7922	0.7853	0.0087
292.6	0.997	0.9907	0.0063	285.5	0.8529	0.8593	0.0076	288.6	0.9015	0.9032	0.0018	284.1	0.6761	0.6762	0.0002
290.3	0.7424	0.7491	0.0090	283.9	0.7029	0.6964	0.0092	287.4	0.7673	0.7655	0.0023	283.1	0.5873	0.5810	0.0107
287.0	0.4699	0.4754	0.0116	282.1	0.5697	0.5596	0.0176	286.0	0.6339	0.6407	0.0107	281.5	0.4760	0.4692	0.0144
283.8	0.2719	0.2750	0.0115	280.7	0.4724	0.4686	0.0080	283.2	0.4448	0.4503	0.0123	280.1	0.3865	0.3828	0.0095
280.9	0.1588	0.1600	0.0076	278.4	0.3487	0.3439	0.0136	280.2	0.2869	0.2910	0.0142	278.4	0.2860	0.2819	0.0143
				276.1	0.2399	0.2385	0.0055								

^aU(T) (0.95 level of confidence) = 0.03 K, U(P) (0.95 level of confidence) = 0.0007 MPa, ^bNgema et al. (2014), ^cValues are in mass fraction for

water + salt, $AAD = \frac{|P_i^{cal} - P_i^{exp}|}{P_i^{exp}}$, P – presents the experimental and calculated pressure in MPa

Table C1. 2. Measured and calculated data for hydrate–liquid water–liquid promoter–vapour for the R410a (1) + water (2) + CaCl₂ (3) + CP (4) system at various salt concentrations^a

^b R410a (1) + water (2)				R410a (1) + water (2) + CP (3)				R410a (1) + water (2) + 0.10 ^c CaCl ₂ (3) + CP (4)				R410a (1) + water (2) + 0.15 ^c CaCl ₂ (3) + CP (4)			
T/K	P ^{exp}	P ^{cal}	AAD	T/K	P ^{exp}	P ^{cal}	AAD	T/K	P ^{exp}	P ^{cal}	AAD	T/K	P ^{exp}	P ^{cal}	AAD
293.0	1.4213	1.3986	0.0160	294.4	1.3852	1.3726	0.0091	293.7	1.0561	1.0448	0.0107	291.9	1.0561	1.0448	0.0107
291.3	1.1847	1.1746	0.0086	293.7	1.1877	1.1784	0.0078	292.7	0.8359	0.8447	0.0106	290.1	0.8359	0.8447	0.0106
290.3	1.0339	1.0260	0.0076	292.6	0.9970	0.9907	0.0063	292.0	0.7772	0.7816	0.0056	287.7	0.7772	0.7816	0.0056
289.0	0.8676	0.8653	0.0027	290.3	0.7424	0.7491	0.0090	290.2	0.5873	0.5923	0.0085	287.8	0.5873	0.5923	0.0085
287.8	0.7414	0.7451	0.0050	287.0	0.4699	0.4754	0.0116	290.2	0.5981	0.6022	0.0069	285.4	0.5981	0.6022	0.0069
286.0	0.5824	0.5900	0.0130	283.8	0.2719	0.2750	0.0115	287.9	0.3859	0.3902	0.0111	282.6	0.3859	0.3902	0.0111
284.6	0.4837	0.4902	0.0134	280.9	0.1588	0.1600	0.0076	285.3	0.2148	0.2174	0.0121		0.2148	0.2174	0.0121
283.1	0.3955	0.3929	0.0066												
280.3	0.2568	0.2604	0.0140												
277.5	0.1788	0.1806	0.0101												

^aU(T) (0.95 level of confidence) = 0.03 K, U(P) (0.95 level of confidence) = 0.0007 MPa, ^bNgema et al. (2014), ^cValues are in mass fraction for

water + salt, $AAD = \frac{|p_i^{cal} - p_i^{exp}|}{p_i^{exp}}$, P – presents the experimental and calculated pressure in MPa

Table C1. 3. Measured and calculated data for hydrate–liquid water–vapour for the R410a (1) + water (2) + Na₂SO₄ (3) system at various salt concentrations^a and literature systems for (R134a and R152b) (1) + water (2)

^b R410a (1) + water (2)				R410a (1) + water (2) + 0.100 ^c Na ₂ SO ₄ (3)				^d R134a (1) + water (2)				^d R152b (1) + water (2)			
T/K	P ^{exp}	P ^{cal}	AAD	T/K	P ^{exp}	P ^{cal}	AAD	T/K	P ^{exp}	P ^{cal}	AAD	T/K	P ^{exp}	P ^{cal}	AAD
293.0	1.4213	1.3986	0.0160	291.6	1.3733	1.3590	0.0104	288.6	1.2710	1.2478	0.0183	288.2	0.4440	0.4404	0.0081
291.3	1.1847	1.1746	0.0086	289.6	1.0671	1.0626	0.0042	286.9	1.0320	1.0244	0.0073	288.1	0.4400	0.4367	0.0074
290.3	1.0339	1.0260	0.0076	288.2	0.9016	0.9054	0.0042	285.5	0.8530	0.8555	0.0029	287.2	0.3980	0.3932	0.0121
289.0	0.8676	0.8653	0.0027	285.4	0.6274	0.6324	0.0080	283.9	0.7030	0.7103	0.0104	286.8	0.3740	0.3699	0.0110
287.8	0.7414	0.7451	0.0050	283.3	0.4639	0.4692	0.0115	282.1	0.5700	0.5740	0.0070	285.9	0.3310	0.3289	0.0062
286.0	0.5824	0.5900	0.0130	281.0	0.3167	0.3201	0.0107	280.7	0.4720	0.4755	0.0075	284.2	0.2740	0.2725	0.0054
284.6	0.4837	0.4902	0.0134	278.3	0.1997	0.2019	0.0110	278.4	0.3490	0.3531	0.0118	283.3	0.2430	0.2432	0.0010
283.1	0.3955	0.3929	0.0066					276.1	0.2400	0.2417	0.0071	279.3	0.1450	0.1462	0.0083
280.3	0.2568	0.2604	0.0140									273.9	0.0440	0.0451	0.0243
277.5	0.1788	0.1806	0.0101												

^aU(T) (0.95 level of confidence) = 0.03 K, U(P) (0.95 level of confidence) = 0.0007 MPa, ^bNgema et al. (2014), ^cValues are in mass fraction for

water + salt, ^dLi et al. (2001), $AAD = \frac{|P_i^{cal} - P_i^{exp}|}{P_i^{exp}}$, P – presents the experimental and calculated pressure in MPa

Table C1. 4. Measured and calculated data for hydrate–liquid water–liquid promoter–vapour for the R507 (1) + water (2) + mixed salts (3) + CP (4) system at industrial salt concentrations^a

^b R507 (1) + water (2)				R507 (1) + water (2) + CP (3)				R507 (1) + water (2) + 0.002 ^c CaCl ₂ (3) + 0.017 ^c NaCl (4)				R507 (1) + water (2) + 0.002 ^c CaCl ₂ (3) + 0.017 ^c NaCl (4) + CP (5)			
T/K	P ^{exp}	P ^{cal}	AAD	T/K	P ^{exp}	P ^{cal}	AAD	T/K	P ^{exp}	P ^{cal}	AAD	T/K	P ^{exp}	P ^{cal}	AAD
283.3	0.8733	0.8644	0.0102	284.6	0.8580	0.8494	0.0100	283.2	0.8311	0.8231	0.0097	284.1	0.7783	0.7699	0.0108
283	0.7401	0.73274	0.0099	284.2	0.7445	0.7365	0.0108	282.9	0.7591	0.7509	0.0109	284	0.7784	0.7702	0.0105
282.2	0.611	0.60736	0.0060	283.6	0.6041	0.6093	0.0086	282.4	0.6783	0.6711	0.0106	283.4	0.6675	0.6615	0.0091
281.3	0.5043	0.5064	0.0042	282.6	0.4744	0.4767	0.0049	282.3	0.6704	0.6636	0.0102	282.5	0.5370	0.5391	0.0038
280.7	0.4442	0.44827	0.0092	282.6	0.4823	0.4843	0.0041	281.5	0.5552	0.5555	0.0005	281.8	0.4479	0.4434	0.0102
280	0.3704	0.37425	0.0104	281.1	0.3459	0.3502	0.0123	281	0.5026	0.5053	0.0053	280.9	0.3649	0.3634	0.0041
279	0.2979	0.30107	0.0106	279.8	0.2489	0.2514	0.0101	280.1	0.4087	0.4115	0.0067	279.5	0.2483	0.2504	0.0084
278.1	0.2417	0.24435	0.0110					279.3	0.3506	0.3534	0.0080				
277.7	0.2212	0.22261	0.0064					277.8	0.2503	0.2526	0.0091				

^aU(T) (0.95 level of confidence) = 0.03 K, U(P) (0.95 level of confidence) = 0.0007 MPa, ^bNgema et al. (2014), ^cValues are in mass fraction for

water + salt, $AAD = \frac{|p_i^{cal} - p_i^{exp}|}{p_i^{exp}}$, P – presents the experimental and calculated pressure in MPa

Table C1. 5. Measured and calculated data for hydrate–liquid water–liquid promoter–vapour for the R410a (1) + water (2) + mixed salts (3) + CP (4) system at industrial salt concentrations^a

R410a (1) + water (2) + 0.002 ^b CaCl ₂ (3) + 0.017 ^b NaCl (4)				R410a (1) + water (2) + 0.002 ^b CaCl ₂ (3) + 0.017 ^b NaCl (4) + CP (5)				R410a (1) + water (2) + 0.013 ^b MgCl ₂ (3) + 0.019 ^b NaCl (4) + CP (5)				R410a (1) + water (2) + 0.013 ^b MgCl ₂ (3) + 0.019 ^b NaCl (4) + CP (5)			
T/K	P ^{exp}	P ^{cal}	AAD	T/K	P ^{exp}	P ^{cal}	AAD	T/K	P ^{exp}	P ^{cal}	AAD	T/K	P ^{exp}	P ^{cal}	AAD
289.4	1.0197	1.0242	0.0044	292.5	1.1193	1.1083	0.0098	288.9	1.0183	1.0219	0.0035	292.9	1.1693	1.1593	0.0086
289.3	1.0083	0.9970	0.0112	290.8	0.9075	0.9085	0.0010	287.6	0.8606	0.8555	0.0058	291.8	0.9903	0.9861	0.0042
288.4	0.8935	0.8875	0.0068	289.5	0.7427	0.7514	0.0116	287.5	0.7674	0.7598	0.0099	291.8	0.9766	0.97711	0.0005
286.9	0.7308	0.7251	0.0078	289.5	0.7319	0.7399	0.0109	286.7	0.6146	0.6147	0.0001	290.0	0.8044	0.8015	0.0036
284.7	0.5629	0.5661	0.0056	286.2	0.4683	0.4708	0.0054	285.0	0.4777	0.4801	0.0051	288.2	0.6573	0.6520	0.0081
281.3	0.3549	0.3586	0.0102	283.3	0.2993	0.3011	0.0058	283.2	0.3923	0.3921	0.0006	285.9	0.4556	0.4567	0.0024
279.6	0.2500	0.2532	0.0127					281.6	0.2442	0.2469	0.0109	282.3	0.2381	0.2366	0.0066
								279.1	0.2446	0.2458	0.0049				

^aU(T) (0.95 level of confidence) = 0.03 K, U(P) (0.95 level of confidence) = 0.0007 MPa, ^bValues are in mass fraction for water + salt,

$$AAD = \frac{|p_i^{cal} - p_i^{exp}|}{p_i^{exp}}, \text{ P - presents the experimental and calculated pressure in MPa}$$

Table C1. 6. Measured and calculated data for hydrate–liquid water–liquid promoter–vapour for the R410a (1) + water (2) + mixed salts (3) + CP (4) system at higher salt concentrations^a

R410a (1) + water (2) + 0.080 ^b CaCl ₂ (3) + 0.050 ^b NaCl (4)				R410a (1) + water (2) + 0.080 ^b CaCl ₂ (3) + 0.050 ^b NaCl (4) + CP (5)				R410a (1) + water (2) + 0.150 ^b CaCl ₂ (3) + 0.050 ^b NaCl (4)				R410a (1) + water (2) + 0.150 ^b CaCl ₂ (3) + 0.050 ^b NaCl (4) + CP (5)			
T/K	P ^{exp}	P ^{cal}	AAD	T/K	P ^{exp}	P ^{cal}	AAD	T/K	P ^{exp}	P ^{cal}	AAD	T/K	P ^{exp}	P ^{cal}	AAD
288.8	1.0672	1.0554	0.0111	291.7	1.0992	1.0892	0.0091	282.2	1.0744	1.0645	0.0092	289.4	1.0413	1.0236	0.0170
288.8	1.0834	1.0777	0.0052	289.8	0.8093	0.7996	0.0120	281.8	0.9963	0.98669	0.0096	286.6	0.74244	0.7384	0.0055
286.6	0.8091	0.7987	0.0129	288.4	0.664	0.6621	0.0029	280.6	0.811	0.80501	0.0074	286.8	0.7615	0.7560	0.0072
284.6	0.651	0.6460	0.0077	286.4	0.4995	0.5053	0.0116	280.7	0.8324	0.82357	0.0106	285.1	0.6211	0.6154	0.0092
282.9	0.532	0.5336	0.0030	286.4	0.513	0.5187	0.0110	279.7	0.6991	0.69603	0.0044	282.8	0.466	0.4689	0.0063
281.2	0.4379	0.4429	0.0115	283.2	0.3144	0.3161	0.0052	279.3	0.6486	0.64796	0.0010	280.2	0.3069	0.3101	0.0104
279.3	0.3588	0.3599	0.0031	280.6	0.1919	0.1939	0.0102	277.9	0.5197	0.5253	0.0108	278.1	0.2041	0.2028	0.0062
276.4	0.2498	0.2521	0.0091					276.1	0.3749	0.37844	0.0094				
								274.5	0.2796	0.28323	0.0130				

^aU(T) (0.95 level of confidence) = 0.03 K, U(P) (0.95 level of confidence) = 0.0007 MPa, ^bValues are in mass fraction for water + salt,

$$AAD = \frac{|P_i^{cal} - P_i^{exp}|}{P_i^{exp}}, \text{ P – presents the experimental and calculated pressure in MPa}$$

Table C1. 7. Measured and calculated data for hydrate–liquid water–liquid promoter–vapour for the CO₂ (1) + water (2) + NaCl (3) + CP (4) system at various salt concentrations^a

^b CO ₂ (1) + water (2) + CP (3)				CO ₂ (1) + water (2) + 0.100 ^c				CO ₂ (1) + water (2) + 0.150 ^c				CO ₂ (1) + water (2) + 0.200 ^c			
				NaCl (3) + CP (4)				NaCl (3) + CP (4)				NaCl (3) + CP (4)			
T/K	P ^{exp}	P ^{cal}	AAD	T/K	P ^{exp}	P ^{cal}	AAD	T/K	P ^{exp}	P ^{cal}	AAD	T/K	P ^{exp}	P ^{cal}	AAD
290.7	2.0600	2.0583	0.0008	276.0	3.2390	3.2210	0.0056	271.9	2.7811	2.7682	0.0046	266.3	2.4461	2.4324	0.0056
289.1	1.5900	1.5428	0.0297	275.3	2.9392	2.9291	0.0034	270.5	2.2819	2.2909	0.0039	265.3	2.1074	2.0833	0.0114
288.1	1.2000	1.1589	0.0342	274.2	2.4011	2.4083	0.0030	269.8	2.0463	2.0562	0.0048	264.2	1.7872	1.7779	0.0052
286.9	0.9300	0.8846	0.0488	273.2	2.1312	2.1329	0.0008	268.5	1.7854	1.7699	0.0087	262.3	1.3381	1.2989	0.0293
285.3	0.6400	0.5983	0.0652	272.1	1.8751	1.8599	0.0081	266.0	1.3584	1.3479	0.0077				
284.3	0.3500	0.3378	0.0349	270.0	1.4881	1.4689	0.0129								

^aU(T) (0.95 level of confidence) = 0.03 K, U(P) (0.95 level of confidence) = 0.0007 MPa, ^bMohammadi and Richon (2009), ^cValues are in mass

fraction for water + salt, $AAD = \frac{|p_i^{cal} - p_i^{exp}|}{p_i^{exp}}$, P – presents the experimental and calculated pressure in MPa

Table C1. 8. Measured and calculated data for hydrate–liquid water–liquid promoter–vapour for the CO₂ (1) + water (2) + CaCl₂ (3) + CP (4) system at various salt concentrations.

^b CO ₂ (1) + water (2) + CP (3)				CO ₂ (1) + water (2) + 0.100 ^c CaCl ₂ (3) + CP (4)				CO ₂ (1) + water (2) + 0.150 ^c CaCl ₂ (3) + CP (4)				CO ₂ (1) + water (2) + 0.200 ^c CaCl ₂ (3) + CP (4)			
T/K	P ^{exp}	P ^{cal}	AAD	T/K	P ^{exp}	P ^{cal}	AAD	T/K	P ^{exp}	P ^{cal}	AAD	T/K	P ^{exp}	P ^{cal}	AAD
290.7	2.0600	2.0583	0.0008	277.2	2.7784	2.7748	0.0013	273.4	2.4881	2.4799	0.0033	267.2	2.3484	2.3387	0.0041
289.1	1.5900	1.5428	0.0297	276.4	2.486	2.5007	0.0059	271.8	1.9993	2.0036	0.0022	264.8	1.7824	1.79	0.0043
288.1	1.2000	1.1589	0.0342	275.2	2.0844	2.0727	0.0056	270.3	1.5913	1.5818	0.0060	263.1	1.3891	1.3787	0.0075
286.9	0.9300	0.8846	0.0488	272.9	1.6322	1.6202	0.0074	268.0	1.1924	1.1817	0.0090	261.4	1.0623	1.0762	0.0131
285.3	0.6400	0.5983	0.0652	271.6	1.3693	1.3595	0.0072								
284.3	0.3500	0.3378	0.0349	268.8	0.9660	0.9506	0.0159								

^aU(T) (0.95 level of confidence) = 0.03 K, U(P) (0.95 level of confidence) = 0.0007 MPa, ^bMohammadi and Richon (2009), ^cValues are in mass

fraction for water + salt, $AAD = \frac{|p_i^{cal} - p_i^{exp}|}{p_i^{exp}}$, P – presents the experimental and calculated pressure in MPa

Table C1. 9. Measured and calculated data for hydrate–liquid water–liquid promoter–vapour for the CO₂ (1) + water (2) + MgCl₂ (3) + CP (4) system at various salt concentrations.

^b CO ₂ (1) + water (2) + CP (3)				CO ₂ (1) + water (3) + 0.100 ^c MgCl ₂ (3) + CP (4)				CO ₂ (1) + water (2) + 0.150 ^c MgCl ₂ (3) + CP (4)			
T/K	P ^{exp}	P ^{cal}	AAD	T/K	P ^{exp}	P ^{cal}	AAD	T/K	P ^{exp}	P ^{cal}	AAD
290.7	2.0600	2.0583	0.0008	287.2	2.4193	2.4179	0.0006	268.6	2.0621	2.0644	0.0011
289.1	1.5900	1.5428	0.0297	286.2	1.9899	2.0001	0.0051	266.0	1.5255	1.5149	0.0069
288.1	1.2000	1.1589	0.0342	285.3	1.6422	1.6400	0.0013	263.3	1.1524	1.1455	0.0060
286.9	0.9300	0.8846	0.0488	284.3	1.3414	1.3389	0.0019	261.1	0.8833	0.8736	0.0110
285.3	0.6400	0.5983	0.0652	282.0	0.8133	0.8087	0.0057				
284.3	0.3500	0.3378	0.0349								

^aU(T) (0.95 level of confidence) = 0.03 K, U(P) (0.95 level of confidence) = 0.0007 MPa, ^bMohammadi and Richon (2009), ^cValues are in mass

fraction for water + salt, $AAD = \frac{|p_i^{cal} - p_i^{exp}|}{p_i^{exp}}$, P – presents the experimental and calculated pressure in MPa

APPENDIX D: DESIGN EQUATIONS

D.1 Reactor design

$$\text{Reactor volume: } V = \frac{F_{AO} X}{-r_A} \quad (\text{D1.1})$$

$$\text{Reaction rate constant: } k_r = k_o e^{-Ea/RT} \quad (\text{D1.2})$$

Power calculations

$$\text{Prandtl number: } \text{Pr} = \frac{C_p \nu}{k} \quad (\text{D1.3})$$

$$\text{Impeller diameter: } d = \frac{D}{3} \quad (\text{D1.4})$$

Rotational speed, N, range between 4.1 and 5.6 rpm

$$\text{Reynold number: } \text{Re}_d = \frac{Nd^2}{\nu} \quad (\text{D1.5})$$

Constant, C₁, range between 0.3 and 1.2

$$\text{Nussel number: } Nu_D = C_1 \text{Re}^{2/3} \text{Pr}^{1/3} \quad (\text{D1.6})$$

$$\text{Constant, C}_2: C_2 = k\nu^{-2/3} \text{Pr}^{1/3} \quad (\text{D1.7})$$

$$\text{Ratio of diameters, } dd = d/D \quad (\text{D1.8})$$

$$\text{Heat transfer coefficient: } h = \frac{Nu_D k}{k} \quad (\text{D1.9})$$

$$\text{For scale-up the heat transfer coeffiecent: } h = C_1 C_2 dd^{3/4} N^{2/3} D^{1/3} \quad (\text{D1.10})$$

$$\text{Froude number: } Fr^y = \frac{N^2 d}{g} \quad (\text{D1.11})$$

$$N_p = C_1 \text{Re}^{2/3} Fr^y \quad (\text{D1.12})$$

$$\text{Power number: } P_o = N_p \rho_l N^3 d^5 \quad (\text{D1.13})$$

$$\text{Power required: } W = \rho_l N^3 d^5 P_o \quad (\text{D1.14})$$

D.2 Compressor design

Using N-method

$$\text{Calculating the inlet specific volume: } v_1 = \frac{ZRT_1}{P_1 * 10^5} \quad (\text{D2.1})$$

$$\text{The polytropic exponent: } \frac{n}{n-1} = \left(\frac{k}{k-1} \right) \eta \quad (\text{D2.2})$$

η is taken from Table B.6

$$k = \frac{MC_p}{MC_p - 8.33} \quad (\text{D2.3})$$

$$\text{The overall head: } H = ZRT \left(\frac{n}{n-1} \right) \left[\left(\frac{P_2}{P_1} \right)^{\frac{n-1}{n}} - 1 \right] \quad (\text{D2.4})$$

Checking the discharge temperature for a need to intercool (for intercool if $T_2 > 478.2 \text{ K}$)

$$\frac{T_2}{T_1} = \left(\frac{P_2}{P_1} \right)^{\frac{n-1}{n}} \quad (\text{D2.5})$$

$$\text{Number of stages: } N_s = \frac{H}{\left(\frac{H}{N^2} \right) * N^2} \quad (\text{D2.6})$$

By using Fan Law relationships adjust the speed: $H \propto N^2$

$$N = N_{nom} \left[\frac{H_{req}}{H} \right]^{\frac{1}{2}} \quad (\text{D2.7})$$

$$\text{Power required: } P_{req} = \frac{mH}{60000 \eta}, \text{ if m is in kg/min} \quad (\text{D2.8})$$

$$P_{req} = \frac{mH}{1000 \eta}, \text{ if m is in kg/s} \quad (\text{D2.9})$$

$$\text{Flow coefficient: } \delta = \frac{700Q}{ND^3} \text{ or } \frac{4Q}{\pi UD^2} \quad (\text{D2.10})$$

where D is impeller diameter (mm), it is taken from Table B.7 base on the frame size, U is tip speed

$$\text{Head coefficient: } \mu = \frac{32.2H}{U^2} \quad (\text{D2.11})$$

$$\text{Tip speed: } U = \sqrt{\frac{H}{N\psi}} \text{ or } \frac{\pi D}{720} \quad (\text{D2.12})$$

$$\text{Equivalent tip speed: } U_e = U \sqrt{\frac{26.2MW}{kZT}} \quad (\text{D2.13})$$

$$\text{Work coefficient: } \phi = \frac{\mu}{\eta} \quad (\text{D2.14})$$

D.3 Horizontal belt filter design

Hydrate slurry filtration

The filtration vacuum (Δp_f) is fixed throughout the process, and α_{av} , C_{av} , m_{av} , effective feed concentration © remain constant. These properties are related to (Δp_f) by using the following equations

$$\alpha_{av} = \alpha_o (1-n) \Delta p_f^n \quad (\text{D3.1})$$

$$C_{av} = C_o \Delta p_f^\beta \quad (\text{D3.2})$$

$$m_{av} = 1 + \frac{\rho_l}{\rho_s} \left(\frac{1-C_{av}}{C_{av}} \right) \quad (\text{D3.3})$$

$$c = \frac{s\rho_l}{1-m_{av}s} \quad (\text{D3.4})$$

where ρ_l is density of liquid and s the mass fraction of solid in feed.

$$L_f = \frac{V_f c}{A_f \rho_s (1 - \varepsilon_{av})} \quad (D3.5)$$

Cumulative filtrate volume is calculated using the following equation

$$V_f = \frac{A_f}{c} \left[-\frac{R}{\alpha_{av}} + \sqrt{\left(\frac{R}{\alpha_{av}}\right)^2 + \frac{2ct_f \Delta p_f}{\mu_l \alpha_{av}}} \right] \quad (D3.6)$$

The cake thickness, where R is the filter medium resistance

$$L_f = \frac{1}{\rho_s C_{av}} \left[-\frac{R}{\alpha_{av}} + \sqrt{\left(\frac{R}{\alpha_{av}}\right)^2 + \frac{2ct_f \Delta p_f}{\mu_l \alpha_{av}}} \right] \quad (D3.7)$$

$$q = \frac{dV_f}{dt_f} \approx \frac{\Delta V_f}{\Delta t_f} \quad (D3.8)$$

$$\text{Solid mass: } M_s(t) = K_l L_f C_{av} \rho_s \quad (D3.9)$$

$$\text{Liquid mass: } M_l(t) = K_l L_f (1 - C_{av}) \rho_l \quad (D3.10)$$

$$\text{Solute mass: } M_{sol}(t) = K_l L_f (1 - C_{av}) \phi_0 \quad (D3.11)$$

$$\text{where } K_l = v_B h_B \quad K_l = v_B h_B \quad (D3.12)$$

$$\text{The hydrate slurry moisture content: } M = 100 \left(\frac{M_l(t)}{M_l(t) + M_s(t)} \right) \quad (D3.13)$$

Washing phase

$$(t_w)_e = \frac{z_w}{v_B} \quad (D3.14)$$

$$A_w = z_w h_B \quad (D3.15)$$

$$\text{Supercritical wash velocity: } u = \frac{\Delta p_w}{\mu \alpha_{av} \rho_s L_w R C_{av}} \quad (D3.16)$$

$$\text{Mean velocity: } v = \frac{u}{\varepsilon_{av}} \quad (D3.17)$$

$$\frac{dV_w}{dt_w} = u A_w = \text{constant} \quad (D3.18)$$

and hence

$$\text{Re } Sc = \frac{vx}{D} \quad (\text{D3.19})$$

Since $\text{Re } Sc > 1$ and $L_w < 10$ cm, then

$$\frac{D_L}{D} = 0.707 + 55.5(\text{Re } Sc)^{0.96} \quad (\text{D3.20})$$

$$\text{The dispersion number: } D_n = \text{Re } Sc \frac{L_w}{x} \left(\frac{D}{D_L} \right) \quad (\text{D3.21})$$

$$\text{Total cycle time: } t_T = t_{pr} + t_w \quad (\text{D3.22})$$

The cumulative volume of liquid extracted from filter:

$$V_T = V_{pr} + V_w = V_{pr} + A_w u t_w \quad (\text{D3.23})$$

$$\text{The distance along the belt: } x_B = x_{pr} + v_B t_w \quad (\text{D3.24})$$

The mass throughput of slurry solute is for $t_w > 0$

$$M_{sol}(t) = (1 - F) \left[(M_{sol}(t))_{pr} - \phi_w u A_w \right] + \phi_w u A_w \quad (\text{D3.25})$$

Deliquoring phase

$$(t_d)_e = \frac{z_d}{v_B} \quad (\text{D3.26})$$

$$A_d = z_d h_B \quad (\text{D3.27})$$

$$\text{Breakthrough vacuum: } p_b = \frac{4.6 C_{av} \sigma}{(1 - C_{av}) x_{av}} \quad (\text{D3.28})$$

$$\text{Hydrate permeability: } k_{av} = \frac{1}{\alpha_{av} \rho_s C_{av}} \quad (\text{D3.29})$$

$$\text{Total cycle time: } t_T(s) = t_{pr} + t_d \quad (\text{D3.30})$$

$$\text{Distance along the belt: } x_B = x_{pr} + v_B t_d \quad (\text{D3.31})$$

$$\text{Dimensionless pressure: } p^* = \frac{\Delta p_d}{p_b} \quad (\text{D3.32})$$

$$\text{Dimensionless deliquoring time: } \theta p^* = \frac{t_d k_{av} \Delta p_d}{\varepsilon_{av} \mu_l (L_d)^2 (1 - S_\infty)} \quad (\text{D3.33})$$

$$\text{Reduced saturation: } S_R = \frac{1}{1+1.08(\theta p^*)^{0.88}} \text{ because } 0.096 \leq (\theta p^*) \leq 1.915 \quad (\text{D3.34})$$

$$\text{Hydrate saturation: } S = S_\infty + S_R(1 - S_\infty) \quad (\text{D3.35})$$

$$\text{The slurry moisture content: } M = \frac{100}{\frac{\rho_s}{S\rho_l} \left(\frac{C_{av}}{1 - C_{av}} \right)} \quad (\text{D3.36})$$

$$\text{At } p_a^* = 5 \text{ then } \bar{u}_a^* = 10^{(0.331+0.4431\log\theta-0.4364(\log\theta)^2-0.0124(\log\theta)^3-0.0058(\log\theta)^4)} \quad (\text{D3.37})$$

$$\text{where } 10^{-4} \leq \theta < 0.8 \quad (\text{D3.38})$$

$$\text{At } p_a^* = 10 \text{ then } \bar{u}_a^* = 10^{(0.4085-0.6765\log\theta-1.3865(\log\theta)^2-0.3329(\log\theta)^3-0.0304(\log\theta)^4)} \quad (\text{D3.39})$$

$$\text{where } 10^{-4} \leq \theta < 0.3 \quad (\text{D3.40})$$

$$\text{Then total cycle for horizontal belt filter: } (t_T)_e = 2(t_T)_{pr} \quad (\text{D3.41})$$

The pressure difference across the cake/slurry

$$p_a^* = p_{aei}^* - p_{aeo}^* = \frac{p_B}{p_b} - \frac{p_B - \Delta p_d}{p_b} \quad (\text{D3.42})$$

$$p_{ao}^* = p_{ai}^* - p_a^* \quad (\text{D3.43})$$

The dimensionless air rate

$$\bar{u}_{ae}^* = 1.1 \bar{u}_a^* \frac{p_{ao}^*}{p_{aeo}^*} \left[\frac{(p_{aeo}^*)^2 - (p_{aei}^*)^2}{(p_{ao}^*)^2 - (p_{ai}^*)^2} \right] \quad (\text{D3.44})$$

$$u_a = \bar{u}_{ae}^* \left(\frac{k_{av} p_b}{\mu_a L_d} \right) \quad (\text{D3.45})$$

$$u_a|_{tot} = u_a \left(\frac{t_d}{(t_T)_e} \right) \quad (\text{D3.46})$$

The design air rate is given by the following expression

$$u_a|_{des} = u_a|_{tot} \left(\frac{p_{aei}^* - \frac{\Delta p_d}{p_b}}{p_{aei}^* - \frac{\Delta p_d + 3300}{p_b}} \right) \quad (\text{D3.47})$$

The cumulative volume of liquid extracted from the filter

$$V_T = V_{pr} + \frac{(t_d)_e M_s(t)}{\rho_l} \left(\frac{M_{pr}}{100 - M_{pr}} - \frac{M}{100 - M} \right) \quad (D3.48)$$

The cake/slurry liquid: $M_l(t) = S(M_l(t))_{pr}$ (D3.49)

The cake/slurry solute: $M_{sol}(t) = S(M_{sol}(t))_{pr}$ (D3.50)

Table D1. 1. Separation and filtration phase

t_f (s)	x_B (m)	V_f (m ³)	L_f (m)	dV_f/dt_f (m ³ /s)	M_s (t)	M_l (t)	M_{sol} (t)
0.0	0.00	0.000	0.000	0.000	0.000	0.000	0.000
1.5	0.15	0.017	0.019	0.011	1.081	2.289	0.102
3.0	0.30	0.024	0.027	0.005	1.565	3.314	0.147
4.5	0.45	0.030	0.034	0.004	1.936	4.101	0.182
6.0	0.60	0.034	0.039	0.003	2.250	4.765	0.212
7.5	0.75	0.039	0.044	0.003	2.526	5.350	0.238
9.0	0.90	0.042	0.048	0.003	2.776	5.879	0.261
10.5	1.05	0.046	0.052	0.002	3.005	6.365	0.283
12.0	1.20	0.049	0.056	0.002	3.219	6.818	0.303
13.5	1.35	0.052	0.059	0.002	3.420	7.243	0.322
15.0	1.50	0.055	0.063	0.002	3.610	7.645	0.340

Table D1. 2. Washing phase

t_w (s)	t_r (s)	x_B (m)	W	F	ϕ	V_T (m ³)	M_{sol} (t)
0.0	15.0	1.50	0.00	0.00	1.000	0.055	0.000
4.5	19.5	1.95	0.13	0.119	1.000	0.081	0.090
9.0	24.0	2.40	0.27	0.252	1.000	0.106	0.110
13.5	28.5	2.85	0.40	0.385	0.994	0.132	0.112
18.0	33.0	3.30	0.53	0.514	0.951	0.157	0.103
22.5	37.5	3.75	0.66	0.635	0.881	0.183	0.087
27.0	42.0	4.20	0.80	0.745	0.755	0.209	0.067
31.5	46.5	4.65	0.93	0.833	0.577	0.234	0.047
36.0	51.0	5.10	1.06	0.897	0.401	0.260	0.031
40.4	55.4	5.54	1.20	0.642	0.254	0.285	0.115
45.0	60.0	6.00	1.33	0.961	0.157	0.311	0.013

Table D1. 3. Deliquoring phase

t_a (s)	t_T (s)	x_b (m)	θ_p^*	S_R	S	M	θ	u_a^*	u_{ac}^*	u_a (m^3/m^2s)	u_a (tot)	u_a (des)	V_T (m^3)	M_I (t)	$M_{sol}(t)$
0	60.0	6.0	0	1	1	73.621	0								
3	63.0	6.3	0.065	0.911	0.938	72.350	0.010	0.049	0.077	2.9×10^{-6}	5.0×10^{-8}	5.0×10^{-8}	0.327	7.168	0.012
6	66.0	6.6	0.131	0.847	0.893	71.368	0.020	0.102	0.162	6.2×10^{-6}	2.1×10^{-7}	2.2×10^{-7}	0.338	6.828	0.012
9	69.0	6.9	0.196	0.795	0.857	70.509	0.030	0.161	0.256	9.7×10^{-6}	4.9×10^{-7}	5.2×10^{-7}	0.347	6.550	0.011
12	72.0	7.2	0.261	0.751	0.826	69.737	0.040	0.224	0.355	1.3×10^{-5}	9.0×10^{-7}	9.6×10^{-7}	0.355	6.312	0.011
15	75.0	7.5	0.327	0.712	0.799	69.032	0.050	0.288	0.457	1.7×10^{-5}	1.5×10^{-6}	1.6×10^{-6}	0.362	6.106	0.011
18	78.0	7.8	0.392	0.679	0.775	68.383	0.060	0.353	0.560	2.1×10^{-5}	2.1×10^{-6}	2.3×10^{-6}	0.368	5.925	0.010
21	81.0	8.1	0.457	0.648	0.754	67.780	0.070	0.419	0.663	2.5×10^{-5}	2.9×10^{-6}	3.1×10^{-6}	0.374	5.763	0.010
24	84.0	8.4	0.523	0.621	0.735	67.218	0.079	0.483	0.766	2.9×10^{-5}	3.9×10^{-6}	4.2×10^{-6}	0.378	5.617	0.010
27	87.0	8.7	0.588	0.596	0.717	66.692	0.089	0.547	0.867	3.3×10^{-5}	4.9×10^{-6}	5.3×10^{-6}	0.383	5.485	0.010
30	90.0	9.0	0.653	0.574	0.702	66.197	0.099	0.610	0.966	3.7×10^{-5}	6.1×10^{-6}	6.5×10^{-6}	0.387	5.364	0.009

APPENDIX E: KINECTICS MEASUREMENTS

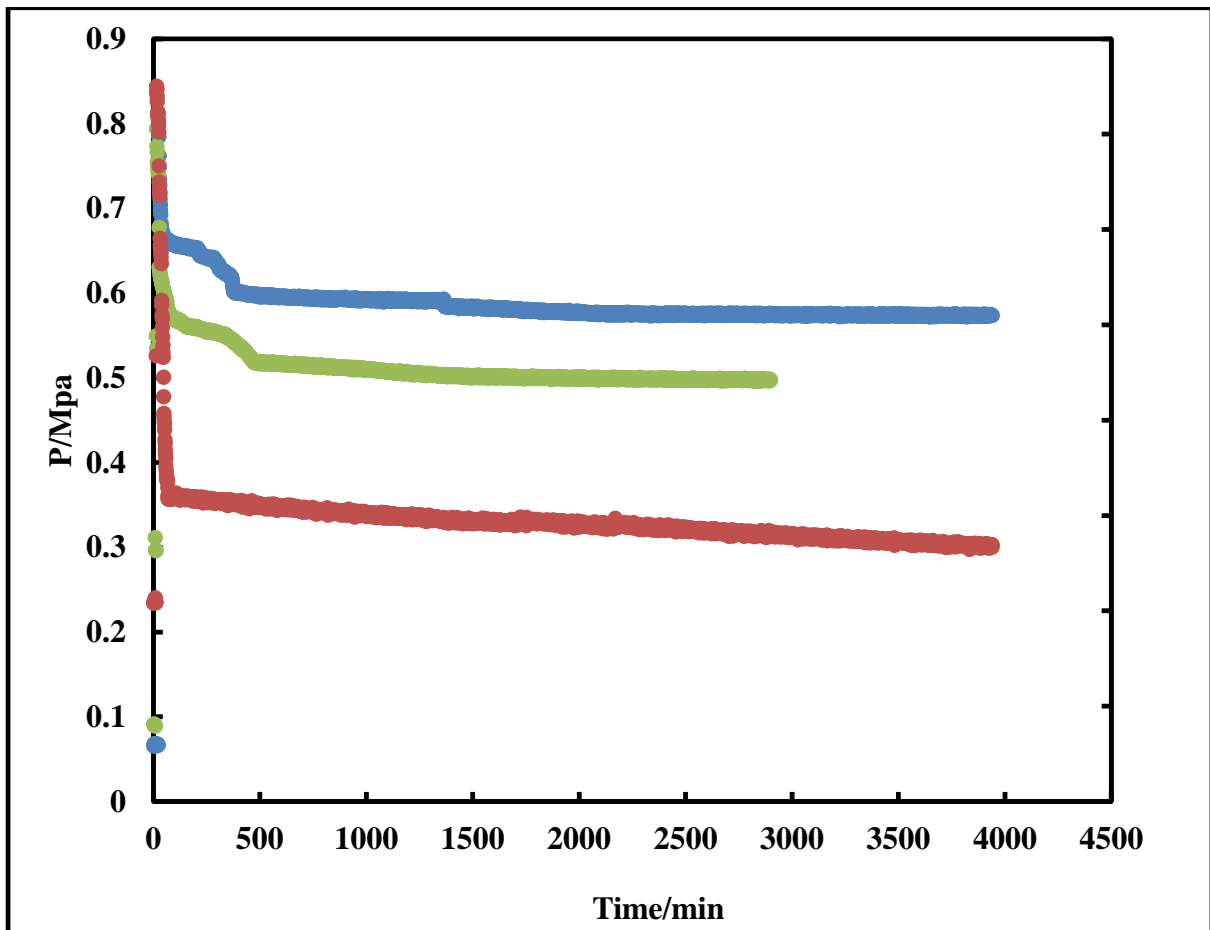


Figure E1. 1: Kinetic measurements for R410a (1) + water (2) + 0.013 mass fraction of MgCl_2 (3) + 0.019 mass fraction of NaCl (4) system at 276.8 K at the following initial pressures; ▲, 0.51 MPa; ■, 0.7 MPa, ◆, 0.91 MPa; ●.

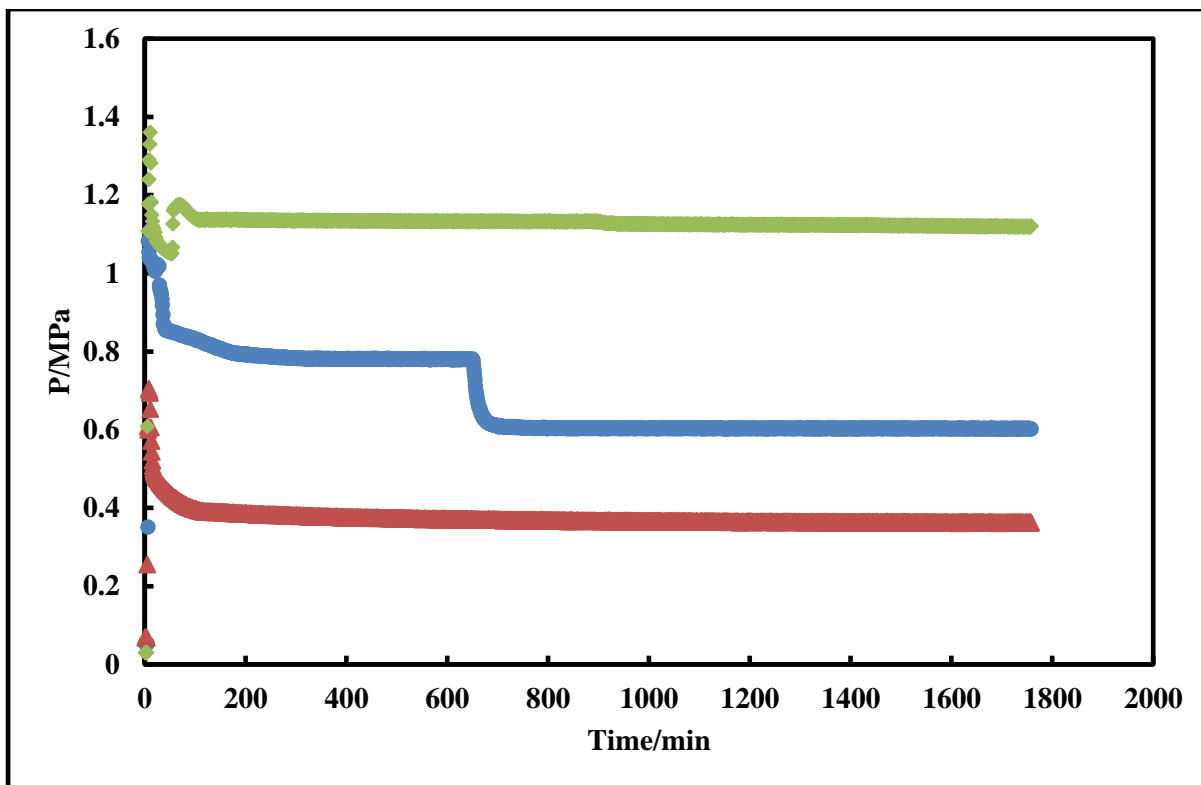


Figure E1. 2: Kinetic measurements for R410a (1) + water (2) + 0.013 mass fraction of MgCl_2 (3) + 0.019 mass fraction of NaCl (4) + CP system at 280.8 K at the following initial pressures; \blacktriangle , 0.70 MPa; \bullet , 1.08 MPa, \blacklozenge , 1.36 MPa.

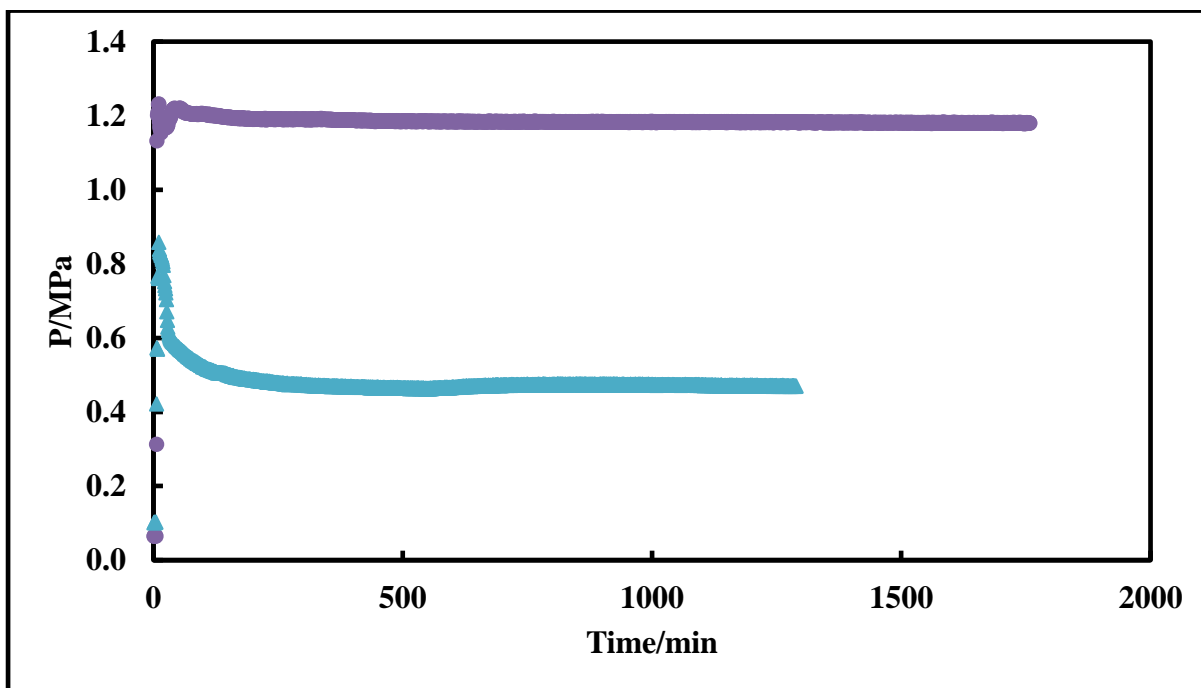


Figure E1. 3: Kinetic measurements for R410a (1) + water (2) + 0.013 mass fraction of MgCl_2 (3) + 0.019 mass fraction of NaCl (4) + CP system at 282.8 K at the following initial pressures; \blacktriangle , 0.85 MPa; \bullet , 1.21 MPa.

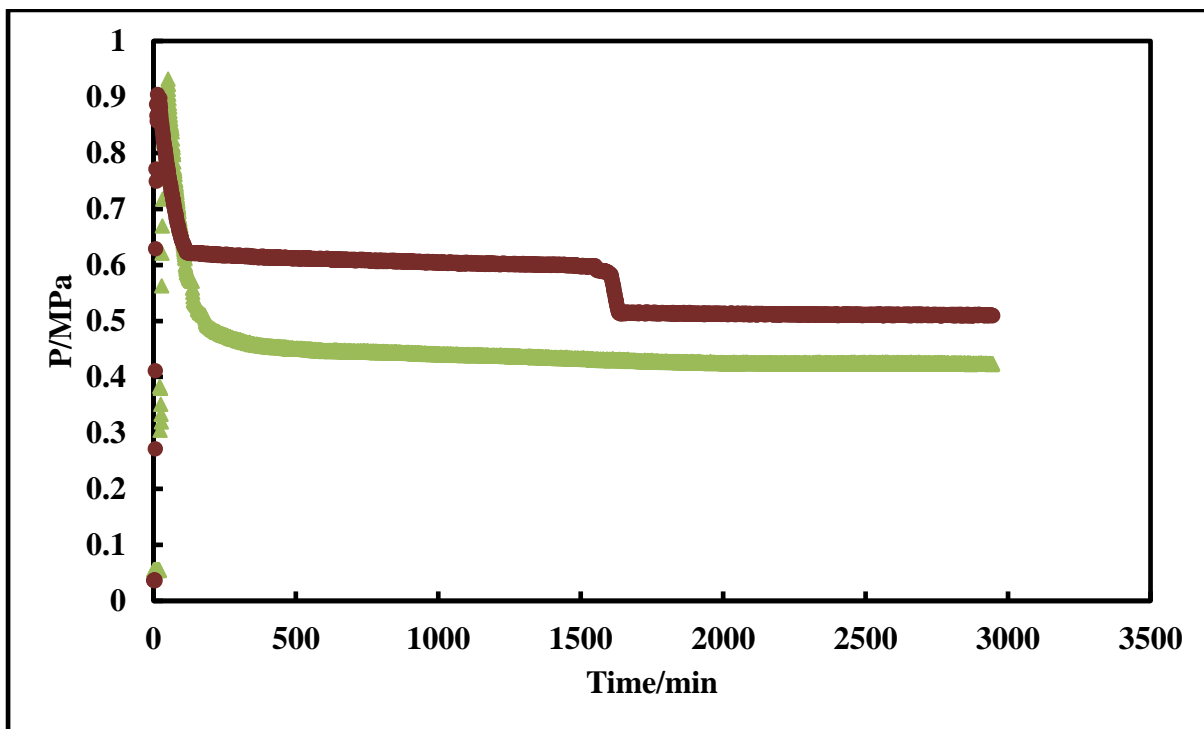


Figure E1. 4: Kinetic measurements for R410a (1) + water (2) + 0.002 mass fraction of CaCl_2 (3) + 0.017 mass fraction of NaCl (4) system at initial pressure of 0.90 MPa; at different temperature; \blacktriangle , 281.9 K; \bullet , 280.9 K.

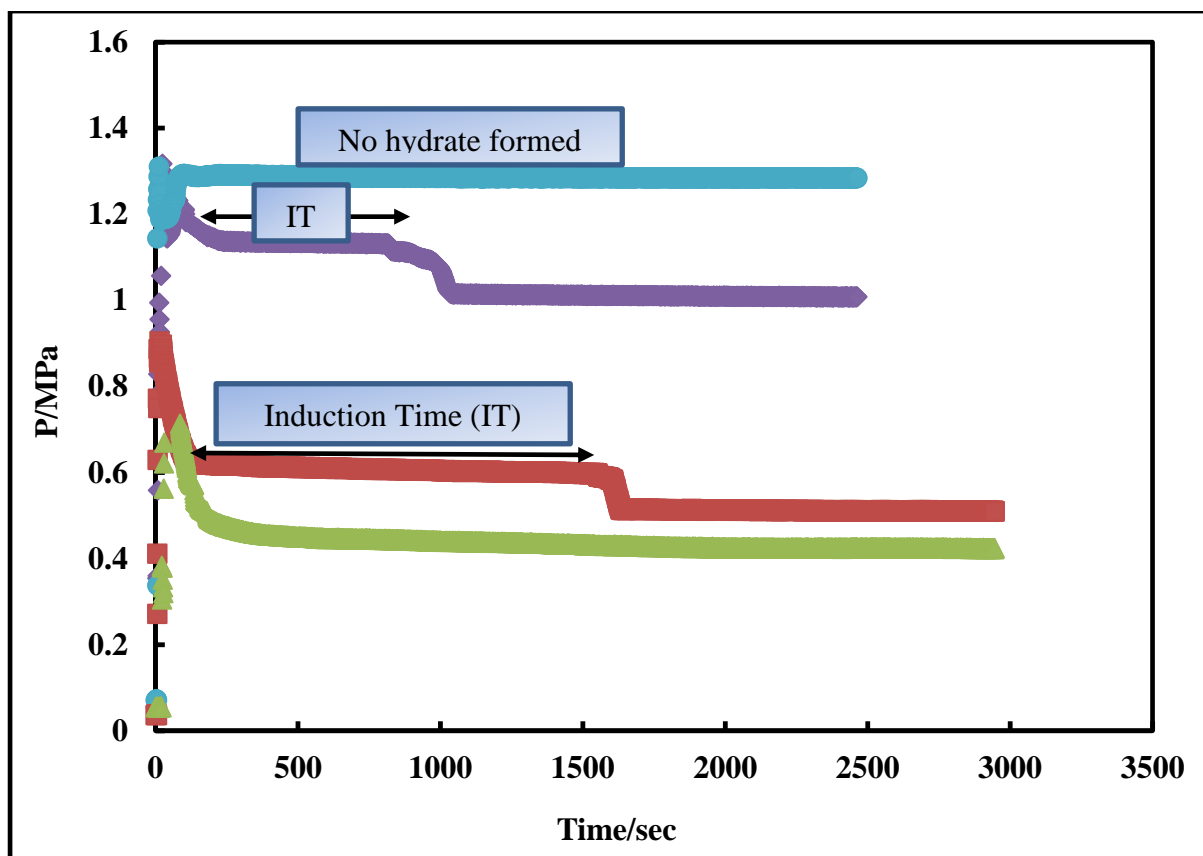


Figure E1. 5: Kinetics measurements for R410a (1) + water (2) + 0.002 mass fraction of CaCl_2 (3) + 0.017 mass fraction NaCl (4) system at 281.8 K at the following initial pressures; \blacktriangle , 0.71 MPa; \blacksquare , 0.9 MPa, \blacklozenge , 1.23 MPa; \bullet , 1.31 MPa.

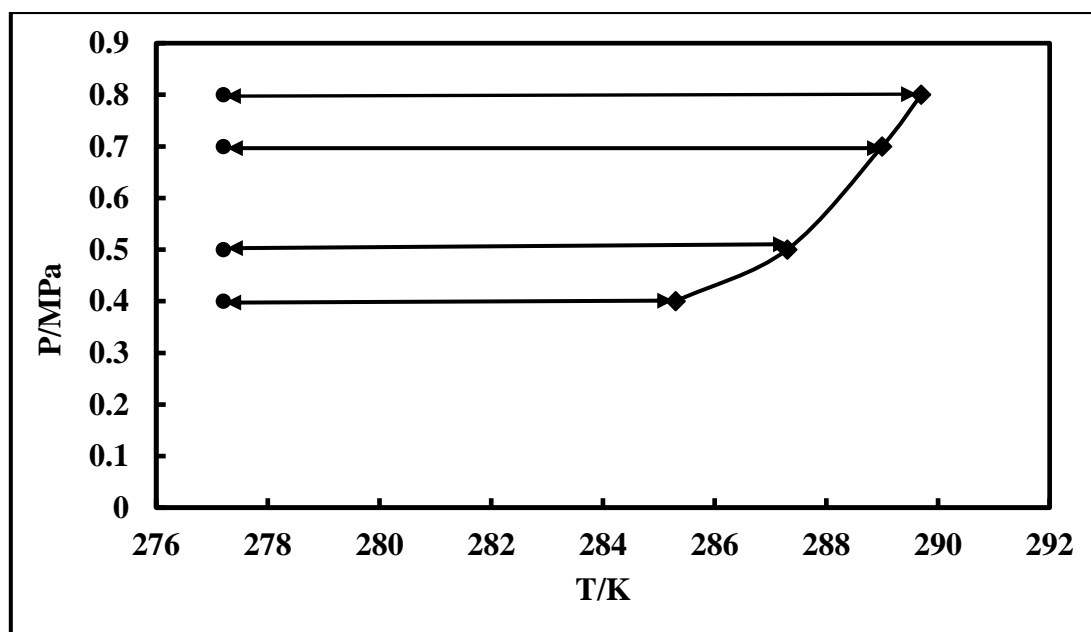


Figure E1. 6: Initial conditions and degree of subcooling for R410a (1) + water (2) + 0.013 mass fraction of MgCl_2 (3) + 0.019 mass fraction of NaCl (4) + CP (5) system: This work; \bullet , 277.2 K; \blacklozenge , gas hydrate equilibrium conditions; Solid lines, model correlations.

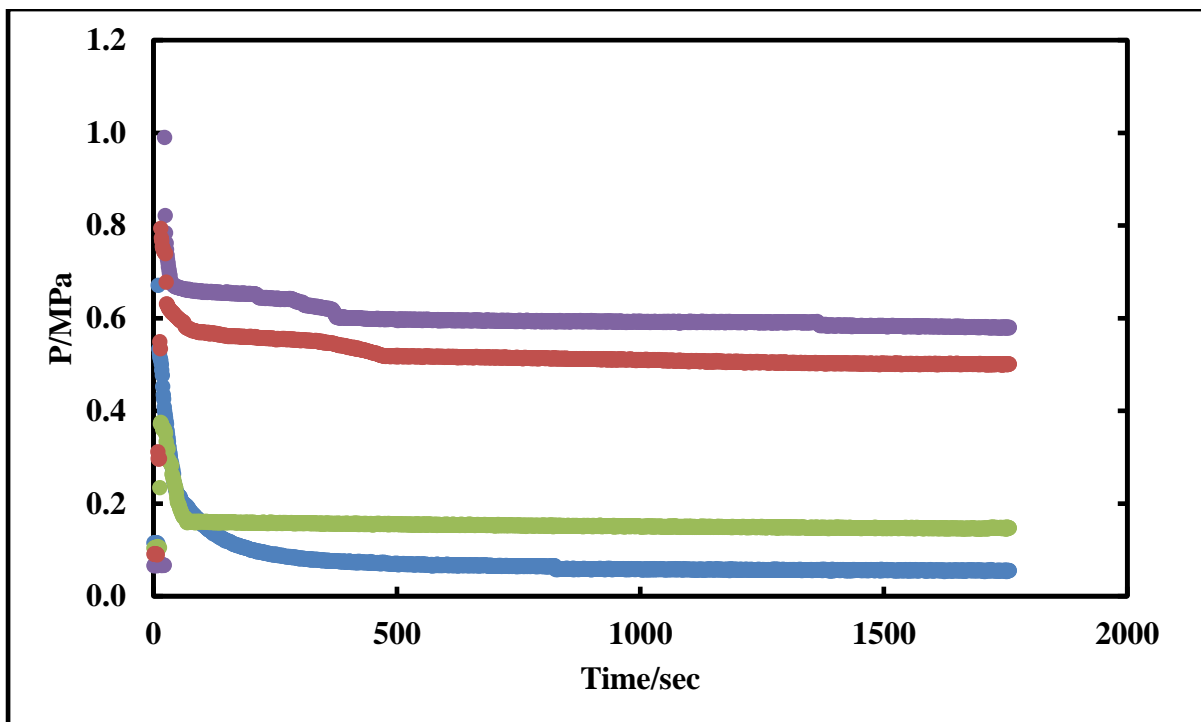


Figure E1. 7: Kinetics measurements for R410a (1) + water (2) + 0.013 mass fraction of MgCl₂ (3) + 0.019 mass fraction of NaCl (4) system + CP (5) at 277.2 K at the following initial pressures; ▲, 0.40 MPa; ●, 0.53 MPa, ■, 0.80 MPa; ●, 1.00 MPa.

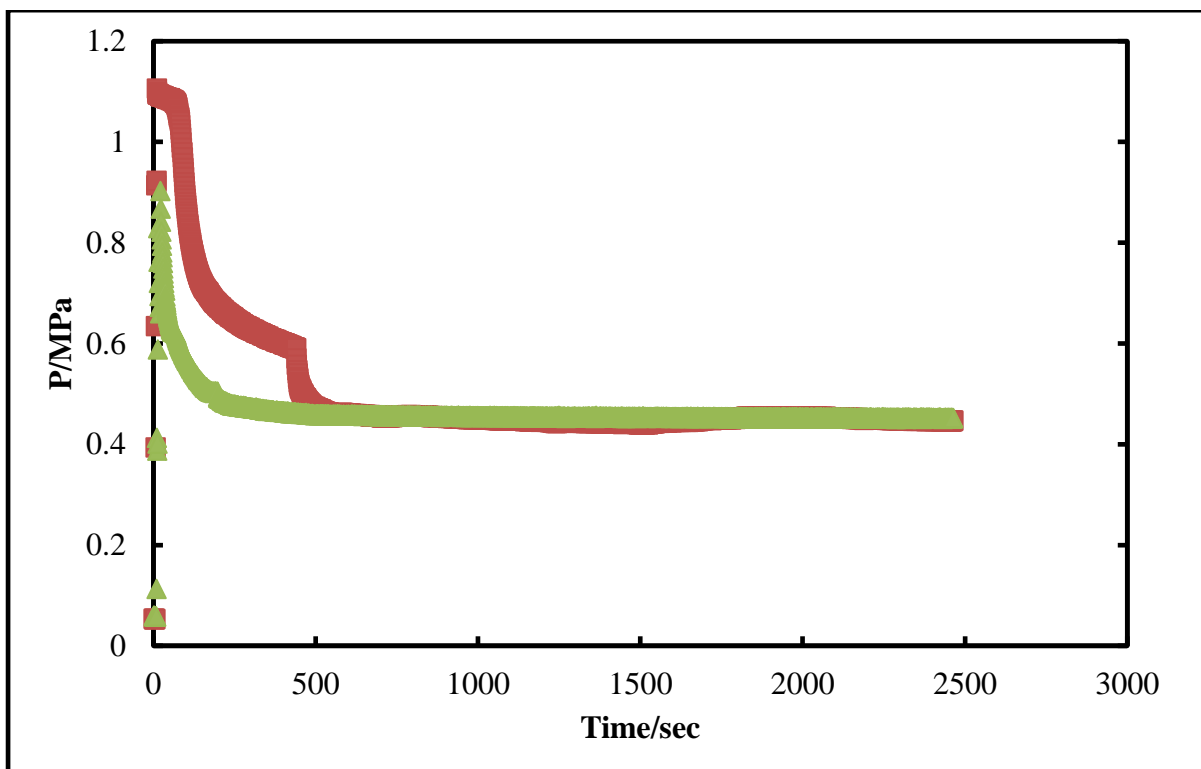


Figure E1. 8: Kinetics measurements for R410a (1) + water (2) + 0.002 mass fraction of CaCl₂ (3) + 0.017 mass fraction of NaCl (4) system at 282.9 K at the following initial pressures; ▲, 0.90 MPa; ■, 1.01 MPa.

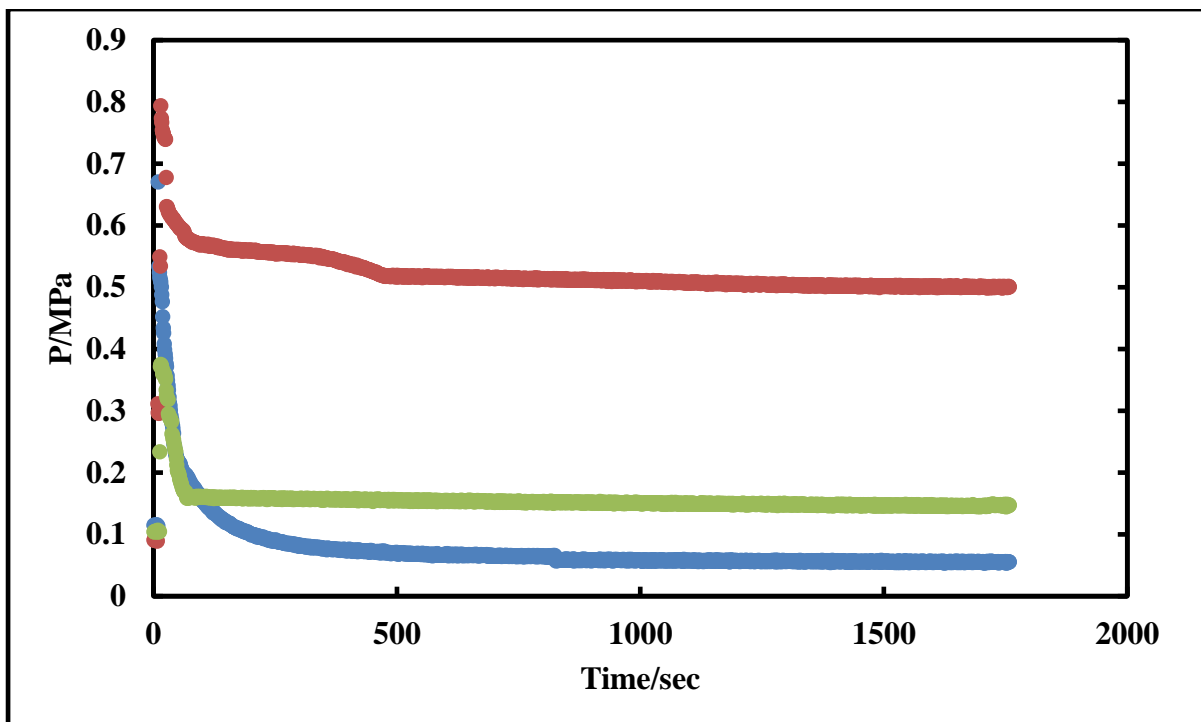


Figure E1. 9: Kinetics measurements for R410a (1) + water (2) + 0.013 mass fraction of MgCl_2 (3) + 0.019 mass fraction of NaCl (4) system + CP at 277.2 K at the following initial pressures; \blacktriangle , 0.37 MPa; \bullet , 0.53 MPa, \blacksquare , 0.80 MPa.

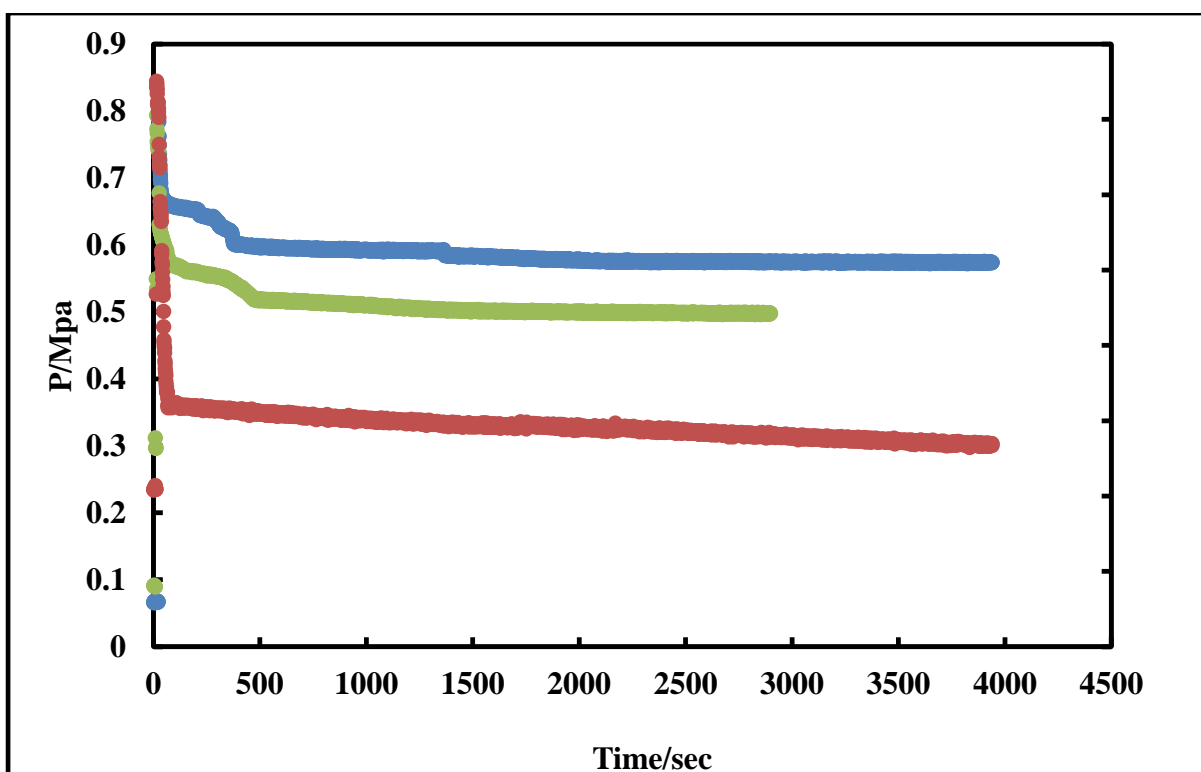


Figure E1. 10: Kinetics measurements for R410a (1) + water (2) + 0.013 mass fraction of MgCl_2 (3) + 0.019 mass fraction of NaCl (4) system at 276.8 K at the following initial pressures; \blacksquare , 0.51 MPa; \blacktriangle , 0.60 MPa, \bullet , 0.80 MPa.

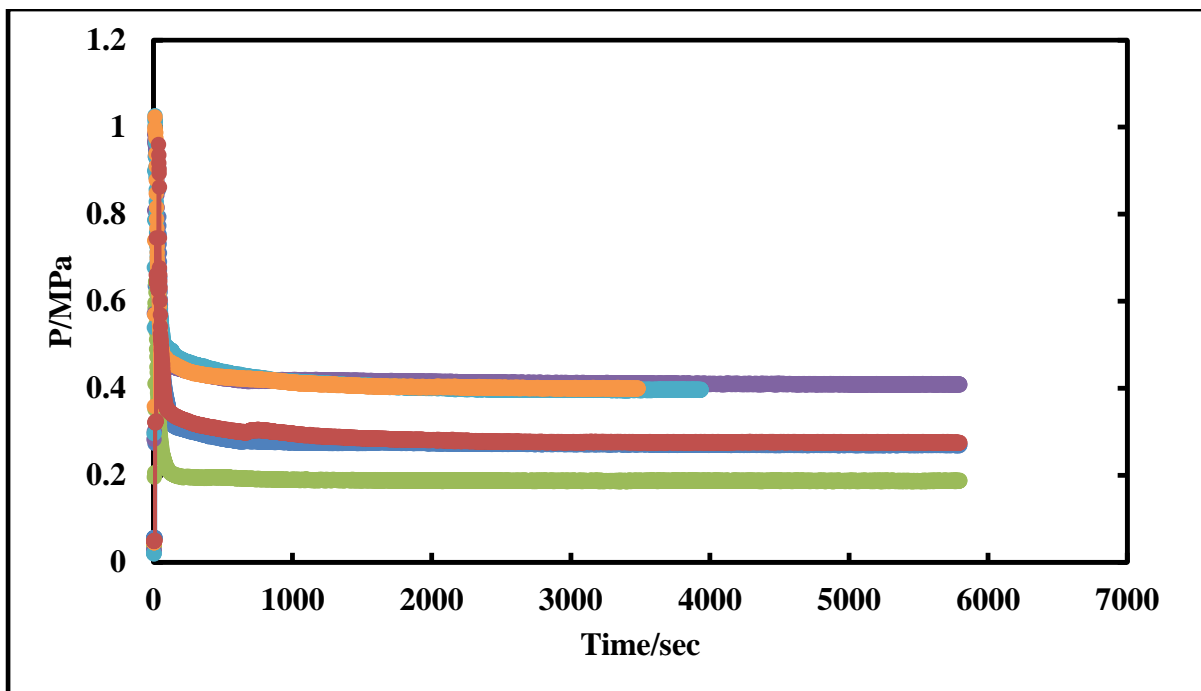


Figure E1.11: Kinetics measurements for R410a (1) + water (2) at the following initial pressures; \blacktriangle , 0.64 MPa; \bullet , 0.92 MPa; \blacksquare , 0.98 MPa, \blacklozenge , 1.11 MPa; \bullet , 1.1 MPa.

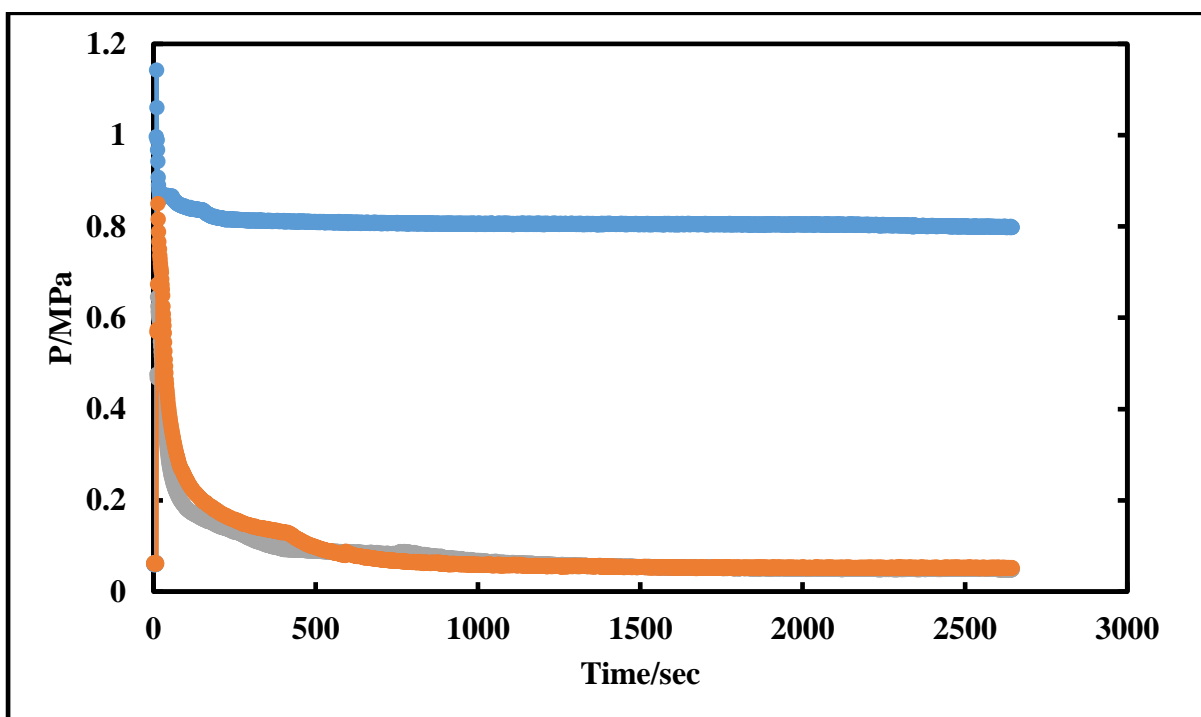


Figure E1.12: Kinetics measurements for R410a (1) + water (2) + 0.002 mass fraction of $CaCl_2$ (3) + 0.017 mass fraction $NaCl$ (4) + CP system at 277.2 K at the following initial pressures; \blacktriangle , 0.65 MPa; \blacksquare , 0.85 MPa, \bullet , 1.14 MPa.

APPENDIX F: JOURNAL PAPERS ABSTRACT

Phase Stability Conditions for Clathrate Hydrate Formation in Fluorinated Refrigerant + Water + Single and Mixed Electrolytes + Cyclopentane System: Experimental Measurements and Thermodynamic Modelling

Peterson Thokozani Ngema^{1,2}, Paramespri Naidoo¹, Amir H. Mohammadi^{*,1}, and Deresh Ramjugernath^{*,1}

¹Thermodynamics Research Unit, School of Engineering, University of KwaZulu-Natal, Howard College Campus, King George V Avenue, Durban, 4041, South Africa

²Thermodynamics Research Unit, Department of Chemical Engineering, Durban University of Technology, Steve Biko, Durban, 4041, South Africa

Abstract

Phase equilibrium data (dissociation data) for clathrate hydrate (gas hydrate) were undertaken for systems involving fluorinated refrigerants + water + single and mixed electrolytes (NaCl, CaCl₂, MgCl₂ and Na₂SO₄) at varying salt concentrations in the absence and presence of cyclopentane (CP). The ternary systems for (R410a or R507) + water + CP were performed in the temperature and pressures ranges of (279.8 to 294.4) K and (0.158 to 1.385) MPa, respectively. Measurements for R410a + water + {NaCl or CaCl₂} + CP were undertaken at salt concentrations of (0.10, 0.15 and 0.20) mass fractions in the temperature and pressure ranges of (278.4 to 293.7) K and (0.214 to 1.179) MPa, respectively. The temperature and pressure conditions for R410a + water + Na₂SO₄ system were investigated at salt concentration of 0.10 mass fraction in range of (283.3 to 291.6) K and (0.483 to 1.373) MPa respectively. Measurements for {R410a or R507} + water + mixed electrolytes {NaCl, CaCl₂, MgCl₂} were undertaken at various salt concentrations of (0.002 to 0.15) mass fractions in the temperature and pressure ranges of (274.5 to 292.9) K and (0.149 to 1.119) MPa in the absence and presence of CP, in which there is no published data related to mixed salt and a promoter. The phase equilibrium measurements were performed using a non-visual isochoric equilibrium cell that co-operates the pressure-search technique. This study is focused on obtaining equilibrium data that can be utilised to design and optimize industrial wastewater, desalination process and the development of Hydrate Electrolyte–Cubic Plus Association (HE–CPA) Equation of State. The results show impressive improvement in the presence of promoter (CP) on hydrate formation, because it increases the dissociation temperatures near ambient conditions. The results obtained were modelled using a developed HE–CPA equation of state. The model results are strongly agree with the measured hydrate dissociation data.

Keywords: Gas hydrate, clathrate hydrate, water desalination, refrigerant, salt, phase equilibrium.

*Corresponding authors: D. Ramjugernath, e-mail: ramjuger@ukzn.ac.za; A.H Mohammadi, e-mail: amir_h_mohammadi@yahoo.com

Accepted Manuscript by the Journal of Chemical Thermodynamics in November 2018

Phase Stability Conditions for Clathrate Hydrate Formation in CO₂ + (NaCl or CaCl₂ or MgCl₂) + Cyclopentane + Water Systems: Experimental Measurements and Thermodynamic Modelling

Peterson Thokozani Ngema^{1,2}, Paramespri Naidoo¹, Amir H. Mohammadi^{*,1}, and Deresh Ramjugernath^{*,1}

¹Thermodynamics Research Unit, School of Engineering, University of KwaZulu-Natal, Howard College Campus, King George V Avenue, Durban, 4041, South Africa

²Thermodynamics Research Unit, Department of Chemical Engineering, Durban University of Technology, Steve Biko, Durban, 4041, South Africa

Abstract

Experimental hydrate dissociation conditions for ternary systems involving CO₂ + water + {sodium chloride (NaCl) or calcium chloride (CaCl₂) or magnesium chloride (MgCl₂)} at various molalities in the absence and in the presence of a water immiscible promoter (cyclopentane) were measured. The ternary systems consist of CO₂ + water + {NaCl or CaCl₂ or MgCl₂} + cyclopentane (CP), which were measured at various molalities of (1.041–4.278) mol.kg⁻¹ in the temperature range of (261.1–287.2) K and a pressure range of (0.813–3.239) MPa. Hydrate dissociation conditions were measured using an isochoric pressure-search method. The main challenge is limited information regarding the use of hydrate technology for the treatment of industrial wastewater and desalination processes, particularly with a water immiscible promoter. A promoter is the substance that is used to increase hydrate dissociation temperatures or lower dissociation pressures. The main aim of this study was to generate hydrate dissociation data, which can be used to design/optimize wastewater treatment and desalination processes using gas hydrate technology. The measured hydrate dissociation data were successfully modelled using the Hydrate Electrolyte–Cubic Plus Association (HE–CPA) equation of state based model.

Keywords - Gas hydrate; clathrate hydrate; electrolyte; dissociation data; water desalination.

*Corresponding authors: Deresh Ramjugernath, e-mail: ramjuger@ukzn.ac.za, Amir H. Mohammadi, e-mail: amir_h_mohammadi@yahoo.com

***This paper was presented on the Fluoro-Chemical Expansion Initiative Conference, Cape Town, South Africa, 14–17 November 2015

Accepted Manuscript by the Journal of Chemical Engineering Data in November 2018

Water Desalination using Clathrate Hydrates: State of the Art

Peterson Thokozani Ngema^{1,2}, Paramespri Naidoo¹, Amir H. Mohammadi^{*1}, and Deresh Ramjugernath^{*1}

¹Thermodynamics Research Unit, School of Engineering, University of KwaZulu-Natal, Howard College Campus, King George V Avenue, Durban, 4041, South Africa

²Thermodynamics Research Unit, Department of Chemical Engineering, Durban University of Technology, Steve Biko, Durban, 4041, South Africa

Abstract

There has been an ongoing research since the 1940s to date, using gas hydrate technique in the production of fresh water from seawater by employing the desalination process. Gas hydrate technology shows tremendous potential compared to traditional conventional processes, which include membrane and distillation processes. This technology is very simple, more economical and low energy consuming, thus, it should be considered as an alternative for future sustainable technology. The operation cost can be reduced more in the presence of a suitable promotor. Gas hydrate technology should be applied in the purification of industrial wastewater and seawater at a large scale. Desalination using gas hydrate technology has potential to recover fresh water from concentrated salinity solution at ambient temperatures and pressures. This review presents desalination technologies and the experimental studies using refrigerant as a hydrate former in the presence of common salts which include NaCl, CaCl₂, KCl, MgCl₂, Na₂SO₄, etc. Refrigerants have an advantage of forming hydrate at ambient conditions. This study presents more theory on hydrate formation with electrolytes, application of gas hydrates and economic studies. However, most of the investigations have been undertaken in the laboratory scale and modelling. Thus, there are limited pilot plant and large industrial scale in the world.

Keywords: Desalination, Gas hydrate, Refrigerant, Electrolytes

***Corresponding authors:** Deresh Ramjugernath, e-mail: ramjuger@ukzn.ac.za,

Amir H. Mohammadi, e-mail: amir_h_mohammadi@yahoo.com

Submitted to the Desalination Journal in December 2018